16 August 2013 | $10

Science

Smarter Pest Control

AAAS

SPECIAL SECTION

Smarter Pest Control

INTRODUCTION

728 The Pesticide Paradox

NEWS

730 Pesticide Planet
732 A Lethal Dose of RNA
>> *Science* Podcast
734 The War Against Weeds Down Under
737 Vietnam Turns Back a 'Tsunami of Pesticides'
738 In Rural Asia, Locking Up Poisons to Prevent Suicides
>> *Science* Podcast
740 Growing Up With Pesticides

REVIEWS

742 Current Challenges and Trends in the Discovery of Agrochemicals
C. Lamberth et al.
746 Pivoting the Plant Immune System from Dissection to Deployment
J. L. Dangl et al.
>> *Science* Podcast
752 Evaluating Pesticide Degradation in the Environment: Blind Spots and Emerging Opportunities
K. Fenner et al.
759 Wildlife Ecotoxicology of Pesticides: Can We Track Effects to the Population Level and Beyond?
H.-R. Köhler and R. Triebskorn

>> Editorial p. 695; Policy Forum p. 717; Perspective p. 722; Reports pp. 783 and 786; and additional resources at www.sciencemag.org/special/pesticides

page 710

POLICY FORUMS

717 Reevaluate Pesticides for Food Security and Safety
P. J. P. Verger and A. R. Boobis
>> Smarter Pest Control section p. 728
719 A U.K. View on the U.S. Attack on Social Sciences
P. Boyle

PERSPECTIVES

720 Long Noncoding RNAs Xist in Three Dimensions
A. Dimond and P. Fraser
>> Research Article p. 767
721 Gauging Greenland's Subglacial Water
M. Lüthi
>> Report p. 777
722 Paths from Pesticides to Parkinson's
F. Kamel
>> Smarter Pest Control section p. 728
724 Earthquake Risk in Turkey
M. Erdik

CONTENTS continued >>

EDITORIAL

695 The Road to Pollinator Health
Catherine Woteki
>> Smarter Pest Control section p. 728

NEWS OF THE WEEK

698 A roundup of the week's top stories

NEWS & ANALYSIS

701 Budget Woes Threaten Long-Term Heart Studies
702 Researchers Scramble to Understand Camel Connection to MERS
703 Senator's Demands Freeze NSF Political Science Grants
704 Europe Aims for a Cut-Rate Superlaser to Power Future Particle Accelerators

NEWS FOCUS

706 New Team, Old Hands
The Women of the Cosmos Club
708 Pluto, the Last Planetary First
710 The Crab That Roared

LETTERS

713 Develop, Then Intensify
J. Hanspach et al.
Extra Oversight for H7N9 Experiments
H. Jaffe et al.
The Systematic Place of Morals in Markets
C. Luetge and H. Rusch
Response
A. Falk and N. Szech
714 CORRECTIONS AND CLARIFICATIONS

BOOKS *ET AL.*

715 Tesla
W. B. Carlson, reviewed by T. J. Misa
716 Fatal Flaws
J. Ingram, reviewed by J. J. McDonald

ON THE WEB THIS WEEK

>> *Science* Podcast
Listen to a special show focused on smarter pesticides, including stories on preventing pesticide suicides, RNA interference for bugs, and manipulating the plant immune system.

>> Find More Online
Check out *Science* Express, our podcast, videos, daily news, our research journals, and *Science* Careers at **www.sciencemag.org**.

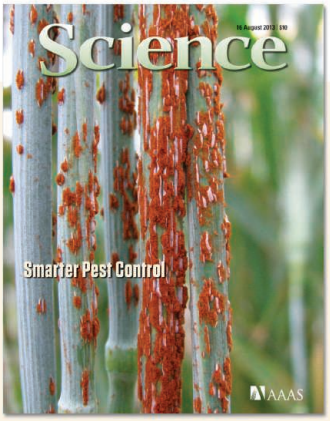

COVER

Stem rust fungus Ug99 is deadly to unprotected wheat strains (two stems on the right), but not to those protected by innate resistance genes (three stems on the left). In this special issue, we explore past and future strategies for responding to diseases and infestations caused by pests. The solutions demand our best knowledge of chemistry, immune responses, and ecosystem stability. See page 728.

Photo: Evans Lagudah and Zak Pretorius

DEPARTMENTS

694 This Week in *Science*
696 Editors' Choice
697 *Science* Staff
803 New Products
804 *Science* Careers

725 Triggering an Optical Transistor with One Photon
J. Volz and A. Rauschenbeutel
>> Report p. 768

726 Mapping Neuronal Diversity One Cell at a Time
H. Wichterle et al.

RESEARCH ARTICLE

767 The Xist lncRNA Exploits Three-Dimensional Genome Architecture to Spread Across the X Chromosome
J. M. Engreitz et al.
A large noncoding RNA uses folds within the chromosome to drive the spread of a chromatin repressive complex.
Research Article Summary; for full text: http://dx.doi.org/10.1126/science.1237973
>> Perspective p. 720

REPORTS

768 All-Optical Switch and Transistor Gated by One Stored Photon
W. Chen et al.
Optical transmission through a cesium-filled cavity can be controlled by a single stored photon.
>> Perspective p. 725

771 Control of Metal Nanocrystal Size Reveals Metal-Support Interface Role for Ceria Catalysts
M. Cargnello et al.
Comparing nanocrystals of different sizes on different oxides shows that ceria-metal interface sites enhance carbon monoxide oxidation.

774 Incision into the Eastern Andean Plateau During Pliocene Cooling
R. O. Lease and T. A. Ehlers
Climate had stronger control of canyon incision than tectonics in the eastern Andes 4 million years ago.

777 Basal Drainage System Response to Increasing Surface Melt on the Greenland Ice Sheet
T. Meierbachtol et al.
Basal drainage structures at the edges of the Greenland ice sheet differ from those found farther in the interior.
>> Perspective p. 721

779 Earliest Evolution of Multituberculate Mammals Revealed by a New Jurassic Fossil
C.-X. Yuan et al.
A fossilized skeleton reveals the origins of diverse feeding and locomotor adaptations of once-common rodent-like multituberculates.

783 Identification of Wheat Gene *Sr35* That Confers Resistance to Ug99 Stem Rust Race Group
C. Saintenac et al.

786 The Gene *Sr33*, an Ortholog of Barley *Mla* Genes, Encodes Resistance to Wheat Stem Rust Race Ug99
S. Periyannan et al.
Two resistance genes are identified that could protect wheat from a virulent fungus that can severely reduce crop yields.
>> Smarter Pest Control section p. 728

789 A Long Noncoding RNA Mediates Both Activation and Repression of Immune Response Genes
S. Carpenter et al.
In mice, a broadly acting RNA, lincRNA-Cox2, regulates the circuit that controls the inflammatory response.

792 Cleavage of Fibrinogen by Proteinases Elicits Allergic Responses Through Toll-Like Receptor 4
V. O. Millien et al.
Allergic inflammation requires proteinase-dependent cleavage of fibrinogen that activates innate immunity through Toll-like receptor 4.

796 Recurrent Insect Outbreaks Caused by Temperature-Driven Changes in System Stability
W. A. Nelson et al.
Seasonal temperature changes destabilize population cycles in the tea tortrix moth and drive the timing of pest outbreaks.

800 A Gut Lipid Messenger Links Excess Dietary Fat to Dopamine Deficiency
L. A. Tellez et al.
In mice, a high-fat diet functionally disrupts a gut lipid that controls the brain's perception of the reward value of food.

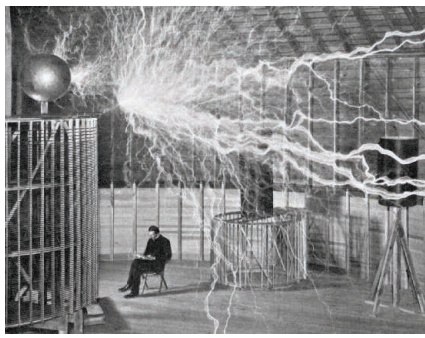

page 715

page 774

page 779

CREDITS: (MIDDLE) TODD A. EHLERS AND RICHARD O. LEASE; (BOTTOM) APRIL ISCH/UNIVERSITY OF CHICAGO

SCIENCE (ISSN 0036-8075) is published weekly on Friday, except the last week in December, by the American Association for the Advancement of Science, 1200 New York Avenue, NW, Washington, DC 20005. Periodicals Mail postage (publication No. 484460) paid at Washington, DC, and additional mailing offices. Domestic individual membership and subscription (51 issues): $149 ($74 allocated to subscription). Domestic institutional subscription (51 issues): $990; Foreign postage extra: Mexico, Caribbean (surface mail) $55; other countries (air assist delivery) $85. First class, airmail, student, and emeritus rates on request. Canadian rates with GST available upon request, GST #1254 88122. Publications Mail Agreement Number 1069624. **Printed in the U.S.A.**

Change of address: Allow 4 weeks, giving old and new addresses and 8-digit account number. **Postmaster:** Send change of address to AAAS, P.O. Box 96178, Washington, DC 20090–6178. **Single-copy sales:** $10.00 current issue, $15.00 back issue prepaid includes surface postage; bulk rates on request. **Authorization to photocopy** material for internal or personal use under circumstances not falling within the fair use provisions of the Copyright Act is granted by AAAS to libraries and other users registered with the Copyright Clearance Center (CCC) Transactional Reporting Service, provided that $30.00 per article is paid directly to CCC, 222 Rosewood Drive, Danvers, MA 01923. The identification code for *Science* is 0036-8075. *Science* is indexed in the *Reader's Guide to Periodical Literature* and in several specialized indexes.

EDITED BY STELLA HURTLEY

A Measure of Metal-Oxide Interfaces

The rate of a catalytic reaction can sometimes be enhanced by using a different metal oxide as the support for adsorbed metal nanoparticles. Such enhancement is often attributed to more active sites at the metal-oxide interface, but it can be difficult to quantify this effect. **Cargnello *et al.*** (p. 771, published online 18 July) synthesized monodisperse nanoparticles of nickel, platinum, and palladium and dispersed them on high-surface-area ceria or alumina supports. High-resolution transmission electron microscopy enabled a detailed analysis of interfacial site structure, which showed that the rate of CO oxidation on ceria was indeed enhanced greatly at interface sites.

Allergy Induction

Proteinases found in fungi and other allergens elicit allergic inflammation, but how they do so is far from clear. It is also unclear how pattern recognition receptors, which detect invading microbes, drive allergic inflammation. **Millien *et al.*** (p. 792) shed light on this puzzle by showing that, in mice, induction of allergic inflammation requires proteinase-dependent cleavage of the clotting factor fibrinogen, leading to generation of a ligand that activates the pattern-recognition receptor, Toll-like receptor 4 (TLR4). Cleaved fibrinogen signals through TLR4 to activate the innate immune system and recruit cells to the airway, which drives both allergic responses and antifungal immunity.

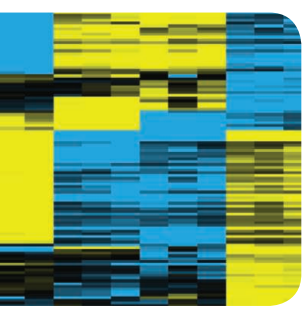

Food as Reward

Why does ice cream taste so good? High-fat foods activate a reward circuit in the brain involving dopamine, a neurotransmitter that regulates pleasure. Overconsumption of high-fat foods is thought to dampen this dopamine-induced reward sensation, leading to compensatory consumption of even more high-fat foods. The mechanisms by which dietary fat in the gut "talks" to the dopamine reward circuit are unclear. **Tellez *et al.*** (p. 800) suggest that an intestinal lipid messenger called oleoylethanolamine (OEA) may play a role—at least in mice. Mice on a high-fat diet had unusually low levels of intestinal OEA and exhibited deficient dopaminergic responses to gut stimulation with high-fat lipids. Infusion of OEA into these mice restored the dopaminergic response, and mice that had been accustomed to a high-fat diet began to eat more low-fat foods.

Draining Through Ice

Water formed by surface melting of the Greenland Ice Sheet is transferred rapidly to the underlying bedrock, but how the water is then dispersed is less clear. This question is important because how the ice-rock interface is lubricated affects how fast the ice sheet moves. Existing conceptual models are based on observations of mountain glaciers, but **Meierbachtol *et al.*** (p. 777; see the Perspective by **Lüthi**) now show that those ideas may not be applicable to the Greenland Ice Sheet. Measuring water pressures in a transect of 23 boreholes revealed that drainage structures differ between the edge, where large melt channels form, and further inland, where more distributed pathways are found.

A Single-Photon Gate

A long-standing goal in optics is to produce an all-optical transistor, in which the transmission of a light beam can be controlled by a single photon. Using a system in which a cloud of cesium atoms is coupled to an optical cavity, **Chen *et al.*** (p. 768, published online 4 July; see the Perspective by **Volz and Rauschenbeutel**) were able to control transmission through the optical cavity by exciting the atomic ensemble using a "gate" laser pulse. Just one gate photon stored was sufficient to detune the system and switch the transmission of source photons through the cavity.

Bringing Down the Andes

Mountain ranges, like the Andes in South America, have a number of forces acting on them that control their elevation. High rates of precipitation can induce rapid incision of canyons, but tectonic forces from deep within the mountain range may balance or even exceed the rate of erosion. **Lease and Ehlers** (p. 774) examined the exhumation histories of the northeastern Andean Plateau. The erosion of sediments older than ~10 million years was controlled largely by tectonic processes. However, more recent sediments suggest that a shift to cooler temperatures increased precipitation 3 to 4 million years ago.

Insect Cycles

Rapid increases in insect population sizes can result in significant crop losses. Seasonal temperature has been proposed to drive such outbreaks. Despite clear evidence that temperature can drive individual insect development, its influence at the population level is much less clear. **Nelson *et al.*** (p. 796, published online 1 August) analyzed data collected over 50 years on the tea tortrix moth, which affects Japanese tea plantations, to reveal the impacts of temperature on cyclical outbreaks.

Resistance May Not Be Futile

Recently, Ug99, a particularly devastating strain of wheat stem rust fungus, has emerged, which could potentially threaten food security. Now, two genes have been cloned that offer resistance to Ug99. **Saintenac *et al.*** (p. 783, published online 27 June) cloned *Sr35* from *Triticum monococcum*, a diploid wheat species not often cultivated. **Periyannan *et al.*** (p. 786, published online 27 June) cloned *Sr33* from *Aegilops tauschii,* a diploid wild grass that contributed to the hexaploid genome of cultivated wheat. The genes both encode proteins that show features typical of other disease resistance proteins and offer opportunities to slow the pace of Ug99 progression.

CREDITS (TOP TO BOTTOM): MARTIN LÜTHI; MILLIEN *ET AL.*

Published by AAAS

Additional summaries

Understanding Xist-ance

Large noncoding RNAs (lncRNAs) are increasingly appreciated to play important roles in the cell. A number of lncRNAs act to target chromatin regulatory complexes to their sites of action. **Engreitz *et al.*** (p. 767, published online 4 July; see the Perspective by **Dimond and Fraser**) found that the mouse Xist lncRNA, which initiates X-chromosome inactivation, was transferred from its site of transcription to distant sites on the X chromosome purely through their close three-dimensional proximity to the *Xist* gene. Xist initially localized to the periphery of active genes on the X chromosome but gradually spread across them using its A-repeat domain, until the Xist RNA bound broadly across the inactive X chromosome in differentiated female cells.

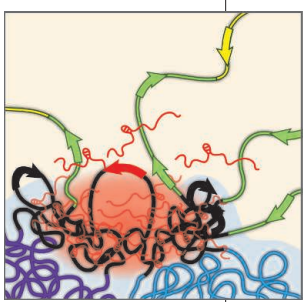

Early Multi

Multituberculate mammals (multis) first arose in the Jurassic and became extinct in the Oligocene, a span of over 100 million years, which makes them the longest-living order of mammals known. This highly diverse and abundant group filled many niches occupied by today's similarly diverse rodents. Multis are known for their complex dentition and unique locomotor adaptations, which facilitated their divergence into a suite of ecosystems. **Yuan *et al.*** (p. 779) describe a new basal multi from a nearly complete skeleton that shows that the underpinnings of these adaptations arose early in the evolution of the order, setting the stage for the major diversification and radiation of the group that came during the Cretaceous and Paleogene.

A New Linc in Innate Immunity

Long noncoding RNAs (lncRNAs) have recently emerged as important regulators of gene expression in a wide variety of biological processes, although specific roles for these molecules in the immune system have not been described. **Carpenter *et al.*** (p. 789, published online 1 August) now define the function of one such lncRNA in the immune system, lincRNA-Cox2. Whole-transcriptome profiling revealed that lincRNA-Cox2 was induced in mouse macrophages in response to activation of Toll-like receptors—molecules that detect microbes and alert the immune system to respond. LincRNA-Cox2 both positively and negatively regulated the expression of distinct groups of inflammatory genes. Negative regulation of gene expression was mediated by lincRNA-Cox interaction with heterogeneous nuclear ribonucleoprotein A/B and A2/B1.

CREDIT: ENGREITZ *ET AL.*

Catherine Woteki is the Chief Scientist and Under Secretary for Research, Education and Economics at the U.S. Department of Agriculture. E-mail: Catherine.woteki@osec.usda.gov.

The Road to Pollinator Health

AGRICULTURAL PRODUCTION IS A BALANCING ACT. ON ONE SIDE IS SUSTAINABLE PRODUCTION OF food and biobased products for a growing population. On the other is protecting our natural resources and the environment. The global decline of the honey bee, a major domestic pollinator of many crops, exemplifies how complex the factors are that contribute to maintaining this balance. Overall bee colony decline, including loss from colony collapse disorder (CCD), poses a serious challenge to agricultural research worldwide. The causes are still not definitive, but stress from pesticides may be a factor. This spring, the European Commission temporarily restricted the use of three neonicotinoid pesticides for specific applications (pending more research). Last year, the U.S. Environmental Protection Agency (EPA) and U.S. Department of Agriculture (USDA) formed a bee health task force to take an even broader look at the pollinator crisis, with a plan to collect interagency input and develop a federal Pollinator Roadmap before the end of 2013.

The United Nations Food and Agriculture Organization has noted that 71 of the 100 crops that provide 90% of human food are pollinated by bees, and the estimated value of those crops is as much as $200 billion annually.* In the United States, honey bees contribute over $17 billion to the nation's economy and are vital to keeping fruits, nuts, and vegetables in our diets. Since 2006, U.S. beekeepers have seen colony loss rates increase to 30 to 35% per year, as compared to historical loss rates of 10 to 15%, a situation that requires beekeepers to rapidly, and at great expense, rebuild their colonies. The honey bee declines have been associated with a combination of many factors, such as poor nutrition, parasites, pests, pathogens, pesticides, and stress from colony transport.

In May, the USDA, EPA, and Pennsylvania State University released a comprehensive scientific report† that focuses on four areas for concentrated work: nutrition; pathogens and arthropod pests; pesticides; and bee genetics, breeding, and biology. We need to examine the interactions of these factors. Because honey bees are social insects, assessing the impact of pesticide exposure, especially at sublethal amounts, requires a different metric that accounts for colony survival. And a decline in nutrient availability in the environment could cause bees to respond poorly to environmental challenges. The symbiotic microbiota that bees need to process and store their food also might be affected by the environment. These impacts could contribute to colony losses weeks or months after exposure.

To fully address the range of interacting factors that contribute to bee declines, and building on the work of the Honey Bee Health and CCD Action Committee that reports to Congress yearly, the EPA-USDA task force is taking a landscape-level systems approach to bee research and rescue, examining land-use patterns, nutritional stress associated with available forage, exposure and susceptibility to parasites and pathogens, bee genetic diversity, and the means to augment pollinator forage in all landscapes, in addition to minimizing pesticide exposures. A meta-analysis should guide attention to the most urgent research. Steps to improve collaboration and information sharing among commercial beekeepers, agricultural producers, the research community, and other stakeholders will also be laid out. The task force's goal is to turn around this decline as we proceed with our work over the next 5 to 10 years. As our knowledge increases during this time, there will be constant evaluation of research priorities and actions.

Exploring the causes of bee colony declines and specifically CCD remains a priority for the USDA, even as funding for agricultural research has been reduced by almost 20%. Our health and environmental well-being are related to the health of honey bees in the complex web of interconnectedness that is our world. Their crisis is ours as well.

– Catherine Woteki

10.1126/science.1244271

*www.fao.org/ag/magazine/0512sp1.htm. †www.usda.gov/documents/ReportHoneyBeeHealth.pdf.

Published by AAAS

EDITED BY GILBERT CHIN AND MARIA CRUZ

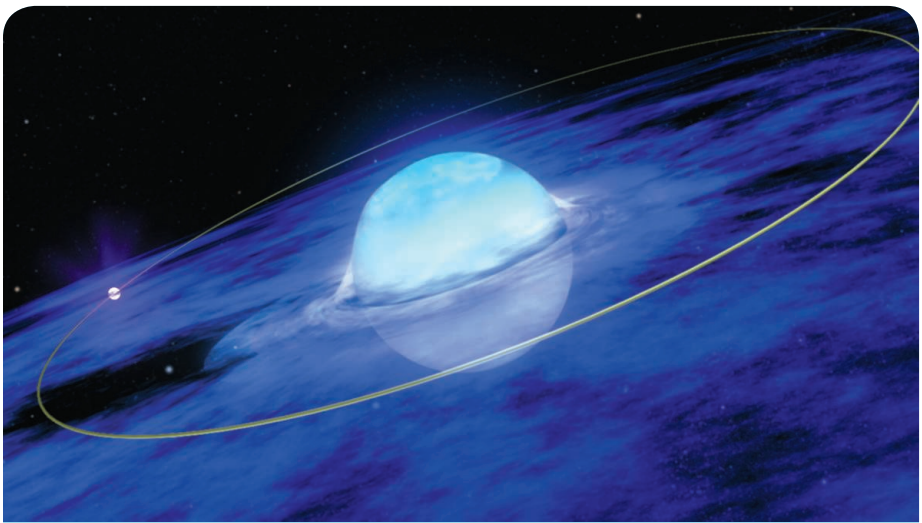

ASTRONOMY

Superorbital Variability

Many stars live in pairs, and sometimes they form rather intriguing binary systems. LS I +61°303 is one such case, where a Be star 10 times as massive as the Sun and a compact object orbit around their common center of mass. Be stars are rapidly rotating B-type stars that show hydrogen Balmer emission lines in their spectrum and lose mass to an equatorial circumstellar disk. The nature of the compact object in LS I +61°303 is unknown, but it is suspected to be a neutron star. The system has been detected across the electromagnetic spectrum all the way from radio to gamma rays, and it has been shown to be highly variable across all frequencies. At most wavelengths, the flux of LS I +61°303 is known to be modulated by the orbital period of about 26.5 days; at radio, x-ray, and optical frequencies, the flux is also modulated on a longer time scale, or superorbital period, of 1667 days. Based on data from the Fermi Gamma-ray Space Telescope, Ackermann *et al.* show that the gamma-ray emission of LS I +61°303 also varies according to the superorbital period. This modulation is more prominently seen at orbital phases around apastron (the point at which the stars in the binary are farthest apart), which could be explained by a quasi-cyclical evolution of the equatorial outflow of the Be star. The authors suggest that gamma-ray observations such as these could be used to study the ouflows of massive stars in eccentric binary systems. — MJC

Astrophys. J. **773**, L35 (2013).

CANCER

Gains in Cancer Epigenetics

With the recent discovery that genes that code for chromatin-modifying enzymes are mutated in human cancers, interest in the oncogenic role of these epigenetic regulators has intensified. Adding a twist to this story is a new study showing how aberrant overexpression of the wild-type (that is, nonmutated) version of an epigenetic regulator can also contribute to the development of tumors. Black *et al.* found that the gene for KDM4A, a histone lysine demethylase, is reproducibly amplified in several tumor types, most notably in ovarian cancer. In order to investigate the functional consequences of this amplification, the authors studied a cell culture model in which KDM4A was overexpressed. Surprisingly, KDM4A overexpression produced transient gains in the number of copies of specific genomic regions, especially at chromosome 1q12 as measured by fluorescence in situ hybridization, but did not cause global genome instability as assessed by spectral karyotyping. In primary tumors, the regions amplified in a KDM4A-dependent manner correlated with amplification of the KDM4A gene itself. The authors hypothesize that the elevated level of this chromatin-modifying enzyme enhances the recruitment of the DNA replication machinery and leads to a repeated replication of some genomic regions, which produces a selective gain in copy number. These findings reveal an unexpected mechanistic link between epigenetic regulation and genomic instability, a hallmark of cancer cells. — PAK

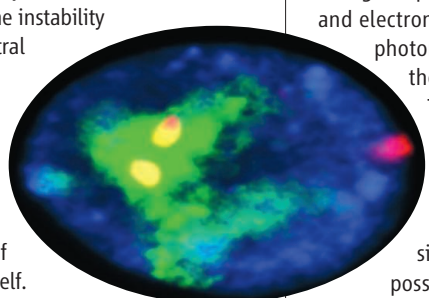

Cell **154**, 541 (2013).

SIGNAL TRANSDUCTION

When a Half-Life Isn't

A common tactic for measuring the rate of turnover of proteins in cells is to block the synthesis of new proteins by treating the cells with cycloheximide, a drug that gums up the ribosomal assembly line that churns out proteins. But Dai *et al.* warn that this methodology only works if cycloheximide treatment does not itself affect the rate of protein degradation. Cells are autonomously regulated machines; as such, they can detect environmental insults and launch a stress response. In human embryonic kidney cells, the authors found that inhibiting protein synthesis with cycloheximide led to the activation of the protein kinase AKT (also called protein kinase B). Among the many targets of AKT are the ubiquitin ligases MDM2 and Skp2. These enzymes promote protein degradation, and phosphorylation by AKT stimulates their activity. Thus, at least for certain proteins, inhibiting protein synthesis can increase the rate of protein degradation. — LBR

J. Biol. Chem. **288**, 10.1074/jbc.M112.445148 (2013).

PHYSICS

Controlling Power Flow

Optoelectronic devices lie at the heart of the technology industry. Shrinking the size (and increasing the operation speed) of the devices are often limited by the optical components, whose sizes generally exceed many tens of wavelengths. Surface plasmons are collective electronic excitations induced by photons interacting with a metal, effectively confining the light to subwavelength dimensions and offering the possibility of bridging the optical and electronic size gap. Much effort in nanophotonics is geared toward controlling the directional flow of plasmons. To this end, Davoyan and Engheta present a theoretical study that combines plasmonic nanostructures with magneto-optical elements. Their numerical simulations show that it may be possible to control the energy flow of the plasmons in such a hybrid structure, thereby providing a possible route to manipulating light at the nanoscale. — ISO

Phys. Rev. Lett. **111**, 047401 (2013).

Published by AAAS

AROUND THE WORLD

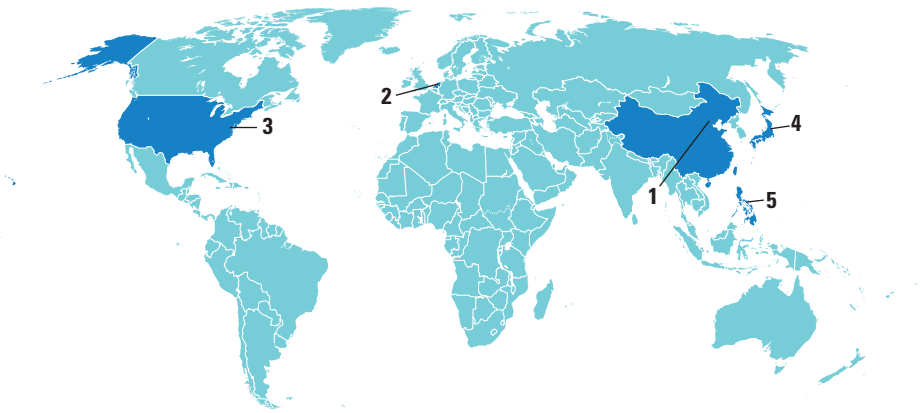

Beijing **1**

China to Share Nuclear-Monitoring Data

Hours after North Korea announced its third nuclear test in February, seismic signals around the world confirmed a massive explosion—but the United States and its allies were unable to detect radioxenon emanating from the test site quickly enough to distinguish whether it was a plutonium bomb or a uranium bomb.

Next time might be different: On 8 August, the Vienna-based Comprehensive Nuclear-Test-Ban Treaty Organization (CTBTO) announced that China has agreed to begin sharing data from 10 stations on its territory. Seven stations register seismic waves and infrasound waves; three stations in Beijing, Lanzhou, and Guangzhou detect radionuclides. Data from the stations would be fed into the International Data Centre maintained by CTBTO. To date, 85% of CTBTO's 337 planned monitoring stations around the world are operational.

The breakthrough came during a visit to Beijing last week by Lassina Zerbo, the new executive secretary of CTBTO's preparatory commission. China is one of eight CTBT signatories whose ratification would bring the treaty into force; other holdouts include the United States and North Korea. (So far, 159 countries have ratified the treaty.) CTBTO now must certify the Chinese stations. **http://scim.ag/ChinaCTBTO**

Luttelgeest, the Netherlands **2**

Return of the Wolf

The good news: A wolf apparently traveled more than 900 kilometers to find a new home in the Netherlands, a densely populated country where the species was last seen more than 140 years ago. The bad news: The animal was killed, probably by a car.

The discovery of the roadside carcass on 4 July triggered a raft of DNA and other studies—first, to determine whether it was really a wolf, and then to trace its origins. On 7 August, researchers from three institutes announced that the animal, a healthy female that lived at least 18 months, didn't peel off from the nearest known wolf populations in Germany and western Poland but most likely wandered in all the way from the Carpathian Mountains or the Balkans. An autopsy revealed that it had died from a high-impact blow.

End of the road. The wolf found in the Netherlands was the first seen in the country in 140 years.

The arrival has bolstered Dutch conservationists' hopes that wolves—which have recently been moving westward in neighboring Germany, close to the Dutch border—will soon make a spontaneous comeback in their country. The government has already ordered experts to write a wolf management plan, to be revealed in November.

Denied. A U.S. agency rejected a request to import captive belugas.

Washington, D.C. **3**

U.S. Blocks Import Of Beluga Whales

The U.S. National Marine Fisheries Service (NMFS) on 6 August denied a request from a consortium of U.S. marine parks and aquariums to import 18 beluga whales (*Delphinapterus leucas*) from Russia's Sea of Okhotsk, finding the move would violate marine mammal protection laws. The June 2012 request for the import permit divided marine mammal scientists and drew extensive opposition from animal rights groups.

The Georgia Aquarium, which led the request, lamented the decision, saying that it would set back efforts to study the species and reduce opportunities for public education. But conservationists applauded.

NMFS determined that the Georgia Aquarium's request fell short in three ways: The agency found that the imports would adversely affect the specific population of whales from which the belugas were captured; that approving the permit would likely lead to the seizure of additional marine mammals for display; and that past captures had not adhered to Marine Mammal Protection Act rules that only adult or juvenile animals be taken. The fate of the 18 captive belugas is unclear. **http://scim.ag/Russiabelugas**

Okuma, Japan **4**

Government Takes Role In Fukushima Cleanup

The government of Japan will intervene in the management of the Fukushima nuclear power plant disaster, which so far has been left to Tokyo Electric Power Co. (TEPCO), the operator of the stricken reactors. Prime Minister Shinzo Abe ordered his administration to "provide multiple, speedy and sure

CREDITS (TOP TO BOTTOM): THINKSTOCK; GUUS SCHOONEWILLE/EPA/LANDOV

Published by AAAS

Biological Art

The winners of the 2013 Federation of American Societies for Experimental Biology (FASEB) BioArt competition each offer a sneak peek into science on the move, using a range of imaging techniques (magnetic resonance imaging, electron microscopy, fluorescence microscopy, and so on). The 10 image winners (plus two video winners), announced on 8 August, captured snapshots from a variety of subjects, including magnetic resonance images that map water motion in the brain tissues of a living monkey, a scanning electron micrograph of the transport of micron-sized silica beads (standing in for targeted drug delivery) to human fibroblast cells, and a tiny embryonic little skate sitting on its yolk sac (pictured; the red strands are external gills).

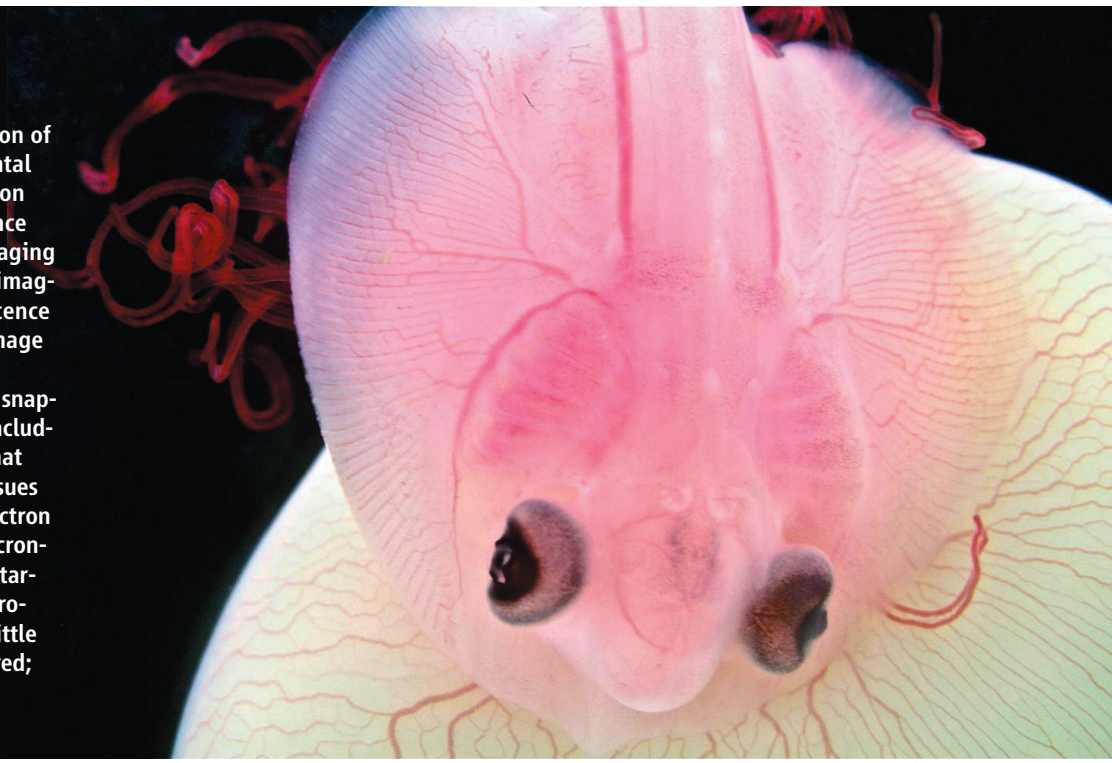

CREDITS (TOP TO BOTTOM): FASEB'S BIOART IMAGE AND VIDEO COMPETITION, KATHERINE O'SHAUGHNESSY AND MARTIN J. COHN; DA-RFU 5 PUBLIC INFORMATION UNIT

solutions" after TEPCO recently admitted that water laden with cesium, strontium, and tritium is leaking into the Pacific Ocean. TEPCO's admission came nearly a year after marine scientists reported that persistently high levels of radionuclides in the ocean near the plant indicated that efforts to contain contaminated water were not working.

The estimated 300 tons of radioactive water flowing into the ocean each day will not have "a significant impact on the marine environment," says Jota Kanda, an oceanographer at the Tokyo University of Marine Science and Technology. But because strontium accumulates in bone, it "may become a greater concern in the seafood supply," says Ken Buesseler, a marine chemist at Woods Hole Oceanographic Institution in Massachusetts.

Japanese officials proposed containing the tainted water by creating a barrier of frozen soil between the reactors and the sea. But ground freezing "has never been done on these scales of size and time," Buesseler says.

NOTED

>Following record numbers of bottlenose dolphin deaths in July—which saw 89 stranded bottlenose dolphins, seven times the average for the month—the U.S. National Oceanic and Atmospheric Administration has declared an **Unusual Mortality Event** for the marine mammals in the mid-Atlantic region from Virginia to New York. Scientists are searching for answers; the dolphins were mostly stranded dead and decomposed, but at least one has tested positive for morbillivirus, the cause of a die-off that killed more than 700 dolphins along the U.S. Atlantic Coast in 1987.

Bicol region, Philippines **5**

Activists Destroy 'Golden Rice' Field Trial

Protestors from two anti-GMO groups, KMB and Sikwal-GMO, on 8 August vandalized a field of genetically modified (GM) "golden rice" in the Philippines, swarming over the field and uprooting stalks. The rice was just weeks away from being harvested, says plant biologist Ingo Potrykus, one of the researchers who originally created the rice strain.

Golden rice is engineered to carry two foreign genes—one bacterial and another from maize—that together produce beta carotene, a precursor of vitamin A. Scientists hope distribution of the modified rice can make inroads against vitamin A deficiency, which can lead to blindness and makes people more susceptible to infectious diseases.

The vandalized field was one of five involved in golden rice trials in the Philippines. Golden rice could be deemed safe and approved by the Philippine government as early as the end of this year, says Robert Zeigler, director general of the International Rice Research Institute. But further trials assessing whether the beta carotene in the rice is absorbed and converted into vitamin A in vitamin A-deficient people could take another 18 months.
http://scim.ag/goldenrice

Mowed down. Uprooted and trampled plants at the vandalized golden rice field.

Published by AAAS

Random Sample

Play Find the Fungus

There's a fungus among … the ash trees. The "ash dieback fungus" (*Chalara fraxinea*) was first identified in Poland in 1992 and quickly spread across Europe. In the United Kingdom, it first appeared in 2012; now, U.K. scientists worry that the fungus is poised to spread to the rest of the country.

Hoping to slow its spread, the U.K. government is using social media—mobile phone apps and open-access crowdsourcing hubs—to help study the emerging pathogen. Now, scientists are adding a new strategy: Facebook gaming.

"I saw an opportunity to take advantage of a new way of working"—using online games to answer questions about variations in the genomes of both the fungus and the ash trees—says Dan MacLean, a genomicist at the Sainsbury Laboratory in Norwich, U.K. "We need to find the genetic variants that are associated with resistance in the ash or with lethality in the fungus." Genomes are pieced together from small overlapping DNA sequences. Once there's a reference genome established for the species, scientists then try to match sequences of DNA to it from samples, hunting for differences between the strains. "The whole puzzle is a pattern-recognition puzzle," MacLean says.

Enter "Fraxinus," a Facebook game that debuted 12 August (after beta-testing by middle schoolers, pictured). Fraxinus takes advantage of the human eye's natural pattern-recognition ability to detect differences in sequences that computers might miss. Players match nucleotide sequences, represented by colorful leaf shapes, to a reference genome to create the best possible alignment. The game also has an element of competition: You get more points for beating someone else's score on a "puzzle." "That's useful scientifically," MacLean says—it means multiple pairs of eyes on the same data point, refining the data.

CREDITS (TOP TO BOTTOM): JOHN INNES CENTRE PHOTOGRAPHY; THE JOHN INNES CENTRE AND THE SAINSBURY LABORATORY; ABRI PEYRONY & PECH-DE-L'AZÉ I PROJECTS (2)

FINDINGS

Neandertals Made Bone Tools, Too

Finely made bone tools found at two prehistoric sites in southwest France suggest that Neandertals independently invented these implements without help from *Homo sapiens*. Neandertals lived in Europe and Asia between about 135,000 and 35,000 years ago. Around the time that modern humans moved into Europe—between about 45,000 and 40,000 years ago—Neandertals' stone tools became more sophisticated, they began to wear jewelry, and they started using bone tools. Archaeologists debate whether these Neandertals copied modern human behavior or developed the behaviors before modern humans appeared.

Now, two teams of archaeologists have found four bone tools dated earlier than the first known existence of modern humans in the region, they reported online on 12 August in the *Proceedings of the National Academy of Sciences*. The tools, made from red deer or reindeer ribs, are a type of implement called a *lissoir*, used to polish animal hides.

This, the teams say, suggests that Neandertal technical abilities have been underestimated. Yet other researchers caution against drawing too many conclusions about Neandertal mental abilities from these tools, noting that specialized implements—for example, bone toothpicks—can be easy to make and are not necessarily an expression of advanced technology. **http://scim.ag/bonetools**

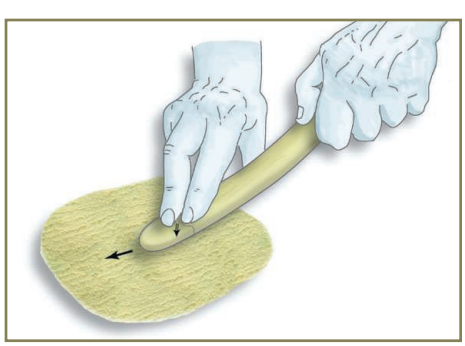

Well-rounded. Neandertals made bone tools (*left*), probably to work animal hides (*right*).

Published by AAAS

EPIDEMIOLOGY

Budget Woes Threaten Long-Term Heart Studies

For more than 6 decades, thousands of residents of Framingham, Massachusetts, have reported every few years to a research clinic, where they undergo a detailed physical exam that now includes electrocardiograms, measures of lung and cognitive function, and the collection of blood and urine samples. The Framingham Heart Study (FHS) is an icon of epidemiology. Its long-term monitoring of a large group, or cohort, has yielded landmark results on everything from the link between cholesterol and heart disease to the genetic risk of stroke. But this year, those exams will be scaled back, and plans for new tests put on hold. Other cohort studies sponsored by the National Heart, Lung, and Blood Institute (NHLBI) are confronting a similar fate.

The immediate culprit is this year's across-the-board federal budget cuts known as the sequester, which trimmed 5%, or $1.55 billion, from the National Institutes of Health (NIH). To preserve investigator-initiated grants and clinical trials, NHLBI is slashing $4 million, or 40%, from the 2013 contract that supports the FHS's core operations. "We have to make cuts," explains Michael Lauer, director of the NHLBI Division of Cardiovascular Sciences. "There are other [cohort studies] that are being affected even more severely," he adds, declining to identify them because of ongoing contract negotiations.

The squeeze on cohort studies is set to continue. NHLBI has already decided to suspend exams scheduled to start 2 years from now at FHS and another study, the Multi-Ethnic Study of Atherosclerosis (MESA). Some observers say NHLBI's plans signal that the era of such large, costly long-term studies is drawing to a close.

In response to this year's cut, FHS plans to lay off 19 of 90 staffers as well as scale back clinical exams and laboratory work. Calling the exams "the lifeblood of the study," FHS principal investigator Philip Wolf of Boston University told *Science* that he is concerned that the study's scientific productivity will decline if investigators can no longer collect the same wealth of data. He also worries that participants will drop out of the study if not routinely brought in for exams. "We've had amazing subject retention over the decades. It obviously has to have a deleterious effect," he says.

Lauer says that NHLBI has no plans to shut FHS altogether. "We have every intention of maintaining and preserving this investment." The Framingham effort has survived money woes before, turning to private funding in 1970 when NIH slashed its budget, and its supporters say they will seek such help again now. But NHLBI's longer term plans for it and other cohort studies worry some epidemiologists.

NHLBI now spends $160 million of its $3 billion budget on epidemiology research, including cohort studies (see table). The institute began scrutinizing these studies 2 years ago, asking whether there are cheaper ways to do the research, for example, by using electronic medical records and Internet surveys of participants instead of costly in-person exams. At a June meeting of the institute's advisory council, NHLBI officials announced that the next contracts for Framingham and MESA, which start in 2015, will run for just a few years, instead of the usual 7 years. And a new working group will look for ways to make these studies more efficient "during this time of big data and small budgets," Lauer says.

Such studies can be scaled back without long-term harm, he adds. One large cohort study, Atherosclerosis Risk in Communities (ARIC), went for 10 years from 1999 to 2009 without conducting exams, yet suffered no apparent loss in participation, Lauer notes. "We've been down this road before and we've seen that it's possible to do this and support terrific science," he says.

But other epidemiologists argue that there's no substitute for in-person exams. "Some things could be done more cheaply; for others you need trained staff doing things in a standardized way," says David Couper of the University of North Carolina, Chapel Hill, one of ARIC's principal investigators. "If all you know is that someone had a heart attack, you lose a chance to better understand disease etiology and potentially new prevention strategies," says Gregory Burke of the Wake Forest School of Medicine in Winston-Salem, North Carolina, a MESA investigator.

Offering a possible model for lower-cost, large cohort research, the University of California, San Francisco (UCSF), has launched a new study called Health eHeart that aims to enroll up to a million people over the Internet and have them use technologies such as a wireless cuff linked to a smart phone to relay blood pressure data. Yet even one of its organizers, UCSF's Mark Pletcher, acknowledges that "the jury's still out on" how well such measures can substitute for in-person exams.

Bruce Psaty of the University of Washington, Seattle, a member of the working group on cohort studies, says he hopes some direct exams will be preserved in NHLBI's efforts. But in the end, he adds, Framingham's troubles are just one sign of something bigger: They are "a poster child for the larger problem of the erosion of funding for biomedical research," he says. **–JOCELYN KAISER**

Selected NHLBI-Sponsored Cohort Studies

	Participants	First exam
Framingham Heart Study—Generations 1–3	14,400	1948
Coronary Artery Risk Development in Young Adults	5100	1985
Atherosclerosis Risk in Communities Study	15,800	1987
Cardiovascular Health Study	5900	1989
Jackson Heart Study	5300	2000
Multi-Ethnic Study of Atherosclerosis	6800	2000
Strong Heart Study	3800	2001
Hispanic Community Health Study/Study of Latinos	16,000	2008

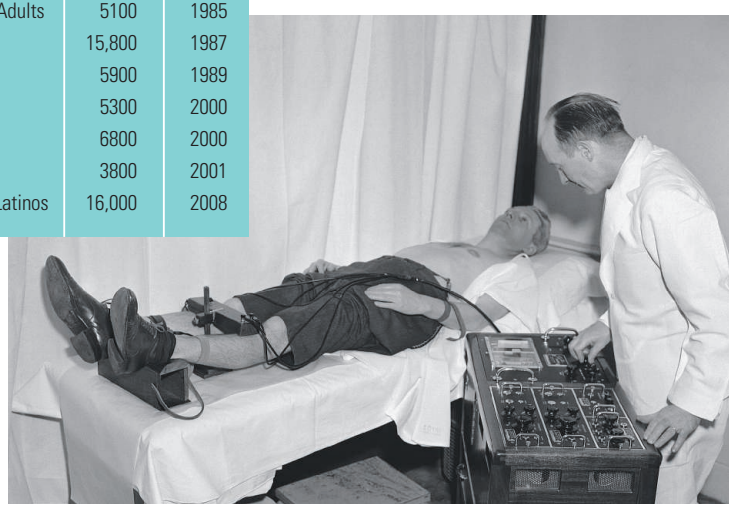

On hold. The Framingham Heart Study has included clinical exams for decades (a 1952 one, *below*), but future ones are at risk.

TABLE SOURCE: NHLBI/P. SORLIE AND G. WEI, *JOURNAL OF THE AMERICAN COLLEGE OF CARDIOLOGY* **58**, 19 (2011); PHOTO CREDIT: ASSOCIATED PRESS

Risk factor? Close contact between a man and a camel at a farm in Qatar.

EMERGING DISEASES

Researchers Scramble to Understand Camel Connection to MERS

The discovery that a dangerous new virus that surfaced in the Middle East last year may be lurking in camels has reenergized the hunt for its source. There had been little progress in finding the origins of the Middle East respiratory syndrome (MERS) coronavirus, which has sickened 94 people and killed 46. But after last week's report in *The Lancet Infectious Diseases,* "everybody's scrambling to figure out what we know about camels," says Anthony Mounts, the point person for MERS at the World Health Organization (WHO) in Geneva, Switzerland.

The team that reported the finding, in retired racing camels in Oman, found only antibodies, not the virus itself, and they acknowledge it's possible that the antibodies were directed at another agent. Gaps in knowledge about camels' biology are also a challenge for researchers pursuing the connection, says Mounts, who notes "the very limited number of camel experts in the world."

Scientists had long suspected that animals harbor and transmit the virus, because some patients have not had contact with other known human cases. Bats are a key suspect, because viruses very closely related to MERS are found in several bat species. But bats rarely cross paths with people, so even if they're the ultimate source, an intermediate host may act as the bridge.

Some scientists tracking the source complain that MERS-affected countries have not allowed a full-fledged epidemiological investigation (*Science,* 15 March, p. 1264). Researchers in the new, multinational study weren't able to obtain samples from these countries either. Instead, they used sheep, goats, cows, and camels from other countries, including Oman, which has not had MERS cases but borders two countries that have: Saudi Arabia and the United Arab Emirates. They tested the samples for antibodies against a protein on the viral surface called the spike; to make sure any signal was specific for MERS, they also tested against two human coronaviruses, severe acute respiratory syndrome (SARS) and OC43. The former is believed to be extinct; the latter is closely related to a bovine coronavirus.

As they expected, none of the animals had antibodies against SARS, and only some against OC43. But all 50 camels from Oman had antibodies against the MERS virus. (So did 16 out of 105 camels from the Canary Islands, but at lower levels.) "There is something circulating in dromedary camels that looks very much like the MERS coronavirus," says co-author Marion Koopmans of the National Institute for Public Health and the Environment in Bilthoven, the Netherlands.

The scientists didn't try to isolate the virus because it's unlikely to be present in animals with high antibody titers. "So it's still a bit of a question whether this is the exact same virus," Mounts says. Columbia University virologist Ian Lipkin calls the results "very intriguing," but says it's "surprising" to see antibodies in each and every Omani camel that was tested. Antibody tests have misled researchers before, he warns; until the agent itself is isolated, "we are just dealing with shadows of what may be MERS virus or a related virus."

Saudi deputy minister of health Ziad Memish is more outspoken. "We don't think camels have anything to with it," he says. Most patients had no contact with camels, Memish says; moreover, camels are "complicated animals with a complicated immune system." Antibodies in humans and most other animals are made up of four chains of amino acids, but camels also have antibodies consisting of just two chains, possibly allowing them to attach to more pathogens. Combined with the fact that serology tests against MERS are so new, this could have led to a wrong result, Memish suggests.

Koopmans says that even if the peculiar antibodies can cause false positives, this wouldn't explain why they recognized only MERS, not SARS. She agrees that more studies are needed, however. "Go ahead: Do studies and prove us wrong," she says. "As long as we look into it." Several countries have already asked for the team's assistance in analyzing animal samples, she adds, including Jordan and Qatar, which both have had MERS cases.

A team led by Lipkin has already collected samples from animals in Saudi Arabia, including 33 camels. Lipkin says he's hoping to submit a paper about them as early as next week. WHO, the Food and Agriculture Organization of the United Nations (FAO), and the World Organisation for Animal Health are planning to embark on a joint research mission to the region within 2 months, says Juan Lubroth, FAO's chief veterinary officer.

The camel connection does not come as a complete surprise. A patient from Abu Dhabi who died in a German hospital in March owned racing camels and reported that he had close contact with a sick camel before falling ill. But other than that, little is known about MERS patients' animal contacts. "We need to go back to [other] patients and question them very carefully about exposures that may be related to camels," Mounts says.

Camels are used for meat and milk and as beasts of burden in the Middle East; camel races are very popular as well. "You have the whole gamut of human contact," Lubroth says. Many camels are imported to the Middle East from African countries like Kenya, Tanzania, and Sudan and from Australia. The virus may have originated in bats in one of these countries, hitched a ride in an exported camel, and started spreading in the Middle East. It's an interesting hypothesis that deserves exploration, Lubroth says—but he urges researchers to keep their eyes wide open for other possible culprits as well.

–KAI KUPFERSCHMIDT

SOCIAL SCIENCE

Senator's Demands Freeze NSF Political Science Grants

Officially, the $10-million-a-year political science program at the National Science Foundation (NSF) remains open for business. But in reality the agency has decided not to fund any political science research this year.

NSF officials aren't talking about the reasons for the move. But it appears to reflect an impasse between NSF's desire to preserve its highly regarded peer-review system and the need to abide by language in a government-wide funding bill that restricts NSF's ability to support research in the discipline.

The dilemma was triggered by a short amendment to the 2013 spending bill passed on 20 March by the U.S. Senate. It allows NSF to fund political science research only when a project is deemed vital to national security or the country's economic interests. Senator Tom Coburn (R–OK), who introduced the amendment, says that the goal is "to restrict funding of low-priority political science grants."

NSF officials initially said that they would fold Coburn's new criteria into the agency's existing metrics for judging proposals. But they appear to have abandoned that effort and seem to be searching for another approach. In the meantime, they have suspended further deliberations on a set of proposals that were highly ranked by a panel of outside reviewers who met this spring. NSF has also held up the paperwork on dozens of grant proposals approved for funding much earlier in the year. The agency appears to be trying to avoid what the American Political Science Association has called "an exceptionally dangerous slippery slope … [that] makes all scientific research vulnerable to the whims of political pressure."

The casualties include this year's edition of Duke University's long-running Ralph Bunche Summer Institute for promising minority students considering academic careers in political science. "We were told this winter we had been recommended for renewal and were waiting for the paperwork when Coburn was passed," says Paula McClain, a professor of political science and dean of the graduate school at Duke University in Durham, North Carolina. Then NSF put its $160,000-a-year contribution on hold. "The students would have started in early June, and in late April I finally decided I couldn't keep people hanging on any longer."

David Lewis, a political scientist at Vanderbilt University in Nashville, received a similar green light from NSF in December on his proposal to mine newly available government employment records to track how personnel policies have affected the quality of the federal workforce over the past quarter-century. Lewis's grant would have supported programmers and Web designers to make the enormous database more accessible to researchers.

Coburn rules. NSF has struggled to implement language from Senator Tom Coburn that restricts funding for political science.

Since getting that good news, however, Lewis has been treading water. His repeated queries about the status of his grant have elicited empathetic but vague responses from NSF officials. In the meantime, he's continuing work on a 2011 grant that explores similar questions but without access to the treasure trove of data coughed up by the U.S. Office of Personnel Management after extended negotiations.

Scientists in the most recent cohort of grant applicants whose proposals were deemed worthy of funding by outside reviewers have encoutered similar delays. "I can tell you that proposals submitted last January are still under consideration," NSF program manager Brian Humes wrote in a June letter to the community that *Science* has obtained. "The regular panel met in May. This panel only considered the normal NSF criteria, intellectual merit and broader impacts. We have been working to evaluate their positive recommendations with regards to the new restrictions on the program imposed by the language in the [2013] continuing resolution."

NSF had planned to convene additional panels that would apply Coburn's two criteria. Agency officials would then meld the results of the two sets of panels and make final funding decisions. But that idea, which Myron Gutmann, head of the research directorate that includes political science, described to *Science* in June, appears to have been scrapped. And it's not clear what has replaced it.

In a 2 August statement, Gutmann said only that the social, behavioral, and economic sciences (SBE) directorate "is working diligently under the constraints of the law to accept and review proposals related to political science. SBE intends to make awards under the political science program and will do so with deliberation and foresight to ensure that NSF continues to be a good steward of taxpayer dollars." When asked to explain how that process would work, Gutmann deferred to Deborah Wing, a press spokeswoman, who said "we do not have anything further to say than what was in the [2 August] statement."

Researchers whose well-reviewed proposals are in limbo remain optimistic that they will see the money eventually. They also hope Congress will have a change of heart.

"I have everything crossed," says McClain about her expectations that NSF will help fund next year's summer institute, which she describes as "a 5-week boot camp" for minority students hoping to go into political science. "I'm also hoping that NSF's 2014 budget doesn't contain Coburn, or that senators will realize the damage that it has done and revise the language."

–JEFFREY MERVIS

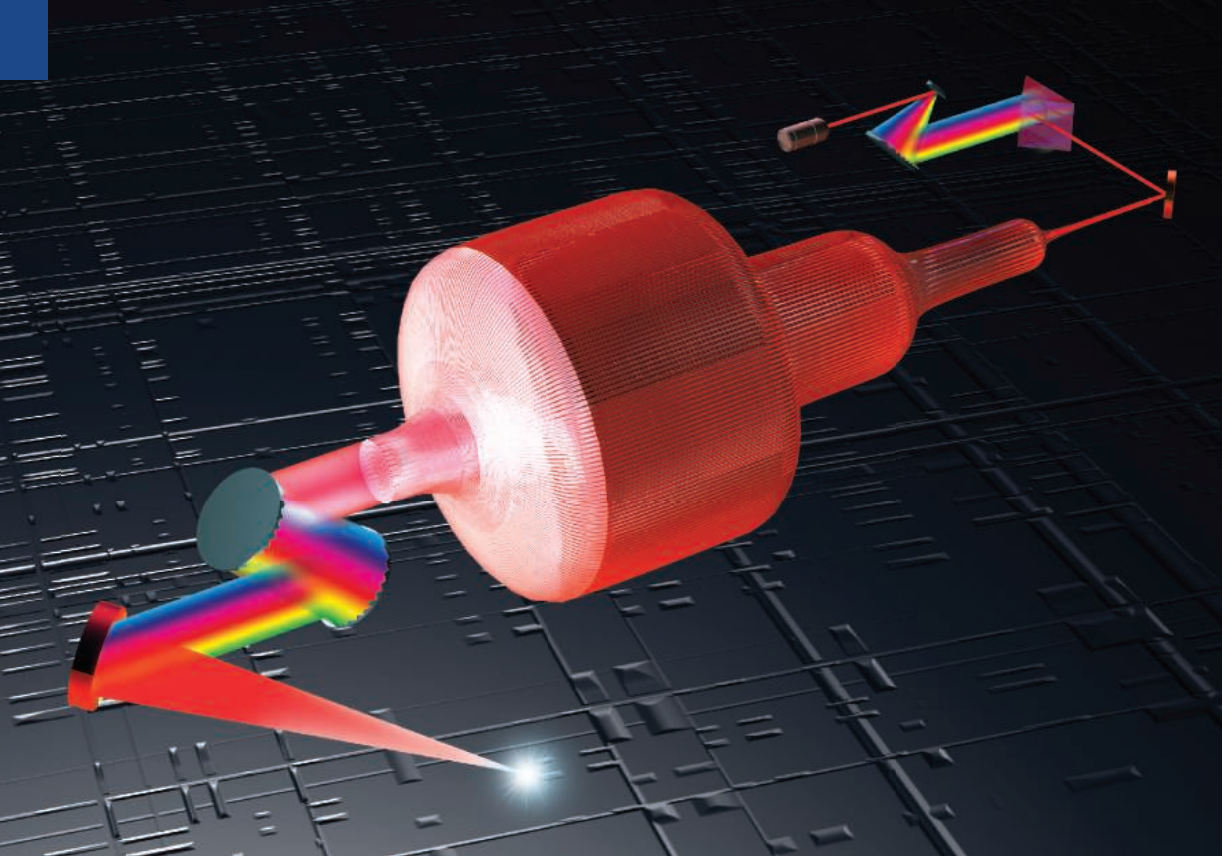

All for one. The ICAN laser would use thousands of fiber lasers to boost power before recombining their beams.

CREDIT: PHIL SAUNDERS/SPACECHANNEL.ORG

PARTICLE PHYSICS

Europe Aims for a Cut-Rate Superlaser To Power Future Particle Accelerators

Could the light at the end of high-energy physics' increasingly long tunnels be … light? The field's appetite for ever more powerful accelerators is running up against society's willingness to pay. The Large Hadron Collider (LHC) at CERN, the European particle physics laboratory near Geneva, Switzerland, with its 27-kilometer circular tunnel and detectors the size of cathedrals, cost close to $10 billion. Next, physicists want to build the 31-kilometer-long International Linear Collider at up to $25 billion, and they are talking about even bigger machines and longer tunnels. Sooner or later, these ambitions will be stymied—unless some new, radically cheaper accelerator technology succeeds. A team of European physicists sees hope in the light of simple fiber-optic lasers.

Researchers have known for decades that laser pulses can accelerate charged particles, but only in the past few years have they produced beams of high enough quality for particle physics. The remaining stumbling block is quantity: Lasers that can produce sufficiently intense pulses at high enough repetition rates with reasonable efficiency just don't exist.

Now, a consortium of European physics labs says that it can meet the necessary spec without building a new superlaser. The trick is to take fiber lasers—a workhorse of the telecommunications industry—and combine their output into a superbeam. In an 18-month pilot project funded by €500,000 from the European Union, the labs coaxed 64 fiber lasers to merge their beams smoothly. If the European Union's next 7-year research budget allows—it is now being finalized—they hope to scale up to a full-size demonstrator with thousands of fibers.

Physicists are reaching the limits not only of national budgets, but also of technology. To search for new physics, they would ultimately like to accelerate leptons, such as electrons and positrons, to energies in excess of 5 trillion electron volts (5 TeV). But doing so with today's technology would consume hundreds of megawatts (MW) of electricity—the entire output of a medium-sized power station. "There is no technology for over-5-TeV lepton colliders," says Roy Aleksan of France's Atomic Energy Commission lab at Saclay. The problem is that the radio-frequency waves now used to accelerate particles don't give them a very big kick, so it takes a lot of microwave cavities in a row to reach high energies. The cavities are also not very efficient at converting wall-plug electricity into beam power.

> *"People said it was crazy."*
>
> —GÉRARD MOUROU
> ÉCOLE POLYTECHNIQUE, PALAISEAU, FRANCE

More than 30 years ago, John Dawson and Toshiki Tajima of the University of California, Los Angeles, proposed a radically different strategy: accelerating particles in a plasma stirred by a laser. A plasma is essentially a gas of charged particles: ions, and electrons stripped from them. If a high-powered pulse of laser light is fired into a plasma, the transverse electric field of the light pushes the featherweight electrons out of the way but barely budges the much heavier ions, leaving in its wake an electron-deficient bubble of positive charge followed by a region of negative charge that forms as electrons rush back in. The result is a powerful electric field parallel to the pulse's direction of travel. This "wakefield" can give a huge boost in speed to electrons, either those from the plasma or bunches of electrons specially injected to take advantage of it.

When Dawson and Tajima proposed this wakefield-acceleration technique, laser pulses could not be made short enough and powerful enough. In the mid-1980s, however, Gérard Mourou and Donna Strickland of the University of Rochester devised chirped pulse amplification (CPA). This takes a moderately powered short laser pulse and stretches it out into a longer, lower-powered one. Passing this elongated pulse through laser amplifiers boosts its energy, and so when it is recompressed to its original length it has greatly increased power. Almost all of the world's highest-power lasers use CPA to produce petawatt (10^{15} watt) pulses.

With such pulses, researchers could produce accelerating wakefields as strong as 10 billion to 100 billion volts per meter (GV/m), three orders of magnitude higher than conventional radiofrequency accel-

eration (10-50 MV/m). But particle physicists didn't take the technique seriously because it produced particle beams of poor quality and low luminosity—too few particles per second.

The skeptics started to sit up and take notice in 2006, however, when researchers at Lawrence Berkeley National Laboratory in California created a high-quality 1-GeV electron beam in a tube of plasma just 3.3 centimeters long. In 2009, the International Committee for Future Accelerators and the International Committee on Ultra-High Intensity Lasers set up a joint task force to investigate how these new laser techniques could help accelerator development. Its report, published in 2011, sketched out a plan for an electron-positron collider with hundreds of laser plasma modules lined up to accelerate particles. The machine would be far smaller than current accelerators—no more than a couple of kilometers long—and potentially much cheaper. Yet it would reach an energy of between 1 and 10 TeV.

> *"They need to develop an accelerator. Then people can say 'This is something we can use.' "*
>
> —ROY ALEKSAN
> CEA SACLAY

But the necessary lasers still don't exist. Although CPA lets researchers create pulses with sufficiently high peak power, such lasers typically fire just once a second, a pace far too slow to generate an intense particle beam. The lasers for a TeV-scale accelerator would need to produce thousands or even millions of pulses per second and, to avoid huge energy costs, would need a high wall-plug efficiency, too. "This is what you have to shoot for overall: high peak power and average power and efficiency," Aleksan says.

The report proposed a long-term R&D program to develop the necessary lasers. But Mourou, now at the École Polytechnique near Paris, had a better idea: use a common and inexpensive tool of the telecommunications industry, the fiber laser—little more than an optical fiber doped with ytterbium. Pumped with light from another source, fiber lasers can produce beams at high repetition rates and with high efficiency. What they lack is the ability to produce ultrashort, high-power pulses.

So Mourou proposed combining the output of many thousands of fiber lasers to create a beam that could drive a TeV accelerator. The system would work by taking short pulses from a seed laser, stretching them out, and then amplifying them in a large number of fiber lasers. The pulses would then be recombined into a single beam and compressed to produce short, high-power pulses. The hitch comes in the penultimate step: recombining the output of thousands of fibers into a single beam. All the beams have to be precisely in phase, otherwise some will destructively interfere with others to reduce the power of the final beam. "People said it was crazy," Mourou says.

Mourou formed the International Coherent Amplification Network (ICAN) in collaboration with colleagues at CERN, the University of Southampton in the United Kingdom, and Germany's Fraunhofer Institute in Jena. After a year and a half of research, they showed that coherent combination could work. In their final demonstration, completed earlier this year, they fed the 64 fiber lasers into an 8-by-8 lattice so that their beams emerged in parallel. Allowing the beams to overlap slightly, the researchers could observe interference patterns between each beam and its four nearest neighbors. A camera recorded the patterns, detecting any differences in phase, and then a feedback loop would go back to the fiber laser in question and tweak its phase back into line in real time.

To monitor and adjust the roughly 30,000 fiber lasers needed for a particle accelerator would be a much more daunting task—one that Mourou likens to the challenge of designing the European Extremely Large Telescope, a 40-meter behemoth in which 6000 actuators will compensate for atmospheric distortion by reshaping a deformable mirror a thousand times a second. But the ICAN demonstration proved the principle.

The ICAN project drew attention from other communities that see the promise of a high-peak-power, fast-pulsing laser. The same technology could provide a low-cost source of electron beams for a type of x-ray light source called a free-electron laser; proton beams for cancer therapy; or medical isotopes. "ICAN heralds a revolution in laser-plasma-based acceleration," says Alexander Pukhov of the Skobeltsyn Institute of Nuclear Physics at Lomonosov Moscow State University.

Even if ICAN's laser scales up successfully, physicists will not build an all-out TeV-scale electron-positron collider anytime soon. But the ICAN team was intrigued by a proposal for a more modest machine: a Higgs factory. Now that researchers at CERN have discovered the Higgs boson, the last missing piece in their standard model, physicists want to make more of them to study their properties. One way of doing that is by colliding high-energy photons called gamma rays. A team at the Fermi National Accelerator Laboratory in Illinois, in collaboration with Mourou and Tajima, has proposed building a conventional accelerator producing two counter-rotating beams of electrons in the tunnel of the retired Tevatron collider at Fermilab. The electron beams—with the relatively low energy of 80 GeV—would be collided with photons from ICAN-style lasers, resulting in back-scattered 63-GeV gamma rays; beams of those photons would then be collided to produce Higgs bosons. The researchers estimate that such a gamma-gamma collider could produce 10,000 Higgs bosons per year, several times the number made by the LHC.

Before any of that can happen, Mourou and his team need to show that they can build a full-scale laser with the required capabilities. If the next E.U. research budget provides the €3 milllion they need, they may be able to show whether their proof-of-principle heralds a bright future for particle physics or is just a flash in the pan. "They need to develop an accelerator," Aleksan says. "Then people can say 'This is something we can use.' " **–DANIEL CLERY**

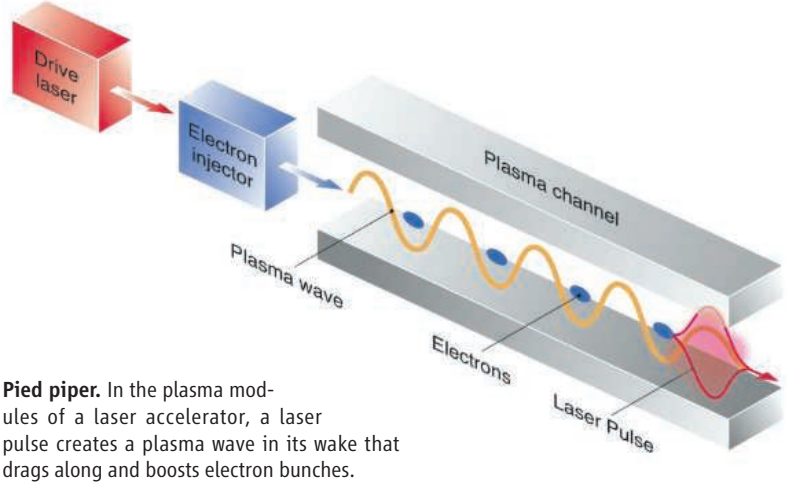

Pied piper. In the plasma modules of a laser accelerator, a laser pulse creates a plasma wave in its wake that drags along and boosts electron bunches.

CREDIT: W. P. LEEMANS AND E. ESAREY, *PHYSICS TODAY* **62**, 44 (2009)

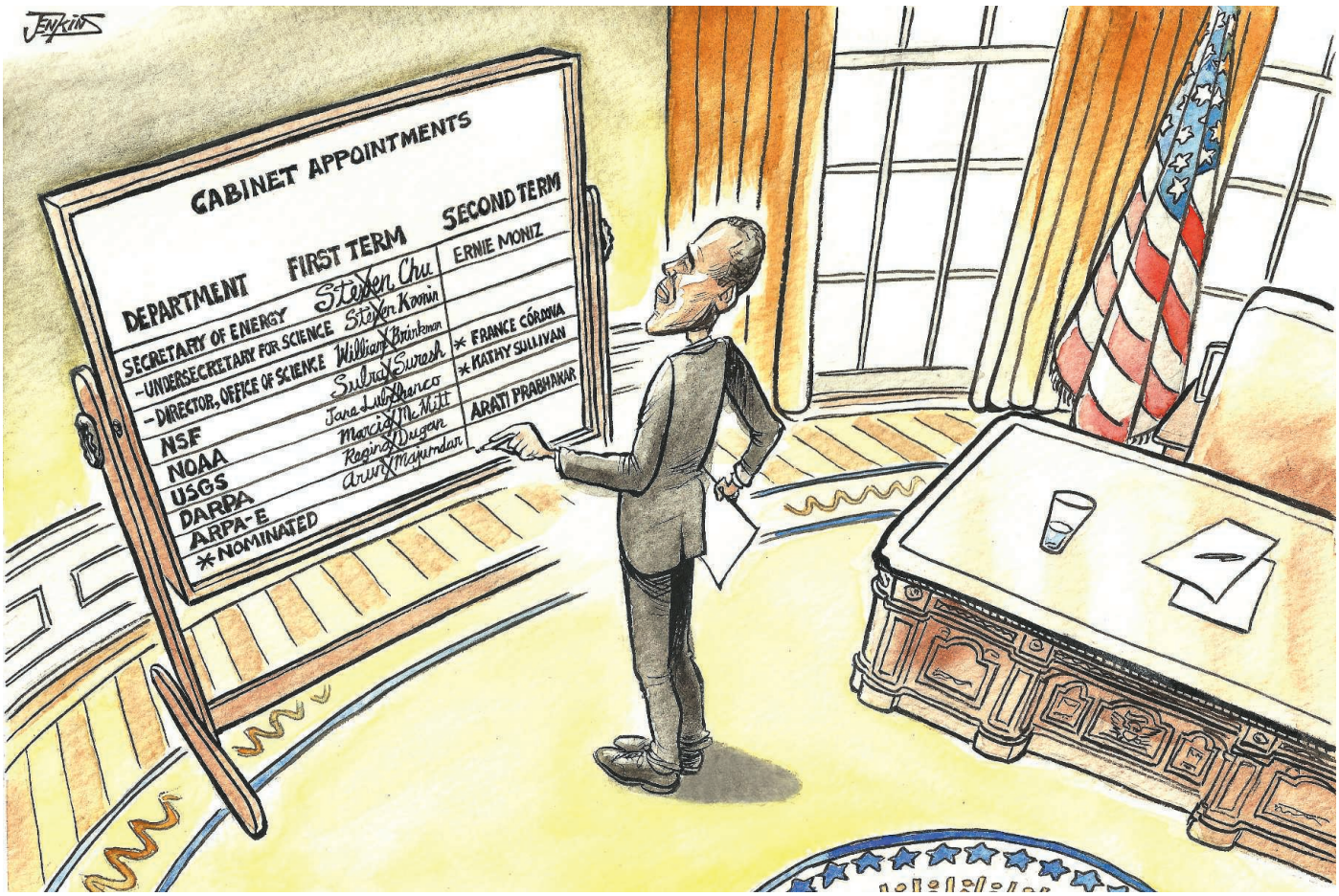

New Team, Old Hands

President Obama is hoping that experienced managers will help him overcome Washington gridlock and leave a legacy of accomplishments in science

Out with the visionary laureates, in with the pragmatic wonks.

That's one intriguing theme emerging from President Barack Obama's recent picks to lead key U.S. science agencies in his second term. That first group, now largely gone, included a slew of Washington outsiders, among them Nobel Prize winners and high-profile academics. They were brought in to shape the administration's research agenda at a time when the White House welcomed fresh ideas and all things seemed possible.

Now, with Washington paralyzed by political gridlock and expectations diminished in a lame-duck presidency, the new corps of leaders possesses a bit less pizzazz but arguably more managerial experience. And many on the new team share a common bond: In the 1990s, they held sometimes obscure but important science policy jobs under President Bill Clinton. Those jobs served as priceless preparation for navigating Washington's convoluted culture.

Researchers who study presidential hiring aren't surprised by the shift. "First-term appointments tend to be more symbolic and ideological, while second term appointments tend to be more technocratic and managerial," says political scientist David Lewis of Vanderbilt University in Nashville. Still, in Obama's case, the contrast can be striking. Here's a look at three new arrivals, and some key posts that are still vacant.

Secretary of Energy: Ernest Moniz for Steven Chu

Chu, a Nobel laureate and director of the Lawrence Berkeley National Laboratory in California, brought scientific star power to the White House's effort to remake the Department of Energy (DOE) into a hotbed of clean power innovation. By the end of his tenure, however, the sparkle had dimmed as a result of repeated clashes with Congress over DOE financing of green energy companies, chronic complaints about cost overruns in the department's nuclear weapons programs, and Chu's often uneasy public persona, which some in Washington interpreted as arrogance.

In contrast, Moniz, a career academic at the Massachusetts Institute of Technology in Cambridge and longtime government adviser, brings a friendly-butcher-at-the-corner-store vibe to the job. That style has played to rave reviews in Congress, with the Senate rapidly and unanimously confirming his appointment in May.

Moniz is at ease in government, observers say. He served 2 years as a senior official in Clinton's science policy shop before moving to a senior position at DOE. Since then, he's been a regular on government and White House advisory panels. "Not many scientists know Washington the way Ernie does," says David Garman, a former senior DOE official.

That familiarity may explain Moniz's move to make DOE man-

ILLUSTRATION: MIKE JENKINS

Published by AAAS

agement reform an initial centerpiece of his tenure. In addition to shaking up DOE's leadership structure, he's discussing ways to streamline its sprawling network of 17 laboratories (*Science*, 12 July, p. 119) and $5 billion Office of Science.

Director, National Science Foundation (NSF): France Córdova for Subra Suresh

Congress spared NSF from the brunt of this year's sequester, and President Obama has asked for a 10.5% increase in 2014. But despite NSF's favored budget status, Córdova will still need the management skills that she developed over the past decade as president of Purdue University and the University of California, Riverside, as well as her knowledge of Washington acquired during 3 years as chief scientist to NASA Administrator Dan Goldin in the first Clinton administration.

Her biggest challenge after being confirmed will be to sustain NSF's bread-and-butter disciplinary research programs without ignoring new opportunities. Her predecessor, Subra Suresh, created the template OneNSF to launch programs that promoted high-risk collaborative research, entrepreneurship, international partnerships, and more family-friendly workplace policies. NSF's 2014 budget request would boost them significantly. But the chair of the Senate Appropriations Committee, Senator Barbara Mikulski (D–MD), has told NSF to tap OneNSF money if Congress, as expected, cannot match the president's overall request for NSF's six research directorates.

Córdova will also need a strategy to advance the White House's plan to reorganize STEM (science, technology, engineering, and mathematics) education. Although Congress has resisted the president's request to make NSF one of three lead agencies and boost overall funding for STEM education, the White House is unlikely to drop the idea. And the perennial challenge of finding room in a tight budget for expensive new scientific infrastructure is also likely to resurface. The National Ecological Observatory Network is still rapidly expanding, and this year NSF got the green light to request money to start building the Large Synoptic Survey Telescope, a wide-angle sky-mapping instrument in Hawaii.

Administrator, National Oceanic and Atmospheric Administration (NOAA): Kathryn Sullivan for Jane Lubchenco

Twenty years ago, after becoming the first American woman to walk in space, Sullivan signed up for a more prosaic job at the National Oceanic and Atmospheric Administration (NOAA). As the agency's chief scientist, "she was a troubleshooter," helping sort out troubled projects, recalls oceanographer James Baker, the NOAA administrator at the time.

Now, as Obama's nominee to replace marine scientist Jane Lubchenco at NOAA's helm, Sullivan will be responsible for completing some of those same projects. Near the top of her list is a $12 billion satellite program, the Joint Polar Satellite System (JPSS), which has struggled through 20 years of cost overruns and reorganizations, threatening to wreck NOAA's $5 billion budget along the way. Sullivan, a geologist, worked on an early version of JPSS as chief scientist and helped implement major reforms since returning to NOAA as a senior leader in 2011. So "she understands the problems that come with big technology," Baker says.

Baker also expects Sullivan's experience running museum and science education programs in Ohio—which occupied her between stints at NOAA—to come in handy as she promotes NOAA's work in everything from building climate models to regulating fisheries. "She's used to explaining why a program is important," he says.

Still to come ...

The White House has yet to announce its picks for a slew of other important science posts. At DOE, open posts include the head of the Office of Science; a new undersecretary position overseeing science and energy programs; and the head of the Advanced Research Projects Agency–Energy, which promotes the commercialization of new technologies. The top job at the U.S. Geological Survey (USGS) is also open, but former director Charles "Chip" Groat says that finding a willing candidate could be tough. As USGS's budgets have stagnated, he says, "it's become a job of managing decline."

–DAVID MALAKOFF AND JEFFREY MERVIS

The Women of the Cosmos Club

Founded in 1878 as a bastion of the powerful in Washington, the Cosmos Club didn't allow women to be members until 1988. But a few years later, a group of local women decided to welcome their newly arrived peers in the Clinton administration with monthly dinners there. As the Obama administration seeks experienced managers (see main story, p. 706), some of the then-newcomers are making a return appearance.

Clinton had appointed a large number of women to several federal research agencies. Many of them "had no social or professional network here," says Florence Haseltine, a scientist emeritus at the National Institutes of Health in Bethesda, Maryland, and founder of the Society for Women's Health Research, who kick-started the meals in 1993. "Dinners were a chance for them to exchange information on how the system works."

The meals triggered discussions on topics that never came up during meeting-filled workdays, says physicist Martha Krebs, who was part of that influx as director of the Office of Science at the Department of Energy (DOE). "At dinner we could talk about how to get things done—the career staff at another agency that your staff needed to deal with, or how to handle interactions with Congress." A glass of wine and some good food also helped the women form bonds that lasted far beyond their tenures in Washington, adds Krebs, who left DOE in 2001 to return to academia and who is now head of research at the University of California, Davis, Energy Institute.

The dinners were once so popular that they almost outgrew the venue. "I can remember a few times we had more than 30 women, and the club liked me to keep it to 12," says Haseltine, who also serves as the group's unofficial secretary. The irony of dining at the Cosmos Club was part of its appeal, Krebs admits. "It was a little bit of 'in your face,' I suppose. And because we could."

Two of the "new faces" in the Obama administration—France Córdova and Kathryn Sullivan—were regulars at those dinners, as was Catherine Woteki, now undersecretary for research at the U.S. Department of Agriculture. Also back in town is the only man who ever attended the dinners: newly confirmed Energy Secretary Ernest Moniz, another Clinton administration veteran. "It was a big, extended group," Córdova recalls fondly. "It was a very good time to be a woman scientist in Washington."

But times change. "It's a different environment now," Córdova says. "There are a lot of women in scientific posts in Washington now, and I'm not sure that [the dinner group] is needed now. I don't think you should do things just to do them."

Haseltine still has a standing reservation at the Cosmos Club for the third Tuesday of the month. Sometimes the only attendees are she and co-founder Mary Clutter, the longtime head of biology at the National Science Foundation who retired in 2005. But she plans to keep the welcome mat out for both newcomers and returnees. "You can see what you're eating, it's got free parking, and the food is better than it used to be," she says.

–J. D. M.

Published by AAAS

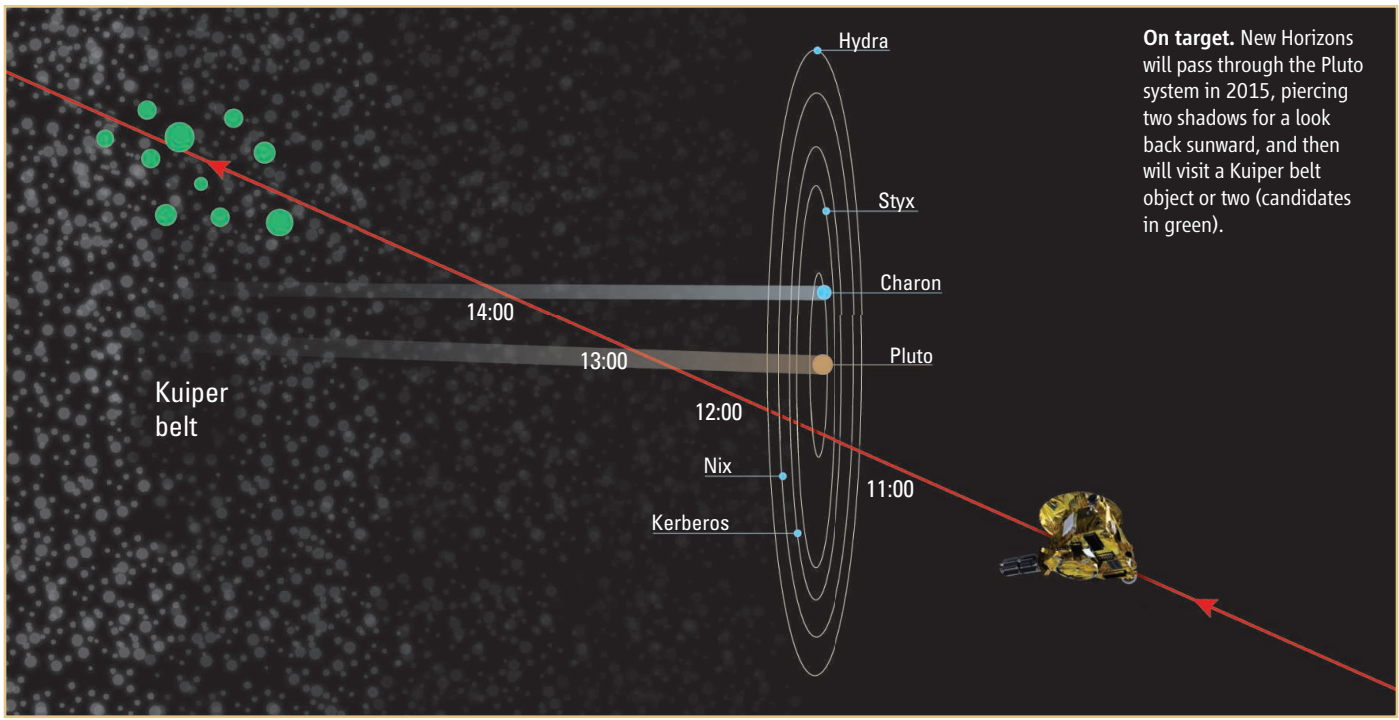

On target. New Horizons will pass through the Pluto system in 2015, piercing two shadows for a look back sunward, and then will visit a Kuiper belt object or two (candidates in green).

CREDIT: (SOURCE AND SPACECRAFT) NASA/JOHNS HOPKINS UNIVERSITY APPLIED PHYSICS LABORATORY/SOUTHWEST RESEARCH INSTITUTE; (ILLUSTRATION) C. SMITH/*SCIENCE*

SOLAR SYSTEM EXPLORATION

Pluto, the Last Planetary First

The New Horizons spacecraft will finally reveal much of Pluto's true nature; scientists are feverishly speculating about what they'll find

LAUREL, MARYLAND—The next planetary first will be our last. After traveling for 10 years and crossing more than 5 billion kilometers, NASA's New Horizons spacecraft will flash by Pluto in a matter of hours, and an age of exploration will be over. Never again will a fuzzy ball of light in astronomers' telescopes crystallize into a new, exquisitely detailed world before everyone's eyes. Pluto aficionados gathered* here last month to anticipate the 14 July 2015 encounter, which Alan Stern, of the Southwest Research Institute (SwRI) in Boulder, Colorado, and principal investigator of the New Horizons mission, called "an epochal milestone in the exploration of the solar system."

It will be epochal because our world knows so little about that world. An ice dwarf planet, Pluto is the archetype of billions of icy bodies that roam the outer solar system, left over from the formation of the "real" planets. The Earth-orbiting Hubble Space Telescope shows it as no more than a smudged disk with an outsized moon, Charon, and four tiny moonlets orbiting the pair. What will flying through that system just 12,500 kilometers above Pluto reveal? Inner fires might still be fueling icy volcanoes, despite surface temperatures just 40° above absolute zero. Or Pluto might disappoint with a surface that has been geologically dead for eons. Or, tragically, a stray fleck of ice might blast New Horizons, ending the mission, as it speeds past Pluto at 49,000 kilometers per hour?

"We can expect the unexpected," said planetary geologist Paul Schenk of the Lunar and Planetary Institute in Houston, Texas, at the meeting. "We are going to be captivated; we are going to be befuddled."

Two faces of Pluto

Speakers bold enough to predict what New Horizons will find on Pluto faced a stark choice: Does Pluto hold geological wonders like those the Voyager 2 probe found in 1989 on Neptune's youthful moon Triton, a close relation of Pluto's? Or will Pluto present an eons-old, crater-pocked face like the one that Voyagers 1 and 2 found on Jupiter's big moon Callisto?

It all depends on how much heat has been generated and retained inside Pluto since it formed. Triton has much in common with Pluto. It is another protoplanetary leftover of similar size and composition to Pluto; Neptune just happened to capture Triton into orbit as a moon. Triton has plenty of internal heat, to judge by images from Voyager 2's flyby, perhaps fueled by lingering stores of heat-generating radioactive elements in its rocky core. Only an internal heat source could have driven icy lavas to the surface over the past few tens of millions of years to form vast smooth plains, which have smothered most impact craters in their path. And heat must have driven the slow churning of solid crustal ice that produced Triton's mottled "cantaloupe" terrains and erased craters as well.

Indeed, Triton appears to be so geologically vigorous that most researchers believe that it probably has an internal ocean of still-liquid water deep beneath an icy outer shell. And where there is liquid water, there could be life.

Callisto, one of the four large moons of Jupiter, is another matter entirely. Not that different in size or composition from Triton, it was never heated much. Scientists are not sure why, but there was not even enough heating to completely separate its rock from its ice to form a rocky core, let alone to reshape its surface. The Voyager spacecraft found a surface with almost every square kilometer scarred by impacts of all sizes, accumulated over billions of years. That doesn't leave geologists with a lot to ponder. And no one is imagining an inner ocean for Callisto.

At the meeting, planetary geologist John Spencer of SwRI stuck his neck out and said

*The Pluto System on the Eve of Exploration by New Horizons, 22–26 July, at the Applied Physics Laboratory.

Published by AAAS

he would be "very surprised" if Pluto were heavily cratered. Because Pluto resembles Triton in size and composition, it, too, could have an internal heat source powerful enough to drive geologic activity, he concluded. "It could be just as wonderful and exotic as Triton's surface," he said.

Planetary geophysicist Francis Nimmo of the University of California, Santa Cruz, predicts disappointment. "I would not be surprised by a totally dead surface" on Pluto, he says. He now thinks the analogy with Triton is flawed. Rather than being heated solely by a stockpile of radioactive elements, he says, Triton is probably also warmed by the rhythmic squeezing of Neptune's gravity. Pluto, with no nearby giant planet, receives no such tidal massaging, Nimmo notes.

The red shift

Even if Pluto is geologically dead, its wisp of an atmosphere most certainly is not. Pluto "is definitely changing color, getting redder," said Marc Buie of SwRI, who has been gleaning what he can from telescopic images of Pluto for more than 30 years. And the color change, which Buie found to occur between 2000 and 2002, almost certainly involves plutonian meteorology of a sort you won't see on The Weather Channel.

On Pluto, the atmosphere—with 1/100,000 the pressure of Earth's—is actually Pluto's crustal "rock" sublimated into a near vacuum. The surface is frozen molecular nitrogen—the stuff we breathe—with traces of methane and carbon monoxide. In recent years, Pluto's northern hemisphere has been gradually turning toward the sun, and the rising warmth of summer may have driven off bright methane or nitrogen frosts deposited during the winter. That would expose underlying nitrogen ice, which is dirtied by dark, reddish gunk that radiation forms from the methane.

New Horizons' cameras, which team with composition-analyzing spectrometers, will reveal details of the distribution of frosts that could help explain the recent reddening. Changing patterns of frosts might also account for the only two surface markings that Buie is sure he can see: an equatorial blotch of material as dark as soot and an adjacent blotch as bright as pure snow.

The cameras may also be able to peer inside Pluto, in a manner of speaking. Precisely gauging the shape of Pluto's gravity field would be the best way to probe the nature of its interior—whether it has a rocky core, for example. New Horizons won't be passing close enough for that, but the cameras will measure the size and shape of Pluto to within a few hundred meters. A precise size will nail down its density, a key indicator of Pluto's overall composition.

A precise shape could also fill in much of Pluto's history of heating and cooling. An oblate Pluto, flattened from pole to pole, could signal that it has retained enough heat to keep water liquid inside it, forming an inner ocean that makes Pluto flexible enough to deform under its own rotation. Or a more extreme oblateness could point to an early ocean that froze top to bottom while Pluto was spinning more rapidly, leaving its mark on the now-rigid dwarf planet.

New Horizon team members are looking forward to measuring not just Pluto's shape, but also its tail. In its origin among the frozen relics of planet formation and its rock-and-ice composition, Pluto is essentially a very big comet. The solar wind of magnetic field and charged particles—mostly protons—streaming from the sun is blowing away about 140 kilograms of Pluto's atmospheric nitrogen each second, presumably into a cometlike tail. But "we absolutely have no idea of what this is going to look like," says space physicist Frances Bagenal of the University of Colorado, Boulder. "That's what's exciting about Pluto."

Out at Pluto—30 times farther from the sun than Earth—the solar wind's enveloping magnetic field is so weak, Bagenal says, that charged nitrogen is far freer to roam. That puts Pluto in a different regime of space physics than ever seen at any comet, a realm two of New Horizons' instruments will explore. "It's an interesting way of tweaking the knobs of physics," she says, impossible to do in any lab.

The danger of dust

A millimeter-size dust speck of ice blasted off a moon of Pluto by an impact could end this scientific harvest. But mission planners are optimistic that the craft will survive the encounter with Pluto.

Astronomers using the Hubble Space Telescope failed to turn up any threatening dust, but they would miss rare but lethal larger particles. Then calculations showed that Charon would quickly sweep up any particles straying into its orbit, so planners chose to send the craft through the Pluto system at Charon's orbit. Project scientist Hal Weaver of the Applied Physics Laboratory here told the meeting that the team now has "a high degree of confidence we'll be safe." He put a number to their confidence: less than 0.3% chance of loss of the mission.

Assuming it survives its trip by Pluto, New Horizons will pass into the heart of the Kuiper belt, the home of many thousands of leftover objects like Pluto and smaller. If funding is renewed, the probe will take distant looks at many of them in the next decade. The team has already found 31 candidates perhaps close enough to the current trajectory that small thruster tweaks would bring New Horizons in for a close encounter with one or two of them.

All in all, the last planetary first is shaping up nicely for Buie. When he picked the planet for his 1984 dissertation, he says, "I knew there was a pretty good chance I'd get a chance to peek in the back of the textbook and see the answers." That chance is coming up.

–RICHARD A. KERR

Two Possible Analogs for Pluto

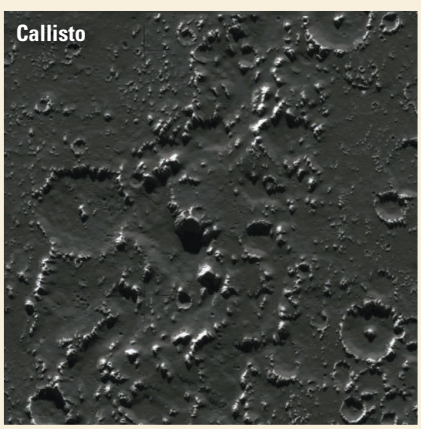

Dead. Pocked by impact craters, Callisto lacks internal heat to drive geologic resurfacing.

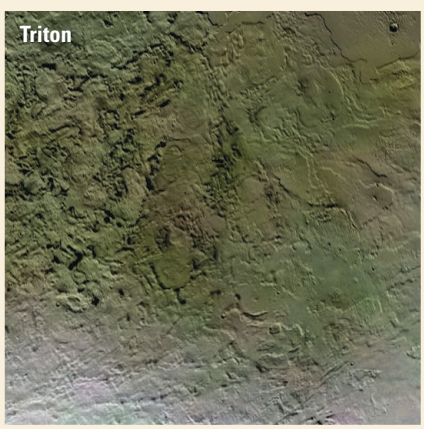

Alive. Resurfaced by icy lavas and churning of its crust, Triton has few impact craters remaining.

CREDITS: PAUL SCHENK/NASA/JPL/LPI (2)

Published by AAAS

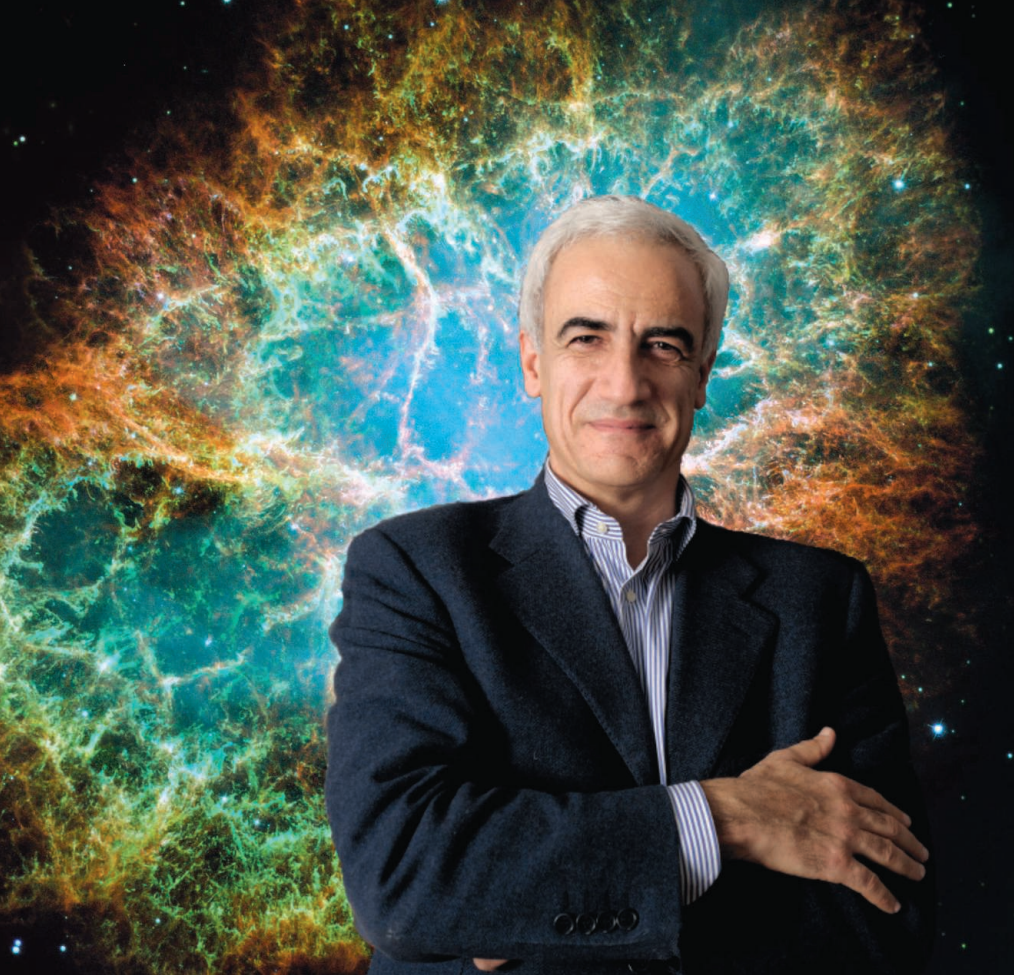

Flare? Where? AGILE PI Tavani in photo composite with the unexpectedly assertive Crab.

ASTRONOMY

The Crab That Roared

The Crab nebula was famous for its rock-steady output of radiation. So when it began spewing gamma rays, at first researchers couldn't believe their instruments

On an October morning in 2007, Marco Tavani took a train from Rome to Bologna to attend a meeting of the scientific team behind AGILE, a gamma ray telescope launched earlier that year by the Italian Space Agency. A researcher at Italy's National Institute for Astrophysics, Tavani had led the AGILE mission since it was conceived in 1997. Now that the observatory was finally in orbit, he and his colleagues were keen to start doing real science. First, however, they had to spend a few months confirming that AGILE was working as planned.

As the train sped toward Bologna, Tavani switched on his laptop and got to work. A trim 57-year-old with silver hair and bushy eyebrows, Tavani has a ready laugh, but his equine face is engraved with deep frown lines. He was frowning as he stared at the slides he'd prepared for the meeting. The irritant was a map of the sky based on observations taken by AGILE in the last week of September, showing three bright gamma ray sources. Each is a rapidly spinning neutron star known as a pulsar: the Vela pulsar, a thousand light-years from Earth; the Geminga, some 500 light-years away; and the Crab, which spins at the center of the iconic Crab nebula, about 6000 light-years away.

For decades, the three pulsars had emitted radiation so steadily that astronomers had come to rely on them as cosmic standards to calibrate their instruments—AGILE included. Geminga, being closer, normally shines brighter than the Crab. But in the AGILE map, the Crab blazed brighter and larger than Geminga. The anomaly raised the troubling prospect of a flaw in the telescope's detectors. Tavani wanted to wish it away.

At the meeting in Bologna, attended by some two dozen researchers, Tavani delivered a technical talk on the satellite. Then he showed the audience the problematic slide. Several scientists expressed surprise. "This is very strange," said Marco Feroci, an astrophysicist at the Institute of Space Astrophysics and Cosmic Physics in Rome. "I have never seen anything like this before." But Tavani had more pressing problems to attend to. "For the moment, we put this week of observations in our drawer," he told the group. "And we do not talk about this to anybody."

Tavani had passed up—for the moment—a chance to make a textbook-changing discovery about one of the most familiar objects in the heavens.

The Crab burst into human awareness in the year 1054, when astrologers in China reported seeing in the constellation Taurus a brilliant star that appeared out of nowhere and then faded away over several months. Centuries later, astronomers recognized the sighting as a massive stellar explosion, a supernova. The blast spread a bright, shiny blob of gas, or nebula, some 11 light-years across space, and in 1968, radio astronomers detected a pulsar at its center.

That pulsar—which sets the entire nebula aglow—formed when the massive star that exploded into the 1054 supernova collapsed into a dense neutron star barely 20 kilometers across, spinning fast and powerfully magnetized. Those magnetic fields cause jets of particles accelerated to nearly the speed of light to shoot out from the star's magnetic poles, generating powerful beams of radiation across different energy bands that sweep Earth 30 times a second. Telescopes see the pulsar as a strobe light flashing with the unwavering precision of a cosmic metronome.

Astrophysicists prize the Crab because it is the only nebula they can trace to its originating event, allowing them to figure out and confirm the physics of how it developed over time. Tavani saw its image in one of his first astronomy textbooks. Later he studied the Crab pulsar along with other neutron stars while working on his doctorate in theoretical astrophysics at Columbia University. In the 1990s, as a postdoctoral researcher, Tavani returned to the Crab nebula yet again in work aimed at understanding how the powerful winds of charged particles gusting from near the pulsar interact with the surrounding gas.

In 1997, he moved back to his native Italy to begin working at the Institute of Space Astrophysics and Cosmic Physics in Milan. The Italian Space Agency had just put out a call for small missions, and Tavani and colleagues immediately started drafting a proposal for an observatory with a gamma ray imager and an x-ray detector on board.

When AGILE was launched, in April 2007, the Crab nebula wasn't on Tavani's list

CREDIT: G. BRUNEAU, M. GIUSTI, NASA HUBBLE

Published by AAAS

of targets to study. It was too familiar and "boring," Tavani says—far less exciting than the exotic new gamma and x-ray sources he expected AGILE to discover.

A year after the Bologna meeting, Carlotta Pittori, a researcher in Tavani's group, met with him to discuss her project: a catalog of the gamma ray sources that AGILE had observed in its first year. There were about four dozen of them. For each, Pittori had calculated the average gamma ray emission observed between July 2007 and June 2008. Scanning the numbers, Tavani's eyes homed in on the value for the Crab. "This cannot be so high," he remarked, noting that Pittori's number was 30% higher than readings NASA's Compton Gamma Ray Observatory had recorded in the 1990s. "See? It's not possible."

The suspect value stemmed from data collected during the anomalous week in September 2007. The pulsar's recorded emissions then had been high enough to skew the average for the entire year. Tavani suggested that the gamma ray detector had temporarily malfunctioned, but Pittori was skeptical. "I would like to publish this table as is, without eliminating anything, with a note saying that this point is under investigation," she said.

"No," Tavani replied. "We have to cut that week out." Scientists would normally frown on such an omission, but Tavani deemed it appropriate for data from a newly launched satellite still in its early phase of observation.

The revised data set brought the emission value back in line with what astronomers were accustomed to seeing from the Crab. Tavani was satisfied. In a concession to Pittori, the paper on the catalog included a sentence stating that the average emission from the Crab had been found to be higher than usual when the researchers merged all the observations from 2007.

The cryptic note went unnoticed when the paper appeared online in *Astronomy & Astrophysics* in September 2009. So did a figure that the authors later realized they had included by mistake. It was an image showing the Crab outshining Geminga—the same slide Tavani had shown his colleagues at the October 2007 meeting in Rome.

In October 2009, Tavani was wracked with anxiety. He'd just got word that AGILE's reaction wheel—the device that helps point a satellite—had failed. Engineers at the Italian Space Agency had tried to restart it, but in vain.

To salvage the mission, Tavani and his colleagues put AGILE into a spin. Every 7 minutes, it made a full rotation, its wide field of view sweeping out a circular band of the sky. The maneuver converted AGILE from a point-and-shoot imager to a sky survey, and by early 2010 the mission was back on track.

To follow the latest observations, the researchers created a website onto which a fresh map of the gamma ray sky, as seen by AGILE, was uploaded every few hours. Tavani got in the habit of accessing it on his iPhone morning, noon, and night.

Shortly before midnight on 20 September 2010, Tavani clicked on the link one last time before going to bed. On the map he saw a bright, yellow spot, right in the position of the Crab nebula. "Who knows what this is?" he said excitedly to his wife, showing her the screen. The Crab was at it again.

The next morning, Tavani hurried to his office at the institute, where a 2-day conference for AGILE team members was about to begin. Before the morning session, he stopped by the office of his graduate student, Edoardo Striani, who was responsible for conducting fast analyses on AGILE data, and asked Striani to take a look at the Crab.

Striani carried his laptop into the conference and settled down in a corner. His attention drifted in and out of the presentations. Analyzing the satellite's observations—downloaded every hour and a half by a receiver in Kenya, then relayed to the AGILE data center—he checked whether the emission from the Crab had been changing over the past few days.

By the afternoon, Striani had confirmed that the emission had been rising. He and Tavani were witnessing a flare. "It immediately occurred to me that we had seen this in 2007," Tavani says. "At that moment, I knew the phenomenon was real."

By the next morning, the Crab's emission had started to go back down, although it was still more than twice as high as normal. After the meeting's morning presentations, Tavani and Striani worked straight through the lunch break, plotting the pulsar's emission. Tavani was scheduled to give a "surprise talk" after lunch. He had planned to discuss a different gamma ray source, but now he had something meatier to present. "We have this phenomenon again," he announced, flashing his freshly made slides. "What do we do now?"

Any postprandial lethargy in the room evaporated instantly. Pittori was jubilant. "Do you remember the note we put in the catalog?" she asked, grinning. It was the day before her birthday.

A few hours later, the researchers put out an astronomical telegram announcing the flare to the broader community. The following day, researchers with NASA's Fermi gamma ray observatory reported that they had seen evidence of the flare in their archived data from the same dates. The teams described the flares in papers in *Science* a few months later (11 February 2011, pp. 736 and 739).

Since 2010, AGILE and Fermi have both seen more flares in the Crab—one or two a year, each lasting a few days. In January, the American Astronomical Society awarded Tavani and the AGILE team its Bruno Rossi Prize "for a significant contribution to High Energy Astrophysics" for the discovery.

What's causing the flares is still a mystery. The data show that the pulsar doesn't emit more energy than usual during the flaring episodes and that it gets brighter only in the gamma ray band of the electromagnetic spectrum, not at optical wavelengths. Tavani and others speculate that the wind of charged particles emanating from near the pulsar could be slamming into the surrounding plasma in a way that destabilizes regions of it. These plasma instabilities could be causing a runaway acceleration of particles that produces the spike in high-energy gamma radiation seen during a flare.

But this explanation and others are still preliminary, says Bruno Coppi, a physicist at the Massachusetts Institute of Technology in Cambridge. "I think it would be unfair to call them theories," he says. Perhaps the solution is lurking in data that's already been collected, waiting to be recognized as such by a receptive mind. **–YUDHIJIT BHATTACHARJEE**

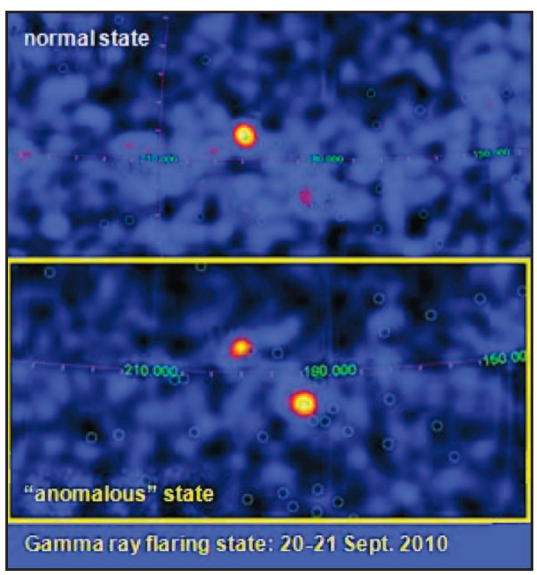

Flash! Normally (*top*) Geminga far outshines the Crab in gamma rays. But in 2010 (*bottom*), the Crab blazed forth.

CREDIT: GERALD BRUNEAU AND MANUELA GIUSTI

Published by AAAS

Assessing pesticide safety 717

Subglacial water flow 721

LETTERS | BOOKS | POLICY FORUM | EDUCATION FORUM | PERSPECTIVES

LETTERS

edited by Jennifer Sills

Develop, Then Intensify

WE APPLAUD THE RECENT EFFORT BY T. GARNETT *ET AL.* ("SUSTAINABLE intensification in agriculture: Premises and policies," Policy Forum, 5 July, p. 33) to place the concept of sustainable intensification into a decision-making context. The authors emphasize that sustainable intensification must be part of a multipronged and context-dependent strategy for food security, which also includes efforts to curb consumption, improve governance, and reduce waste.

However, we question the framing of sustainable intensification as one of several issues to be tackled in parallel. Such parallel framing rests on a fundamental misunderstanding. Food insecurity is most frequently caused by poverty and political and structural problems (*1*, *2*). If a lack of production is not the primary cause of food insecurity, then an increase in production cannot be the primary solution (*3*). Only if issues such as equity, access, and distribution are addressed can increases in production improve food security. Addressing these issues offers other important benefits. For example, improved gender equality and education have been related to reduced population growth, as well as increased food production and food security (*4*, *5*).

Progress. Sustainable development programs in the Democratic Republic of Congo have led to the formation of community farming groups, which now grow enough food for their families and for sales to local markets.

Sustainable development must be the overarching framework, which incorporates food security and also provides criteria for judging whether intensification of agricultural systems is sustainable or not. Sustainable intensification cannot be a meaningful goal without regard for who intensifies, where, and who benefits from the changes. Whereas higher yields are needed in some areas (such as parts of sub-Saharan Africa), the mechanisms by which the hungry are going to benefit from intensification in other locations (such as Eastern Europe) are far less certain.

JAN HANSPACH,[1]* DAVID J. ABSON,[2] JACQUELINE LOOS,[1] MURIEL TICHIT,[3] M. JAHI CHAPPELL,[4] JOERN FISCHER[1]

[1]Institute of Ecology, Leuphana University, Lueneburg, 21335 Lueneburg, Germany. [2]FuturES Research Center, Leuphana University, Lueneburg, 21335 Lueneburg, Germany. [3]INRA, UMR 1048 SADAPT, AgroParisTech, 75235 Paris, France. [4]School of the Environment, Washington State University, Vancouver, WA 98684, USA.

*Corresponding author. Email: hanspach@leuphana.de

References

1. A. Sen, *Poverty and Famines: An Essay on Entitlement and Deprivation* (Oxford Univ. Press, Oxford, 1984).
2. L. Christiaensen, *Rev. Business Econ*. **54**, 345 (2009).
3. O. De Schutter, G. Vanloqueren, *Solutions J*. **2**, 33 (2011).
4. W. Lutz, S. KC, *Science* **333**, 587 (2011).
5. O. De Schutter, "Our secret weapon against hunger: Gender equality and women's empowerment," *Asian Development Network Gender Network E-News* **6**, issue 2 (2012).

Extra Oversight for H7N9 Experiments

THE U.S. DEPARTMENT OF HEALTH AND Human Services (HHS) announces a new review process for certain gain-of-function (GOF) experiments with the avian influenza A (H7N9) virus, some of which were proposed last week by influenza scientists (*1*). Specifically, before being undertaken using funds from the HHS, proposed studies that are reasonably anticipated to generate H7N9 viruses with increased transmissibility between mammals by respiratory droplets will undergo an additional level of review by the HHS.

The HHS review will consider the acceptability of these experiments in light of potential scientific and public-health benefits as well as biosafety and biosecurity risks, and will identify any additional risk-mitigation measures needed. The review will be carried out by a standing, multidisciplinary panel of federal experts with backgrounds in public health, medicine, security, science policy, global health, risk assessment, U.S. law, and ethics. This approach, similar to that for certain H5N1 influenza virus experiments (*2*, *3*), allows the HHS to focus special oversight efforts on experiments of concern while allowing routine characterization and other fundamental research to proceed rapidly, thereby enabling a robust public-health response.

GOF studies can provide important insights into how the A (H7N9) virus adapts to mammalian hosts, causes disease, and spreads to other hosts, but they may also pose biosafety and biosecurity risks. To ensure that research involving H7N9 virus is conducted safely and securely, the U.S. Centers for Disease Control and Prevention recently reexamined the requisite biosafety conditions for conducting experiments involving H7N9 and, in June 2013, issued interim risk assessment and biosafety level recommendations (*4*).

HAROLD JAFFE,[1] AMY P. PATTERSON,[2]* NICOLE LURIE[3]

[1]Centers for Disease Control and Prevention, Atlanta, GA 30329–4018, USA. [2]National Institutes of Health, Bethesda, MD 20852, USA. [3]Department of Health and Human Services, Washington, DC 20201, USA.

*Corresponding author. E-mail: pattersa@od.nih.gov

References

1. R. A. M. Fouchier *et al.*, *Science* **341**, 612 (2013).

2. A. P. Patterson, L. A. Tabak, A. S. Fauci, F. S. Collins, S. Howard, *Science* **339**, 1036 (2013).
3. A Framework for Guiding U.S. Department of Health and Human Services Funding Decisions about Research Proposals with the Potential for Generating Highly Pathogenic Avian Influenza H5N1 Viruses that are Transmissible among Mammals by Respiratory Droplets (https://www.phe.gov/s3/dualuse/Documents/funding-hpai-h5n1.pdf).
4. CDC, Interim Risk Assessment and Biosafety Level Recommendations for Working with Influenza A(H7N9) Viruses (www.cdc.gov/flu/avianflu/h7n9/risk-assessment.htm).

Published online 7 August 2013; 10.1126/science.1244158

The Systematic Place of Morals in Markets

IN THEIR RESEARCH ARTICLE "MORALS AND markets" (10 May, p. 707), A. Falk and N. Szech gave participants a choice between saving the life of a mouse and receiving money. The value of the mouse's life was higher when participants sold it directly to the experimenter than when they bargained over the price with other participants.

For the particular comparison they draw between selling a mouse's life directly and bargaining for it, the findings mark a substantial advance in experimental economics and experimental moral philosophy. We do not believe, however, that the general claim that "markets erode moral values" (p. 710) can be justified by this observation. The real-world examples of "immoral markets" chosen by the authors—slave trade and the sale of indulgences—are extreme cases. It is easy to find counterexamples in which markets lead to moral improvements. For example, as Falk and Szech acknowledge, replacing potentially arbitrarily acting private or state authorities with markets can benefit all affected parties (*1*, *2*) and is a direct moral improvement. More important, free markets can sometimes even create incentives for their participants to morally improve, such as by yielding lower returns to vendors who discriminate against certain groups of customers (*3*, *4*).

The moral consequences of real markets, we think, are mostly determined by the regulatory framework in which those markets are embedded (*5*, *6*). Falk and Szech's conclusions reach too far in that they claim to discuss "the market" without taking into account that different markets, while using the same mechanism of supply and demand, are subject to quite distinct rules.

Finally, Falk and Szech's design, ingenious as it is, is unable to answer the crucial question: Which institutional alternative to markets would cause less moral erosion? Therefore, their critique of the market mechanism does not lead to any constructive policy recommendation.

CHRISTOPH LUETGE[1]* AND HANNES RUSCH[1,2]

[1]TU München, D-80333 Munich, Germany. [2]JLU Giessen, Behavioral and Institutional Economics, D-35394 Giessen, Germany.

*Corresponding author: luetge@tum.de

References
1. W. L. Megginson, J. M. Netter, *J. Econ. Lit.* **39**, 321 (2001).
2. R. A. Posner, *J. Pol. Econ*. **83**, 807 (1974).
3. G. Becker, *The Economics of Discrimination* (Univ. of Chicago Press, Chicago, IL, 1971).
4. O. Ashenfelter, T. Hannan, *Quart. J. Econ*. **101**, 149 (1986).
5. S. Storm, C. W. M. Naastepad, *Industrial Relations* **48**, 629 (2009).
6. M. Olson, *The Logic of Collective Action* (Harvard Univ. Press, Cambridge, MA, 1965).

Response

IN OUR RESEARCH ARTICLE, WE RAN A SERIES of controlled laboratory experiments and report a causal effect of market institutions on moral transgression. Our findings contribute to the literature on the malleability of morality in general and the effects of institutions on moral transgression in particular.

As we argue in our Research Article, we do not aim at questioning market economies per se. Markets often improve social welfare for market participants in efficiently allocating goods (*1*). Competition in markets may also pressure firms to reduce discrimination against certain groups of workers or customers (*2*). Our research interest, however, was not to study effects of markets on active market participants but on third parties—i.e., those who are not directly involved in market trading, and who potentially suffer from trade. Our study shows that market interaction reduces how people value harm and damage done to third parties.

To study how markets affect moral outcomes, we implemented bilateral and multilateral markets, using the double auction institution. This is a well-established and widely used market set-up in economics, which displays the positive properties of allocation mentioned above (*3*). We deliberately abstained from imposing additional regulatory details, to allow for more general conclusions. As is standard in economics, these markets are real, with real participants and real incentives. Thus, we are convinced that the chosen market institution is well suited for the research questions at hand.

We agree that our findings raise the pressing question of how to design policies that mitigate the problem of moral erosion in markets. This, however, requires a thorough understanding of the relevant underlying mechanisms, as we discuss in our Research Article. First, markets generate information about selling and buying behavior and thus provide systematic social information about prevailing norms. Second, because trading involves at least two parties, market interactions allow traders to share guilt associated with immoral outcomes. Third, in markets with many buyers and sellers, the notion of being pivotal is diffused: Traders may apply a "replacement logic" (*4*), telling themselves that if they do not trade, some other trader may. These mechanisms potentially play a crucial role not only in markets but also in many nonmarket contexts. For example, in group decision-making, sharing of guilt and diffusion of pivotality may contribute to moral transgression. In recent work, we used the same mouse paradigm and found causal evidence that the diffusion of pivotality in groups erodes moral behavior compared with individual decision-making (*5*).

We hope that our study laid ground for thinking about moral consequences of market interaction and that it will stimulate research on relevant mechanisms.

ARMIN FALK[1]* AND NORA SZECH[2]*

[1]Center for Economics and Neuroscience, University of Bonn, 53127 Bonn, Germany. [2]Department of Economics, University of Bamberg, 96047 Bamberg, Germany.

*Corresponding author. E-mail: armin.falk@uni-bonn.de (A.F.); nora.szech@uni-bamberg.de (N.S.)

References
1. K. Arrow, *An Extension of the Basic Theorems of Welfare Economics* (Univ. of California Press, Berkeley, CA, 1951).
2. G. Becker, *The Economics of Discrimination* (Univ. of Chicago Press, Chicago, IL, 1971).
3. C. R. Plott, V. L. Smith, Eds., *Handbook of Experimental Economics Results* (Elsevier, Amsterdam, 2008), vol. 1.
4. J. Sobel, *Markets and Other-Regarding Preferences* (Discussion Paper, Economics Department, Univ. of California, San Diego, CA, 2010).
5. A. Falk, N. Szech, *Organizations, Diffused Pivotality, and Immoral Outcomes* (Discussion Paper, Centre for Economic Policy Research, London, 2013).

Letters to the Editor

Letters (~300 words) discuss material published in *Science* in the past 3 months or matters of general interest. Letters are not acknowledged upon receipt. Whether published in full or in part, Letters are subject to editing for clarity and space. Letters submitted, published, or posted elsewhere, in print or online, will be disqualified. To submit a Letter, go to www.submit2science.org.

CORRECTIONS AND CLARIFICATIONS

News Focus: "Insistence on gathering real data confirms low radiation exposures" by D. Normile (10 May, p. 678). The article and the caption for the image on p. 679 incorrectly describe the location of solar-powered radiation monitors and radiation monitors that plug into wall sockets as being Minamisoma. These programs are actually in Soma City. The HTML and PDF versions online have been corrected.

HISTORY OF TECHNOLOGY

Electrifying the Imagination

Thomas J. Misa

Somewhere, surely, Nikola Tesla (1856–1943) is smiling. After all, he's still in the news with visionary technology. The stock price of namesake Tesla Motors (brainchild of Paypal co-founder Elon Musk) has quintupled in 12 months. In July, it replaced Oracle on the NASDAQ 100 index of high-tech heavies. To celebrate, Tesla would have chosen a celebratory dinner at the legendary Delmonico's in New York.

A set piece on "Dinner at Delmonico's" introduces W. Bernard Carlson's carefully researched and thoughtfully written biography. Author also of *Innovation as a Social Process* (*1*), Carlson (University of Virginia) knows the historical terrain. He uses letters, patents, and autobiographical writings to draw a generally sympathetic portrait of Tesla as the most colorful inventor of his generation. Tesla collected around 300 patents worldwide, most notably his landmark alternating-current motor and three-phase alternating current, both of which George Westinghouse deployed to overcome Thomas Edison's direct-current system. While scientists today might use the tesla unit of magnetic flux and the Tesla coil, the public more likely remembers his schemes for communicating with other planets, the giant radio towers, and the much-vaunted "death ray."

Tesla arrived in New York as an immigrant in 1884 and remained something of an outsider his entire life. Born in present-day Croatia to Serbian parents, and with schooling in Slovenia and Austria, he was a walking geography lesson. The delights of an intensely visual and imaginative boyhood were shadowed by his parents' hope that he would enter the Serbian Orthodox priesthood. As with Andrew Carnegie, Tesla grew up in the shadow of a strong-willed mother. Nine months spent in the Croatian mountains on the lam from military recruiters, armed only with "a hunter's outfit and a bundle of books," confirmed his tendencies as a loner.

Before leaving for the New World, Tesla learned firsthand about motors at electrical laboratories in Prague, Budapest, and Paris. An unusual instance of technical creativity took place—if his 1919 autobiography is accurate—in a Budapest city park during 1882. While reciting lines from Goethe's Faust, he experienced a eureka moment: a design for an alternating-current motor "came like a flash of lightning. … The images were wonderfully sharp and clear and had the solidity of metal and stone." The vision profoundly shaped Tesla's career. Across the next six years (supported by two American investors), he worked up a successful alternating-current motor that relied on rotating magnetic fields, lectured to the American Institute of Electrical Engineers, and then sold the patents to Westinghouse for a tidy sum. He briefly went to Pittsburgh to assist Westinghouse's engineers. As soon as he could, however, Tesla returned to New York, where he lived in the fanciest hotels, cultivated the era's newspaper reporters, and raised money from the likes of John Jacob Astor IV and J. Pierpont Morgan.

Tesla
Inventor of the Electrical Age

by W. Bernard Carlson
Princeton University Press, Princeton, NJ, 2013. 516 pp. $29.95, £19.95.
ISBN 9780691057767.

Carlson describes Tesla's innovation strategy as "patent-promote-sell." Usually, he did not build factories, as did the better-funded Edison, Westinghouse, and Thomson. His opportunistic strategy relied on continual doses of promotion and publicity, which *Electrical World*, *Harper's Weekly*, and newspapers were delighted to bestow. Crafting a stage persona as "magician" or "wizard," Tesla gave showy public lectures where he used high-frequency electrical energy (something very much like radio waves) to light up gas-filled tubes, create great crackling jags of lightning, and generally wow the audience.

As Carlson sees it, Tesla careened uneasily between "ideal and illusion." He aimed to go beyond merely workable inventions; he aimed to create an "ideal." In his mind, he ran motors forward and backward, devised efficient turbines, and built frictionless pumps. Eventually he had a compelling vision for moving massive quantities of energy. While Marconi and other radio inventors sent electromagnetic waves "out" from their antennas and used the earth as a convenient ground return, Tesla proposed to do just the opposite. He believed Earth, with its resonant frequency, might be charged up with carefully applied electrical bursts to create a means for sending huge quantities of electricity through and around the world, with radio waves serving as the current's return.

Carlson charitably labels Tesla's promotions as a necessary "illusion" to achieve his innovation strategy, and successes mounted through 1894. But a fire gutted his New York City laboratory in March 1895, leading to a nervous breakdown. After his recovery, it seems, Tesla stepped over the line between genius and crackpot. In 1889, he set up a large radio tower in Colorado Springs to

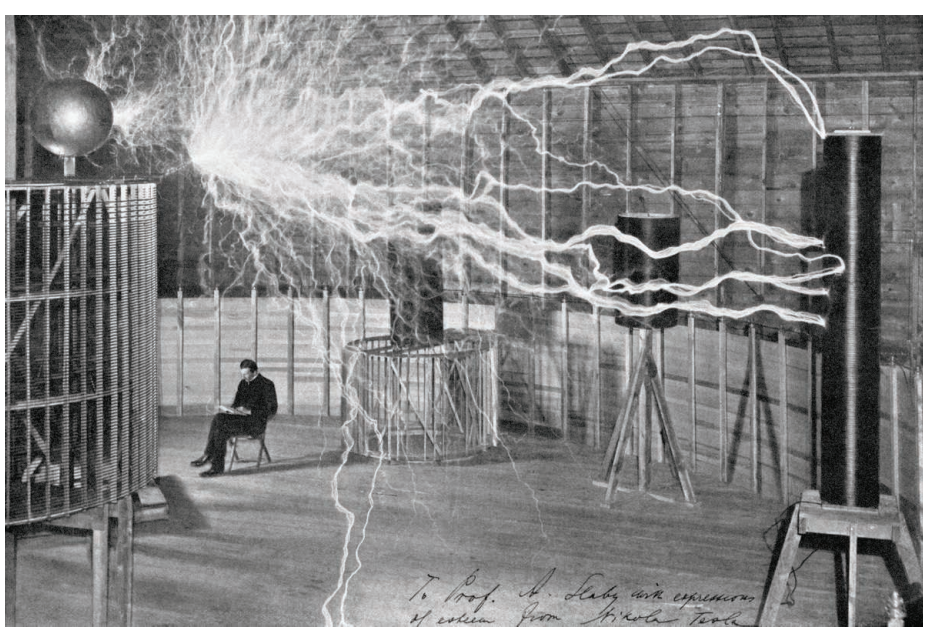

CREDIT: BETTMANN/CORBIS

Trick image. Tesla was photographed before the magnifying transmitter was turned on.

The reviewer is at the Charles Babbage Institute, University of Minnesota, Minneapolis, MN 55455, USA. E-mail: tmisa@umn.edu

"test" his unusual theories, then promptly returned to New York and those useful dinners at Delmonico's with tantalizing stories about communicating with Mars. Flush with $150,000 from J. P. Morgan, he built a laboratory and quarter-size radio tower on Long Island. Not even Morgan would bankroll the immense 600-foot tower that Tesla had planned to "shake the earth." When Earth and the ether refused to behave, Tesla resorted to increasingly outlandish claims, still needing a flow of money to keep the lights on and the laboratory mortgage paid. (He infrequently settled his luxury-hotel bills.) Photographs made for illusions. The famous image of Tesla peacefully reading in his laboratory while surrounded by dangerous bolts of electricity turns out to be a contrived double exposure.

Carlson also admirably surveys the clashes among Edison, Tesla, and Westinghouse covered by Jill Jonnes (*2*). Clearly surpassing earlier accounts (*3*–*5*), his will be the gold standard for Tesla biography.

References

1. W. B. Carlson, *Innovation as a Social Process: Elihu Thomson and the Rise of General Electric* (Cambridge Univ. Press, Cambridge, 1991).
2. J. Jonnes, *Empires of Light: Edison, Tesla, Westinghouse, and the Race to Electrify the World* (Random House, New York, 2003).
3. J. J. O'Neill, *Prodigal Genius: The Life of Nikola Tesla* (Washburn, New York, 1944).
4. M. Cheney, *Tesla, Man Out of Time* (Prentice-Hill, Englewood Cliffs, NJ, 1981).
5. M. Seifer, *Wizard: The Life and Times of Nicola Tesla* (Carol, Secaucus, NJ, 1996).

10.1126/science.1242282

BIOMEDICINE

Burgers, Brains, and Blasphemy

Jessica J. McDonald

Don't eat brains. And don't let animals you find tasty eat brains, either. These are just two of the lessons readers will take away from science writer and former Discovery Channel Canada cohost Jay Ingram's *Fatal Flaws*. The multivalent title alludes not only to the prion proteins themselves—which when misfolded trigger deadly neurodegenerative diseases—but also to the involved researchers and governments, who, like everything else, are sometimes imperfect.

In contrast to several previous general-audience books that center on bovine spongiform encephalopathy (mad cow disease), *Fatal Flaws* tells a broader story of prions. Ingram ranges from the curious cases of kuru in Papua New Guinea to current speculations about the role of prions in other diseases, including Alzheimer's and Parkinson's.

At its height in the late 1950s, kuru struck up to 200 members of the Fore tribe a year, predominantly women and children. Victims curiously lacked any typical signs of infection. The disease would start with poor coordination and always progressed to death. The story of kuru is also the story of an American field physician, Carleton Gajdusek, who by all accounts was brilliant and dedicated ("Indiana Jones with extra empathy")—but also an unabashed pedophile. Gajdusek was awarded the 1976 Nobel Prize in Medicine for showing that he could transmit the disease to chimpanzees by exposing their brains to extracts from human kuru patients.

Focusing on the process of science rather than providing a detailed and comprehensive survey of the field, Ingram argues that Gajdusek's success was largely dependent on contributions from other researchers. Anthropologist Robert Glasse serendipitously connected kuru to the Fore tribe's cannibalism after reading a short article in *Time*, and Bill Hadlow, an observant veterinarian, linked the human disease to sheep scrapie after the timely arrival of a traveling kuru exhibit.

Ingram devotes much of the book to the now 40-year quest to understand the nature of the infectious agents responsible for transmissible spongiform encephalopathies such as kuru, scrapie, and Creutzfeldt-Jakob disease. They were originally presumed to be unusually "slow" and hardy viruses, given long incubation periods, remarkable resistance to sterilization, and size estimates. But repeatedly, experiments suggested that perhaps they were not viruses—and heretical under molecular biology's central dogma, perhaps they had no DNA or RNA at all.

Neurologist Stanley Prusiner staked his career on the bold claim that proteins could be infectious in and of themselves. He named the novel scrapie agents "prions," a slightly disordered neologism combining "protein" and "infectious" (*1*). Initially highly controversial—even in 1997 at the time of Prusiner's Nobel Prize—his idea is now accepted by most researchers, although a few holdouts remain.

The most valuable aspect of Ingram's account is his careful consideration of how such a blasphemous notion played out in the scientific community, including the politics that all too often are elided in favor of casting scientists as entirely rational automatons. By focusing on the battle as waged in the journals, he infuses the tale with a humanity that captures how science actually works, including the power of language to alter the direction of research.

For an author so clearly taken with the importance of language, this account lacks the vital voices of the scientists themselves, beyond their scientific publications. In the early chapters, Ingram liberally quotes from Gajdusek's letters and field notes—including his 1957 observation (disputed by some) that the Fore were "still spearing each other as of a few days ago, and only a few weeks ago cooking and feeding the children the body of a kuru case." Such snippets capture what it was like for the young doctor to trek into the wild tropics in an attempt to understand the mysterious affliction. Yet when Ingram deals with the conceptual understanding of prions in the mid-1980s, and the research and controversy that followed, equivalent voices are missing. That is no doubt due in part to Prusiner's unwillingness to talk to the press (which extended to Ingram), but the absence deprives the story of the human elements stressed elsewhere.

Fatal Flaws
How a Misfolded Protein Baffled Scientists and Changed the Way We Look at the Brain

by Jay Ingram
Yale University Press, New Haven, CT, 2013. 292 pp. $30, £20. ISBN 9780300189896.

Even more disappointing, the discussions of prions and their connection to the (generally considered) nontransmissible neurodegenerative diseases prove fairly superficial. The chapters dedicated to Parkinson's, amyotrophic lateral sclerosis, and chronic traumatic encephalopathy run only four to five pages and fail to provide much beyond sketches of our current understandings of each disease. Nevertheless, like prions themselves, the story told in *Fatal Flaws* is quite infectious.

References

1. S. B. Prusiner, *Science* **216**, 136–144 (1982).

10.1126/science.1241317

The reviewer, a 2012 AAAS Mass Media Fellow, is at the Department of Immunobiology, Yale University School of Medicine, New Haven, CT 06520, USA. E-mail: jessica.mcdonald@yale.edu

GLOBAL FOOD SUPPLY

Reevaluate Pesticides for Food Security and Safety

Generic pesticides, vital in the developing world, present assessment challenges.

Philippe J. P. Verger[1]* and Alan R. Boobis[2]

With global population projected to increase above 9 billion by 2050, food security—the availability of food and one's access to it—is increasingly important (*1*). Crop-protection products can help reduce yield losses caused by pests, pathogens, and weeds, to help feed the world's population sustainably. Given potential harm for human health and the environment, regulation of pesticide use in agriculture has been controversial.

Although most pesticides are developed and patented by large multinational companies, ~30% of total sales are by producers of generic versions (*2*). For these chemicals, the initial name-brand producer is often no longer interested in commercialization or in investing resources to generate updated toxicological data critical for sponsoring international health impact assessments (see below). But cheaper, generic compounds are necessary for developing countries to increase their food production, feed their population, and trade internationally.

Without a committed sponsor of assessments for generics, sufficient data may not be available to update their safety assessment. Thus, ~30% of pesticides marketed in developing countries, with an estimated annual market value of U.S. $900 million, may not meet internationally accepted criteria for safe pesticide residues in the food supply (*3*). They could pose unacceptable dietary risk to human health, with repercussions for food security, safety, and trade that could disproportionately affect developing countries (*1*). We discuss an approach to address this.

International Scientific Risk Assessment

The *Codex Alimentarius* Commission (CAC) of the United Nations' Joint Food and Agricultural Organization–World Health Organization (FAO-WHO) Food Standards Programme is recognized by the World Trade Organization (WTO) as the normative body to produce international science-based standards (e.g., for food hygiene), guidelines (e.g., for safety assessment of food derived from biotechnology), and codes of practice (e.g., for fish and fishery products) that are used in case of trade disputes involving sanitary or phytosanitary considerations (*5*). *Codex* involves 185 member countries (99% of the world's population). *Codex* standards protect public health in developing countries that lack infrastructure for proper national evaluation of hazards in food. These standards are also important in facilitating market access and ensuring fair practices in trade—indirectly contributing to development and reducing poverty.

The maximum residue limit (MRL) is the maximum pesticide residue in a specific crop grown with recognized good agricultural practices (GAP) that is expected not to cause harm to human health from dietary consumption. The *Codex* establishes MRLs for pesticides based on scientific risk assessment by the Joint FAO-WHO Meeting on Pesticide Residues (JMPR), a group of independent scientific experts. Countries can use MRLs to develop national regulations.

Compounds already evaluated in the *Codex* process are to be reviewed at least every 15 years. For compounds prioritized by the *Codex* Committee on Pesticide Residues (CCPR), at the request of member countries, an up-to-date toxicological dossier—and crop residue data corresponding to proposed GAP—should be submitted to JMPR by the sponsor, generally the company holding the patent.

JMPR uses the most relevant science available (*5*) but is constrained by the information provided. In general, such data are generated to support the establishment of MRLs and other regulatory decisions by national or regional authorities, such as the U.S. Environmental Protection Agency (EPA), Health Canada, European Food Safety Authority (EFSA), and the Ministry of Health, Labor, and Welfare in Japan.

The information provided should cover oral disposition, including metabolic fate; acute, chronic, and subchronic toxicity; carcinogenicity; reproductive and developmental toxicity; and genotoxicity. Information should be sufficient to assess neurotoxic and immunotoxic potential. This information is used to establish acceptable daily intake (ADI), an estimate of the amount of pesticide residue that can be ingested daily over a lifetime without appreciable health risk.

Where possible, JMPR has paid increasing attention to potential acute effects of pesticide residues. Guidance on the establishment of an acute reference dose (ARfD) was published (*6*). JMPR uses information on mode and mechanism of action for toxic effects to determine human relevance, interpret the dose-response relation, and identify inter- and intraspecies safety and uncertainty factors (*7*, *8*).

CREDIT: ECO IMAGES/GETTYIMAGES

Potential Outcomes for Generic Pesticides

For old compounds no longer supported by their initial producer, a decision needs to be made on whether to prioritize them for dietary risk assessment or to withdraw the previously established MRLs. Removal of MRLs renders crops with residues of the pesticide in question subject to enforcement actions. A procedural solution is needed to replace the compound's original sponsor when their assessment is requested by member countries.

As manufacturers change from the original patent holder to generics companies, the technical specifications of the substance may change—for example, impurity profiles or isomeric composition. The specification

[1]World Health Organization, Geneva 1211 Switzerland. [2]Imperial College London, London W12 0NN, UK.

*Corresponding author. E-mail: vergerp@who.int

Published by AAAS

of the active substance in current use must be provided for JMPR to assess toxicity.

Ideally, JMPR should have access to original, quality-assured reports containing all summary and individual animal toxicity test data. This will not always be possible. Where secondary sources, containing only summary information, are used, these must contain sufficient information to enable study findings to be reconstructed, with adequate information on the response at all dose levels for all key end points. Secondary sources might be reviews by other authoritative bodies, such as EPA or EFSA, or previous assessments by JMPR or WHO's International Programme on Chemical Safety.

As with all substances, whether fully supported by the original commercial sponsor or not, a full search of the peer-reviewed literature will be undertaken. For some compounds no longer supported by the original sponsor, greater reliance will need to be placed on such publications. JMPR will weigh these publications, as with any study report, for their quality and design.

JMPR is not a regulatory body, so it does not prescribe mandatory data requirements. Hence, minor data gaps may be tolerable. JMPR will use its best judgment as to whether gaps are of such a concern that it would not be appropriate to confirm or establish an ADI and/or an ARfD. Where data gaps prohibit confirming or establishing an ADI and/or ARfD, JMPR will provide guidance information that would be useful for further evaluation of the compound. Depending on need, the necessary studies may be commissioned by a member country, manufacturer, research organization, or other party.

Areas where outcomes are likely to differ, depending on whether a comprehensive data package is provided by the original sponsor, include the following:

Establishment of an ARfD. Due to differences in study design, earlier studies may place less emphasis on nonpathological effects than modern studies.

Information on mode of action, the intermediate biochemical and pathological processes leading to an adverse effect. Substances no longer supported by the original sponsor are less likely to have follow-up information on mode of action for cancer or noncancer end points. When irrelevant modes of action are not ignored, risk assessments could become more conservative.

In the absence of mode-of-action information, it is less likely that it will be possible to use chemical-specific considerations in the choice of safety and uncertainty factors. The default judgment is that, on average, humans may be 10 times as sensitive as experimental animals, on a per-body weight basis, and that some human subpopulations may be 10 times as sensitive as the average (*5*). The two factors of 10 can be subdivided into subfactors for differences in how the substance enters and is processed by the body (toxicokinetics) and in toxicological response to the substance (toxicodynamics). Information on intermediate processes underlying mode of action may support substance-specific modification, which would not be possible without knowledge of the mode of action (*5*).

Toxicity of metabolites. Where metabolites formed in plants or livestock contribute to the residue that is consumed, JMPR will seek assurance that there is sufficient information to assess toxicity. It may be that sufficient information is formed in laboratory species that it would have been covered in assessment of the toxicity of the pesticide itself. If specific to treated plants or livestock, additional information on toxicity would normally be required unless structural similarity was sufficient to rely on the toxicity profile of the pesticide itself.

Recent JMPR assessment of dicofol and fenvalerate illustrates these issues. Neither compound was supported by original sponsors, but JMPR was provided with sufficient information to establish ADIs and ARfDs. The original dicofol manufacturer provided original reports of toxicological studies to the sponsoring government, India, where dicofol is used to control mites on tea. The EPA was authorized to permit access to reports of toxicological studies from the original fenvalerate manufacturer. In no case was it necessary to use a safety and uncertainty factor >100 (in 2005, a safety factor of 500 was used with ethoxyquin owing to inadequate information). For both compounds, the ARfD was based on acute effects observed after a single dose. Information provided on the likely mode of action of fenvalerate for microgranulomatous lesions observed in lymph nodes and other tissues provided reassurance that these were of low biological significance to humans (*9*).

Proposals to Update Procedures

In 2013, the CCPR updated one of its fundamental documents dealing with risk analysis principles and the roles of JMPR, CCPR, and CAC to account for new needs of member countries (*10*). Member countries agreed that when the company owning a pesticide's patent is no longer interested in commercialization, a member country may submit to JMPR a dossier that need not necessarily contain raw data generated by the original sponsor. This will allow trade of food containing residues from these compounds, which should be an incentive for generating data for safety assessment and ultimately to discourage use of pesticides not (re)evaluated.

Member countries also agreed that all compounds listed for reevaluation after 15 years could remain on this list for up to 10 years, during which time a member country would need to express interest in supporting the compound. This time frame seems more realistic to allow generation of adequate data without support of the original sponsor. In the absence of member country interest, MRLs should be automatically deleted and the compounds no longer used in food for international trade. Where there is interest in continued availability, a member country should propose that CCPR prioritize the compound for reevaluation and provide the JMPR with adequate data for its evaluation.

The *Codex Alimentarius* process of developing international MRLs, started 50 years ago, is essential but insufficient. Ensuring that pesticides are used properly so as not to violate MRLs requires proper licensing of pesticides, clear instructions on their use, pesticide application education and training, and enforcement of pesticide regulations.

References and Notes

1. FAO, *Feeding the World in 2050.* World Agricultural Summit on Food Security, 16 to 18 November, 2009 (FAO, Rome, 2009); ftp://ftp.fao.org/docrep/fao/meeting/018/k6021e.pdf
2. Phillips McDougall AgriService, *Industry Overview: 2009 Market* (Vineyard Business Centre, Saughland Pathhead Midlothian, 2010).
3. J. Popp *et al.*, *Agron. Sustain. Dev.* **33**, 243 (2013).
4. WTO, *The WTO Agreement on the Application of Sanitary and Phytosanitary Measures* (WTO, Geneva, 1994); www.wto.org/english/tratop_e/sps_e/spsagr_e.htm.
5. World Health Organization, *Environmental Health Criteria 240: Principles and Methods for the Risk Assessment of Chemicals in Food* (WHO, Geneva, 2009); www.who.int/foodsafety/chem/principles/en/index1.html.
6. R. Solecki *et al., Food Chem. Toxicol.* **43**, 1569 (2005).
7. A. R. Boobis *et al.*, *Crit. Rev. Toxicol.* **36**, 781 (2006).
8. A. R. Boobis *et al.*, *Crit. Rev. Toxicol.* **38**, 87 (2008).
9. FAO, Report of the Joint Meeting of the FAO Panel of Experts on Pesticide Residues in Food and the Environment and WHO Core Assessment Group (FAO, Rome, 2013); www.fao.org/fileadmin/templates/agphome/documents/Pests_Pesticides/JMPR/Report12/JMPR_2012_Report.pdf.
10. CCPR, Report of the 45th Committee Meeting, Beijing, 6 to 13 May 2013; ftp://ftp.fao.org/codex/meetings/CCPR/CCPR45.

Acknowledgments: A.R.B. is a paid consultant for Sumitomo Chemical and Endura Fine Chemicals.

10.1126/science.1241572

SOCIAL SCIENCE

A U.K. View on the U.S. Attack on Social Sciences

U.S. politicians should refrain from a self-defeating critique of the world's leading social science community.

Paul Boyle[1,2]

Social science is under attack in the United States. The National Science Foundation (NSF) is prohibited from funding political science, except for grants identified by its director as "promoting national security or the economic interests of the United States." The High Quality Research Act is being drafted with the aim of guarding against "questionable projects" at NSF. A bill was proposed that would exclude health economics research at the National Institutes of Health (NIH). Such developments provide cause for concern.

First, this represents political interference in the delivery of science. It is unreasonable for scientists to be oblivious to the political reality of budget constraints and responsibility to the taxpayer, particularly in periods of austerity. However, there are good reasons why, in most of the world, decisions about science funding are left to the experts. In the United Kingdom, the "Haldane Principle" espouses the idea that once the overall science budget is set by the government, researchers should decide where specific research project funds are spent, so that funding decisions are autonomous.

Second, even if we agreed that politicians should influence whether specific grant applications are supported, they will rarely have the expertise to make such decisions. Expert peer reviewers are best placed to judge whether proposed research is novel, methodologically rigorous, and likely to succeed. Should politicians without a scientific background judge social science research, based on little more than grant titles and brief descriptions?

Third, this attitude fails to recognize the value in the breadth of scientific endeavor. Politicians' negative comparisons of the value of social science relative to medical science are ironic, because 40% of premature deaths can be explained by behavioral choices. Americans, including those with high incomes, get sicker sooner than their equivalents in other wealthy nations, not because of the quality of care but because of lifestyle factors (*1*). Indeed, many of the world's most pressing problems require input from social scientists. People's attitudes, beliefs, and behaviors underpin so many issues that to question the need for social science research is short-sighted.

Fourth, the value of social science is recognized by experts outside the social science community, including academics in other disciplines (*2*), business leaders (*3*), and those influencing government. The value of social science is understood in U.K. political circles, including in the incumbent coalition government. First, the Economic and Social Research Council (ESRC) received a funding deal in the most recent 2010 Comprehensive Spending Review in line with the other six U.K. research councils. Second, the Behavioral Insights Team in the Prime Minister's office is evidence of support for social science at the very heart of government (*4*). Third, ESRC and a number of government departments are jointly funding a series of "What Works" centers to synthesize evidence from social research on topics such as local economic growth, policing, early-life interventions, and aging, in part to better shape government policy (*5*). Fourth, the Parliamentary Office of Science and Technology (POST)—the Parliament's in-house source of independent advice on policy issues related to science and technology—has recently expanded to include social science. Fifth, there are ongoing discussions about appointing a chief social scientist to assist the government's chief scientific adviser.

Government also recognizes that, while academics need to strive to share insights from their research, it is unrealistic to assume that all studies will have immediate, anticipated impacts. Some research impacts are unforeseen. Measuring impact is challenging in all scientific disciplines, and some studies will not, and should not, have any impact at all. If every project succeeded, scientists would not be pushing the boundaries far enough into riskier or more innovative ideas which, if successful have the ability to transform our ways of thinking.

Social science advice is similarly valued by many in U.S. political circles, but politicians from across the spectrum need to be convinced of its value. Undermining this research community can be done very quickly, and reversing the effects may take a long time. Equally, researchers need to engage in an ongoing and dedicated mission to legitimize the value of social science in the United States, so that their work is not taken for granted. At ESRC, we can have an extensive list of social science research that has delivered significant social and economic impact [e.g., (*6*)], and American social scientists and funding agencies will be able to identify similar impressive impacts from their work. The United States has benefited enormously from social science research in the past. Politicians would be wise to acknowledge this and refrain from a self-defeating critique of the world's leading social science community.

...there are good reasons why, in most of the world, decisions about science funding are left to the experts.

[1]U.K. Economic and Social Research Council (ESRC), Swindon SN21UJ, UK. [2]Science Europe, Brussels B–1040 Belgium.

E-mail: ESRC.CEO@esrc.ac.uk

References and Notes

1. National Research Council and Institute of Medicine, *U.S. Health in International Perspective: Shorter Lives, Poorer Health* (National Academies Press, Washington, DC, 2013).
2. J. Calvert, P. Martin, *EMBO Rep.* **10**, 201 (2009).
3. R. Mann, Impact of Social Sciences Blog, "Five Minutes with Neil Carberry, CBI" (30 November 2012); http://blogs.lse.ac.uk/impactofsocialsciences/2012/11/30/five-mins-neil-carberry-cbi.
4. H. M. Government, Cabinet Office, "Applying Behavioural Insights to Reduce Fraud, Error and Debt" (2012); www.gov.uk/government/uploads/system/uploads/attachment_data/file/60539/BIT_FraudErrorDebt_accessible.pdf.
5. H. M. Government, Cabinet Office, "What Works: Evidence Centres for Social Policy" (2013); www.gov.uk/government/uploads/system/uploads/attachment_data/file/136227/What_Works_publication.pdf.
6. Economic and Social Research Council, "ESRC Celebrating Impact Prize" (2013); www.esrc.ac.uk/news-and-events/events/celebrating-impact-prize/index.aspx.

10.1126/science.1242563

MOLECULAR BIOLOGY

Long Noncoding RNAs Xist in Three Dimensions

The three-dimensional organization of the mammalian genome spatially guides the binding of an RNA to loci for silencing gene expression.

Andrew Dimond and Peter Fraser

RNA has traditionally been viewed as the genomic "messenger" molecule, carrying the coding information from DNA to make proteins. However, an abundance of short and long noncoding RNAs also exist, many of which are likely to have regulatory roles. Little is known about the mechanisms of action of long noncoding RNAs, but many appear to act as "guides" that recruit protein regulatory complexes to specific genomic loci to control gene expression (*1*). Where these long noncoding RNAs contact the genome, and how they locate these regulatory targets, have been open questions. On page 767 of this issue, Engreitz *et al*. (*2*) show that the mouse long noncoding RNA called X-inactive specific transcript (Xist) is initially targeted to specific loci across the X chromosome using a targeting mechanism that exploits three-dimensional chromosome topology.

The Xist RNA orchestrates dosage compensation in female mammalian cells. Because female mammals have two X chromosomes, inactivating one of them prevents the expression of twice as many X-chromosome genes as in males, which possess only one X chromosome. In X-inactivation, Xist is synthesized (17 kilobases in length) from the X chromosome that will ultimately become inactivated. It recruits the polycomb repressive complex 2 (PRC2) to switch off gene expression from one X chromosome in each female cell (*3*). Eventually, Xist appears to encapsulate the entire inactive X chromosome in a "cloud" (as seen by microscopy), forming a silencing compartment. The few genes that escape silencing are seen looping out of the condensed core (*4*). By developing and applying a technique to map RNA interaction sites in the genome, Engreitz *et al*. describe these images at a genomic level. Consistent with microscopic observations, the authors found that Xist interaction sites are distributed broadly across the X chromosome in mouse fibroblasts, whereas "escape" genes showed reduced association with Xist.

However, the most interesting questions relate to how Xist establishes this pattern of binding during the initiation of X-chromosome inactivation. To investigate these early events, Engreitz *et al*. used an inducible system in mouse embryonic stem cells that allowed them to activate Xist expression and map Xist interaction sites at defined time points. They observed that Xist does not spread uniformly outwards along the chromosome sequence, but rather appears to preferentially "jump" from its site of transcription to certain early binding sites.

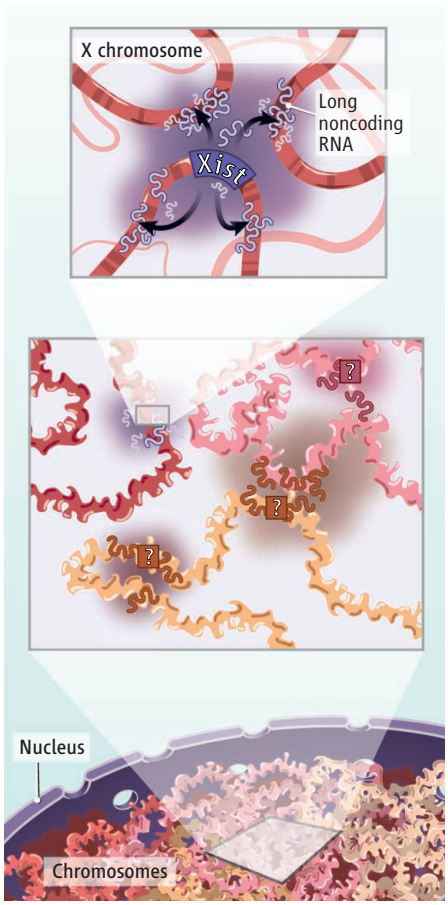

Organizing silence. The Xist long noncoding RNA binds to sites in close spatial proximity on the X chromosome. A mechanism based on the three-dimensional genome architecture could be a general strategy for targeting long noncoding RNAs.

One mechanism to explain how Xist could target specific distal loci would be the presence of high-affinity binding sites at these locations. Intriguingly, Engreitz *et al*. could not identify any genomic feature to explain the pattern of Xist early binding. Instead, the authors considered the three-dimensional organization of the genome by using published data from "Hi-C" (*5*), a high-throughput "chromosome conformation capture" technology that allows identification of DNA sequences in close proximity to each other within the nucleus. The authors discovered that the early binding sites for Xist correspond to loci that are spatially close to the Xist transcription site. This suggested that Xist might find its targets by binding sequences nearby in space, rather than those that are close along the linear sequence. Importantly, the authors tested their hypothesis by expressing Xist from a different position on the X chromosome and found a new pattern of Xist early binding sites that corresponded to sites in close spatial proximity to the new location.

From these early binding sites, Engreitz *et al*. show that Xist requires its A-repeats to spread across and silence active genes. The A-repeats are required for PRC2 recruitment (*6*) and for repositioning active genes into the Xist silencing compartment (*4*). A model is thus proposed whereby the three-dimensional chromosome conformation is exploited to extrude Xist onto its early binding site targets where it then helps to modify and reorganize the X-chromosome architecture.

Several key questions remain regarding the secondary spreading of Xist and control mechanisms to prevent inappropriate spreading across genes that escape inactivation or from transferring to other chromosomes. Engreitz *et al*. found sharp transitions of Xist binding surrounding escape genes, which may relate to previous work implicating CCCTC-binding factor (CTCF) in blocking Xist spreading (*7*). In addition to transcription, CTCF controls chromatin architecture by binding together strands of DNA and forming chromatin loops. CTCF binding sites that are adjacent to escape genes may play a role in segregating these regions from Xist binding. Preventing spread to other chromosomes requires the nuclear matrix protein heterogeneous nuclear ribonucleoprotein U (hnRNP U) (*8*), which may facilitate transfer of Xist from the transcription site to contacting regions. Although hnRNP U is located throughout the nucleus, differences in con-

Nuclear Dynamics Programme, The Babraham Institute, Cambridge, UK. E-mail: peter.fraser@babraham.ac.uk

Published by AAAS

tact frequency between cis-linked loci and interchromosomal interactions may inhibit Xist from establishing a foothold on other chromosomes. The biggest gaps still to fill are details that explain how Xist eventually encompasses the entire chromosome. Does Xist spread from early sites into adjacent sites by diffusion or transfer across a fairly static chromosome structure, or do chromosome dynamics allow other binding sites to iteratively contact and collect RNA from the Xist locus to eventually produce the broad distribution seen in all cells? Conformational studies at later time points of X-inactivation or live-cell studies could potentially provide a timeline to fill these gaps in RNA and chromatin dynamics.

Other long noncoding RNAs (*9*–*11*) have been described that exert their regulatory effects by exploiting the three-dimensional folding of the genome. The similarities with Xist suggest that this may be a general targeting mechanism (see the figure). It will be interesting to see if other, trans-acting noncoding RNAs (both long and short) also exploit three-dimensional genome organization to target loci on other chromosomes (*12*, *13*). With tools to map RNA binding sites and describe genome conformation now at hand, answers to these questions are within reach.

References

1. V. A. Moran, R. J. Perera, A. M. Khalil, *Nucleic Acids Res.* **40**, 6391 (2012).
2. J. M. Engreitz *et al*., *Science* **341**, 1237973 (2013); 10.1126/science.1237973.
3. J. T. Lee, *Nat. Rev. Mol. Cell Biol.* **12**, 815 (2011).
4. J. Chaumeil, P. Le Baccon, A. Wutz, E. Heard, *Genes Dev.* **20**, 2223 (2006).
5. J. R. Dixon *et al*., *Nature* **485**, 376 (2012).
6. J. Zhao, B. K. Sun, J. A. Erwin, J.-J. Song, J. T. Lee, *Science* **322**, 750 (2008).
7. G. N. Filippova *et al., Dev. Cell* **8**, 31 (2005).
8. Y. Hasegawa *et al*., *Dev. Cell* **19**, 469 (2010).
9. K. C. Wang *et al*., *Nature* **472**, 120 (2011).
10. P. G. Maass *et al*., *J. Clin. Invest.* **122**, 3990 (2012).
11. F. Lai *et al*., *Nature* **494**, 497 (2013).
12. J. L. Rinn *et al*., *Cell* **129**, 1311 (2007).
13. M. Guttman *et al*., *Nature* **477**, 295 (2011).

10.1126/science.1243257

GEOPHYSICS

Gauging Greenland's Subglacial Water

Subglacial water flow regimes differ between the interior and the margins of the Greenland Ice Sheet.

Martin Lüthi

The supply, storage, and flow of water under an ice sheet are crucial for its overall dynamics. The density difference between ice and water limits subglacial water pressure to the pressure from overlying ice. Near this limit, the ice gradually becomes decoupled from the base (see the figure), water-filled cavities form, and sediments become weakened. The velocity of ice moving over the bedrock increases due to reduced friction and faster sediment deformation. Subglacial water pressure is therefore the key parameter that controls basal motion, ice flux, and the future evolution of an ice sheet. On page 777 of this issue (*1*), Meierbachtol *et al*. present a detailed record of water pressure variability under one region of the Greenland ice sheet.

Glacier hydrology has been investigated in great detail on mountain glaciers, providing insights into their drainage over the course of the melt season (*2*–*5*). However, similar measurements have been mostly missing on the ice sheets. Only very recently, dye-tracing experiments provided information on the evolution of the hydraulic properties of subglacial drainage (*6*, *7*) and their link to surface velocity variations (*8*). The reason for the sparse observational data are the difficulty of investigating an extended karst-like system that can change its characteristics within days and that is drained by big, violent, and sediment-laden rivers. Some of the biggest such rivers are invisible as they emerge from the ice sheet at great depth in deeply incised fjords filled with icebergs. Directly exploring the under-ice environment is a difficult endeavor because of thick ice, rapidly freezing boreholes, and ice flow that can stretch and rip instrumentation cables.

CREDIT: MARTIN LÜTHI

Freshly exposed, glacially carved bedrock. Sediment-covered areas and solid bedrock form the base of the Greenland ice sheet. Scratch marks from rocks dragged along this freshly exposed bedrock in West Greenland illustrate the sliding motion of ice over its base. Meierbachtol *et al*. provide insights into the mechanisms of water flow, which controls sliding motion.

Meierbachtol *et al*. explore subglacial conditions on a transect from the Greenland ice sheet's margin to its interior, sampling water pressure at several drill sites. Their main finding is the different characteristics of subglacial water drainage between marginal and inland areas of the ice sheet. Whereas boreholes close to the ice sheet margin showed large diurnal variations of water pressure, the inland sites showed persistent high water pressure with small fluctuations. Their interpretation is that an efficient system of high-capacity channels exists under the marginal parts of

Laboratory of Hydraulics, Hydrology and Glaciology (VAW), ETH Zürich, 8093 Zürich, Switzerland. E-mail: luethi@vaw.baug.ethz.ch

the ice sheet, but that the interior is drained by a network of linked cavities.

With the help of a numerical model, the authors conclude that the growth of efficient subglacial channels is limited by the surface geometry of the ice sheet. The ice sheet margins usually exhibit steep surface slopes reminiscent of mountain glaciers, but the ice sheet interior is very flat, with a small hydraulic gradient driving water flow. In other words, little potential energy is available to enlarge water pathways by melting, while creep closure of channels by ice flow is faster than in the thinner marginal areas. Both effects preclude the development of an efficient channelized system, and water flux might be constrained to a system of linked cavities at high pressure.

These results suggest that current research of subglacial processes may be too narrowly focused on the efficient drainage system that evacuates surface water. Such channelized systems, by their very nature, occupy only a small fraction of the total area. Basal hydrology often differs considerably between neighboring boreholes, and many holes show little water pressure variation. Water pressure is often not even recorded in such boreholes, or the data are discarded because of their seemingly random variations, but they might hold important information on the conditions in large parts of the under-ice environment. Moreover, drill sites are usually restricted to areas lacking crevasses for practical and security reasons. Nothing is known about processes under the crevassed zones, which are subject to an extensional flow regime, in contrast to the compressional regime at topographic lows. The focus of past investigations on fast pressure variations in easily accessible areas might skew our perception of the system under investigation.

Basal motion is a distributed process that is controlled by water pressure and conditions everywhere on the ice sheet's bed and that is undoubtedly controlled by water drainage to the ice sheet base (*8*). But it is far from obvious how water pressure variations in a spatially confined area influence the behavior of the whole system. Lacking detailed information on bed geometry and sediment properties, one might reasonably consider the boundary zone between ice and bedrock as a self-organized critical system with interacting entities that exchange water depending on pressure gradients and evolving state variables (*3*–*5*), and tightly coupled with a spring-block model of stress transfer through the surrounding ice (*9*).

Considering the under-ice environment as a self-organized critical system explains why widely different conditions are simultaneously encountered in neighboring boreholes. To obtain a meaningful sample of variations in basal conditions requires a large number of holes spread over a representative area of the ice sheet, at distances of less than one ice thickness. Such an effort is larger than any of today's small research groups can handle. Drilling and instrumenting hundreds of holes simultaneously would require a concentrated and coordinated effort.

Even after decades of theoretical and experimental progress, we are just starting to understand the variety and interrelation of processes active in the inaccessible subglacial environment. In situ observations such as those presented by Meierbachtol *et al*. (*1*) and others (*6*, *7*) are urgently needed to develop, test, and quantify predictive theories of subglacial processes. Only by understanding the dynamics at the base of the ice sheets will it be possible to predict their future evolution under a changing climate.

References

1. T. Meierbachtol, J. Harper, N. Humphrey, *Science* **341**, 777 (2013).
2. G. C. K. Clarke, *Annu. Rev. Earth Planet. Sci.* **33**, 247 (2005).
3. C. Schoof, *Nature* **468**, 803 (2010).
4. C. Schoof, I. J. Hewitt, M. A. Werder, *J. Fluid Mech.* **702**, 126 (2012).
5. I. J. Hewitt, C. Schoof, M. A. Werder, *J. Fluid Mech.* **702**, 157 (2012).
6. T. Cowton *et al*., *J. Geophys. Res.* **118**, 29 (2013).
7. D. M. Chandler *et al*., *Nat. Geosci.* **6**, 195 (2013).
8. I. Bartholomew *et al*., *J. Geophys. Res.* **117**, F03002 (2012).
9. J. Faillettaz, M. Funk, D. Sornette, *Nat. Hazards Earth Syst. Sci.* **12**, 2977 (2012).

10.1126/science.1242672

EPIDEMIOLOGY

Paths from Pesticides to Parkinson's

Freya Kamel

High-quality studies of specific chemical pesticides are needed to determine the relationship between exposure and risk of Parkinson's disease.

Interest in the relationship between exposure to pesticides and the risk of neurodegenerative diseases including Alzheimer's disease, amyotrophic lateral sclerosis, and Parkinson's disease (PD) is long-standing (*1*). PD, in particular, has been the subject of much debate in this context (*2*). Its symptoms typically occur later in life (at age 60 or older), with the destruction of neurons manifesting most obviously as loss of motor function. Decades of epidemiological studies have suggested that pesticide exposure is connected to the development of PD. Yet there is still much that is not clear about this relationship. The disorder likely has multiple contributing genetic and environmental factors, but how exposure to a particular chemical leads to neuronal loss and the symptoms of PD is not known. A recent meta-analysis indeed shows that epidemiologic data generally support an association between pesticides and the risk of PD (*3*). But what is needed is detailed information on the nature of exposure—which pesticides, at what dose, and for how long—to help design policies and practices that prevent the relevant exposures. Also needed is information on the cellular and molecular mechanisms that, over time, lead from pesticide exposure to neurodegeneration and ultimately to PD. Although many questions still linger, some recent studies appear to be advancing the field.

It is well known that some pesticides are toxic to humans after acute exposure to a very high amount (poisoning). However, the effects of chronic, low-dose exposure to this diverse group of chemicals are not so clear. An analysis of over 100 epidemiologic studies establishes that pesticide exposure (in the absence of poisoning) is indeed linked to PD (*3*). PD risk increased with exposure to any pesticide (1.8-fold), to herbicides (1.3-fold), or to insecticides (1.5-fold). Risk associated with exposure to any pesticide (1.6-fold) and to herbicides (1.4-fold) was elevated in high-quality studies—those with adequate size, minimal potential for bias, and good information on PD diagnosis and pesticide exposure. Although its general conclusions are not surprising, the study highlights why such a wealth of data has limited impact. Heterogeneity of study quality and lack of detailed exposure information prevent results from being definitive.

Epidemiology Branch, National Institute of Environmental Health Sciences, P.O. Box 12233, Research Triangle Park, NC 27709, USA. E-mail: kamel@niehs.nih.gov

Perhaps one of the most important unanswered questions is which pesticides are associated with PD. Of several specific pesticides or chemical classes of pesticides evaluated in the meta-analysis, only the herbicide paraquat was significantly associated with PD (2.2-fold increase in risk for ever having used the chemical). Paraquat, used to kill weeds and desiccate foliage before harvesting crops such as cotton, is one of the most widely used herbicides in the world. Thirty years ago, recreational drug users rapidly developed parkinsonism after acute exposure to a contaminant whose active agent,1-methyl-4-phenylpyridinium (MPP+), has a chemical structure similar to that of paraquat (*2*). Epidemiological data collected since then have been considered insufficient to establish a role for paraquat in PD. Recent studies, however, have provided stronger support. Notably, risk was increased not only for farmers and pesticide applicators (*4*, *5*), but also for individuals working or living near sites where paraquat was used (*6*). Among farmers, those who had used paraquat for less than 8 days had smaller increases in risk (2.4-fold) than those who had used it for more time (3.6-fold) (*5*). The compound rotenone is also of interest because like MPP+, it disrupts mitochondrial energy production. Rotenone, which is used as an insecticide and as a piscicide (toxic to fish), is less well studied than paraquat, but a recent study of farmers suggests that it too may be associated with PD (*5*).

Exposure. Epidemiological studies suggest that pesticide exposure may increase risk of Parkinson's disease.

The strong evidence from these epidemiological studies of paraquat and rotenone is particularly important because animal models have shown that chronic, low-dose exposure of adult animals to either pesticide results in many features of PD (*7*). Long-term exposure of adult mice to a low dose of rotenone was also found to replicate the gastrointestinal dysfunction found in PD, a nonmotor feature of the disease (*8*). Further, experimental studies using these pesticides and cultured cells are providing great insights into the cellular processes involved in PD, including mitochondrial dysfunction, oxidative stress, and inflammation (*9*, *10*). These processes are affected by genetic variants found in familial PD and also play a role in sporadic PD (*9*). Paraquat increases oxidative stress whereas rotenone causes mitochondrial dysfunction, but the processes are interrelated and both pesticides ultimately affect both mechanisms (*1*, *9*).

Other specific pesticides with more recent and stronger evidence of association include organochlorine insecticides. A large study of French farmers found that these pesticides as a group are associated with PD (*11*). Although for most pesticides the amounts found in blood or urine reflect only current exposures, organochlorine insecticides are an exception, with half-lives of years. Two studies that measured the amounts of organochlorines in serum determined that dieldrin (*12*) and beta-hexachlorocyclohexane (*13*) were elevated in PD patients. This corroborates an earlier observation that the amounts of dieldrin and gamma-hexachlorocyclohexane (lindane) were increased in the brains of PD patients (*14*). Notably, dieldrin and lindane increase oxidative stress and inflammation, cellular processes involved in PD pathogenesis (*1*, *10*).

While there is good progress in examining the effects of individual pesticides, they are frequently used in combination, and the effects of mixtures need to be evaluated. Exposure to multiple pesticides may increase the risk of PD more than exposure to any one alone. For example, paraquat increased risk only 1.3-fold, but paraquat with either of the fungicides maneb or ziram increased risk up to threefold (*6*). Head injury increases risk of PD, probably by increasing inflammation. By itself, head injury increased risk twofold, whereas head injury together with paraquat exposure increased risk threefold (*15*). Smoking, by contrast, is inversely associated with PD, and effects of dieldrin were evident only in nonsmokers (*12*). These studies are intriguing, but each combination of risk factors has been evaluated in only a few studies, and replication is crucial.

Genetic susceptibility may also modify effects of pesticides on the risk of PD. Studies of gene variants related to pesticide metabolism and transport, to mitochondrial dysfunction and oxidative stress, and to familial forms of PD suggest that associations of pesticides with PD are stronger in genetically susceptible individuals (*7*). Again, most studies have assessed effects of pesticides as a group; studies of genetic susceptibility will prove most fruitful when they focus on specific pesticides.

As for other neurodegenerative diseases, recent work is also expanding our understanding of the role of pesticides. Two high-quality prospective studies—one in France and one of an agricultural community in the United States—found that chronic, low-dose exposure to any type of pesticide increased the risk of cognitive impairment, Alzheimer's disease, and other forms of dementia that arise later in life (*16*, *17*). In a meta-analysis of nine epidemiologic studies, exposure to any type of pesticide increased the risk of amyotrophic lateral sclerosis nearly twofold (*18*), and a prospective study of U.S. farmers found that organochlorine insecticides were associated with amyotrophic lateral sclerosis (*18*). These results must now be confirmed, and as with PD, more details are needed regarding the effects of specific compounds.

The recent epidemiological studies provide much needed advances in clarifying the pesticide-PD relationship. That cellular processes important to PD are affected by specific pesticides underscores the importance of the epidemiologic findings. The most pressing need is for high-quality studies with data that are sufficiently detailed to identify essential aspects of exposure. What is the important life stage and time frame for exposure? Is it duration or intensity of exposure that is important—or both? Does exposure affect the progression of PD as well as risk? Above all, information on specific pesticides is imperative, not only to create a basis for prevention but also to provide clues for experimental mechanistic studies that may suggest therapeutic strategies.

References and Notes

1. S. Mostafalou, M. Abdollahi, *Toxicol. Appl. Pharmacol.* **268**, 157 (2013).
2. K. Wirdefeldt, H. O. Adami, P. Cole, D. Trichopoulos, J. Mandel, *Eur. J. Epidemiol.* **26** (suppl. 1), S1 (2011).
3. G. Pezzoli, E. Cereda, *Neurology* **80**, 2035 (2013).
4. C. M. Tanner *et al.*, *Arch. Neurol.* **66**, 1106 (2009).
5. C. M. Tanner *et al.*, *Environ. Health Perspect.* **119**, 866 (2011).
6. A. Wang *et al.*, *Eur. J. Epidemiol.* **26**, 547 (2011).
7. J. R. Cannon, J. T. Greenamyre, *Neurobiol. Dis.* **57**, 38 (2013).
8. R. E. Drolet *et al.*, *Neurobiol. Dis.* **36**, 96 (2009).
9. D. T. Dexter, P. Jenner, *Free Radic. Biol. Med.* **62**, 132 (2013).
10. T. Taetzsch, M. L. Block, *J. Biochem. Mol. Toxicol.* **27**, 137 (2013).
11. A. Elbaz *et al.*, *Ann. Neurol.* **66**, 494 (2009).
12. M. G. Weisskopf *et al.*, *Neurology* **74**, 1055 (2010).
13. J. R. Richardson *et al.*, *Arch. Neurol.* **66**, 870 (2009).
14. F. M. Corrigan, C. L. Wienburg, R. F. Shore, S. E. Daniel, D. Mann, *J. Toxicol. Environ. Health* **59**, 229 (2000).
15. P. C. Lee *et al.*, *Neurology* **79**, 2061 (2012).
16. I. Baldi *et al.*, *Neuroepidemiology* **22**, 305 (2003).
17. K. M. Hayden *et al.*, *Neurology* **74**, 1524 (2010).
18. F. Kamel *et al.*, *Neurotoxicology* **33**, 457 (2012).

Acknowledgments: This work was supported by the intramural research program of the National Institutes of Health, National Institute of Environmental Health Sciences.

10.1126/science.1243619

GEOPHYSICS

Earthquake Risk in Turkey

Recent efforts are helping to increase earthquake preparedness in a region of high earthquake risk.

Mustafa Erdik

Turkey has been the site of devastating earthquakes. Two massive earthquakes in Antioch (today Antakya) in CE 115 and 526 reportedly claimed more than 500,000 lives. Since 1900, ~90,000 people have lost their lives in 76 earthquakes, with a total affected population of ~7 million and direct losses of ~25 billion U.S. dollars (USD). About half the lives lost were due to two earthquakes associated with the North Anatolian Fault in 1939 and 1999 (*1*). The resulting losses place Turkey in the top 20% of all countries exposed to earthquake hazard with regard to mortality and economic losses (*2*). Recent efforts are helping to increase Turkey's earthquake preparedness.

Turkey lies on the great Alpine belt that extends from the Atlantic Ocean to the Himalaya Mountains. This belt was formed during the Tertiary Period when the Arabian, African, and Indian continental plates began to collide with the Eurasian Plate. Today, the African Plate continues to converge with the Eurasian Plate, while the Anatolian Plate moves toward the west and southwest along strike-slip faults. The North Anatolian Fault Zone forms the present-day plate boundary of Eurasia near the Black Sea coast, and the East Anatolian Fault Zone forms part of the boundary of the North Arabian Plate in the southeast (see the figure).

The North Anatolian Fault Zone, a close analog of the San Andreas Fault in California, saw a remarkable level of earthquake activity between 1939 and 1999. During this time, seven large westward-migrating earthquakes created a 900-km-long continuous surface rupture along the fault zone from Erzincan to the Marmara Sea, stopping just short of Istanbul. Earthquake records spanning two millennia indicate that, on average, at least one medium intensity [Io = VII to VIII, (*3*)] earthquake has affected Istanbul in every 50 years. The average return period for high intensity (Io = VIII to IX) events has been 300 years. The last two major earthquakes that affected Istanbul were in 1509 and 1766.

Based on a time-dependent model that includes coseismic and postseismic effects of the 1999 Kocaeli earthquake with moment magnitude (M_w) = 7.4, Parsons (*4*) concluded that the probability of an earthquake with $M_w > 7$ in the Sea of Marmara near Istanbul is 35% to 70% in the next 30 years. This high probability is shared by Tokyo and San Francisco; however, the earthquake fragility of the pre-2000 building stock in Turkey is much higher than that of California or Japan.

Istanbul has a population of about 13,000,000 and houses about 1,000,000 buildings. According to a 2011 study, an earthquake with $M_w = 7.25$ on the Main Marmara Fault is expected to heavily damage or destroy 2 to 4% of buildings, with 9 to 15% of the buildings receiving medium damage and 20 to 34% of buildings damaged lightly (*5*). Between 400,000 and 800,000 housing units would become inhabitable. From 0.2 to 0.4% of Istanbul's inhabitants are expected to lose their lives or be seriously injured, and ~130,000 people may need hospitalization. The direct economic losses due to building damage are estimated as ~11 billion USD, with total economic losses of 40 billion USD. Similar building damage results for Istanbul have been obtained in (*6*, *7*). However, an unsubstantiated extrapolation of the damage from the 1999 Düzce earthquake suggests much higher extensive and complete damage levels, reaching 40% of the building stock in Istanbul (*8*).

After the losses suffered during the two major earthquakes that struck Turkey in 1999, there has been broad recognition of the need for extensive earthquake preparedness and response planning on the basis of detailed earthquake risk analysis across the country. Particular emphasis has been given to Istanbul. Istanbul houses about one-sixth of the total population and one-half of the industrial potential of Turkey. Several risk-assessment studies have provided information on the expected earthquake losses in Istanbul and led to the preparation of a comprehensive "Earthquake Masterplan for Istanbul" (*9*), which has been promoted as an example for other cities (*10*). The Masterplan assessed the seismic vulnerability of the existing building stock in Istanbul and identified the technical, social, administrative, legal, and financial measures needed to implement such methods. Further,

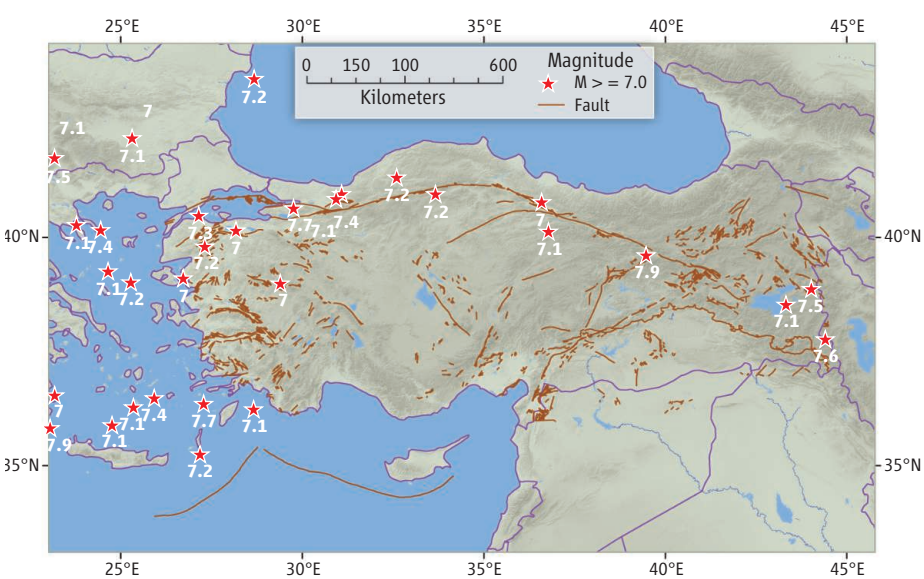

Main faults and major earthquakes in and around Turkey. Since 1900, 33 earthquakes with $M_w \geq 7$ have struck this region. Data for earthquakes from the Kandilli Observatory and Earthquake Research Institute; data for faults from the General Directorate of Mineral Research and Exploration.

Department of Earthquake Engineering, Kandilli Observatory and Earthquake Engineering Research Institute, Bogazici University, 34684 Cengelkoy, Istanbul, Turkey. E-mail: erdik@boun.edu.tr

Published by AAAS

it provided a strategy for sustained progress in a range of areas, including seismic assessment and rehabilitation of existing buildings, urban planning, education, and risk and disaster management.

Earthquake risk management measures are now being implemented in Istanbul and in other cities in Turkey, including a 20-year, 400 billion USD urban renewal program that foresees the demolition and rebuilding of about seven million fragile housing units, most of them residential. It is to be hoped that when the next earthquake strikes at or near one of the major cities in Turkey, these measures will reduce the numbers of lives lost.

References and Notes

1. The International Disaster Database, www.emdat.be.
2. M. Dilley, R. S. Chen, U. Deichmann, A. L. Lerner-Lam, M. Arnold, *Natural Disaster Hotspots: A Global Risk Analysis* (The World Bank Hazard Management Unit, Washington, DC, 2005).
3. Io refers to the maximum intensity as measured by the European Macroseismic Scale [EMS-98, see (*11*)]. Intensities and magnitudes cannot be easily compared. Magnitude is related to the earthquake energy released at the source, whereas intensity is a measure of damage created by the earthquake that depends on the distance from the source as well as the geological conditions.
4. T. Parsons, *J. Geophys. Res.* **109**, B05304 (2004).
5. M. B. Demircioglu, Assessment of Earthquake Risk in Istanbul, in Seismic Risk Management in Urban Areas, PEER Report 2011/07 (University of California, Berkeley, 2011).
6. I. E. Bal *et al.*, *J. Earthquake Eng.* **12**, 12 (2008).
7. F. O. Strasser *et al.*, *J. Earthquake Eng.* **12**, 246 (2008).
8. J. H. Pyper Griffiths *et al.*, *Earthq. Spectra* **23**, 63 (2007).
9. Earthquake Masterplan for Istanbul, Istanbul Metropolitan Municipality, prepared by Bogazici University, Istanbul Technical University, Middle East Technical University, and Yildiz Technical University (2003).
10. See the Earthquakes and Megacities Initiative (http://emi.pdc.org/emi/emihome.html) and PreventionWeb (www.preventionweb.net).
11. G. Grünthal, Ed., *European Macroseismic Scale 1998*, Cahiers du Centre Européen de Géodynamique et de Séismologie, Volume 15 (European Centre for Geodynamics and Seismology Luxembourg, 1998).

10.1126/science.1238945

APPLIED PHYSICS

Triggering an Optical Transistor with One Photon

The coherent absorption of a single photon by atoms in an optical cavity can control the transmission of a more intense light beam.

Jürgen Volz and Arno Rauschenbeutel

Transistors are the key element in all electronic circuits, and a single computer chip may contain billions of these elements. However, in recent years, data communication underwent a paradigm shift away from electronic schemes to light-based communication with optical fibers. In the wake of this transformation, a considerable amount of research has gone into trying to replace active electronic circuits with optical ones. One major research direction focuses on all-optical transistors that allow a large optical "source" signal to be controlled by a weak "gate" light field. On page 768 of this issue, Chen *et al*. (*1*) report on the realization of such a device and demonstrate that even the smallest possible gate field—a single photon—can control the transmission of a source optical field consisting of hundreds of photons.

Under normal circumstances, pulses of light do not interact with each other. This property enables the simultaneous use of multiple-wavelength channels for transmitting data over optical fibers. However, the absence of direct interaction prevents the direct implementation of active photonic elements such as optical transistors. To circumvent this problem and to realize a strong effective light-light interaction, Chen *et al*. combined two central elements of modern quantum optics research in their experiment: a high-finesse optical cavity (one that has very low absorption losses) and an optical quantum memory (*2*, *3*). The latter enables light to be stored in an ensemble of laser-cooled atoms and to be retrieved later on.

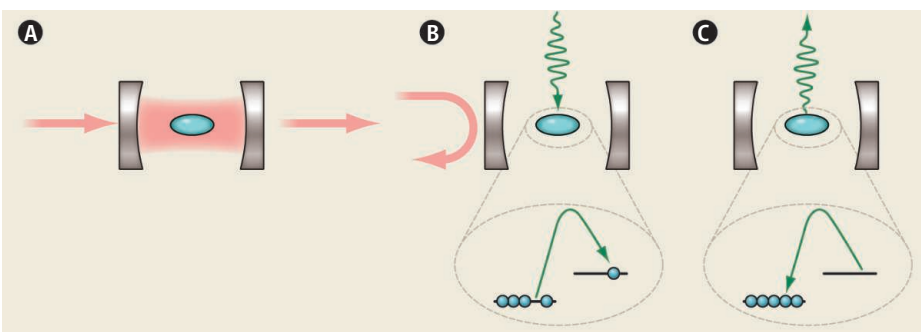

An optical "light switch." The schematic setup and operation principle of the all-optical transistor is shown. (**A**) An ensemble of laser-cooled atoms (blue) is trapped inside an optical resonator in the off-resonant ground state. As a consequence, the incident source field (red) is transmitted though the cavity. (**B**) In the first step of the switching process, the gate light field (green) containing about one photon is stored in the ensemble. A collective state is formed in which one atom is transferred to a state resonant with the cavity, which blocks the transmission of source photons through the cavity. (**C**) If the source field is weak enough, no information on the position of the transferred atom becomes available and the gate photon can be retrieved.

The high-finesse optical cavity consists of two highly reflective mirrors that can reflect light back and forth about 25,000 times. Inside the cavity, an ensemble of around 20,000 cesium atoms were trapped by means of optical tweezers (*4*) and laser-cooled to a temperature of a few microkelvin. Initially, all of the atoms were prepared in an internal state that did not interact with the light in the cavity. The atomic ensemble was thus transparent for the cavity light, and, because the length of a round trip between the cavity mirrors equaled an integer multiple of the wavelength of the incident source light field, the cavity transmitted the source light.

In order to realize an all-optical transistor, it is necessary to control the cavity transmission with an external light field that acts as the gate. Chen *et al*. accomplished this feat by sending the gate light field from the side into the cavity where each photon induced—through interplay with an additional control light field—a coherent scattering process that changed the state of just one of the atoms (see the figure) (*2*, *3*). For their experimental conditions, the interaction between the source light and atoms was strongly enhanced because of the high finesse of the cavity. Remarkably, transferring just a single

Vienna Center for Quantum Science and Technology, Atominstitut, Vienna University of Technology, Stadionallee 2, 1020 Wien, Austria. E-mail: arno.rauschenbeutel@ati.ac.at; jvolz@ati.ac.at

atom to another internal atomic state that was resonant with the optical field inside the cavity sufficed to change the resonance wavelength of the cavity substantially and block the transmission of the source field (*5*). Thus, as soon as a single gate photon underwent a coherent scattering event in the ensemble, the cavity transmission was reduced and most of the source light incident on the cavity was reflected. In this way, the authors showed that a gate field that contained only a single photon could switch between the transmission and reflection of the source light field containing hundreds of photons.

The performance of the device even went beyond that of a classical switch operated by a single photon. As long as no information is available about which atom changed its state, quantum interference allows the coherent scattering process to be reversed. Thus, the initial gate photon could be retrieved from the atomic ensemble after blocking the transmission of the source photons. In this case, the atomic ensemble was operated as a so-called quantum memory (*2*, *3*). Here, the number of source photons that could be redirected was smaller than in this previous experiment: Because of experimental imperfections, a small fraction of the source light will still enter the cavity and can then be scattered outside of the cavity by the atom. This process will more likely occur for a larger number of incident source photons and will reveal which atom changed its state, thereby destroying the quantum interference necessary for retrieving the gate photon. Chen *et al*. found that a single gate photon that was stored in their quantum memory could redirect a source field containing up to two photons before the retrieval of the gate photon was impeded. Although this number seems small, it exceeds 1 and is above the critical threshold for a positive gain of their transistor.

With their experiment, Chen *et al*. demonstrated the feasibility of an all-optical transistor that can be triggered by only a single gate photon. That such a system can be operated in the quantum regime opens the way to future photonic devices that could be used for light-based quantum information protocols (*6*). To this end, the next critical step will be to optimize the performance of such systems, which requires enhancing the absorption probability of the gate light in the atomic ensemble. Moreover, the efficiency of coupling the source light into and out of the optical resonator will have to be improved. In independent experiments, highly efficient quantum memories (*7*) and optical resonators with coupling efficiency close to 1 (*8*, *9*) have been realized. Combining these improvements in the same system would allow the realization of an efficient all-optical transistor, which in turn might enable the implementation of deterministic quantum logical operations between individual photons (*6*)—the key element of an optical quantum computer.

References

1. W. Chen *et al*., *Science* **341**, 768 (2013); 10.1126/science.1238169.
2. A. I. Lvovsky, B. C. Sanders, W. Tittel, *Nat. Photonics* **3**, 706 (2009).
3. K. Hammerer *et al*., *Rev. Mod. Phys.* **82**, 1041 (2010).
4. R. Grimm *et al*., *Adv. At. Mol. Opt. Phys.* **42**, 95 (2000).
5. P. R. Berman, *Cavity Quantum Electrodynamics* (Academic Press, Boston, 1994).
6. M. Nielsen, I. Chuang, *Quantum Computation and Quantum Information* (Cambridge Univ. Press, Cambridge, 2000).
7. M. Hosseini *et al*., *Nat. Commun.* **2**, 174 (2011).
8. T. Aoki *et al*., *Nature* **443**, 671 (2006).
9. C. Junge *et al*., *Phys. Rev. Lett.* **110**, 213604 (2013).

10.1126/science.1242905

NEUROSCIENCE

Mapping Neuronal Diversity One Cell at a Time

A universal method for classifying neuronal subtypes will increase our understanding of the human brain.

Hynek Wichterle,[1] David Gifford,[2] Esteban Mazzoni[3]

How many types of nerve cells are there in the mammalian central nervous system (CNS)? We still do not have a satisfactory answer to this deceptively simple question, and yet the precise assignment of nerve cells to well-defined subtype categories is critical both for elucidating the function of neural circuits and for the success of neural regenerative medicine. Amid the anatomical, electrophysiological, and biochemical diversity of nerve cells, the field is struggling to devise simple and clear criteria for neuronal classification. A universally applicable classification system should be based on traits that are objectively quantifiable, sufficiently diverse, and reproducible in independent laboratories. Such a classification method would provide new insights into CNS organization, development, and function, and might reveal unexpected relationships between neuronal subtypes.

To fully characterize nerve cells and appreciate their diversity, they are analyzed at all three phenotypic levels—anatomical, biochemical, and electrophysiological. Complete anatomical mapping was accomplished for the CNS of the worm *Caenorhabditis elegans* by reconstruction of serial electron micrographs (*1*). Ultrastructural mapping is complemented by analysis of anatomy and connectivity based on cell type–specific expression of reporter genes to effectively study the much larger mammalian CNS (*2*, *3*). At the biochemical level, ongoing efforts to map expression patterns of developmentally regulated genes provide fundamental insights into molecular diversity and developmental programs of individual nerve cells (*4*, *5*). And at the electrophysiological level, new research programs, such as the recently announced Brain Research through Advancing Innovative Neurotechnologies (BRAIN) initiative, are supporting development of technologies for global mapping of neuronal activity in behaving animals (*6*). Although integration of the three complementary approaches is essential for the ultimate understanding of brain structure and function (*7*, *8*), at the single nerve cell level such detailed analysis poses a problem as it allows assignment of each nerve cell to multiple different subtype groups.

Currently we do not have a system to provide a definitive count of neuronal subtypes, even in a small region of the mammalian CNS. A recent review on subtype diversity of neocortical interneurons provided a partial solution by proposing to focus on a few easily distinguishable morphological phenotypes to categorize inhibitory interneurons (*9*). Although such an approach is practical and immediately applicable to classification of cortical interneurons, it is not sufficiently universal to be easily transferable to other types of neurons and might miss important

[1]Departments of Pathology and Cell Biology, Neurology, and Neuroscience, Center for Motor Neuron Biology and Disease, Columbia Stem Cell Initiative, Columbia University Medical Center, 630 168 Street, New York, NY 10032, USA. [2]Computer Science and Artificial Intelligence Laboratory, Massachusetts Institute of Technology, 32 Vassar Street, Cambridge, MA 02139, USA. [3]Department of Biology, New York University. 100 Washington Square East, New York, NY 10003, USA. E-mail: hw350@columbia.edu

functional differences among interneurons that are not manifested by anatomically discernible features.

Differential expression of developmentally regulated genes determines most aspects of neuronal identity. The expressed genes not only define neuronal connectivity and physiology but also determine and reflect neuronal responses to external signals and patterns of neuronal activity. Unlike other types of phenotypic characterization (morphology or electrophysiology), gene expression provides extremely rich and diverse data sets with large numbers of measurable attributes. Advances in next-generation sequencing make analysis of global gene expression relatively easy, quantitative, and highly reproducible (*10*).

Current gene expression studies typically rely on profiling neuronal populations that have been partially purified on the basis of reporter gene expression. A systematic approach to profile all neuronal populations has been recently completed for the mouse retina (*5*). While the resulting data provide insights into the diversity of principal neuronal classes, reliance on reporter genes expressed in multiple neuronal subtypes implies that the resulting expression profiles are composites (*5*). Computational deconvolution of such complex data sets requires a priori knowledge of neuronal diversity within the sorted cell populations, thereby limiting the discovery of new neuronal subtypes (*11*).

Given the utility and generality of expression data, we propose that single-cell expression profiling be used to characterize neuronal diversity (see the figure) (*12*). Single-cell RNA sequencing (RNA-seq) provides an unbiased and systematic method of "fingerprinting" an aspect of cellular state that enables similar cells to be computationally identified (*13*). However, several challenges need to be overcome to ensure the success of this approach. One is that universally adoptable protocols that yield consistent data in different laboratories will need to be developed, so that data can be progressively built into a universal "neuronal gene expression reference library" (*4*).

Another challenge will be to devise strategies for assigning expression profiles to discrete subtype categories. Computational methods could determine the degree of similarity between individual profiles and draw subtype boundaries between groups of cells. For example, existing algorithms for high-dimensional single-cell cytometry data arrange cells in a branched tree structure defining their relatedness (*14*). Once subtype identities are determined, it will be possible to extract a core set of differentially expressed genes defining neuronal subtype identity (subtype signature). The flexibility of this system will make it easy to continuously add expression profiles, update models, and define finer neuronal subtype categories.

Relating the expression signatures to nerve cell function will also be key to the success of this approach. Focused analysis of neuronal subsets based on reporter expression will decrease the cellular complexity of studied samples and provide a link between expression profiles and functional attributes derived from parallel morphological and electrophysiological studies. Some neuronal phenotypes such as the neurotransmitter and electrophysiological properties will correlate with expression of core signature genes encoding enzymes involved in neurotransmitter biosynthetic pathways, and receptors and ion channels defining neuronal membrane properties (*15*, *16*). Other phenotypes such as position within the CNS, morphology of the cell, or connectivity might be harder to correlate with expression profiles as these phenotypes are controlled by programs active during neuronal development. Whether a footprint of these developmental programs is carried over into the terminal neuronal signature remains to be determined.

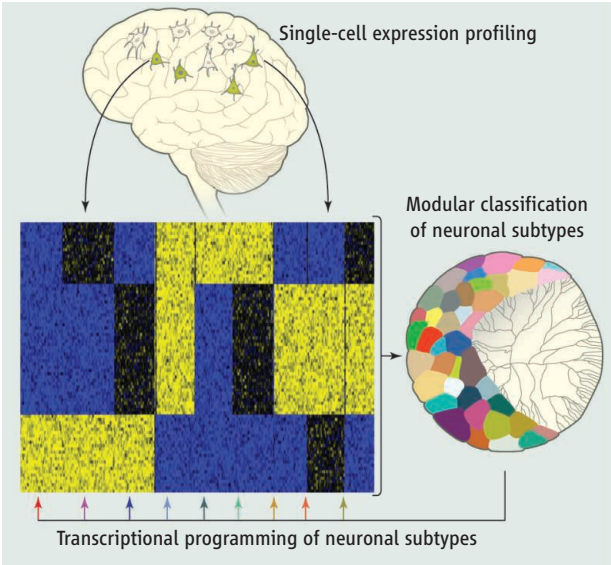

Classifying neuronal subtypes. Clustering of single-cell expression profiles provides an objective method for subtype classification. Regulatory relationships between genes can be computationally extracted from the expression profiles, defining sets of transcription factors (TFs) critical for the establishment and maintenance of subtype-specific expression profiles. Discovered transcription factor modules can be used to reprogram other cell types to desirable neuronal subtypes.

Single-cell RNA-seq data for classifying neuronal subtypes will have additional applications. For example, correlation of differentially expressed genes with connectivity and electrophysiology might decipher effects of neuronal activity, cell signaling, and memory formation on neuronal transcriptomes. The discovered molecular signatures might provide novel insights and tools for studying CNS function.

Another area that will benefit from the expression data is transcriptional programming of neuronal identity. Programming factors are typically discovered by a tedious trial-and-error method, and their ability to program functional nerve cells matching their in vivo counterparts is frequently questioned. Cross-referencing expression profiles of programmed cells with the neuronal reference expression library will provide an unambiguous measure of the quality and subtype identity of programmed cells. Furthermore, RNA-seq data can be used to estimate transcriptional networks and to predict key transcription factors controlling subtype-specific expression profiles (*17*). Such prospectively identified transcription factors, capable of programming neuronal subtype identity in diverse cellular contexts, will have a practical impact on production of specific nerve cells either from pluripotent stem cells in vitro or by reprogramming endogenous neural stem cells in vivo. Effective and subtype-specific neuronal programming might find application in cell replacement therapies or for modeling neurodegenerative diseases in vitro.

References and Notes

1. D. H. Hall, R. L. Russell, *J. Neurosci.* **11**, 1 (1991).
2. I. R. Wickersham *et al.*, *Neuron* **53**, 639 (2007).
3. S. Gong *et al.*, *Nature* **425**, 917 (2003).
4. M. J. Hawrylycz *et al.*, *Nature* **489**, 391 (2012).
5. S. Siegert *et al.*, *Nat. Neurosci.* **15**, 487, S1 (2012).
6. L. Tian *et al.*, *Nat. Methods* **6**, 875 (2009).
7. K. Sugino *et al.*, *Nat. Neurosci.* **9**, 99 (2006).
8. G. A. Ascoli *et al.*, *Nat. Rev. Neurosci.* **9**, 557 (2008).
9. J. DeFelipe *et al.*, *Nat. Rev. Neurosci.* **14**, 202 (2013).
10. Z. Wang *et al.*, *Nat. Rev. Genet.* **10**, 57 (2009).
11. S. S. Shen-Orr *et al.*, *Nat. Methods* **7**, 287 (2010).
12. S. Qiu *et al.*, *Front. Genet.* **3**, 124 (2012).
13. G. Gerber *et al.*, *PLoS Comp. Biol.* **3**, 1426 (2006).
14. P. Qiu *et al.*, *Nat. Biotechnol.* **29**, 886 (2011).
15. K. D. Winden *et al.*, *Mol. Syst. Biol.* **5**, 291 (2009).
16. T. Kodama *et al.*, *J. Neurosci.* **32**, 7819 (2012).
17. A. A. Margolin *et al.*, *Nat. Protoc.* **1**, 662 (2006).

Acknowledgments: We thank O. Hobert and R. Bonneau for helpful discussions. H.W. and D.G. are supported by NIH grants R01NS078097 and P01NS055923. E.M. and H.W. are supported by Project A.L.S.

10.1126/science.1235884

Smarter Pest Control

CREDIT: G. GRULLON/SCIENCE

INTRODUCTION

The Pesticide Paradox

PESTICIDES—A VAST RANGE OF CHEMICALS THAT KILL INSECTS, WEEDS, FUNGI, AND other organisms humans would rather do without—bring some great benefits to society. They have made it possible to feed a growing human population, and they protect millions from malaria and other insect-borne diseases. They also support important economic sectors such as the cotton and flower industries and help make our lives easier and more enjoyable; for instance, by reducing mosquito, ant, and cockroach populations. Yet the potentially serious threats they pose to human health and the environment have led to a series of bans on the most dangerous chemicals and to calls to go much further. This spring, the European Union took a new step by issuing a partial ban on three neonicotinoids, a widely used group of insecticides suspected of harming bees, butterflies, and other nontarget species.

Although science is guiding some policy changes, there is still room for major improvement when it comes to pesticides, by more carefully tracking their effects, using them more judiciously, reducing their negative impacts, and finding alternatives. Scientists are making strides in precisely understanding the effects of the chemicals now in our arsenal, including the myriad ways in which they are broken down in the environment and the harm they cause to wildlife. Meanwhile, cohort studies in the United States are beginning to map out their troubling effects on the young developing brain.

Reducing the negative fallout from pesticides is possible in many ways. Australia's wheat farmers are tackling one of the worst weed problems in the world (a crisis that, ironically, partly arose from overreliance on herbicides) by using a more diverse set of tools. Pesticide overuse is a big problem in Asia, too; although cheap, they hurt the farmer's bottom line in the long run. Vietnam has developed a pioneering program that is paying dividends to farmers who spray less. Also in Asia, scientists are tackling one of the biggest problems: More than 300,000 people are believed to commit suicide every year by swallowing pesticides.

Others, meanwhile, are looking ahead. New synthetic chemicals to protect crops hold the promise of stronger and more specific protection with less collateral damage. And some crops won't need pesticides at all: Scientists are developing plants whose immune systems can ward off fungal, bacterial, or viral diseases, and they are using RNA interference to help plants fight insects—a new technology that could hit the market before the decade ends.

We may never be able to abandon pesticides altogether, but as this collection of Reviews, News stories, and research papers shows, pest control can become much smarter, and science has a major role to play.

– MARTIN ENSERINK, PAMELA J. HINES, SACHA N. VIGNIERI, NICHOLAS S. WIGGINTON, JAKE S. YESTON

CONTENTS

News

730 Pesticide Planet
732 A Lethal Dose of RNA
734 The War Against Weeds Down Under
737 Vietnam Turns Back a 'Tsunami of Pesticides'
738 In Rural Asia, Locking Up Poisons to Prevent Suicides
740 Growing Up With Pesticides

Reviews

742 Current Challenges and Trends in the Discovery of Agrochemicals
C. Lamberth et al.
746 Pivoting the Plant Immune System from Dissection to Deployment
J. L. Dangl et al.
752 Evaluating Pesticide Degradation in the Environment: Blind Spots and Emerging Opportunites
K. Fenner et al.
759 Wildlife Ecotoxicology of Pesticides: Can We Track Effects to the Population Level and Beyond?
H.-R. Köhler and R. Triebskorn

See also Editorial p. 695; Policy Forum p. 717; Perspective p. 722; Reports pp. 783 and 786; Podcasts; and additional resources at www.sciencemag.org/special/pesticides

Science

Published by AAAS

PESTICIDE PLANET

In a world of humanmade chemicals, pesticides are second only to fertilizer in the amount applied and the extent of use. They are effective tools for protecting crops, fighting disease-causing insects, and dealing with nuisance animals such as rodents, fleas, and ticks. But herbicides, insecticides, and their kin can harm the environment and are dangerous to workers if improperly used.

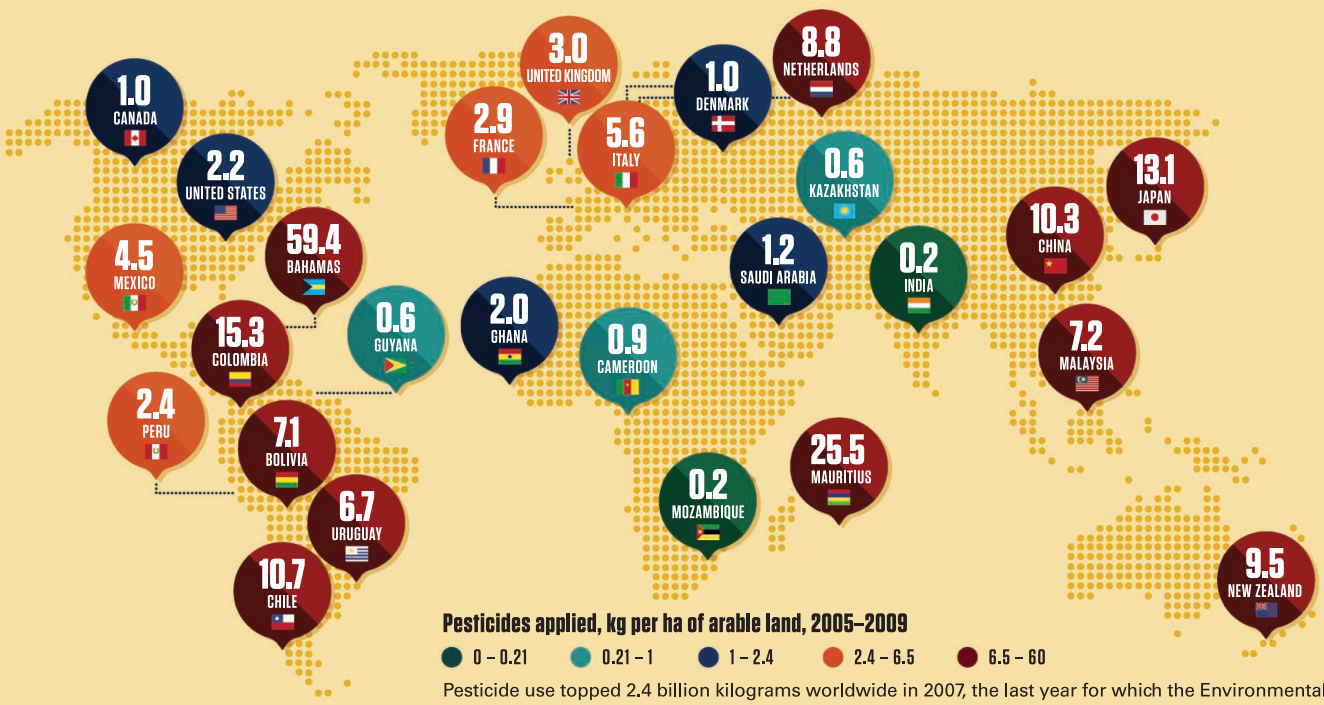

Pesticide use topped 2.4 billion kilograms worldwide in 2007, the last year for which the Environmental Protection Agency produced global figures, and the United States accounted for 20%. Application rates were higher in other countries, such as China, where farmers are less trained and also in valuable crops where pest pressures are high, including Colombian coffee and Dutch tulips.

MORE DEMAND, MANY USES

Global pesticide sales by region

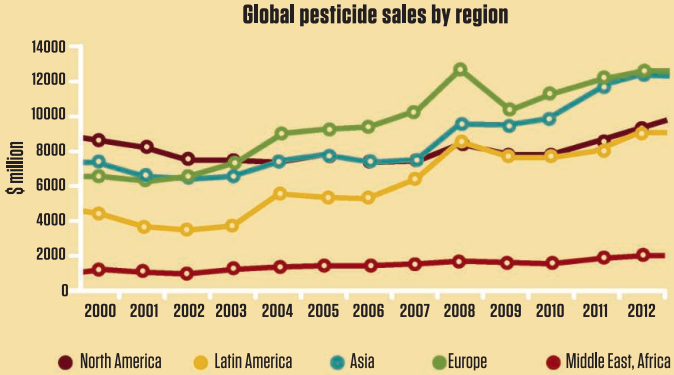

Pesticide sales are increasing in Asia, Latin America, and Eastern Europe. In addition, companies often charge lower prices for older products and in poorer markets, boosting sales. Africa uses far less pesticide than any other region.

Pesticide use by sector, U.S.

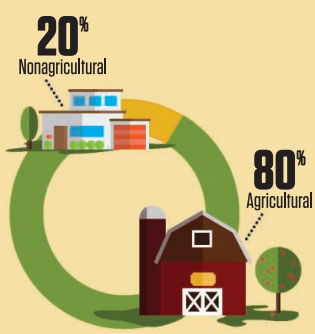

Weeds remain the largest concern of farmers. Yet in the United States, 20% of pesticides are applied in nonagricultural settings, such as homes, lawns, and gardens, where more is often used per square meter.

Pesticide use by type, worldwide

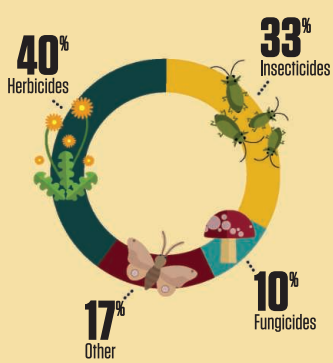

"Other" includes sulfur, oil, insect repellent, moth control, and other chemicals.

SOURCES: (TOP TO BOTTOM): *FAO STATISTICAL YEARBOOK 2013*; PHILLIPS MCDOUGALL LTD; *EPA PESTICIDES INDUSTRY SALES AND USAGE 2006 AND 2007 MARKET ESTIMATES*

ENHANCING YIELDS

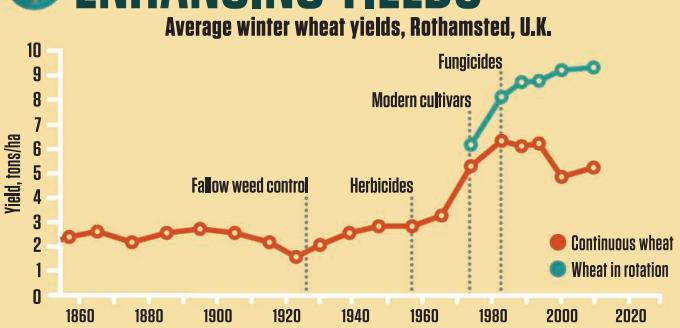

Long-term research plots have shown increases in wheat yield from controlling weeds and disease. Gains from plowing fallow fields were exceeded by the advent of chemical herbicides and fungicides.

PREVENTING DISEASE

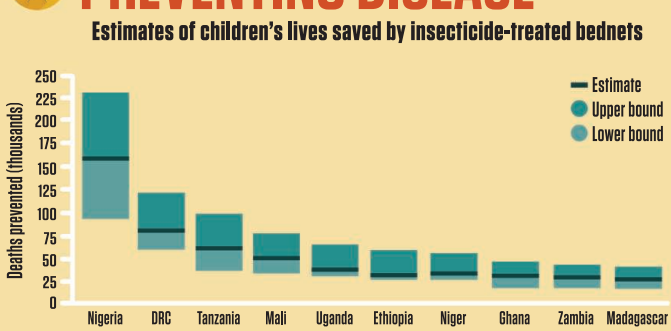

Between 2000 and 2010, household spraying and insecticide-treated bednets prevented the deaths from malaria of an estimated 831,100 children in 43 countries, according to a recent model—almost 230 a day. Insecticide resistance in the mosquito threatens these gains.

GETTING SAFER, USING LESS

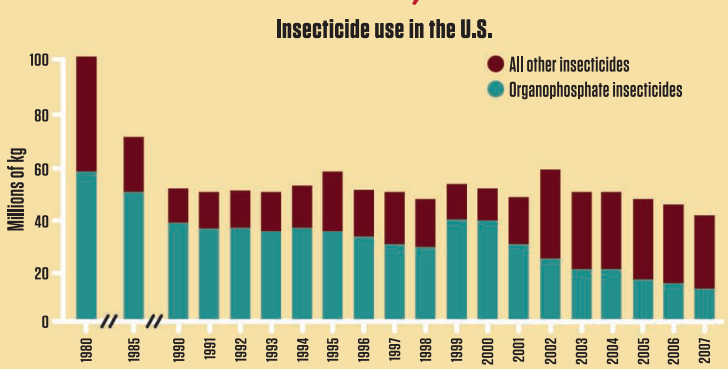

Developed countries have phased out the more dangerous compounds, such as parathion and other organophosphates. After the U.S. Food Quality Protection Act of 1996, several more have been banned altogether, limited to farm use, or further restricted to protect workers or the environment. They are still widely used in many developing countries.

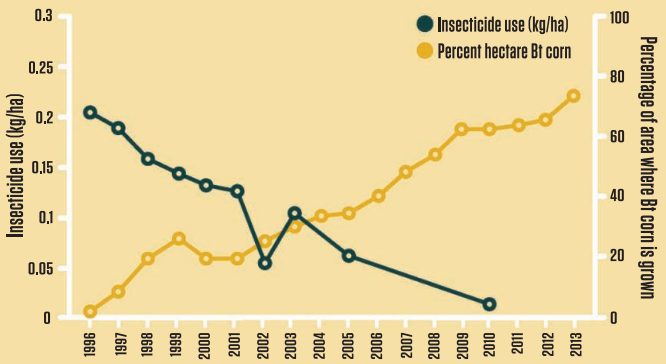

Overall pesticide use on U.S. farms dropped 0.6% a year from 1980 to 2007. The declines were even greater in corn fields, thanks in part to genetically modified varieties with the Bt toxin. But resistant insects have led to a recent uptick in insecticide applications. Herbicide-tolerant crops, and resistant weeds, have led to an increase in herbicide use.

UNINTENDED HARM

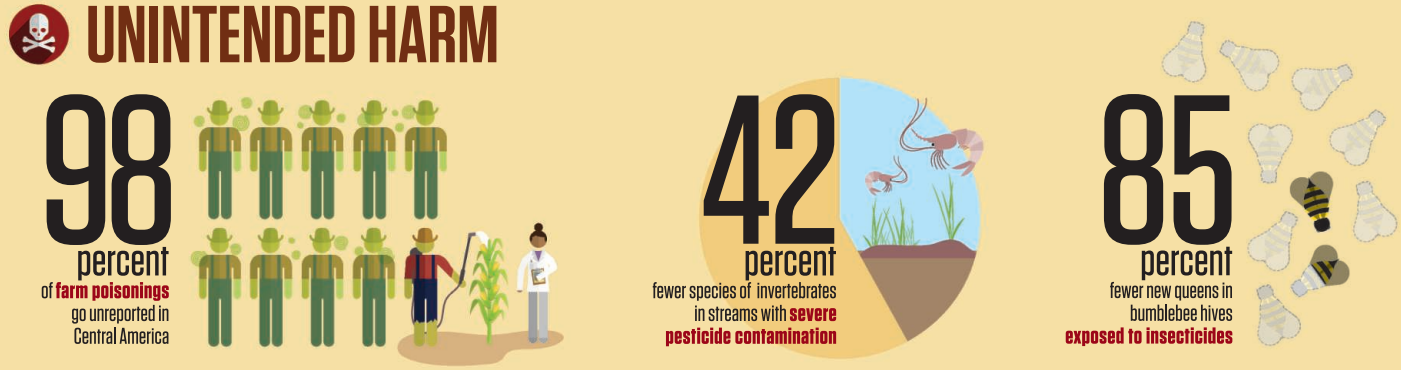

Surveys of farm worker health are scarce, but it's clear that pesticides cause more harm in the developing world. More toxic chemicals are still used, and basic safety equipment is often lacking. Despite many studies on wildlife toxicology, ecosystem-wide impacts are poorly understood (see p. 759).

Research: Erik Stokstad
Design: Garvin Grullón

SOURCES: (TOP TO BOTTOM): ROTHAMSTED RESEARCH; *MALARIA JOURNAL* **11** (28 MARCH 2012); *EPA PESTICIDES INDUSTRY SALES AND USAGE 2006 AND 2007 MARKET ESTIMATES*, FEBRUARY 2011; USDA, ECONOMIC RESEARCH SERVICE, NATIONAL AGRICULTURAL STATISTICS SERVICE; *INTERNATIONAL JOURNAL OF OCCUPATIONAL AND ENVIRONMENTAL HEALTH* **8**, 3 (JUL–SEP 2002); *PNAS* **110**, 27 (2 JULY 2013); *SCIENCE* **336**, 6079 (20 APRIL 2012)

A Lethal Dose of RNA

A new generation of genetically modified crops will kill insects by silencing their genes

WHEN ANDREW FIRE AND CRAIG MELLO WON a Nobel Prize in 2006 for a revolutionary technique to silence genes, there were high hopes that the discovery would lead to new treatments for disease. RNA interference (RNAi) might help tackle a wide variety of ailments, such as virus infections, cancer, and cardiovascular disease, the Nobel committee noted. Seven years on, the technology is almost ready to be applied—but rather than healing humans, it will kill insects.

Scientists are using RNAi to build a new generation of crops that can fend off pests by making them express small bits of RNA, carefully chosen to match, and silence, crucial genes in the target insects. "It's the next big thing" in crop protection, says Andreas Vilcinskas, an entomologist at the University of Giessen in Germany. "Symposia on this are standing room only," says William Moar, a researcher at Monsanto in St. Louis, Missouri.

The idea to equip plants with built-in pesticides is nothing new. Bt corn, on the market since 1996, produces the protein Cry, derived from a bacterium called *Bacillus thuringiensis*, which is toxic to moth larvae like the European corn borer. It may harm benign insects as well, and like most genetically modified (GM) organisms, it's controversial, yet Bt corn has taken the market by storm, leading to a drop in pesticide use. RNAi would take the concept to a new level by targeting harmful insects with surgical precision—although critics have suggested that the RNA molecules could also harm humans.

Major seed companies are betting heavily on the technology. Last year, Syngenta bought Belgian RNAi pioneer Devgen for $522 million and Monsanto paid $29.2 million for the exclusive rights to intellectual property on RNAi technology from Alnylam Pharmaceuticals. "There is a race to get this to the field," Vilcinskas says.

Targeted for destruction

RNAi technology exploits a pathway first discovered in the 1990s. In an attempt to make petunias a deeper purple, researchers introduced an additional copy of a gene producing its purple pigment. But instead of darker petunias, they bred lighter ones. The reason was RNAi, an unknown defense mechanism that allows cells to break down double-stranded RNA (dsRNA) introduced from outside. The system likely evolved as a defense against viruses, which often have dsRNA. A protein called Dicer cuts the foreign RNA into small bits, which tag any complementary RNA they bind to for destruction by other cellular proteins.

If an introduced RNA molecule isn't viral but corresponds to a gene in the cell itself, the system will turn against itself, destroying transcripts of that gene and silencing it. "We fool the defense system," says Guy Smagghe, an entomologist at Ghent University in Belgium. Millions have been spent on trials to use RNAi for silencing genes involved in cardiovascular and infectious diseases. But getting RNA into human cells has proven very difficult. For insects, on the other hand, it was surpris-

CREDIT: JOHN OBERMEYER/PURDUE EXTENSION ENTOMOLOGY

Published by AAAS

Corn consumers. Adult western corn rootworms. RNAi can kill their larvae, which feed on roots.

ingly easy: Just feed them the RNA. Cells in the midgut of many larvae take up the molecules and help spread the signal throughout the insect's body.

Scientists were quick to see the potential of killing insect pests by making plants produce insect RNA. The technology can be very specific because it affects only insects that have the target sequence, says entomologist Wayne Hunter of the U.S. Department of Agriculture in Fort Pierce, Florida. "You can feed it to psyllids and kill them, and you can feed it to leaf hoppers that eat the same plant and it won't kill them," he says. Indeed, by choosing highly specific gene sequences, scientists in 2009 showed they could kill any one of four fruit fly species while not harming the other three.

Resisting resistances

Monsanto will likely be the first to sell RNAi-based pesticidal seeds to farmers. The company has developed a transgenic corn plant expressing dsRNA based on a gene from the western corn rootworm, a beetle whose larvae cause a billion dollars' worth of damage in the United States alone. The RNA targets *Snf7*, a gene that helps ferry proteins to their destination inside the cell. In a 2012 paper, Monsanto scientists showed that silencing *Snf7* stunts the growth of the larvae and kills them within days. Earlier this year, they also showed that it affects very few other species. "We think the science has been done," Moar says; getting regulatory approval is next. "We definitely expect to have a product out by the end of the decade."

Others are working on different crops. Smagghe, in collaboration with the International Potato Center in Lima, is looking for genes to target in the sweet potato weevil, a beetle whose larvae ravage sweet potato fields all over the world. Researchers are also trying to silence genes in ants, caterpillars, and pollen beetles.

But while locusts and beetle larvae respond well to RNAi, other insects seem less susceptible, Smagghe says, possibly because their saliva is better at breaking down RNA. Butterflies and moths are particularly resistant, and they include many major crop pests such as the cotton bollworm, the beet armyworm, and the Asiatic rice borer.

Another potential problem is resistance. In a few places, the western corn rootworm has already become resistant to Bt corn—that's why scientists are urgently looking for alternatives in the first place. To develop resistance to RNAi, the western corn rootworm would have to change the genetic sequence of its *Snf7* gene at multiple sites, which some experts say is unlikely to happen. Blair Siegfried, an expert on pesticide resistance at the University of Nebraska, Lincoln, disagrees. "My sense is that resistance to RNAi traits is just as likely to emerge as resistance against other agents we have developed," he says. However, combining Bt and RNAi in one plant, as Monsanto is doing, could delay that moment significantly, he says.

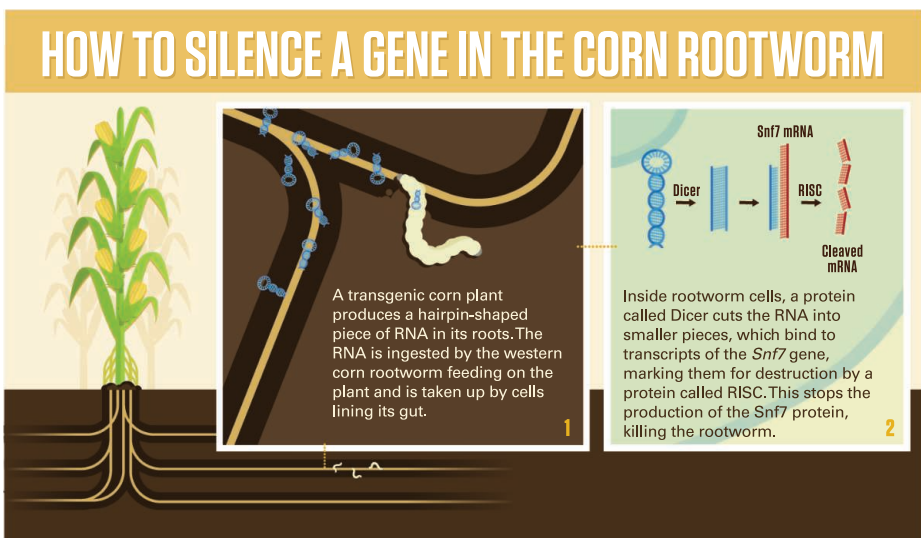

Plants as patients

But the biggest resistance may well come from a public that is skeptical, or even opposed, to GM crops. Environmental groups have already raised worries that RNA incorporated into plants could find its way into consumers' cells. They point to a 2012 paper by Chen-Yu Zhang of Nanjing University, who detected small RNAs from food plants in the blood of mice and humans. RNA intended to kill target insects could also end up in the human bloodstream, critics warn, with unknown consequences.

Zhang's findings are controversial, however, and they have yet to be confirmed. Scientists have pointed out that a variety of biological barriers—including enzymes in saliva and blood and the ferociously acidic stomach environment—should break down any RNA. Monsanto researchers have argued that the RNAs found by Zhang could be the result of lab contamination and say the human equivalent of the mouse diet in his study would be 33 kilograms of cooked rice a day.

Two recent studies published in *RNA Biology* also call the results into question. A team at Brigham and Women's Hospital in Boston fed athletes a diet of apples and bananas; they failed to detect RNAs abundant in these fruits in their blood afterward. Scientists at Johns Hopkins University School of Medicine in Baltimore, Maryland, gave monkeys a fruit shake and couldn't reliably detect plant RNAs in their blood either. "These two studies combined show that there is negligible uptake of microRNA from diets in mammals," says Kenneth Witwer, who led the Hopkins study.

There's another strategy—Hunter calls "treating the plant as a patient"—in which dsRNA is simply added to the water used for irrigation. The molecules are sucked into the plants' vascular system and poison insects feeding on the sap. RNA could also be sprayed onto plants like a conventional pesticide, Hunter says. This would allow faster adaptation if resistance arises; scientists would just choose a new RNA snippet to apply, without having to build it into the plant's genome. Although humans would still ingest the RNA, the fact that plants aren't GM might make this approach an easier sell.

Other scientists are skeptical. RNA molecules are so expensive that it's far more viable to have the plant itself produce them, Smagghe says. What's more, when applied to the water or sprayed onto leaves, RNA might rapidly degrade. Rather than treating our crops as patients, Smagghe says, it's better to give them the weapons to defend themselves.

–KAI KUPFERSCHMIDT

CREDIT: G. GRULLÓN/*SCIENCE*

Published by AAAS

The War Against Weeds Down Under

For decades, Australia's wheat farmers have had the worst weed problem in the world. Now, nonchemical weapons are helping to turn the tide

In 1788, when the First Fleet brought more than 700 English convicts to Australia, it also transported dozens of sheep. The animals were intended to help feed the penal colony, but they soon provided more than meat: Wool became one of Australia's main exports, which it remained for nearly 2 centuries. As settlers moved across the dry continent, they planted pastures for their flocks. Ryegrass, nutritious and fast-growing, was particularly popular forage. "Our early history is full of things that seemed like good ideas at the time, but that have come back to haunt us," says Christopher Preston, a weed scientist at the University of Adelaide in Australia. "The planting of ryegrass is one of them."

The trouble started as the wool market crashed in the 1970s. Many sheep farmers switched to exclusively growing wheat in their pastures. Then ryegrass showed its ugly side. In wheat fields, the grass is an aggressive weed that competes for water and light, reducing yield. The plants produce so many seeds that, if left unchecked, they will choke a field completely. "It's our greatest nemesis," says Ray Harrington, a wheat farmer in Darkan, Western Australia.

For a while, the solution was simple. Although there are many ways to fight weeds—plowing them up and rotating crops both help—the easiest and cheapest approach is to spray herbicides. Weed-killer was so effective that it allowed fewer workers to farm more land, boosting efficiency. By eliminating the need to plow, it also prevented soil erosion. Throughout the 1980s, production and profits continued to climb. But new difficulties arose. Within little more than a decade, ryegrass and other weeds began to develop resistance to herbicides. Farmers had to apply more and more of them to kill the plants, until the chemicals became virtually useless. Some moved on to other herbicides, often more toxic.

It is a mistake that could easily be repeated around the world, making farming more complicated and expensive for large producers. "The real danger of resistance," says Dale Shaner, a weed scientist who recently retired from the U.S. Department of Agriculture, is that farmers will lose "the major tool that's given us inexpensive food and fiber." Through a combination of errors, this happened early, quickly, and widely in Australia. "There's never been so large a problem anywhere else in the world," says Stephen Powles of the University of Western Australia (UWA), Crawley.

Thanks in part to Powles, Australia is also pioneering ways to deal with the problem. "He's the undeniable global leader in herbicide resistance," says Ford Baldwin, formerly a weed scientist with the University of Arkansas and now a consultant.

The key to beating herbicide-resistant weeds, Powles says, is to abandon the hope of a silver bullet from the chemical industry. Instead, farmers must return to fighting weeds with a diverse arsenal of techniques. In Australia, these tactics are finally working,

CREDIT: RODNEY MESSINA

Scorched earth. One tool in Australia's approach to fighting weeds is to burn them after harvest, preventing seeds from germinating the next year.

and Powles hopes to promote them in the rest of the world before more farmers lose effective herbicides. In Australia, he says, "we learned the hard way."

What went wrong

Powles grew up poor, milking cows on his grandparents' struggling dairy farm in New South Wales. By age 15, he had dropped out of school. After several years working at a feed supply company, he entered Hawkesbury Agricultural College to study farming. He wound up with a Ph.D. in plant physiology and biochemistry from the Australian National University. By the time he finished a postdoc at Stanford University, he felt that his studies of photosynthesis were too far removed from the real world of agriculture.

Just then, in 1983, the first cases of herbicide resistance were being reported in Australia. Sensing opportunity, Powles moved to the University of Adelaide. Patches of ryegrass had become immune to Hoegrass, a hugely popular herbicide. The product belongs to a family of herbicides that inhibit an enzyme called acetyl coenzyme A carboxylase, which helps plants make fatty acids. Farmers sprayed Hoegrass—which leaves the wheat unscathed—in early spring, to kill ryegrass seedlings.

Tough opponent. Stephen Powles and his colleagues test weeds, such as these wild radish, for resistance to herbicides.

Several factors boosted the evolution of resistance. Ryegrass populations were large, and they had tremendous genetic diversity, thanks to the many varieties planted by sheep farmers over the century. In addition, ryegrass is cross-pollinated by wind, so genes shuffle frequently. But farmers made the situation far worse. By spraying Hoegrass year after year, they put a strong selection pressure on the plants. They were also diluting the herbicide in order to save money, which increases the risk of resistance. "Convincing people that it's a bad thing to do is not easy," Powles says. "We had to do the science."

When Hoegrass stopped working well, farmers turned to a group of herbicides that block acetolactate synthase, an enzyme involved in making amino acids. But weeds soon evolved resistance to these herbicides as well. "Those are the ones that really hurt [to lose]," says Michael Walsh of UWA, a longtime collaborator of Powles. "They've been the most effective in our cropping system."

Weeds will often become resistant to a specific herbicide while remaining vulnerable to others with different modes of action. Thanks to the weak concentrations that farmers were applying, however, ryegrass evolved a kind of cross-resistance that allowed it to rapidly break down a wide variety of herbicides. The mechanisms behind this are not fully understood. But it meant that Australian farmers lost four classes of herbicides in a matter of years. "They are absolutely cursed with the worst scenario you could come up with," says weed scientist David Shaw of Mississippi State University. Only two herbicide classes, called Photosystem II and long-chain fatty acid inhibitors, remain effective everywhere as a last line of chemical defense.

In 1998, Powles founded the Australian Herbicide Resistance Initiative (AHRI), based at UWA. The group is primarily funded by government and industry fees on harvests. Fifteen scientists and technical staff members conduct field surveys, collect seeds, and test the plants for resistance. They also study the biochemical and genetic mechanisms of resistance. One of the first successes was a collaboration with DuPont that led to the introduction of a mandatory herbicide labeling program, in which each mode of action is clearly identified by a letter. AHRI also launched an educational effort called the ABC campaign to encourage farmers to use different types of herbicides each year.

Catching seeds

The key innovation of the AHRI approach has been to focus on weed seeds. Ryegrass seeds don't last more than a few years in the soil, so if farmers can prevent new seeds from getting into the soil, the number of sprouting weeds will shrink each year. For a long time, farmers were unintentionally doing exactly the opposite. When combine harvesters collect wheat, they loosen the ryegrass seeds from their stalks and cast them over the fields with the chaff, creating a worse problem the following year.

Luckily, the propensity of ryegrass (and many other Australian weeds) to hang onto its seeds until harvest time is also a weakness that can be exploited. In the mid-1980s, a few Australian farmers hitched covered trailers, called chaff carts, behind their harvesters. They catch the chaff and weed seeds, then dump it in piles for burning. Their design took much trial and error. "A lot of guys couldn't get the chaff carts to work properly," Walsh says. "Some threw up their hands and walked away." Further tinkering has made chaff carts easier to use, notes Walsh, who expects them to become more popular despite their AUD $70,000 price tag.

Rodney and Andrew Messina, farmers who grow wheat about 380 km north of Perth, developed a cheaper way to tackle weed seeds. In 1997, they modified their combines so that the chaff from each 10-meter swath would drop into a half-meter-wide line called a windrow. The idea was to burn the windrows after all the wheat has been harvested. Now, the brothers drive across all of their 12,000 hectares, igniting the windrows from a pickup truck outfitted with a gas torch. They set the fires at night, when the heat has eased, cre-

CREDIT: COURTESY OF STEPHEN POWLES

Published by AAAS

ating an eerie panorama of blazing lines as far as the eye can see. "It's a phenomenal amount of work," Rodney says. "But we've seen huge results from it." A few years ago, they bought a farm choked with ryegrass and wild radish. After a few years of burning windrows and spraying herbicides, the weeds are gone.

The Messinas wanted scientists to evaluate the technique, so Walsh and Peter Newman of AHRI measured the temperatures inside the burning windrows and determined that they were highly effective at killing weed seeds. Since the research was completed in 2003, Powles says, windrow burning has been adopted by about 70% of farmers in Western Australia.

The newest tool is an invention called the Harrington Seed Destructor. In 2005, Harrington, the Western Australia farmer, was looking for a way to crush weed seeds. He heard about a mining machine called a cage mill, which pulverizes coal with steel bars whirling at up to 1500 rpm. "I took one look at it and said, 'Nothing will survive in there,'" Harrington recalls. He built a prototype on a one-axle trailer, but ended up parking it behind a barn for a few years because he couldn't figure out how well it would work.

Then he met Powles, who arranged for AHRI to build and test a research version of the contraption. Students spent hundreds of hours picking smashed ryegrass seeds out of the dust to see if they would germinate. Last year they reported in *Crop Science* that at least 95% are destroyed. An engineering company has launched a commercial version. Although the machine costs AUD $250,000, it is better for the soil than burning piles or rows of chaff because it returns all the nutrients in the chaff back into the fields.

Measuring success

Destroying weed seeds can be highly effective. AHRI researchers have studied a total of 31 large wheat fields with multiple-herbicide-resistant ryegrass. They've shown that farmers who target the seeds reduced weeds by 98%. A key to that success is also using herbicides—judiciously and at the correct dose—that are still widely effective, such as trifluralin and clethodim. Equally important is dedication: Farmers who managed their weed seeds every single year had much quicker success than those who did so less frequently, Walsh and colleagues report in *Weed Technology* this month.

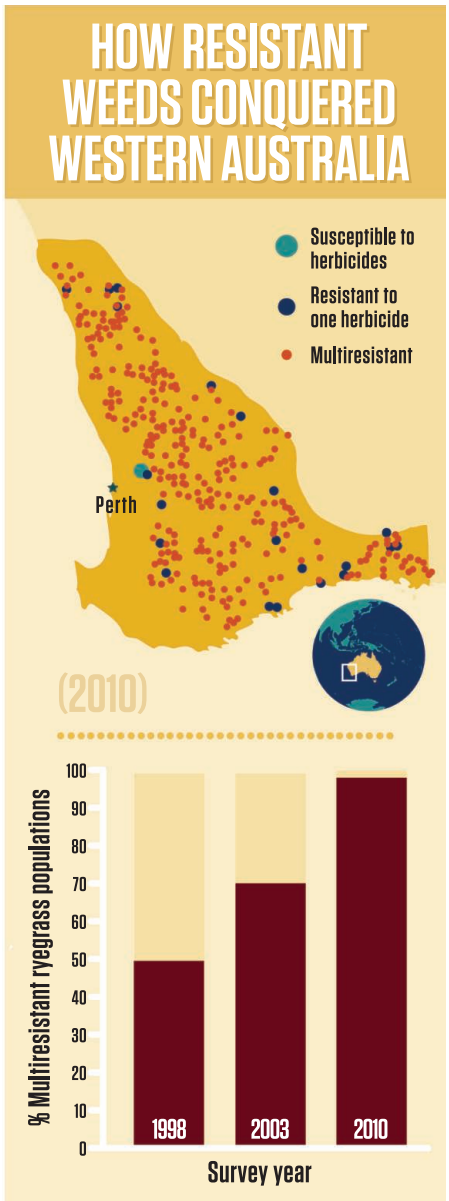

Like wildfire. Weeds have quickly evolved resistance to multiple herbicides all across Western Australia. On the map, each dot represents a study site.

The benefit of mixing weed-seed-capture with herbicides and agronomic approaches, like crop rotation, is that it lowers the odds that resistance will evolve to any one approach. "You confuse the enemy," Powles says. "It's a bit like guerrilla warfare."

AHRI puts a good deal of effort into disseminating these results—Powles himself has a knack for imagery—and encouraging farmers to adopt the techniques. Powles and his team have given thousands of presentations and workshops across the country. "Australian farmers will listen to this message because they've had a crisis," he says. Other researchers credit Powles's easy rapport with farmers, who consider him one of their own.

Powles hopes to persuade farmers in other major agricultural countries to diversify their weed management as well. It's not an easy sell. In 2005, he spent 3 months in the United States, telling farmers what had happened in Australia and urging them to add more diversity to their weed management to prevent the evolution of resistance to glyphosate, which is widely used with genetically modified crops. "It was about a complete waste of time," Powles grumbles. North American weed scientists know the feeling. "We preach and preach and preach," says Patrick Tranel of the University of Illinois, Urbana-Champaign. "At the end of the day, [most farmers] will spend as little money as they can to produce as profitable a crop as they can." Later this month, Powles will try again, embarking on a 6-week speaking tour of the United States. It's not a minute too soon: Palmer amaranth and other herbicide-resistant weeds are becoming a nightmare, particularly in the South.

Despite the progress in Australia, Powles knows that he can't turn his back for long. The most recent survey of Western Australia, in which AHRI staff members drove 15,000 km and sampled 466 wheat fields, found a large increase of herbicide-resistance in wild radish, a particularly nasty competitor with crops. Ultimately, Powles says, the measure of success in the war against weeds is whether farmers can grow their crops over the long haul and earn a decent income. It's a goal that is personal; when he was 10, his grandparents' failed farm was sold. The memory is still vivid.

Seven years ago, Powles bought a farm himself, in Quairading, 180 km east of Perth. ("Probably an emotional rather than a rational judgment," he admits.) The 648-hectare property was thick with weeds resistant to multiple herbicides. Now he's running experiments there to check out the potential for ryegrass to also evolve resistance to the weed seed management he has advocated for so many years. If it can mature earlier and spread its seeds before harvest, for example, the weed might render the carts, the fires, and the seed destruction machines ineffective. But even if that happens, it will only reinforce his main message: Don't rely on any single tool.

–ERIK STOKSTAD

CREDIT: M. OWEN, S. POWLES (MAP); M. OWEN, S. POWLES/*AUS. J. AG. RES.* **58**, 711; *WEED TECH.* **15**, 242 (CHART); G. GRULLÓN/*SCIENCE*

Vietnam Turns Back A 'Tsunami of Pesticides'

Convincing Vietnamese rice farmers to use less pesticide came down to letting them see the benefits for themselves

For years, the entomologists at Vietnam's Southern Regional Plant Protection Center in Long Dinh had tried to sell rice farmers on the benefits of reducing pesticide use—to little effect. So in 2001, they took a different tack: They challenged 950 farmers to try for themselves.

In one plot, the farmers grew rice using their usual amounts of seed and fertilizer, spraying insecticide whenever they thought it was needed—which was often. In a nearby plot, they didn't spray at all for 40 days after planting and used less seed and fertilizer as well. To the farmers' surprise, the yield from the experimental fields was as good or better, while costs were lower, generating 8% to 10% more net income. From then on, they were convinced, recalls Chien Van Ho, who collaborated on the project.

The exercise, designed with colleagues at the International Rice Research Institute (IRRI) of Los Baños, Philippines, was the first step in a campaign that Chien says has led Mekong Delta farmers to cut insecticide spraying from five times per crop cycle to once—or even none at all. Experts are now trying to replicate that success throughout Southeast Asia.

Thanks to misunderstandings about pest control and heavy marketing, Asia's pesticide use has skyrocketed in recent decades. Pesticide imports by 11 Southeast Asian countries grew nearly sevenfold in value between 1990 and 2010, according to U.N. Food and Agriculture Organization (FAO) statistics, with disastrous results. Overuse indiscriminately kills beneficial as well as harmful insects and decimates bird and amphibian populations. Pesticides are also suspected of harming human health and are a common means for rural Asians to commit suicide (see story, p. 738).

Ironically, the main target of this chemical warfare, the brown planthopper (*Nilaparvata lugens*), has become increasingly resistant to it. Over the past 5 years, planthopper outbreaks have devastated rice harvests throughout Asia—"but not in the Mekong Delta," says K. L. Heong, an IRRI insect ecologist. Thanks to the more judicious use of chemicals, natural predators helped keep planthoppers in Vietnam in check.

Clean as a swimming pool

The Green Revolution of the 1960s and '70s introduced sturdier plants that could support the heavier grain loads resulting from intensive fertilizer use. Rice production in Asia more than doubled. But it left farmers believing more is better—whether it's seed, fertilizer, or pesticides.

Rice farmers became accustomed to spraying soon after planting, when they first saw signs of the leaf folder, which appears early in the crop cycle. That bug causes only superficial damage that doesn't reduce yields. Worse, early spraying also takes out the frogs, spiders, wasps, and dragonflies that prey on the brown planthopper, which arrives later and is far more dangerous.

Instead of "landing in a sea of sharks," planthoppers find something as "clean as a swimming pool," Heong says. What's more, tests have shown that killing planthoppers now takes pesticide doses 500 times greater than in the past. More and more planthoppers survive to suck sap from the young rice plants, causing them to wither.

As early as the 1980s, IRRI and the FAO convinced some Southeast Asian governments that with so-called integrated pest management (IPM), natural predators could control planthopppers. In 1986, Indonesia banned 57 pesticides and completely stopped subsidizing their use. But progress was reversed in the 2000s, when growing production capacity, particularly in China, unleashed a "tsunami of pesticides," says FAO entomologist Peter Kenmore. Even some in the agrochemical industry concur. "We all agree that in Vietnam, farmers have overapplied pesticides in some production environments," says Kee Fui Kon, who oversees rice-related R&D at the Swiss agrochemical giant Syngenta.

Radio soap opera

In Vietnam, the Mekong Delta trial helped change conventional wisdom among farmers and agricultural officials. The study led to the "three reductions, three gains" campaign, to convince farmers that cutting the use of seed, fertilizer, and pesticide would boost yield, quality, and income. Word was spread through posters, leaflets, TV commercials, and a serialized radio soap opera, broadcast in 2004, that featured a rice farmer who gradually became convinced of the ben-

Let 100 flowers bloom. Vietnamese rice farmers are encouraged to use less pesticide and to grow flowers and vegetables on the banks of their paddies.

CREDIT: IRRI IMAGES/FLICKR

Published by AAAS

efits of IPM. It didn't hurt that a 2006 planthopper outbreak hit farmers using insecticides harder than those who didn't.

More recently, the Plant Protection Center and IRRI have also been encouraging farmers to grow flowers, okra, and beans on the banks of paddies, instead of stripping vegetation, as was typical. The plants attract bees and a tiny wasp that parasitizes planthopper eggs, while the vegetables diversify farm incomes. Chien says that few Mekong Delta farmers now routinely use insecticides, though many still use fungicides.

"I think that there are signs that things have gone pretty well in Vietnam recently," Kenmore says. Other experts are reserving judgment. "I take the reports [of reduced insecticide use] at face value, but as a scientist I would like to see data," says agroecologist Steve Wratten of Lincoln University in Canterbury, New Zealand. Geoff Gurr of Charles Sturt University, Orange, in Australia, who collaborates with Heong and Chien, says that they are now crunching data from studies on pesticide use and the effects of planting flowers and vegetables; a paper will be ready soon.

Farmers' foe. Brown planthoppers have become increasingly resistant to insecticides.

Syngenta's Kon says that there is still a role for insecticides, especially those targeting other pests, such as stem borers, the larvae of several moth species that feed on rice plants. The company's internal data show that yield gains of 21% can be achieved with the proper use of pesticides, he says.

Other countries are taking note of Vietnam's approach. In 2010 and 2011, massive planthopper outbreaks hit 400,000 hectares of Thai rice fields, causing losses of about $64 million. "We're starting to increase the awareness that farmers are losing a lot because of the misuse of pesticides," says Kukiat Soitong, an extension specialist with the Thai Ministry of Agriculture and Cooperatives. The Thai government is now pushing the "no spray in the first 40 days" approach.

All of these initiatives, Heong says, "have to overcome very powerful marketing forces," such as bundling pesticides in packages with seeds and fertilizer, offering incentives for volume purchases, and hyping the benefits. Here, too, Vietnam is taking action. A proposed law calls for licensing pesticide dealers and government approval of advertisements to prevent exaggerated claims. FAO pest management expert Kevin Gallagher thinks that such regulation is needed throughout the region. "Farmers everywhere are influenced by advertisements," he says. There is "a lot of misinformation everywhere, all the time."

–DENNIS NORMILE

In Rural Asia, Locking Up Poisons to Prevent Suicides

Pesticide ingestion accounts for one-third of the world's suicides. Can a simple plastic lockbox keep toxic chemicals out of desperate people's hands?

When Flemming Konradsen arrived in Sri Lanka's North Central Province in 1993, he aimed to find new ways to control malaria and Japanese encephalitis. But Konradsen, an environmental health biologist at the University of Copenhagen, quickly realized that these mosquito-borne diseases were hardly the region's worst health problem. As others documented in a paper a few years later, people who had intentionally swallowed pesticides occupied far more beds in a provincial hospital than did patients with any one disease.

Farmers in the area used insecticides and herbicides liberally, giving them and their family members ready access to very toxic chemicals at moments of stress. The prevalence of self-poisoning was "very difficult to ignore," Konradsen recalls. Before long, he had shifted his research from mosquitoes to self-harm. Twenty years later, he and colleagues have embarked on a massive study to find out if a specially developed lockbox can reduce the suicide rate by keeping pesticides out of the hands of desperate people.

A little-known problem in the Western world, pesticide ingestion is the leading global means of suicide, accounting for roughly one-third of the estimated 1 million cases annually. Scientists say the easy availability of pesticides contributes to rural Asia's high suicide rates. Asians who kill themselves often have no discernible mental illness; rather, they make impulsive decisions during brief periods of emotional distress (*Science,* 23 November 2012, p. 1025). In the United States, a loaded gun in the home makes adolescents significantly more likely to die by suicide; in Asia, people "don't have guns—they have pesticides," says toxicologist Michael Eddleston of the University of Edinburgh in the United Kingdom.

Reducing access to highly toxic pesticides, Eddleston and colleagues say, is critical to lowering the region's suicide rate. But until recently, international discourse was "dominated by the view that pesticides were an environmental and maybe an occupational issue," Konradsen says.

Fatal gulps

During the Green Revolution of the 1970s, countries like Sri Lanka turned to organic chlorines and organic phosphates to boost crop production. Suicide rates also shot up, Eddleston says: "People taking poison would say 'I'm going to go do a Folidol' "—a brand of methyl parathion, a potent insecticide. With some pesticides, as little as 50 milliliters—a few gulps—can be fatal. Depending on the chemical, death can be triggered by convulsions, respiratory failure, or organ or lung damage.

Drawing attention to this problem was far from easy. Two major treaties governing hazardous pesticides don't mention self-harm at all. Environmental activists don't often address the misuse of pesticides as poison because it makes it "more difficult to highlight the responsibility of the producer," Konradsen says.

Nonetheless, Sri Lanka phased out imports of all World Health Organization (WHO) hazard class I pesticides—the most

CREDIT: IRRI IMAGES/FLICKR

Published by AAAS

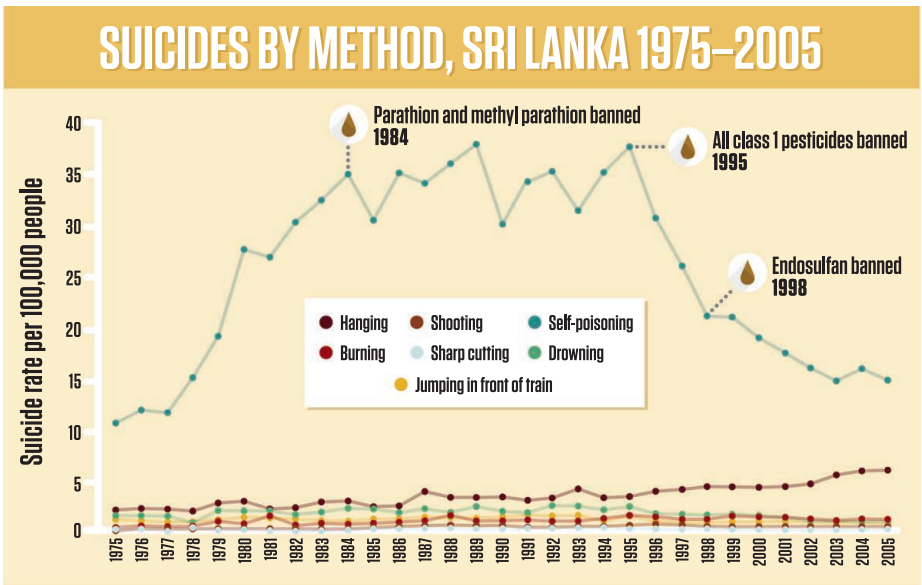

Deadly toll. Easy availability of pesticides has made self-poisoning the most common means to commit suicide in Sri Lanka. Bans on some chemicals have helped reverse the trend.

CREDITS: ADAPTED FROM D. GUNNELL *ET AL.*, *INTERNATIONAL JOURNAL OF EPIDEMIOLOGY* **36** (2007), (CHART) G. GRULLON/*SCIENCE*; MICHAEL EDDLESTON

toxic group—between 1991 and 1995. In 1998, the country also banned endosulfan, a moderately toxic class II pesticide. The suicide rate fell by 50% between 1995 and 2005, even though hospital admissions for pesticide poisoning increased, Eddleston and epidemiologist David Gunnell of the University of Bristol in the United Kingdom noted in a 2007 paper. "It wasn't that people stopped poisoning themselves—they just didn't die," Eddleston says.

Still, self-poisoning remained a major cause of death. In search of additional solutions, Konradsen began working with a local community-based organization and manufacturers in 2004 to fashion a lockbox to store the chemicals safely. Since then, they've tried out a range of designs. A wooden version was too popular with bees and termites. Another prototype made of cement led to broken pesticide bottles, while versions with flimsier lids got trampled by elephants.

For the trial, the team settled on a waterproof, UV-resistant contraption made of plastic, featuring a padlocked inner lid inside a sturdy outer lid that protects the lock from weather damage. The box is partly buried in a field, and the key is generally kept by the family member who applies pesticides—typically the father. The 5-year study, on which Eddleston, Gunnell, and Konradsen are co-investigators, involves 225,000 people and is funded by the Wellcome Trust. Researchers began distributing the lockboxes in 2011 in dozens of randomly selected villages, using another group of villages as controls. The last of 18,980 boxes was distributed in May.

The goal is to see whether the boxes lower the incidence of suicide attempts—and if so, at what cost per life saved. "It seems like a bit of a no-brainer" that there would be a clear effect, Gunnell says. But smaller studies have found mixed or even adverse results. Some farmers moved the box closer to home—apparently feeling that the locked chemicals posed less of a threat—bringing them into closer reach during an impulsive outburst. Waning enthusiasm was another problem: In one study of more than 160 Sri Lankan households, only 55% of containers remained locked after 2 years. And several people in the current study have already broken into boxes and ingested pesticides. (None have died.)

Konradsen says that industry is enthusiastic, touting his previous research as "the solution to all kinds of issues." But at best, lockboxes should supplement bans on toxic chemicals, says Shah Ebrahim, a public health scholar at the London School of Hygiene & Tropical Medicine who chairs the study's independent ethics and data monitoring board. "This is not a panacea."

Richard Brown, head of global stewardship for Syngenta, says that the company is running its own pilot studies on secure storage in India, Sri Lanka, and Suriname with WHO and other partners; Brown is also on the larger trial's advisory board. (The trial receives no industry funding.) There is no "magical fix" for suicide, he says; counseling services and social norms need to be addressed as well. But lockboxes encourage community involvement on the issue of suicide, Brown says, while bans "may encourage farmers to look for banned products on the unregulated black market."

If they prove effective and affordable, lockboxes may be a viable option for other countries as well, such as India and China. Konradsen ultimately hopes to see them become part of a "more holistic" approach to pesticides, including bans. Promoting minimal pesticide use, he notes, would hit a number of key targets—reducing environmental impact, contamination in food, occupational and suicide poisonings, and the development of resistance in disease vectors—all in one fell swoop.

–MARA HVISTENDAHL

Desperate measure. A man is treated after ingesting pesticides in a hospital in Sri Lanka.

Published by AAAS

Growing Up With Pesticides

Long-term studies of the effects of pesticides and other environmental chemicals on the very young brain are coming up with worrisome results

SALINAS VALLEY, CALIFORNIA—It's a sunny July day, sweltering by midmorning. Fields with meticulously maintained rows of lettuce and bushy, berry-laden strawberry plants stretch to the horizon. Farm workers wearing brightly shaded headscarves and layers of clothing—most of them low-income Mexican immigrants—dot the fields. This is "America's salad bowl," a region that grows much of the produce found in grocery stores throughout the country.

At about 3 p.m. in the afternoon, Guillermina Aguilar walks into a small office with her husband and their 12-year-old son Eric, who's about to undergo a series of tests. Aguilar and her family are part of a long-term study into the effects of pesticides and other environmental chemicals at the Center for the Health Assessment of Mothers and Children of Salinas, or CHAMACOS, which is also Mexican slang for "little kids."

Aguilar enrolled in the study when she was pregnant with Eric. At the time, the family lived two blocks from the fields, where the pungent, sweet odor of pesticides often hung heavy in the air. "Sometimes in the mornings I remember I would ask my husband, 'What's that smell?' " Aguilar recalls. But they became accustomed to it. "That was normal for us at that time," Aguilar says. Today she lives in Arkansas; Eric's 12-year assessment takes place during a family visit.

The program, run by the University of California (UC), Berkeley, is one of three U.S. studies that have followed children since the late 1990s to investigate the impact of chemicals in the environment on their brains. The Berkeley program focuses on an agricultural area in California; studies at Columbia University and Mount Sinai School of Medicine look at multiethnic, low-income inner city families in New York City.

The outcomes so far are troubling, although they have been questioned by the pesticide industry. The studies suggest that organophosphates, a widely used class of pesticides that act on the central nervous system, hamper the development of some parts of the brain in children, leading to lower IQs and attention problems. Preliminary evidence also suggests that pesticide exposure may affect sexual differences in certain brain regions during early childhood development.

A main culprit in the Columbia study, chlorpyrifos, was phased out in 2001 for most residential use, and urban exposure in the United States has dropped dramatically—but it's still widely used in agriculture. And a whole generation may already be suffering subtle but prolonged effects, says epidemiologist Virginia Rauh, deputy director of the Columbia Center for Children's Environmental Health.

Critical stages

Research in lab animals and farm workers has shown that chronic exposure to high doses of pesticides is associated with neuro-degenerative diseases such as Parkinson's disease and cognitive deficits. More recently, researchers started looking at how exposure in the womb and in infancy affects the developing brain—a quest spurred in part by a growing awareness of neurobehavioral and neurodevelopmental disorders such as attention deficit hyperactivity disorder (ADHD) and learning disabilities. In the 1990s, "we realized that we needed to understand what children were being exposed to in the womb and in the early months and years of their lives," says Frederica Perera, director of the Columbia center.

All three studies recruited hundreds of pregnant mothers in the late 1990s, measured their exposure to environmental chemi-

CREDIT: KIMBERLY L. PARRA

Published by AAAS

Mind at risk? A boy is playing near a lettuce field in Salinas Valley.

cals, and gave their kids a battery of tests at various intervals. The Columbia researchers also obtained umbilical cord blood samples directly after birth, allowing them to measure fetal exposure to several pesticides directly; the Berkeley team collected urine samples during pregnancy and early childhood, and searched for pesticides' breakdown products. The researchers compared the intellectual development of children with varying levels of pesticide exposure within each group, controlling for confounding variables such as sex, race or ethnicity, maternal education, family income, and other toxic exposures.

Early on in the Berkeley study, infants with high fetal exposures showed abnormal reflexes. At age 2, the highly exposed children had lower mental development, and the researchers found an increase in ADHD-like behaviors at age 5. At age 7, highly exposed children scored 7 points lower on the full-scale IQ score, which includes tests of verbal comprehension, working memory, processing speed, and perceptual reasoning—a drop similar to that found in studies of childhood lead exposure. It translates to about a 6-month developmental lag, says reproductive epidemiologist Kim Harley of the UC Berkeley center.

While the California study looked at a range of organophosphates used in agriculture, the Columbia team zoomed in on chlorpyrifos, which was widely used indoors to kill ants, termites, and cockroaches. Even after indoor use largely ended in 2001, it's still used to control agricultural pests under the Dow Chemical trade name Lorsban. The company also continues marketing chlorpyrifos for residential use in developing countries.

The Columbia team realized that chlorpyrifos might be important after they discovered detectable levels in the umbilical cord blood samples from 71% of their pregnant women in the late 1990s. "That was a wake-up call for all of us," says Columbia University molecular epidemiologist Robin Whyatt. "Whereas one generally thought about pesticides as an agricultural risk, it really became clear that in New York City, because of the cockroach problem, they are definitely an urban risk as well."

The team found that infants with high exposures to chlorpyrifos and another commonly used organophosphate called diazinon had lower birth weight and birth length, "on the order of what one would see with active cigarette smoking during pregnancy," Whyatt says. The team also reported abnormal reflexes in newborns, as well as deficits in IQ and attention, and behavioral problems as the children matured.

Rauh, along with Columbia developmental neuropsychiatrist Bradley Peterson, also performed an MRI study on the brains of 40 children aged 5 to 11, half of them from the high exposure group. In a 2012 paper in the *Proceedings of the National Academy of Sciences*, they reported that the volumes of a number of brain regions that are important in emotion, social cognition, and inhibition were altered in highly exposed children. What's more, some normal sex-specific differences in the sizes of certain brain regions were not seen in children with high prenatal exposure—findings consistent with effects seen in animals. That suggests chlorpyrifos may interfere with normal sexual differentiation of the brain, Rauh says—although what that means for the kids is unclear. The team is now conducting a study in 250 children to confirm the results.

> "Pesticides were designed to be neurotoxic. Why should we be surprised if they cause neurotoxicity?"
>
> —Bruce Lanphear, Simon Fraser University

Chlorpyrifos and other organophosphates work by inhibiting cholinesterase, a family of enzymes that break down acetylcholine, a neurotransmitter that plays many key roles in the brain. When exposure occurs during prenatal development, these compounds "essentially misdirect the assembly of the brain," says Theodore Slotkin of Duke University in Durham, North Carolina, who has extensively studied pesticides' effects on animals.

State of the art

Dow Chemical has long tried to poke holes in the research that finds detrimental effects from pesticides. In response to the imaging study, for instance, the company issued a statement pointing to what it says are limitations in the research, such as the fact that the scans "provide only a single snap-shot in time," and that confounding factors were controlled "only imperfectly or not at all." A company spokesman adds that "no mechanism of action has been determined by these researchers that would explain how these outcomes would come about."

Joseph Braun, an epidemiologist at Brown University, calls the imaging study "cutting edge and very novel" but cautions that replication is necessary. Bruce Lanphear, a pediatric epidemiologist at Simon Fraser University, Vancouver, in Canada, says that the MRI results weren't surprising. In 2008, he and others reported similar structural brain changes associated with childhood lead exposure. Lanphear calls the cohort studies "highly regarded" and "state of the art." "Pesticides were designed to be neurotoxic," he says. "Why should we be surprised if they cause neurotoxicity?" (Neither Braun nor Lanphear was involved in the study.)

The indoor regulation on chlorpyrifos has reduced exposure in some populations, and use of that compound and other organophosphates is steadily declining in U.S. agriculture as well. But researchers worry about the safety of their replacements, such as the pyrethroids, which now comprise the majority of household pesticides and are also heavily used on farms. Harley likens the succession of chemicals to a game of "whack-a-mole," in which one compound is banned, only to be replaced by another whose safety is not assured.

As noon approaches under the relentless California sun, workers—men and women—are bent over, quickly and methodically shaking the strawberry plants, plucking the reddest and ripest of the berries, then stacking them inside clear, plastic cartons labeled with common household names. It would be difficult to grow all of this produce at the current prices without pesticides; the CHAMACOS researchers are the first to admit that it's a complex problem. "Now that we've been in the Salinas Valley for 13 years, we get to see all sides of the issue," says Berkeley epidemiologist Brenda Eskenazi, who heads the study.

Harley agrees—but given the choice, she buys mostly organic produce. Not just to protect her own children, she says, but those of the men and women working in these fields.

–AMANDA MASCARELLI

Amanda Mascarelli is a science writer in Denver. Her reporting was supported by the California Endowment Health Journalism Fellowships, a program of the University of Southern California's Annenberg School of Journalism.

REVIEW

Current Challenges and Trends in the Discovery of Agrochemicals

Clemens Lamberth,* Stephane Jeanmart, Torsten Luksch, Andrew Plant

Crop protection chemistry has come a long way from its "alchemic" beginnings in the late 19th century to a high-tech science that supports the sustainable production of food, feed, and fiber for a rapidly growing population. Cutting-edge developments in the design and synthesis of agrochemicals help to tackle today's challenges of weed and pest resistance, higher regulatory safety margins, and higher cost of goods with the invention of selective, environmentally benign, low use rate, and cost-effective active ingredients.

Since the earliest days of agriculture, humans have had to protect their crops against yield loss from weeds, insect pests, and diseases. Seedlings are in competition with undesired vegetation (weeds) for light, space, nutrients, and water. Harvest devastation by insects and fungal diseases has been known since biblical times. Many of these problems could be solved over time, but feeding a steadily growing population, which is projected to reach more than 9 billion people in 2050 (*1*), remains a vital global challenge that necessitates the integration of different technologies into modern agriculture: improved agrochemicals, seeds, fertilizers, mechanization, and precision farming. Here, we review current and emerging technologies for chemical crop protection (*2*–*4*). Developments over the past 50 years have enabled dramatic reduction of use rates, with concomitant improvements in environmental impact. Whereas even as recently as the 1960s more than 1 kg of a crop protection chemical was typically applied per ha, today application rates can be as low as 10 g/ha, only 1% of that formerly required. Examples of low-use-rate active ingredients (AIs) include the sulfonylurea herbicides (*5*), the piperidinylthiazole fungicides (*6*), and the mectin insecticides and acaricides (*7*). To put this in perspective, 10 g/ha means that only one teaspoon of an AI is required to protect the area of a soccer pitch. There is already a clear trend toward molecules that combine such low use rates with a more favorable toxicology profile (*8*). However, increasing resistance of weeds and pests to established agrochemical compound classes, an increasingly stringent regulatory environment, as well as market growth has stimulated demand for more selective, safer, resistance-breaking, cost-effective chemicals.

Scientists in crop protection research use a variety of chemical inputs from which new lead areas of chemistry are derived: natural products (*9*, *10*), competitor-inspired chemistry (*11*, *12*), compound acquisition from universities, chemical vendors (*13*, *14*), combinatorial chemistry libraries (*15*, *16*), intermediates from projects in other indications (*2*, *11*), and compound collections from pharmaceutical and animal health companies (*2*, *11*). Despite these varied sources of new chemistry, the number of new molecule introductions to the market place has declined in recent years (*17*). Furthermore, the R&D costs to bring a new AI to market have been rising (from U.S. $152 million in 1995 to $256 million in 2005), as have the number of compounds synthesized to deliver one new market introduction (from 52,500 in 1995 to 140,000 in 2005) (*16*). The screening hits obtained from the above-mentioned sources are usually optimized through diverse rounds of a design-synthesis-test-analysis cycle (Fig. 1). Typical for agrochemical research is the testing of all compounds directly on the whole organism, that is, the weed, fungus, or insect. However, molecular target-based approaches using in vitro assays are becoming more and more common. Three major challenges facing R&D-focused companies today are resistance and its impact on the performance of an agrochemical product, increasing regulatory safety margins, and cost of goods. In what follows, we seek to demonstrate how the application of new design strategies as well as state-of-the-art organic chemistry can deliver solutions for the discovery of agrochemicals fit for purpose for the 21st century.

Special Requirements of Agrochemicals

Modern agrochemicals and pharmaceuticals interact with their target receptors or enzymes via the same molecular recognition processes. In several cases, a homologous enzyme/receptor is addressed, so it is not altogether surprising that one compound class can give rise to (different) AIs serving both industries, for example, the triazole antimycotics or fungicides (*18*). However, although bioavailability is vital to both pharmaceuticals and agrochemicals, the chemical environments the AIs encounter en route from the site of application to the biochemical target are very different and generally require differing physicochemical properties (*15*, *19*). Notably, Tice, Clarke, and Delaney have shown that agrochemicals have a lower number of hydrogen bond donors (*20*–*22*). For example, over 70% of the insecticides have no hydrogen bond donor, and over 90% of herbicides have two or fewer hydrogen bond donors (*20*). Also, for agrochemicals to meet growers' needs of longest possible spray intervals, they

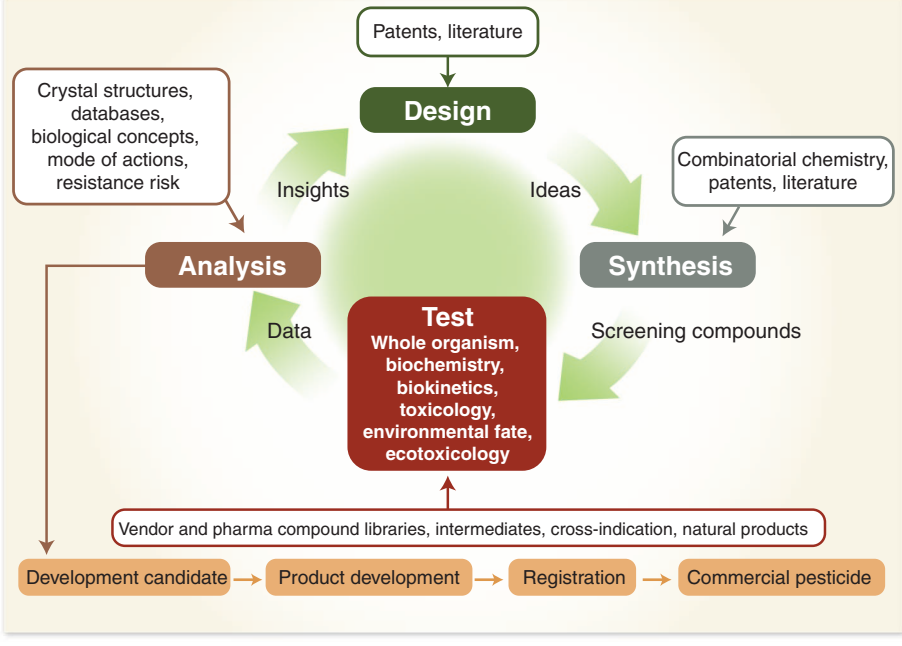

Fig. 1. Innovation and optimization process in crop protection research. There are many similarities to the design-synthesis-test-analysis cycle applied in the pharmaceutical industry.

Syngenta Crop Protection AG, Research Chemistry, Schaffhauserstrasse 101, CH-4332 Stein, Switzerland.

*Corresponding author. E-mail: clemens.lamberth@syngenta.com

should have residual activity and persistence of effect, lasting up to several weeks. The fact that the majority of heterocycles found in agrochemicals are heteroaromatics illustrates this point (*20*). In addition, the product cost of an agrochemical is generally much more constrained compared with that of a pharmaceutical invented to meet an unmet medical need. Thus, the selection of the most cost-effective molecule for a particular market, coupled with an inexpensive manufacturing route, plays an important role.

Efficient Synthesis of Agrochemicals

More than 70% of AIs introduced to the market within the past 30 years possess heterocyclic scaffolds (*23*), and a similar number contain halogen substituents (*24*, *25*). Around one-third of all agrochemicals are chiral compounds, a trend that appears to be increasing (*26*, *27*), and some of the most important and most abundantly manufactured have been introduced in an enantiomerically or diastereomerically enriched form, such as the herbicide (*S*)-metolachlor, the fungicide (*R*)-metalaxyl, and the insecticide indoxacarb (**12**). Notably, the manufacture of the grass herbicide (*S*)-metolachlor, which has its basis in the Ir-catalyzed enantioselective hydrogenation of an imine and is manufactured on a scale of >10,000 tons/year, is among the masterpieces of large-scale crop protection chemical synthesis (*28*). Further examples for the state-of-the-art organic chemistry used in the manufacturing of modern crop protection chemicals include the production of three different commercial fungicides, which incorporate the world's largest production volumes (in tons/year) of three well-known named reactions: boscalid is produced via a Suzuki-Miyaura coupling as a key step (*29*), cyproconazole via a Simmons-Smith cyclopropanation (*30*), and fludioxonil via a van Leusen (p-toluenesulfonylmethyl isocyanide–based) pyrrole synthesis (*31*). Another modern name reaction, the copper-promoted Chan-Lam arylation, was discovered in the research department of DuPont Crop Protection (*32*). Further proof of the fact that crop protection chemistry is often at the forefront of organic chemistry is the large-scale production of pinoxaden (**3**), a new herbicide for the selective postemergence control of grass weeds in cereals, which inhibits acetyl-coenzyme A carboxylase (ACC), an important enzyme in fatty acid biosynthesis. During the development of the most efficient synthetic route to **3**, it turned out that the introduction of a malonyl equivalent into a highly sterically hindered position of a benzene ring in starting material **1** was hitherto unknown (Fig. 2). The transition-metal–catalyzed C-C coupling between the aryl bromide **1** and malononitrile, developed by scientists at Syngenta and Solvias, delivers arylmalonitrile **2**, which is then converted in only three further steps into pinoxaden (**3**) (*33*, *34*). Two elegant routes have been worked out at Bayer CropScience toward tetrasubstituted biphenyl derivatives **8**, which are key intermediates in the synthesis of bixafen (**9**), a broad-spectrum fungicide that blocks the fungal respiratory chain by inhibition of succinate dehydrogenase (*35*). One possibility for the synthesis of **8** is the Goossen-type Pd/Cu-catalyzed decarboxylative cross-coupling of the potassium benzoate **4** with 1-bromo-3,4-dichlorobenzene (**5**), delivering the nitrosubstituted trihalogenated

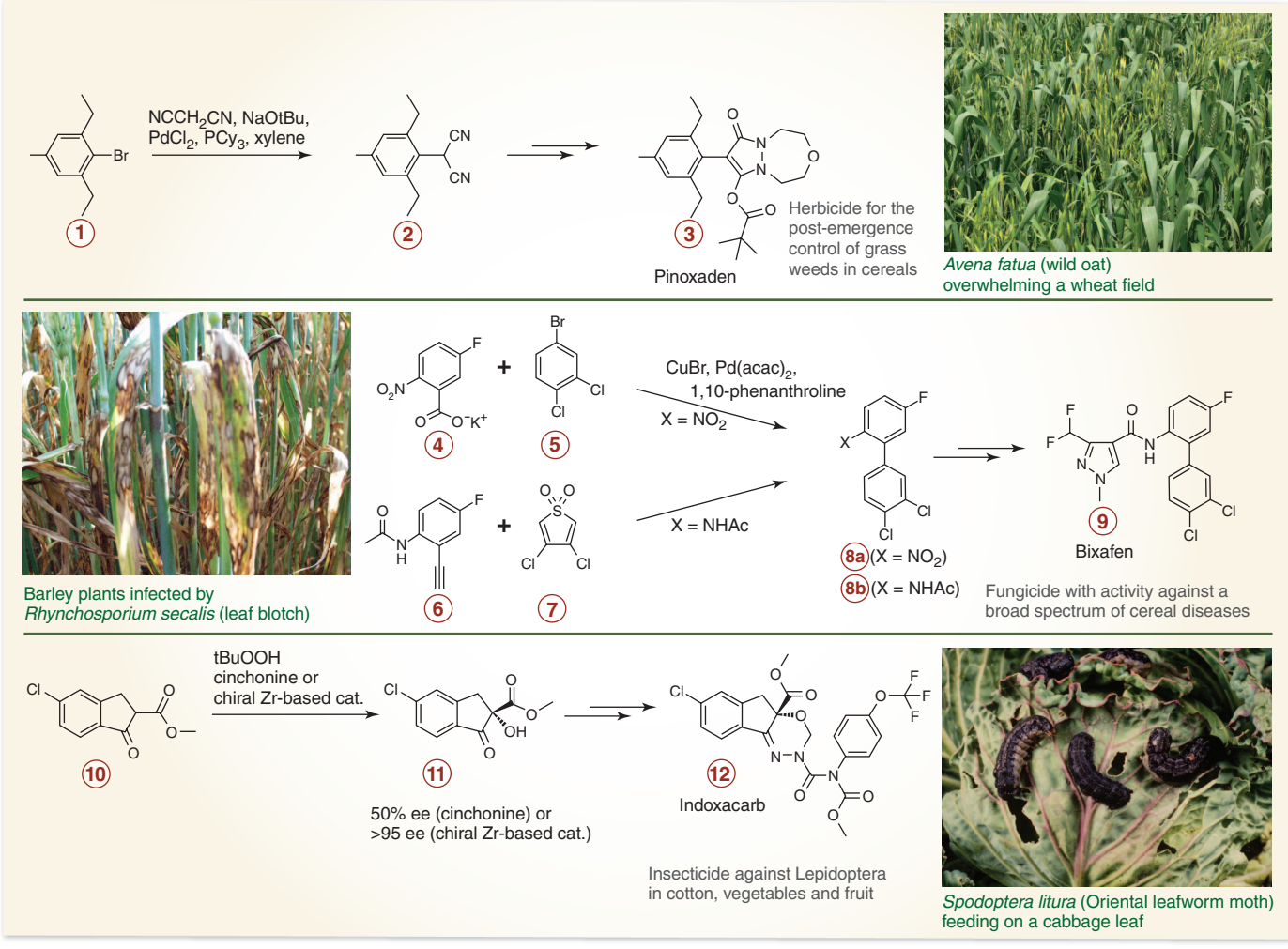

Fig. 2. Key steps in the synthesis of selected agrochemicals. Cy, cyclohexyl; acac, acetylacetonate; Bu, butyl group; Ac, acetyl group.

biphenyl **8a** (*35*). Alternatively, the phenylacetylene derivative **6**, which is readily prepared in two steps from the corresponding bromobenzene precursor, is converted in a tandem Diels-Alder cycloaddition-cycloreversion sequence with 3,4-dichlorothiophene 1,1-dioxide (**7**) to the anilide **8b** (*37*). Both key intermediates, **8a** and **8b**, are then transformed to the unprotected aniline and acylated to obtain bixafen (**9**). The finding that only the (*S*)-enantiomer of the insecticide indoxacarb (**12**), which blocks the voltage-gated sodium channel of the target pests, possesses insecticidal activity created the desire for an efficient enantioselective synthesis. Besides the complexity of the tricyclic core scaffold, the tetrasubstitution at the chiral carbon center rendered the synthesis especially challenging. Scientists at DuPont solved this problem by asymmetric α-hydroxylation of the indanone ester **10** with *tert*-butyl hydroperoxide and cinchonine as a chiral base, obtaining a 3:1 product ratio in favor of the biologically active (*S*)-enantiomer [50% enantiomeric excess (e.e.)]. The enantioselectivity could be increased to 95% e.e. by application of a chiral zirconium-based catalyst. The resulting 2-hydroxyindanone ester **11** was transformed in four further steps to indoxacarb (**12**) (*37*, *38*).

Structure-Based Design

Structure-based design is an iterative and multidisciplinary process that is well-established in the pharmaceutical industry (*39*–*41*). It played an important role in the development of several registered drugs and clinical candidates, for example, nelfinavir (*42*), zanamivir (*43*), and aleglitazar (*44*). In contrast, structure-based design is relatively new in the agrochemical industry, and there are currently no products on the market that are the direct result of this approach (*2*). However, there are several examples of discovery programs where structure-based design has had a strong impact.

The development of scytalone dehydratase inhibitors as rice blast fungicides is one of the most detailed examples that has been reported in the field of crop protection (*45*). Scytalone dehydratase is part of the fungal melanin biosynthetic pathway, and its disruption leads to a loss of fungal pathogenicity (*46*, *47*). The crystal structure of *Magnaporthe grisea* scytalone dehydratase in complex with a salicylamide ligand **13** (*48*) served as the starting point for the design of novel inhibitors [Protein Data Bank (PDB) code 1STD; Fig. 3 left] (*49*). It was hypothesized that the binding pocket would be large enough to accommodate elongated inhibitors. To investigate this, a phenoxypropyl salicylamide **14** (Fig. 3, right) was designed and synthesized, and indeed, although the activity dropped ninefold in comparison to the starting compound, in the enzyme assay it still remained in the picomolar range. Next, crossover compounds with diclocymet, a commercial rice blast fungicide, were designed. The aryl ring in the acid moiety of **14** was replaced, but the phenoxypropyl fragment retained, leading to compound **15**, which has an inhibition constant of 20 pM and provides excellent control of rice blast disease in field trials (*50*). Crystal structures of the enzyme in complex with the new lead compounds were subsequently solved, and a comparative analysis of these structures indicated the presence of conformationally flexible regions in the binding pocket. This information was incorporated into the design, and inhibitor **16**, which carries an additional phenyl substituent, was envisaged to optimize interactions with an adjacent phenylalanine (*50*). The binding mode was again validated and confirmed by x-ray crystallography. The scytalone dehydratase inhibitors are buried in a lipophilic binding site, and therefore potency can be improved by adding lipophilic groups that fit in the binding pocket. However, activity on the whole organism depends not only on enzyme activity but also on bioavailability, which decreases when hydrophobicity becomes too high. Basarab *et al.* showed that the analysis of scytalone dehydratase crystal structures can generate new ideas for increasing ligand hydrophilicity (*51*). For example, the salicylamide **13** makes a hydrogen bond with Asp^{131}; by replacing the hydroxyphenyl group with a butyrolactam, as was done in **17**, two hydrogen bonds can be formed with this residue. As a result, polarity is increased and excellent in vivo activity obtained, which was not present in the initial salicylamide **13** (*50*).

Structure-based design is a growing discipline within crop protection research. One of the key drivers has been the huge increase in the number of protein structures in the public domain, which has increased from 13,600 to 92,700 over the past 13 years (www.pdb.org) (*52*). This increase is due to advances in gene sequencing, recombinant protein production and purification, protein crystallography, and the organization of structural genomics centers (*53*). Many crystal structures of agrochemicals bound to their target sites are now in the public domain, for example, ACC in complex with pinoxaden enolate in the herbicide indication (PDB code

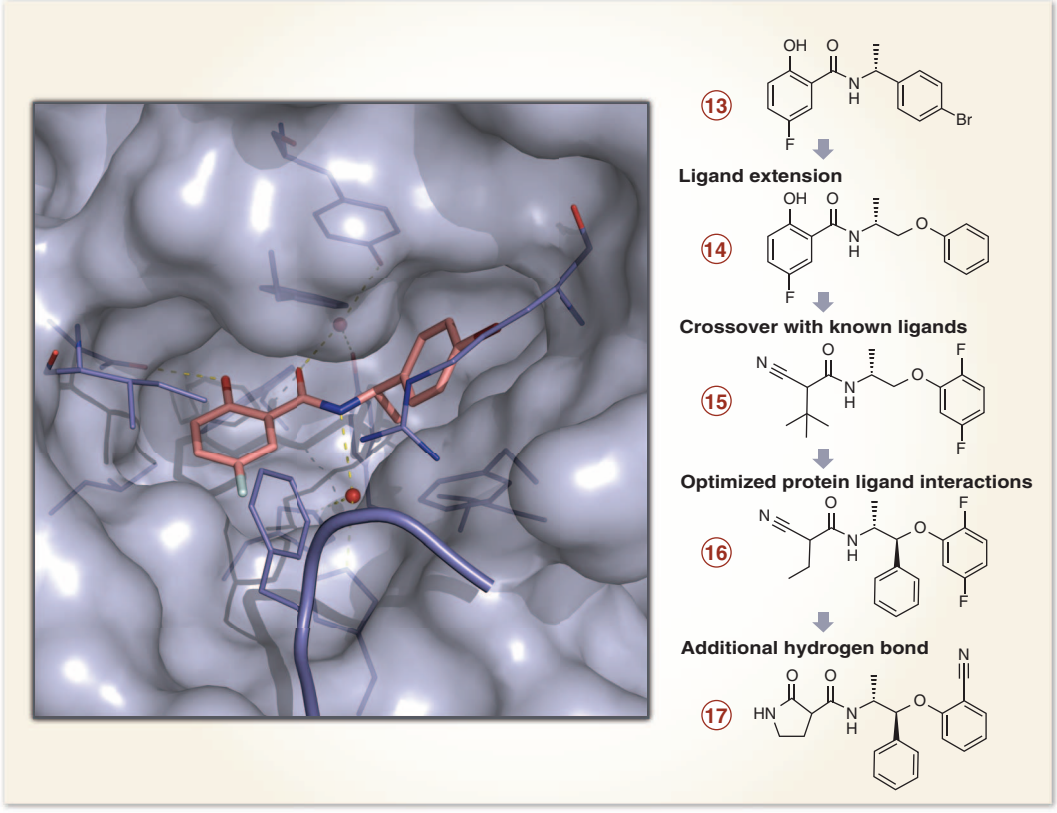

Fig. 3. Iterative structure-based design steps leading to fungicidal scytalone dehydratase inhibitors. (Left) Crystal structure of *M. grisea* scytalone dehydratase in complex with a salicylamide ligand (PDB code 1STD). The protein is displayed as a surface with key amino acids involved in ligand interactions shown as blue sticks. The ligand is displayed as pink sticks, hydrogen bonds as yellow dotted lines, and water molecules as red dots. **(Right)** Optimization of scytalone dehydratase inhibitors through multiple design-synthesis-test-analysis cycles.

3PGQ) (*54*), azoxystrobin bound to the cytochrome bc_1 complex in the fungicide indication (PDB code 3L71), and methamidophos bound to acetylcholinesterase in the insecticide indication (PDB code 2JGE) (*55*); these can be used for structure-based design. Moreover, the structures of several ion channels—notoriously difficult to crystallize but of high interest to crop protection research—are now in the public domain. For example, the crystal structure of a glutamate-gated chloride channel in complex with ivermectin, a member of the mectin class of insecticides, was reported in 2011 (*56*) and represents a solid starting point for the design of novel insecticidal glutamate-gated chloride channel activators. In 2009, a crystal structure of a pentameric ion channel was published (*57*). On the basis of this structure, researchers at Mitsui recently generated a homology model for a related γ-aminobutyric acid (GABA)–gated chloride channel and proposed a binding mode for the *meta*-diamides (*58*), a class of potent insecticides that is currently being investigated by many agrochemical companies. This last example demonstrates how valuable starting points for structure-based design can be obtained from the structure of a related protein in cases where the actual target structure is unknown. Such a homology modeling approach can be very powerful if validated by experimental techniques like site-directed mutagenesis.

Fragment- and Target-Based Design

"Chemistry first" has been, until recently, the sustained basis for the discovery of agrochemicals (*59*). The fact that chemicals could be directly tested in vivo favored this approach. Nowadays, the above-mentioned challenges are forcing the industry to consider alternative ways of finding new leads. Also, new technologies offer additional opportunities to generate leads in different and faster ways. Modern techniques like fragment-based design (*60*), virtual screening, and genome sequencing—developed primarily in the pharmaceutical or biotechnology industries—have been successfully applied for the generation of drug leads. These tools can also be applied to the discovery of agrochemicals as long as the differences between pharmaceuticals and agrochemicals are accounted for, for example, the aforementioned physicochemical properties. Thus far, however, published examples of fragment-based design in the agrochemical context have been comparatively rare. In one instance, the method was used to generate new fungicidal inhibitors of ACC, an enzyme already successfully targeted by herbicides and insecticides (*61*). Dow AgroSciences, in collaboration with Locus Pharmaceuticals, used a combination of in silico fragment-based design with in-house protein-ligand crystal structures to yield synthetically amenable compounds (*61*). These compounds broadened the chemical scope in the ACC inhibitor area, which has been extensively studied by many companies over the past 30 years (*33*, *62*). Recently, Hao *et al.* reported a virtual fragment screening to discover cytochrome bc_1 inhibitors (*63*). Common to all inhibitors is the methoxyacrylate warhead, whose interactions and position are well known from the strobilurin fungicides (*64*). Fragments were linked to the warhead to form a virtual library. In the pharmacophore-linked fragment virtual screening, the position of the warhead was kept constant, and the interactions of the side chains were explored. Picomolar inhibitors of the cytochrome bc_1 complex were found. Although weaker than the commercial compounds such as azoxystrobin, the molecules described by Hao *et al*. showed good biological activity in vivo.

The likelihood of finding active analogs on the basis of a screen hit from a novel scaffold can be increased by virtual screening techniques (*65*). This approach, successfully applied in drug discovery programs, has been validated in agrochemical research (*19*, *66*). Because the pharmacophore of the reference ligand is well defined, a virtual library of potential herbicidal inhibitors of the enzyme anthranilate synthase (*15*) was generated by keeping the core scaffold constant and attaching different linkers to it. The scores obtained from the docking studies were used for ranking these molecules. Novel compounds were then synthesized, tested, and showed a primary hit rate of 10.9%, which is a much higher rate than for conventional high-throughput screening (*15*). Of course, it is rarely the case that the pharmacophore is well defined within a lead generation program. Other tools like three-dimensional (3D) shape, atom-type similarity, or 2D extended connectivity fingerprints also retrieve molecules of interest out of a database with success rate matching the data found in the pharmaceutical literature (*67*). Scaffold-hopping is also efficiently achieved by virtual screening, with 2D and 3D variants providing the best results (*66*).

Progress in genome-sequencing technologies over the past decade has made available the DNA sequences of many organisms. This, combined with gene-knockout or antisense knockdown techniques, has provided agrochemists with a method for validating potential new biochemical targets for pesticides (*59*, *67*–*69*). However, two key factors have to date restricted this approach from yielding effective leads. On one hand, some genes, like avirulence genes or proteins responsible in the development of the infection, are not appropriate targets because they are not essential for the organism (*68*, *69*). On the other hand, there is a lack of known inhibitors for many potential targets. Such hits can be found by screening compound libraries against the identified biochemical target. Recent examples of applying this procedure include the search for new herbicidal compounds of the nonmevalonate pathway (*70*). For example, Witschel *et al*. found new inhibitors of 2-C-methyl-D-erythritol 4-phosphate cytidylyltransferase (IspD, Enzyme Commission (EC) number 2.7.7.60) with the best hit having a half maximal inhibitory concentration (IC_{50}) of 140 nM (*71*). This hit showed good activity in the greenhouse at 3 kg/ha (*71*). Thanks to an x-ray crystal structure of *Arabidopsis thaliana* IspD enzyme cocrystallized with the inhibitor, a more potent inhibitor with an IC_{50} of 35 nM was designed (*70*, *71*). Mitochondrial serine-hydroxymethyl transferase (SHMT) inhibitors were also found by the same group at BASF. Three hundred thousand compounds were tested against the SHMT enzyme, and 24 hits were found. Among those hits, a subclass was followed with in vivo screening and compounds were promoted to field trials (*72*).

Conclusions and Outlook

The new research technologies described above will need to prove their worth further still and provide a sustained industry pipeline leading to commercial products that meet growers' needs. Despite the modern arsenal of crop protection chemicals available to growers and farmers today, the grand challenge of providing food security to a world population of 9 billion people in 2050 will test the innovative capabilities of industry and academia alike. Overcoming the hurdles of limited arable land, increasingly frequent extreme weather events, and weed and pest resistance and reaching the goal of enhanced toxicological and environmental safety will require the crop protection industry and the academic community to continue to develop new research tools. New commercial opportunities are emerging, such as providing farmers with products that enhance plant performance and secure yield potential under conditions of abiotic stress, such as drought and salinity. Science and technology, including novel chemistry, will need to be developed to allow growers to fully bring the potential of plants to life.

References and Notes

1. Population Division of the United Nations Department of Economic and Social Affairs, www.un.org/en/development/desa/index.html.
2. A. Plant, *Agrow Silver Jubilee Issue*, XI–XV (2010).
3. U. Müller, *Pure Appl. Chem.* **74**, 2241–2246 (2002).
4. J. Stetter, F. Lieb, *Angew. Chem. Int. Ed.* **39**, 1724–1744 (2000).
5. O. Ort, in *Modern Crop Protection Compounds*, W. Krämer, U. Schirmer, P. Jeschke, M. Witschel, Eds. (Wiley-VCH, Weinheim, Germany, 2012), pp. 50–88.
6. M. A. Hanagan, R. J. Pasteris, R. Shapiro, Y. Henry, B. Klyashchitsky, paper presented at the 242nd American Chemical Society (ACS) National Meeting, Denver, CO, 28 August to 1 September 2011, abstr. no. AGRO-79.
7. T. Pitterna *et al*., *Bioorg. Med. Chem.* **17**, 4085–4095 (2009).
8. R. M. Hollingworth, in *Agrochemical Discovery*, D. R. Baker, N. K. Umetsu, Eds. (American Chemical Society, Washington, DC, 2001), pp. 238–255.
9. C. L. Cantrell, F. E. Dayan, S. O. Duke, *J. Nat. Prod.* **75**, 1231–1242 (2012).
10. F. E. Dayan, C. L. Cantrell, S. O. Duke, *Bioorg. Med. Chem.* **17**, 4022–4034 (2009).
11. C. Lamberth, *Nachr. Chem.* **55**, 130–134 (2007).
12. K. N. Winzenberg, *Chem. Aust.* **63**, 491–493 (1996).
13. G. Phillips *et al*., *Org. Process Res. Dev.* **6**, 357–366 (2002).
14. J. A. Sternberg *et al*., *Pest Manag. Sci.* **57**, 143–152 (2001).
15. S. D. Lindell, L. C. Pattenden, J. Shannon, *Bioorg. Med. Chem.* **17**, 4035–4046 (2009).
16. S. Smith, *Pestic. Outlook* **14**, 21–26 (2003).
17. P. McDougall, presentation for the ABIM (Annual Biocontrol Industry Meeting) Conference, Lucerne,

Switzerland, 22 to 24 October 2012; www.abim.ch/fileadmin/documents-abim/Presentations_2012/ABIM_2012_6_McDougall_John.pdf.
18. L. Zirngibl, *Antifungal Azoles* (Wiley-VCH, Weinheim, Germany, 1998).
19. K.-J. Schleifer, in *Pesticide Chemistry*, H. Ohkawa, H. Miyagawa, P. W. Lee, Eds. (Wiley-VCH, Weinheim, Germany, 2007), pp. 77–88.
20. C. M. Tice, *Pest Manag. Sci.* **57**, 3–16 (2001).
21. C. M. Tice, *Pest Manag. Sci.* **58**, 219–233 (2002).
22. E. D. Clarke, J. S. Delaney, *Chimia (Aarau)* **57**, 731–734 (2003).
23. C. Lamberth, J. Dinges, in *Bioactive Heterocyclic Compound Classes - Agrochemicals*, C. Lamberth, J. Dinges, Eds. (Wiley-VCH, Weinheim, Germany, 2012), pp. 3–20.
24. P. Jeschke, in *Modern Methods in Crop Protection Research*, P. Jeschke, W. Krämer, U. Schirmer, M. Witschel, Eds. (Wiley-VCH, Weinheim, Germany, 2012), pp. 73–128.
25. G. Theodoridis, in *Fluorine and the Environment – Agrochemicals, Archaeology, Green Chemistry and Water*, A. Tressaud, Ed. (Elsevier, Amsterdam, 2006), pp. 121–175.
26. N. Kurihara, J. Miyamoto, Eds., *Chirality in Agrochemicals* (Wiley, Chichester, UK, 1998).
27. G. M. Ramos Tambo, D. Belluš, *Angew. Chem. Int. Ed. Engl.* **30**, 1193–1215 (1991).
28. H.-U. Blaser, *Adv. Synth. Catal.* **344**, 17 (2002).
29. J. Rheinheimer, in *Modern Crop Protection Compounds*, W. Krämer, U. Schirmer, P. Jeschke, M. Witschel, Eds. (Wiley-VCH, Weinheim, Germany, 2012), pp. 627–639.
30. A. B. Charette, A. Beauchemin, *Org. React.* **58**, 1–415 (2001).
31. C. Lamberth, in *Bioactive Heterocyclic Compound Classes - Agrochemicals*, C. Lamberth, J. Dinges, Eds. (Wiley-VCH, Weinheim, Germany, 2012), pp. 155–162.
32. D. M. T. Chan, P. Y. S. Lam, in *Boronic Acids*, D. G. Hall, Ed. (Wiley-VCH, Weinheim, Germany, 2005), pp. 205–240.
33. J. Wenger, T. Niderman, C. Mathews, in *Modern Crop Protection Compounds*, W. Krämer, U. Schirmer, P. Jeschke, M. Witschel, Eds. (Wiley-VCH, Weinheim, Germany, 2012), pp. 447–477.
34. A. Schnyder, A. F. Indolese, T. Maetzke, J. Wenger, H.-U. Blaser, *Synlett* **2006**, 3167–3169 (2006).
35. H. Walter, in *Bioactive Heterocyclic Compound Classes - Agrochemicals*, C. Lamberth, J. Dinges, Eds. (Wiley-VCH, Weinheim, Germany, 2012), pp. 175–193.
36. C. Lamberth, *Bioorg. Med. Chem.* **17**, 4047–4063 (2009).
37. S. F. McCann, D. Cordova, J. T. Andaloro, G. P. Lahm, in *Modern Crop Protection Compounds*, W. Krämer, U. Schirmer, P. Jeschke, M. Witschel, Eds. (Wiley-VCH, Weinheim, Germany, 2012), pp. 1257–1273.
38. S. F. McCann *et al.*, *Pest Manag. Sci.* **57**, 153–164 (2001).
39. I. D. Kuntz, *Science* **257**, 1078–1082 (1992).
40. G. Klebe, *J. Mol. Med.* **78**, 269–281 (2000).
41. A. C. Anderson, *Chem. Biol.* **10**, 787–797 (2003).
42. S. W. Kaldor *et al.*, *J. Med. Chem.* **40**, 3979–3985 (1997).
43. J. N. Varghese, *Drug Dev. Res.* **46**, 176–196 (1999).
44. A. Bénardeau *et al.*, *Bioorg. Med. Chem. Lett.* **19**, 2468–2473 (2009).
45. M. W. Walter, *Nat. Prod. Rep.* **19**, 278–291 (2002).
46. R. J. Howard, B. Valent, *Annu. Rev. Microbiol.* **50**, 491–512 (1996).
47. C. Bechinger *et al.*, *Science* **285**, 1896–1899 (1999).
48. T. Lundqvist *et al.*, *Structure* **2**, 937–944 (1994).
49. D. B. Jordan *et al.*, *Bioorg. Med. Chem. Lett.* **9**, 1607–1612 (1999).
50. G. S. Basarab, D. B. Jordan, T. C. Gehret, R. S. Schwartz, Z. Wawrzak, *Bioorg. Med. Chem. Lett.* **9**, 1613–1618 (1999).
51. G. S. Basarab, D. B. Jordan, T. C. Gehret, R. S. Schwartz, *Bioorg. Med. Chem.* **10**, 4143–4154 (2002).
52. H. M. Berman *et al.*, *Nucleic Acids Res.* **28**, 235–242 (2000).
53. H. M. Berman, *Acta Crystallogr. A* **64**, 88–95 (2008).
54. L. P. Yu, Y. S. Kim, L. Tong, *Proc. Natl. Acad. Sci. U.S.A.* **107**, 22072–22077 (2010).
55. A. Hörnberg, A. K. Tunemalm, F. Ekström, *Biochemistry* **46**, 4815–4825 (2007).
56. R. E. Hibbs, E. Gouaux, *Nature* **474**, 54–60 (2011).
57. N. Bocquet *et al.*, *Nature* **457**, 111–114 (2009).
58. T. Nakao, S. Banba, M. Nomura, K. Hirase, *Insect Biochem. Mol. Biol.* **43**, 366–375 (2013).
59. K. Tietjen, P. H. Schreier, in *Modern Methods in Crops Protection Research*, P. Jeschke, W. Krämer, U. Schirmer, M. Witschel, Eds. (Wiley-VCH, Weinheim, Germany, **2012**), pp. 197–216.
60. D. A. Erlanson, R. S. McDowell, T. O'Brien, *J. Med. Chem.* **47**, 3463–3482 (2004).
61. W. K. Brewster, *et al.*, paper presented at the 244th ACS National Meeting, Philadelphia, PA, 19 to 23 August 2012, abstr. no. AGRO-241.
62. T. Bretschneider, R. Fischer, R. Nauen, in *Modern Crop Protection Compounds*, W. Krämer, U. Schirmer, P. Jeschke, M. Witschel, Eds. (Wiley-VCH, Weinheim, Germany, 2012), pp. 1108–1126.
63. G.-F. Hao *et al.*, *J. Am. Chem. Soc.* **134**, 11168–11176 (2012).
64. H. Sauter, W. Steglich, T. Anke, *Angew. Chem. Int. Ed.* **38**, 1328–1349 (1999).
65. S. Kar, K. Roy, *Expert Opin. Drug Discov.* **8**, 245–261 (2013).
66. M. López-Ramos, F. Perruccio, *J. Chem. Inf. Model.* **50**, 801–814 (2010).
67. R. Beffa, *Pflanzenschutz Nachr. Bayer* **57**, 46–61 (2004) (English edition).
68. S. Kamoun *et al.*, *Can. J. Plant Pathol.* **24**, 6–9 (2002).
69. K. Okada *et al.*, *Planta* **215**, 339–344 (2002).
70. M. Witschel, F. Röhl, R. Niggeweg, T. Newton, *Pest Manag. Sci.* **69**, 559–563 (2013).
71. M. C. Witschel *et al.*, *Angew. Chem. Int. Ed.* **50**, 7931–7935 (2011).
72. M. Witschel, paper presented at the 244th ACS National Meeting, Philadelphia, PA, 19 to 23 August 2012, abstr. no. AGRO-242.

Acknowledgments: The authors are grateful to their colleagues R. Viner and D. P. Kloer for helpful comments.

10.1126/science.1237227

REVIEW

Pivoting the Plant Immune System from Dissection to Deployment

Jeffery L. Dangl,[1,2,3,4,5]*† Diana M. Horvath,[6]* Brian J. Staskawicz[7]*

Diverse and rapidly evolving pathogens cause plant diseases and epidemics that threaten crop yield and food security around the world. Research over the last 25 years has led to an increasingly clear conceptual understanding of the molecular components of the plant immune system. Combined with ever-cheaper DNA-sequencing technology and the rich diversity of germ plasm manipulated for over a century by plant breeders, we now have the means to begin development of durable (long-lasting) disease resistance beyond the limits imposed by conventional breeding and in a manner that will replace costly and unsustainable chemical controls.

Plants turn sunlight into sugar. Thus, plants are rich sources of nutrients and water that are, to no one's surprise, host to diverse microbial communities both above and below the ground. Microbes are likely to have accompanied the first plants that emigrated from water to land 400 to 500 hundred million years ago. Many of their descendant contemporary microbes are adapted to take advantage of the nutrient niches afforded to them by the huge diversity of plants all over the earth. Plants are protected from infection by a "skin," a waxy cuticular layer atop the cell wall. Would-be pathogens breaching this barrier encounter an active plant immune system that specifically recognizes pathogen and altered-self molecules generated during infection. Consequent regulation of a network of inducible defenses can halt pathogen proliferation and signal distal plant organs to become nonspecifically primed against further infection.

Nevertheless, fungal, oomycete, bacterial, and viral pathogens cause devastating epidemics that have affected human civilizations since the dawn of agriculture (*1*). The late blight Irish potato famine of the 1840s was caused by the oomycete *Phytophthora infestans* (*2*); the loss of the world's first mass-cultivated banana cultivar *Gros Michel* in the 1920s to Panama disease was caused by the fungus *Fusarium oxysporum* (*3*); and the current wheat stem, leaf, and yellow stripe rust epidemics spreading from East Africa into the Indian subcontinent caused by rust fungi *Puccinia graminis* and *P. striiformis* (*4*) are all testament to the recurring impact of plant diseases. Plant pathogens can spread rapidly over great distances, vectored by water, wind, insects, and humans (http://rusttracker.cimmyt.org/). Despite various cultural practices, crop protection chemicals, and available disease-resistant crop varieties, an estimated 15% of global crop production is lost to preharvest plant disease (*5*).

Plant Breeding and Disease Resistance

Humans have selected for disease-resistant crops throughout the history of agriculture, at times unwittingly (*6*). As a practiced science, plant breeding for disease resistance originated with Sir Rowland Biffen in Cambridge, England, who

[1]Department of Biology, University of North Carolina, Chapel Hill, NC 27599, USA. [2]Howard Hughes Medical Institute, University of North Carolina, Chapel Hill, NC 27599, USA. [3]Curriculum in Genetics and Molecular Biology, University of North Carolina, Chapel Hill, NC 27599, USA. [4]Department of Microbiology and Immunology, University of North Carolina, Chapel Hill, NC 27599, USA. [5]Carolina Center for Genome Sciences, University of North Carolina, Chapel Hill, NC 27599, USA. [6]Two Blades Foundation, 1630 Chicago Avenue, Evanston, IL 60201, USA. [7]Department of Plant and Microbial Biology, 111 Koshland Hall, University of California, Berkeley, CA 94720–3120, USA.

*These authors contributed equally and are listed alphabetically.
†Corresponding author. E-mail: dangl@email.unc.edu

identified a single recessive gene for resistance to wheat yellow rust caused by *P. striiformis* (*7*). The ensuing century of breeding in nearly every crop species resulted in deployment of disease resistance (*R*) genes, many of which were introduced by introgression from sexually compatible wild relatives. Dominant or semidominant *R* genes were easier to breed into existing crop cultivars, as they could be selected functionally in each generation. We now know that *R* genes are present in multigene clusters and can occur as true alleles across naturally variant genetic backgrounds. The function of each R protein is activated by the product of a specific pathogen virulence gene (*8*), now generically termed "effector genes." Each pathogen isolate can express an array of effectors, and the diversity of effectors across the population of any pathogen species can be stunning (*9*, *10*).

Unfortunately, the utility of most *R* alleles can be short-lived in the field, because their deployment in monoculture selects for pathogen variants, wherein the corresponding effector allele has suffered mutation or been lost. Effectors are virulence factors, but each typically contributes only partially to virulence. Unrelated effectors can act redundantly by altering the same host signaling pathway. Therefore, effector genes can often be lost without significant impact on pathogen virulence. Likely exceptions to this principle are "core effectors," defined operationally by their wide distribution across the population of a particular pathogen and their substantial contribution to pathogen virulence. Genomics-based identification of core effectors and their utilization to functionally define new *R* alleles that they activate in diverse plant germ plasm is a particularly promising strategy for research and deployment that we discuss below.

The Plant Immune System

Research using both tractable experimental systems (*Arabidopsis*) and the irreplaceable germ plasm toolkits provided by plant breeders and plant pathologists (notably in flax, tomato, and barley) led to the isolation of the first pathogen effector genes (*11*) and plant *R* genes (*12*). Additional fundamental discoveries demonstrated that plants could perceive diverse structures generally encoded by microbes via high-affinity cell surface pattern-recognition receptors (PRR) (*13*). These lines of research converged to describe a plant immune system that consists of two interconnected tiers of receptors, one outside and one inside the cell, that govern recognition of microbes and response to infection (*14*–*18*).

The first tier of the plant immune system is governed by extracellular surface PRRs that are activated by recognition of evolutionarily conserved pathogen (or microbial)–associated molecular patterns (PAMPs or MAMPs). These receptors are typically leucine-rich repeat kinases and lysine motif (LysM) kinases (although some lack the kinase domain and thus require a co-receptor to provide signaling function) and are broadly analogous to Toll-like receptors in animals. Activation of PRRs leads to intracellular signaling, transcriptional reprogramming, and biosynthesis of a complex output response that limits microbial colonization (*13*) (Fig. 1, step 1).

Successful pathogens use their effector repertoire to subvert PRR-dependent responses, to facilitate nutrient acquisition, and to contribute to pathogen dispersal. Effector repertoires have been described from pathogens with diverse lifestyles. These include effectors from extracellular plant bacterial pathogens that are delivered into host cells by the type III secretion system (TTSS) (*9*, *19*); effectors from oomycetes and fungi (*10*, *20*) that invaginate specialized feeding organelles, called haustoria, into host cells; and salivary proteins delivered to plant cells during aphid and nematode feeding (*21*) (Fig. 1, step 2). Effector suites from at least two evolutionarily diverse pathogens interact with a limited set of plant "targets," a high proportion of which have immune system functions (Fig. 1, step 3) (*22*).

Most *R* genes encode members of an extremely polymorphic superfamily of intracellular nucleotide-binding leucine-rich repeat (NLR) receptors, which function intracellularly and anchor the second tier of the plant immune system (*14*–*18*). Specific NLR proteins are activated by specific pathogen effectors. This can be via direct interaction, as receptor and ligand, respectively (*23*) (Fig. 1, step 4a). Alternatively, an effector can modify its host cellular target (or a molecular decoy of that target), and a specific NLR associated with the target or decoy can be activated by the modification (*14*, *24*) (Fig. 1, steps 4b and 4c). NLR activation coordinates effector-triggered immunity, a rapid and high-amplitude reboot of effector-suppressed, PRR-dependent outputs that limits pathogen proliferation (Fig. 1, step 5). Animal NLR proteins are likely to follow similar activation models (*25*).

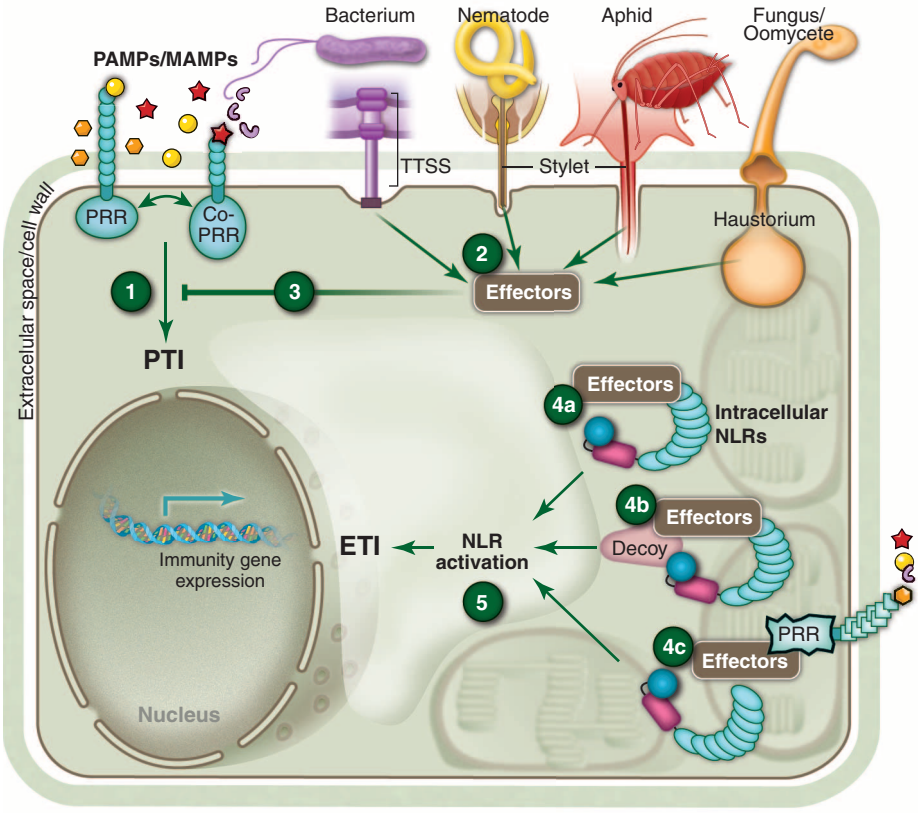

Fig. 1. Schematic of the plant immune system. Pathogens of all lifestyle classes (color coded and labeled) express PAMPs and MAMPs as they colonize plants (shapes are color coded to the pathogens). Plants perceive these via extracellular PRRs and initiate PRR-mediated immunity (PTI; step 1). Pathogens deliver virulence effectors to both the plant cell apoplast to block PAMP/MAMP perception (not shown) and to the plant cell interior (step 2). These effectors are addressed to specific subcellular locations where they can suppress PTI and facilitate virulence (step 3). Intracellular NLR receptors can sense effectors in three principal ways: first, by direct receptor ligand interaction (step 4a); second, by sensing effector-mediated alteration in a decoy protein that structurally mimics an effector target, but has no other function in the plant cell (step 4b); and third, by sensing effector-mediated alteration of a host virulence target, like the cytosolic domain of a PRR (step 4c). It is not yet clear whether each of these activation modes proceeds by the same molecular mechanism, nor is it clear how, or where, each results in NLR-dependent effector-triggered immunity (ETI). [Modified from (*17*) by Sarah R. Grant]

Table 1. Published examples of transgenic disease resistance in crops and development status.

Pub. year	Crop	Disease resistance	Mechanism	Development status	Ref.
2012	Tomato	Bacterial spot	*R* gene from pepper	8 years of field trials	(*46*)
2012	Rice	Bacterial blight and bacterial streak	Engineered *E* gene	Laboratory	(*56*)
2012	Wheat	Powdery mildew	*R* gene from wheat, overexpressed	2 years of field trials at time of publication	(*82*)
2011	Apple	Apple scab fungus	Thionin gene from barley	4 years of field trials at time of publication	(*83*)
2011	Potato	Potato virus Y	Pathogen-derived resistance	1 year of field trial at time of publication	(*84*)
2010	Apple	Fire blight	Antibacterial protein from moth	12 years of field trials at time of publication	(*85*)
2010	Tomato	Multibacterial resistance	PRR from *Arabidopsis*	Laboratory scale	(*43*)
2010	Banana	*Xanthomonas* wilt	Novel gene from pepper	Now in field trial	(*86*)
2009	Potato	Late blight	*R* genes from wild relatives	3 years of field trials	(*87*)
2009	Potato	Late blight	*R* gene from wild relative	2 years of field trials at time of publication	(*88*)
2008	Potato	Late blight	*R* gene from wild relative	2 years of field trials at time of publication	(*89*)
2008	Plum	Plum pox virus	Pathogen-derived resistance	Regulatory approvals, no commercial sales	(*90*, *91*)
2005	Rice	Bacterial streak	*R* gene from maize	Laboratory	(*92*)
2002	Barley	Stem rust	*RLK* gene from resistant barley cultivar	Laboratory	(*93*)
1997	Papaya	Ring spot virus	Pathogen-derived resistance	Approved and commercially sold since 1998, sold into Japan since 2012	(*94*, *95*)
1995	Squash	Three mosaic viruses	Pathogen-derived resistance	Approved and commercially sold since 1994	(*96*)
1993	Potato	Potato virus X	Mammalian interferon-induced enzyme	3 years of field trials at time of publication	(*97*)

Fig. 2. Hawaiian papaya plot in 2011. Hawaiian papaya plot showing diseased, devastated, non-transformed trees in the foreground and healthy transgenic trees behind. [Photo courtesy of Dennis Gonsalves, Agricultural Research Service, U.S. Department of Agriculture, Hawaii]

The molecular architectures of NLR proteins in their resting, transition, and active signaling states are poorly defined (*26*, *27*). There are limited and conflicting data on the role of self-association or oligomerization for sensor NLR protein function, at both pre- and postactivation steps (*28*). Resting state oligomerization (in some cases), activation-dependent intramolecular rearrangements (in essentially all cases), and activation-dependent N-terminal signaling domain dimerization (in many but not all cases) have been documented. Some effector-triggered responses require a pair of NLR proteins (*28*): One is activated by the effector and is a "sensor NLR"; the other is required for its function and is a "helper NLR" (*27*, *29*). Heteromeric pairing could expand NLR repertoires (*30*, *31*). Similar NLR pairs can function in animal NLR systems (*32*, *33*). Exceptions abound, and generalizable models for NLR activation may not exist; evolution may have favored a mix of mechanisms that were refined by coevolutionary conflict between effectors, targets or decoys, and sensor NLRs.

The cellular site(s) of NLR activation and action are likely to be diverse. Some NLRs may require nucleocytoplasmic shuttling for function, whereas others appear to be activated at the plasma membrane (*18*, *27*). These different sites of activation suggest a more idiosyncratic model for NLR function, dictated in part by the localization of, and functional constraints on, the effector targets whose integrity each NLR monitors.

The presence of NLRs with diverse N-terminal signaling domains in both plants and animals suggests that this architecture confers a fundamental advantage in host defense. This advantage may include recruitment of diverse cofactors after activation, as suggested by the functionally relevant interaction of NLR N-terminal domains with transcription factors in some cases (*34*). NLRs may facilitate tightly regulated "cooperative" threshold responses to ligands within an evolutionarily flexible scaffold that permits innate immune systems with limited germ line–encoded repertoires to keep pace with functionally diverse pathogen effectors acting at a variety of intracellular sites.

Engineering Disease Resistance in Crops: Early Successes

Successful transgenic disease resistance was demonstrated in 1986. Constitutive *in planta* expression of viral coat protein gene sequences conferred virus resistance via small RNAs, now understood to be a widely applicable mechanism for inhibiting viral replication (*35*). By combining coat protein genes from three different viruses, scientists developed squash hybrids with field-validated, multiviral resistance (Table 1). The Asgrow Seed Company obtained regulatory approvals for transgenic commercial squash in 1994, and these continue to be sold by Seminis today. Similar levels of resistance to this variety of viruses had not been achieved by conventional breeding.

A similar strategy was deployed to combat papaya ringspot virus, which, by 1994, threatened to destroy Hawaii's papaya industry. Field trials demonstrated excellent efficacy and high fruit quality (Table 1), and by 1998, the first transgenic virus-resistant papaya was approved for sale in Hawaii. Disease resistance has been durable for over 15 years of commercial use, and transgenic papaya currently accounts for ~85% of Hawaiian production (Fig. 2). The fruit is now approved for sale in Canada and Japan.

Since the approval and commercialization of these two crops in the late 1990s, not a single new crop with engineered disease resistance has reached the market. Research successes exist (Table 1), and there is still potential to reduce yield losses and chemical inputs associated with crop disease.

Effector-Targeted Strategies for Durable Disease Resistance—An Emerging Paradigm

R gene isolation using genetics and genomics is now a reality in even the most complex plant genomes (*36*, *37*). Rapid and inexpensive DNA-sequencing technologies can provide the genomes of natural field isolates of plant pathogens with impact on breeding strategies for durable control of plant diseases (*38*). It is now possible to define the genomes, and thus the effector complement, of plant pathogens isolated from infected plants in a rapid and efficient manner. Defining core effectors facilitates identification of suites of corresponding *R* genes from wild germ plasm by using transient coexpression assays, followed by either marker-assisted breeding or transgenic deployment (Box 1). Validation of these new *R* genes could be enhanced by new genome-editing methods that use transcription activator–like effector nuclease (TALEN) (*39*) and clustered regularly interspaced short palindromic repeat (CRISPR) technologies (*40*, *41*).

The function of any particular *R* gene is likely to be durable only if the effector that activates it is present and important for virulence in the pathogen strains that one is trying to control. Knowledge of the effector content in local pathogen isolates can inform *R* gene deployment or chemical treatment in the control of potato late blight (*38*). Another exmaple is *Xanthomonas axonopodis* pv. *manihotis* (*Xam*), the causal agent of cassava bacterial blight (*42*). This disease devastates a staple crop in East Africa. The sequence of ~65 *Xam* strains collected over a 70-year time frame, from 12 countries and three continents, revealed a core effector set that can now serve as targets to define *R* genes activated by them in wild species of *Manihot* and potentially other related plants in the *Euphorbiaceae.*

Deployment of Immune System Receptors

Research aimed at deployment of the two classes of immune receptors currently follows two main strategies. One is to transfer PRRs that detect common microbial products into species that lack them. For example, the *Arabidopsis* PRR EF-Tu receptor (EFR) recognizes the bacterial translation elongation factor EF-Tu. Deployment of EFR into either *Nicotiana benthamiana* or *Solanum lycopersicum* (tomato), which cannot recognize EF-Tu, conferred resistance to a wide range of bacterial pathogens (*43*). The expression of EFR in tomato was especially effective against the widespread and devastating soil bacterium *Ralstonia solanacearum*. Also, the tomato PRR *Verticillium 1* (*Ve1*) gene can be transferred from tomato to *Arabidopsis*, where it confers resistance to race 1 isolates of *Verticillium* (*44*). Identification of functional PRRs and their transfer to a recipient species that lacks an orthologous receptor could provide a general pathway to additional examples of broadened PRR repertoires (*13*).

The second strategy exploits immune responses in contexts where multiple *NLR* genes are deployed simultaneously, a breeding strategy known as stacking. Such cultivars, generated by either DNA-assisted molecular breeding or gene transfer, should provide more durable disease resistance because pathogen evasion would require mutations in multiple effector genes. Recent breakthroughs in DNA sequencing allow access to the huge genetic diversity of our major crops and their relatives to functionally "mine" *NLR* genes directed against different core effectors. This approach will ultimately overcome inherent barriers to traditional crop breeding (Box 1). Illustrative examples follow.

The first "effector-rationalized" search for a potentially durable *R* gene was predicated on the finding that the *avrBs2* effector gene from *Xanthomonas perforans,* the causal agent of bacterial spot disease of pepper and tomato, is found in most species of *Xanthomonas* that cause disease and is required for pathogen fitness (*45*). The *Bs2* NLR gene from the wild pepper, *Capsicuum chacoense,* was transformed into tomato, where it inhibited growth of pathogen strains that contained *avrBs2*. Successful field trials of transgenic tomato plants that express *Bs2* demonstrated robust resistance to *X. perforans* without bactericidal chemicals (*46*). However, rare strains of *Xanthomonas* have overcome *Bs2*-mediated resistance in pepper by acquisition of *avrBs2* mutations that avoid recognition but retain virulence (*47*). Stacking of multiple *R* genes that each recognize a different core effector could delay or prevent this problem.

The oomycete *Phytophthora infestans* causes late blight disease of potato (*2*). Cultivated potato, *Solanum tuberosum*, is tetraploid and clonally propagated via cuttings, which significantly hampers introgression of disease resistance from diploid wild species in the genus *Solanum.* Furthermore, the pathogen is aggressive and has repeatedly adapted to evade host resistance mediated by single *R* genes and chemical treatments. Most potato cultivars are thus susceptible to *P. infestans* infection, which necessitates continual updating of chemical treatments.

Genome-wide definition of effector suites across pathogen isolates collected worldwide and of *R* gene distribution across *Solanum* sp. will have a major impact on management of resistance to *P. infestans* (*38*). Sequencing of several *P. infestans* genomes has identified a core set of effectors that can now be used to identify new sources of disease resistance across the genus *Solanum*. This approach has been validated in the potato cultivar *Sarpo mira*, which contains four naturally stacked *R* genes activated by already known *P. infestans* effectors (*48*). Rational stacking of *R* genes is a general approach (*49*, *50*) and the method of choice for producing sustainable, durable disease resistance that will require fewer chemical inputs.

In modern wheat and its many relatives, more than 50 different loci have been described that confer disease resistance against wheat stem, leaf, and yellow stripe rust pathogens. A few were known to confer resistance to the pandemic wheat rust isolate Ug99 and its derivatives, but these were not readily incorporated into hexaploid wheat or provide only partial resistance. The *Stem rust 35* (*Sr35*) NLR gene was very recently cloned from a diploid relative of cultivated wheat, *Triticum monococcum*, and transferred into cultivated hexaploid wheat to derive resistance to Ug99 (*36*). Similarly, the *Stem rust 33* (*Sr33*) NLR gene from the wheat relative *Aegilops tauschii* was also very recently cloned and shown to encode a wheat ortholog to the barley *Mla* powdery mildew–resistance genes (*37*). Both *Sr35* and *Sr33* are fairly rare in wheat and its relatives, which accentuates the importance of diverse germ plasm screening to identify useful new *R* genes. It is hoped that *Sr35* and *Sr33,* combined with the *Sr2* gene that is known to act additively with at least *Sr33* (*51*), could provide durable disease resistance to Ug99 and its derivatives.

Deployment of Executor-Mediated Disease Resistance

In contrast to PRRs and NLRs, another class of plant disease resistance genes has evolved to coopt pathogen virulence functions and open a "trap door" that stops pathogen proliferation. *Xanthomonas* and *Ralstonia* transcription activator–like (TAL) effectors are DNA-binding proteins delivered into plant cells, where they activate host gene expression to enhance pathogen virulence (*39*). In a neat evolutionary trick, however, both the rice and pepper lineages independently evolved TAL-effector binding sites in the promoters of genes whose products induce hypersensitive host cell death when up-regulated and thus inhibit pathogen proliferation. The known "executor" genes, *Xa27* from rice (*52*) and *Bs3* and *Bs4c* from pepper (*53*, *54*), encode plant proteins of unknown function that share no homology. Executor genes are not expressed in the absence of infection, but expression of each is strongly induced by a specific TAL effector.

Engineered executor genes provide unique opportunities to deliver enhanced and potentially durable disease resistance. This was demonstrated by successfully redesigning the pepper *Bs3* promoter to contain two additional binding sites for TAL effectors from disparate pathogen strains (*55*). Subsequently, an engineered executor gene was deployed in rice by adding five different TAL effector binding sites to the *Xa27* promoter. The synthetic *Xa27* construct was activated by TAL effectors from, and conferred resistance against, both bacterial blight and bacterial leaf streak species of *Xanthomonas* (*56*) (Table 1).

Defining and Deploying Altered Host "Susceptibility Alleles" to Control Plant Diseases

Most plant pathogens reprogram host plant gene expression patterns to directly benefit pathogen fitness, as exemplified above for TAL effectors. Host genes reprogrammed by pathogens that are required for pathogen survival and proliferation can be thought of as "disease-susceptibility genes." Identification and isolation of these would provide useful sources for breeding disease resistance: their loss or alteration of function would deprive the pathogen of a host factor required for its proliferation (*57*, *58*). We highlight a few here.

Recessive disease-resistance genes, long known to breeders, are candidates for disease-susceptibility genes. For example, a loss-of-function mutation in an *Arabidopsis* gene encoding pectate lyase, an enzyme involved in cell wall degradation, conferred resistance to the powdery mildew pathogen *Golovinomyces* (syn. *Erysiphe*) *cichoracearum* (*59*). Similarly, the Barley *mlo* gene has been deployed against powdery mildew for more than 70 years, and it is required for pathogen invasion (*60*). Spontaneous mutations in pea and tomato *MLO* orthologs confer resistance to powdery mildew pathogens of these plants (*61*, *62*). And the *Pseudomonas syringae* bacterial effector HopZ2 targets the *Arabidopsis* ortholog, *MLO2*, to contribute to bacterial virulence (*63*).

Similarly illustrative is the cloning and deployment of *Lr34*, a gene that provides partial resistance to leaf and yellow rusts and powdery mildew in wheat and that has been durable for nearly a century. *Lr34* encodes an adenosine triphosphate (ATP)–binding cassette (ABC) transporter. The dominant allele that provides disease resistance was recently derived in cultivated wheat (it is not present in wild progenitors of wheat) and, like *mlo*, is associated with ectopic plant cell death that may establish a "sensitized" defense state or accelerate senescence. Transfer of the wheat *Lr34* resistance allele provides broad-spectrum resistance in barley, although with the expected cell death–lesion formation (*64*–*66*). It is unclear whether the wheat allele that provides durable resistance is also functional for the inferred ABC transporter activity of Lr34, and thus, the mechanism by which Lr34 confers disease resistance remains obscure.

Naturally occurring alleles of the host translation elongation initiation factors *eif4e* and *eif4g* double as recessive viral-resistance genes. Some have been deployed to control important potyviruses in barley, rice, tomato, pepper, pea, lettuce, and melon (*67*). The discovery of natural recessive alleles prompted a successful mutant screen for chemically induced *eif4e* alleles in tomato (*68*).

Natural variation in the promoters of key plant-susceptibility genes can also lead to the evolution of recessive disease-resistance alleles. For example, the recessive resistance gene *xa13* in rice is an allele of *Os-8N3*. *Os-8N3* is transcriptionally activated by *Xanthomonas oryzae* pv. *oryzae* strains that express the TAL effector PthXo1. The *xa13* gene has a mutated effector-binding element in its promoter that eliminates PthXo1 binding and renders these lines resistant to strains of the pathogen that rely on PthXo1 as their essential virulence factor. This finding also demonstrates that Os-8N3 is required for susceptibility (*69*).

The deployment of mutant alleles of host disease-susceptibility genes can be problematic if the disease-susceptibility phenotype comes at the cost of altered function in other cellular and developmental processes. This is the case for *Xa13/Os-8N3*, which is also required for pollen development (*70*). Nevertheless, it is possible to separate disease susceptibility from normal development. For example, mutations in the *Os11N3* (*OsSWEET14*) TAL effector–binding element were made by using TAL effectors fused to nucleases (TALENs). Genome-edited rice plants with altered *Os11N3* binding sites were resistant to *Xanthomonas oryzae* pv. *oryzae* infection, but they were unaltered for the normal *Os11N3* (*OsSWEET14*) developmental function (*71*).

The identification of new susceptibility genes in crops will come from forward genetic screens that uncover new recessive disease-resistance genes—which may, indeed, turn out to be host-susceptibility genes—and from identification of host targets of effectors. For example, mutant screens in *Arabidopsis* identified additional recessive mutations that confer recessive resistance to the obligate biotrophs, *G. cichoracearum* (*72*) and *Hyaloperonospora arabidopsidis* (*73*). These genes have orthologs in other plants, thus making them obvious targets for identification of mutant alleles in crop species (Box 1).

Looking Forward: Future Challenges, Technical and Societal

In the past century of disease-resistance breeding, we were largely limited to germ plasm from sexually compatible wild species that can recognize and resist infection, without a priori knowledge of the effector *R* gene mediating the outcome (Box 1). This strategy is slow, and field efficacy is often shortened by selection of effector gene mutants that evade host recognition. Our current challenge is to leverage evolutionary genomic information stored in the worldwide germ plasm diversity. The goal is to define and to stack multiple resistance specificities active against the daunting array of economically important pathogens, including *Phytophthora*, *Magnaporthe*,

Box 1. Breeding for disease resistance.

Current practices involved in breeding for disease resistance

1. Discover single *R* genes in wild relative species and cross into agronomic cultivars by interspecific hybridization, followed by successive generations of recurrent selection for resistance. This process is slow.
2. Use pathogen inoculations to test plant germ plasm for resistance without a priori knowledge of which effector is being detected by the new *R* gene.
3. *R* gene–mediated disease resistance can be short-lived, as pathogens can mutate to evade activating *R* function.
4. Interspecific hybrid breeding is sometimes difficult because of sexual incompatibilities and/or linkage drag of undesirable traits.

Improved practices for breeding durable resistance by genomic strategies

1. Use next-generation sequencing technologies to sequence and assemble pathogen genomes causing disease in local fields.
2. Use computational biology to identify the most highly successful core effectors in these strains.
3. Identify *R* genes that are activated by those effectors.
4. Deploy multiple, stacked *R* genes that recognize defined core effectors to reduce the chance that pathogens will overcome resistance.
5. Identify and edit within the genome disease-susceptibility genes to reduce pathogen growth and symptom development.
6. Identify and deploy antipathogenic probiotic and/or antipathogenic microbial mixtures as seed coats.

Fusarium, *Pseudomonas*, *Ralstonia*, *Xanthomonas*, and gemini and potyviruses (*74*). At the same time, we must maintain complex agronomic traits—such as yield, form, and flavor—and avoid yield penalties. The precision offered by transgenic and genome editing technologies offers considerable advantages over conventional breeding (Box 1).

Prospects for the development of durable disease resistance have improved markedly because of the ongoing molecular dissection of the plant immune system and the advent of ever-faster, ever-cheaper genome-sequencing technologies. Many exciting challenges are emerging to exploit that knowledge. We can contemplate rational, stacked deployment of multiple NLRs that each recognize a different core effector (Box 1). We will eventually be able to engineer novel NLR recognition specificities, though this requires detailed structural knowledge only now beginning to be unraveled (*75*). Combinations of stacked NLRs, new PRRs, and genome-edited disease-susceptibility alleles that reduce or stop pathogen proliferation are realistic possibilities. We can now monitor pathogen populations and their effector complements in the field over space and time to inform deployment of better-suited cultivars requiring less chemical control (*38*). We harbor ambitions to enhance plant immune system function by managing defined probiotic, antipathogenic microbial consortia isolated from the plant's own microbiome (*76*, *77*). A holistic, mechanism-based approach will ultimately improve plant immune system function to deliver durable and sustainable disease resistance, with minimum or no chemical input, where it is needed most in the future.

Among the greatest challenges remaining for deployment of next-generation disease-resistant plants are those posed by regulatory and consumer acceptance hurdles. Virus resistance in modified papaya and squash has been durable, and the crops have been safely consumed for nearly 20 years, with no negative environmental impacts (*78*). Nevertheless, significant anxiety remains. Sadly, commercial deployment by BASF Corporation (Badische Anilin Soda Farbrik, AG) of a potentially valuable potato cultivar, Fortuna, containing two stacked and potentially durable *NLR* genes from a wild potato species, was canceled because of pressure from lobbies opposing genetic modification, despite the fact that it would likely eliminate some or all of the up to 25 fungicide treatments required in Northern Europe per year to control late blight (*79*). If the examples of the introduction of coffee as a beverage, and the use of hybrid crops, such as corn, serve as guidelines, acceptance of transgenic crops should become mainstream in about 50 to 200 years (*80*, *81*). That timeline is simply too long to wait to confront the issues of food security and environmental sustainability posed by the plethora of microbes that value our crops as food sources as much as we do.

References and Notes

1. G. N. Agrios, *Plant Pathology* (Academic Press, San Diego, 1988).
2. K. Yoshida *et al.*, *eLife* **2**, e00731 (2013).
3. D. Koeppel, *Banana: The Fate of the Fruit That Changed the World* (Penguin Books, New York, 2008).
4. R. P. Singh *et al.*, *Annu. Rev. Phytopathol.* **49**, 465–481 (2011).
5. J. Popp, K. Hantos, *Stud. Agric. Econ.* **113**, 47 (2011).
6. P. Piffanelli *et al.*, *Nature* **430**, 887–891 (2004).
7. R. H. Biffen, *J. Agric. Sci.* **1**, 4 (1905).
8. H. H. Flor, *Annu. Rev. Phytopathol.* **9**, 275–296 (1971).
9. D. A. Baltrus *et al.*, *PLoS Pathog.* **7**, e1002132 (2011).
10. S. Raffaele *et al.*, *Science* **330**, 1540–1543 (2010).
11. B. J. Staskawicz, D. Dahlbeck, N. T. Keen, *Proc. Natl. Acad. Sci. U.S.A.* **81**, 6024–6028 (1984).
12. B. J. Staskawicz, F. M. Ausubel, B. J. Baker, J. G. Ellis, J. D. G. Jones, *Science* **268**, 661–667 (1995).
13. J. Monaghan, C. Zipfel, *Curr. Opin. Plant Biol.* **15**, 349–357 (2012).
14. J. L. Dangl, J. D. Jones, *Nature* **411**, 826–833 (2001).
15. J. D. Jones, J. L. Dangl, *Nature* **444**, 323–329 (2006).
16. S. T. Chisholm, G. Coaker, B. Day, B. J. Staskawicz, *Cell* **124**, 803–814 (2006).
17. P. N. Dodds, J. P. Rathjen, *Nat. Rev. Genet.* **11**, 539–548 (2010).
18. T. Maekawa, T. A. Kufer, P. Schulze-Lefert, *Nat. Immunol.* **12**, 817–826 (2011).
19. A. Block, J. R. Alfano, *Curr. Opin. Microbiol.* **14**, 39–46 (2011).
20. M. Koeck, A. R. Hardham, P. N. Dodds, *Cell. Microbiol.* **13**, 1849–1857 (2011).
21. J. I. Bos *et al.*, *PLoS Genet.* **6**, e1001216 (2010).
22. M. S. Mukhtar *et al.*, *Science* **333**, 596–601 (2011).
23. P. N. Dodds *et al.*, *Proc. Natl. Acad. Sci. U.S.A.* **103**, 8888–8893 (2006).
24. R. A. van der Hoorn, S. Kamoun, *Plant Cell* **20**, 2009–2017 (2008).
25. L. M. Stuart, N. Paquette, L. Boyer, *Nat. Rev. Immunol.* **13**, 199–206 (2013).
26. F. L. Takken, A. Goverse, *Curr. Opin. Plant Biol.* **15**, 375–384 (2012).
27. V. Bonardi, K. Cherkis, M. T. Nishimura, J. L. Dangl, *Curr. Opin. Immunol.* **24**, 41–50 (2012).
28. T. K. Eitas, J. L. Dangl, *Curr. Opin. Plant Biol.* **13**, 472–477 (2010).
29. V. Bonardi *et al.*, *Proc. Natl. Acad. Sci. U.S.A.* **108**, 16463–16468 (2011).
30. M. Narusaka *et al.*, *Plant J.* **60**, 218–226 (2009).
31. D. Birker *et al.*, *Plant J.* **60**, 602–613 (2009).
32. E. M. Kofoed, R. E. Vance, *Nature* **477**, 592–595 (2011).
33. B. Zhao, D. Dahlbeck, K. V. Krasileva, R. W. Fong, B. J. Staskawicz, *PLoS Pathog.* **7**, e1002408 (2011).
34. C. Chang *et al.*, *Plant Cell* **25**, 1158–1173 (2013).
35. J. A. Lindbo, W. G. Dougherty, *Mol. Plant Microbe Interact.* **5**, 144–153 (1992).
36. C. Saintenac *et al.*, *Science* **341**, 783–786 (2013).
37. S. Periyannan *et al.*, *Science* **341**, 786–788 (2013).
38. V. G. A. A. Vleeshouwers *et al.*, *Annu. Rev. Phytopathol.* **49**, 507–531 (2011).
39. S. Schornack, M. J. Moscou, E. R. Ward, D. M. Horvath, *Annu. Rev. Phytopathol.* 10.1146/annurev-phyto-082712-102255 (2013).
40. M. Jinek *et al.*, *eLife* **2**, e00471 (2013).
41. T. Gaj, C. A. Gersbach, C. F. Barbas 3rd, *Trends Biotechnol.* **31**, 397–405 (2013).
42. R. Bart *et al.*, *Proc. Natl. Acad. Sci. U.S.A.* **109**, E1972–E1979 (2012).
43. S. Lacombe *et al.*, *Nat. Biotechnol.* **28**, 365–369 (2010).
44. E. F. Fradin *et al.*, *Plant Physiol.* **156**, 2255–2265 (2011).
45. B. Kearney, B. J. Staskawicz, *Nature* **346**, 385–386 (1990).
46. D. M. Horvath *et al.*, *PLoS ONE* **7**, e42036 (2012).
47. W. Gassmann *et al.*, *J. Bacteriol.* **182**, 7053–7059 (2000).
48. H. Rietman *et al.*, *Mol. Plant Microbe Interact.* **25**, 910–919 (2012).
49. H. J. Kim *et al.*, *Theor. Appl. Genet.* **124**, 923–935 (2012).
50. S. Zhu, Y. Li, J. H. Vossen, R. G. Visser, E. Jacobsen, *Transgenic Res.* **21**, 89–99 (2012).
51. M. Ayliffe *et al.*, *Mol. Plant Microbe Interact.* **26**, 658–667 (2013).
52. K. Gu *et al.*, *Nature* **435**, 1122–1125 (2005).
53. P. Römer *et al.*, *Science* **318**, 645–648 (2007).
54. T. Strauss *et al.*, *Proc. Natl. Acad. Sci. U.S.A.* **109**, 19480–19485 (2012).
55. P. Römer, S. Recht, T. Lahaye, *Proc. Natl. Acad. Sci. U.S.A.* **106**, 20526–20531 (2009).
56. A. W. Hummel, E. L. Doyle, A. J. Bogdanove, *New Phytol.* **195**, 883–893 (2012).
57. F. Gawehns, B. J. C. Cornelissen, F. L. W. Takken, *Microb. Biotechnol.* **6**, 223–229 (2013).
58. S. Pavan, E. Jacobsen, R. G. Visser, Y. Bai, *Mol. Breed.* **25**, 1–12 (2010).
59. J. P. Vogel, T. K. Raab, C. Schiff, S. C. Somerville, *Plant Cell* **14**, 2095–2106 (2002).
60. M. Humphry, C. Consonni, R. Panstruga, *Mol. Plant Pathol.* **7**, 605–610 (2006).
61. S. Pavan *et al.*, *Theor. Appl. Genet.* **123**, 1425–1431 (2011).
62. Y. Bai *et al.*, *Mol. Plant Microbe Interact.* **21**, 30–39 (2008).
63. J. D. Lewis *et al.*, *BMC Genomics* **13**, 8 (2012).
64. S. G. Krattinger *et al.*, *Theor. Appl. Genet.* **126**, 663–672 (2013).
65. S. G. Krattinger *et al.*, *Plant J.* **65**, 392–403 (2011).
66. J. M. Risk *et al.*, *Plant Biotechnol. J.* **10**, 477–487 (2012).
67. A. Wang, S. Krishnaswamy, *Mol. Plant Pathol.* **13**, 795–803 (2012).
68. F. Piron *et al.*, *PLoS ONE* **5**, e11313 (2010).
69. B. Yang, A. Sugio, F. F. White, *Proc. Natl. Acad. Sci. U.S.A.* **103**, 10503–10508 (2006).
70. Z. Chu *et al.*, *Genes Dev.* **20**, 1250–1255 (2006).
71. T. Li, B. Liu, M. H. Spalding, D. P. Weeks, B. Yang, *Nat. Biotechnol.* **30**, 390–392 (2012).
72. J. Vogel, S. Somerville, *Proc. Natl. Acad. Sci. U.S.A.* **97**, 1897–1902 (2000).
73. M. Van Damme *et al.*, *Mol. Plant Microbe Interact.* **18**, 583–592 (2005).
74. R. N. Strange, P. R. Scott, *Annu. Rev. Phytopathol.* **43**, 83–116 (2005).
75. Z. Hu *et al.*, *Science* **341**, 172–175 (2013).
76. D. Bulgarelli, K. Schlaeppi, S. Spaepen, E. Ver Loren van Themaat, P. Schulze-Lefert, *Annu. Rev. Plant Biol.* **64**, 807–838 (2013).
77. J. A. Vorholt, *Nat. Rev. Microbiol.* **10**, 828–840 (2012).
78. M. Fuchs, D. Gonsalves, *Annu. Rev. Phytopathol.* **45**, 173–202 (2007).
79. C. Dixelius, T. Fagerström, J. F. Sundström, *Nat. Biotechnol.* **30**, 492–493 (2012).
80. R. C. Sutch, "Henry Agard Wallace, the Iowa corn yield tests, and the adoption of hybrid corn" (National Bureau of Economic Research working paper 14141, NBER, Cambridge, MA, 2008).
81. C. Juma, "'Satan's drink' and a sorry history of global food fights," *Financial Times*, 6 February 2006.
82. S. Brunner *et al.*, *Plant Biotechnol. J.* **10**, 398–409 (2012).
83. F. A. Krens *et al.*, *Transgenic Res.* **20**, 1113–1123 (2011).
84. F. Bravo-Almonacid *et al.*, *Transgenic Res.* **21**, 967–982 (2012).
85. E. Borejsza-Wysocka, J. L. Norelli, H. S. Aldwinckle, M. Malnoy, *BMC Biotechnol.* **10**, 41 (2010).
86. L. Tripathi, H. Mwaka, J. N. Tripathi, W. K. Tushemereirwe, *Mol. Plant Pathol.* **11**, 721–731 (2010).
87. S. J. Foster *et al.*, *Mol. Plant Microbe Interact.* **22**, 589–600 (2009).
88. J. M. Bradeen *et al.*, *Mol. Plant Microbe Interact.* **22**, 437–446 (2009).
89. D. Halterman, L. Kramer, S. Wielgus, J. Jiang, *Plant Dis.* **92**, 339–343 (2008).
90. T. Malinowski *et al.*, *Plant Dis.* **90**, 1012–1018 (2006).
91. J. Polák *et al.*, *J. Plant Pathol.* **90** (suppl.), S1.33–S1.36 (2008).
92. B. Zhao *et al.*, *Proc. Natl. Acad. Sci. U.S.A.* **102**, 15383–15388 (2005).
93. H. Horvath *et al.*, *Proc. Natl. Acad. Sci. U.S.A.* **100**, 364–369 (2003).
94. S. Ferreira *et al.*, *Plant Dis.* **86**, 101–105 (2002).
95. S. Lius *et al.*, *Mol. Breed.* **3**, 161–168 (1997).
96. D. M. Tricoli *et al.*, *Biotechnology* **13**, 1458–1465 (1995).
97. E. Truve *et al.*, *Biotechnology* **11**, 1048–1052 (1993).

Acknowledgments: We thank our many colleagues who provided insight and unpublished information that contributed to the development of this review. J.L.D. is a cofounder of AgBiome, LLC. J.L.D. is a Howard Hughes Medical Institute (HHMI) Investigator, and work in his lab on this topic is funded by HHMI, the Gordon and Betty Moore Foundation, and grants from NSF. B.J.S. is a cofounder of Mendel Biotechnology, Inc., and is funded by grants from NSF and NIH.

10.1126/science.1236011

REVIEW

Evaluating Pesticide Degradation in the Environment: Blind Spots and Emerging Opportunities

Kathrin Fenner,[1,2]* Silvio Canonica,[1] Lawrence P. Wackett,[3] Martin Elsner[4]

The benefits of global pesticide use come at the cost of their widespread occurrence in the environment. An array of abiotic and biotic transformations effectively removes pesticides from the environment, but may give rise to potentially hazardous transformation products. Despite a large body of pesticide degradation data from regulatory testing and decades of pesticide research, it remains difficult to anticipate the extent and pathways of pesticide degradation under specific field conditions. Here, we review the major scientific challenges in doing so and discuss emerging opportunities to identify pesticide degradation processes in the field.

An estimated 1 to 2.5 million tons of active pesticide ingredients are used annually, mainly in agriculture (*1*, *2*). Since the discovery of certain synthetic organochlorine compounds as insecticides in the 1940s, a large number of chemical pesticide classes with different uses and modes of action have been developed and brought to market (Table 1). Despite different chemical structures and target organisms [i.e., 40% used as herbicides, followed by insecticides and fungicides (*2*)], pesticides have in common that they are applied extensively over large areas in agriculture and urban settings. Their use therefore represents an important source of diffuse chemical pollution that is difficult to control.

In principle, pesticides are only registered for use if they are demonstrated not to persist in the environment considerably beyond their intended period of use (i.e., soil half-lives in the range of a few days to weeks). Nonetheless, residues of many pesticides are found ubiquitously in the natural environment in ng/liter to low µg/liter concentrations. For instance, surveys of groundwater and raw drinking water in industrialized countries typically detect 10 to 20 substances in recurrent findings above 0.1 µg/liter, the maximal accepted drinking water concentration for pesticides in many countries (Table 1) (*3*, *4*). An even more striking indication of widespread pesticide persistence is that about half of the detected substances have long been phased out of use, and another 10 to 20% are stable transformation products. Pesticide contamination is not limited to groundwater, as transport from groundwater may lead to a low-level, yet continuous presence of pesticides in surface waters (*5*). Current-use pesticides have further been detected in high-altitude regions, demonstrating sufficient persistence to carry them over hundreds of kilometers in the atmosphere (*6*). To protect natural and human food resources such as plants, aquatic biota, and drinking water, it is therefore important to understand what controls pesticides' environmental fate, and particularly their degradation—being the only process that actually clears pesticides from the environment.

Degradation of pesticides involves both biotic transformation processes—mediated by microorganisms or plants—and abiotic processes such as chemical and photochemical reactions. What transformation processes a given pesticide undergoes is determined by its structural affinity to specific types of transformation, and the environmental conditions it is exposed to as a result of its distribution and transport behavior (Fig. 1). For instance, redox gradients in soils, sediments, or aquifers often determine which biotic and/or abiotic transformations can occur. Similarly, photochemical transformations are restricted to compartments exposed to sunlight—e.g., the topmost meter(s) of lakes or rivers, the surfaces of plants, or submillimeter layers of soil. Although atmospheric phototransformation may also strongly affect the chemical nature and transport potential of pesticides, this topic has been treated elsewhere (*7*) and will not be covered here.

For pesticides as a strictly regulated category of substances, a large body of information is available from regulatory testing for market authorization. This includes data from laboratory-based tests on aqueous hydrolysis, photolysis in water and air, biodegradability in soils and water-sediment systems under aerobic and anaerobic conditions, and fate in soil lysimeters. The drawback of these rather phenomenological studies is that they provide little insight into how individual transformation processes contribute to observed bulk degradation. Therefore, they do not support a mechanistic understanding of how specific environmental conditions (i.e., the presence of certain reactants) affect pesticide transformation. Regulatory studies further fail to cover less frequently encountered environmental conditions such as those present in strongly sulfidic environments (e.g., estuaries, prairie potholes) or in different types of water treatment units, nor are they able to highlight transformations at low residual pesticide concentrations at which biodegradation may not take place. Thus, although chemists can generally predict intrinsic reactivity of a pesticide from its molecular structure, their ability to quantitatively predict or interpret degradation under actual field conditions is still limited.

In the following, we will present current understanding, but also prevalent knowledge gaps for pesticide transformation in the terrestrial and aquatic environment. Specifically, given the mentioned shortcomings of most available data, we will address the major challenges in extrapolating from laboratory to field conditions and discuss emerging methods to address these challenges.

The Dominating Role of Microorganisms

Biodegradation is generally recognized as the mass balance–wise most important route of pesticide degradation. Whereas plants, animals, and fungi (Eukaryota) typically transform pesticides for detoxification or through fortuitous metabolism by broad-spectrum enzymes, bacteria (Prokaryota) more commonly metabolize them for assimilation as essential nutrients and energy. This dichotomy is likely due to a wider range of sensitive targets in Eukaryota. For example, the organophosphate esters that interfere with nerve signal transmission in insects do not affect microbial processes and may therefore serve as sources of carbon and phosphorus for microorganisms if they harbor enzymes capable of hydrolyzing phosphotriesters. Bacteria are further more likely to contain such enzymes because of their well-documented propensity for rapid evolution of new enzymes and metabolic pathways that are strongly selected for when they supply one or more essential nutrients for the cell (*8*). In addition, facile horizontal transfer of biodegradation genes is known to occur within microbial populations, and this has been observed to spread newly evolved biodegradation pathways globally (*9*).

Some pesticide transformation reactions, particularly substitutions, can proceed both biotically and abiotically, but typically higher rates are observed for enzyme-catalyzed reactions. For example, the hydrolytic dechlorination of atrazine to hydroxyatrazine in soil had previously been attributed to abiotic processes, but later studies identified atrazine-dechlorinating enzymes in bacteria that produced hydroxyatrazine with a second-order rate constant of 10^5 M^{-1} s^{-1} (*10*) (Fig. 1D). A comparison of these rates with rates of abiotic atrazine dechlorination and the presence of detectable levels of the gene encoding

[1]Eawag, Swiss Federal Institute of Aquatic Science and Technology, 8600 Dubendorf, Switzerland. [2]Institute of Biogeochemistry and Pollutant Dynamics, ETH Zurich, 8092 Zurich, Switzerland. [3]Department of Biochemistry, Molecular Biology and Biophysics, University of Minnesota, St. Paul, MN 55108, USA. [4]Institute of Groundwater Ecology, Helmholtz Zentrum Munchen, 85764 Neuherberg, Germany.

*Corresponding author. E-mail: kathrin.fenner@eawag.ch

those enzymes in most soils surveyed make it highly likely that biotic atrazine degradation dominates in the environment. In cases where biotic and abiotic reactions may both contribute to observed biotransformation, the ability to evaluate their respective contribution is critical to enable extrapolation to structurally similar compounds or to other environmental conditions. In other cases, enzymes have been shown to facilitate reactions that have no counterpart in abiotic chemistry, as with the herbicide glyphosate. Glyphosate contains a C-P bond that is stable to light, reflux in strong acid or base, and other abiotic conditions. Yet, microbes that cleave the C-P bond are now known to be fairly widespread in the environment, and some of those systems can

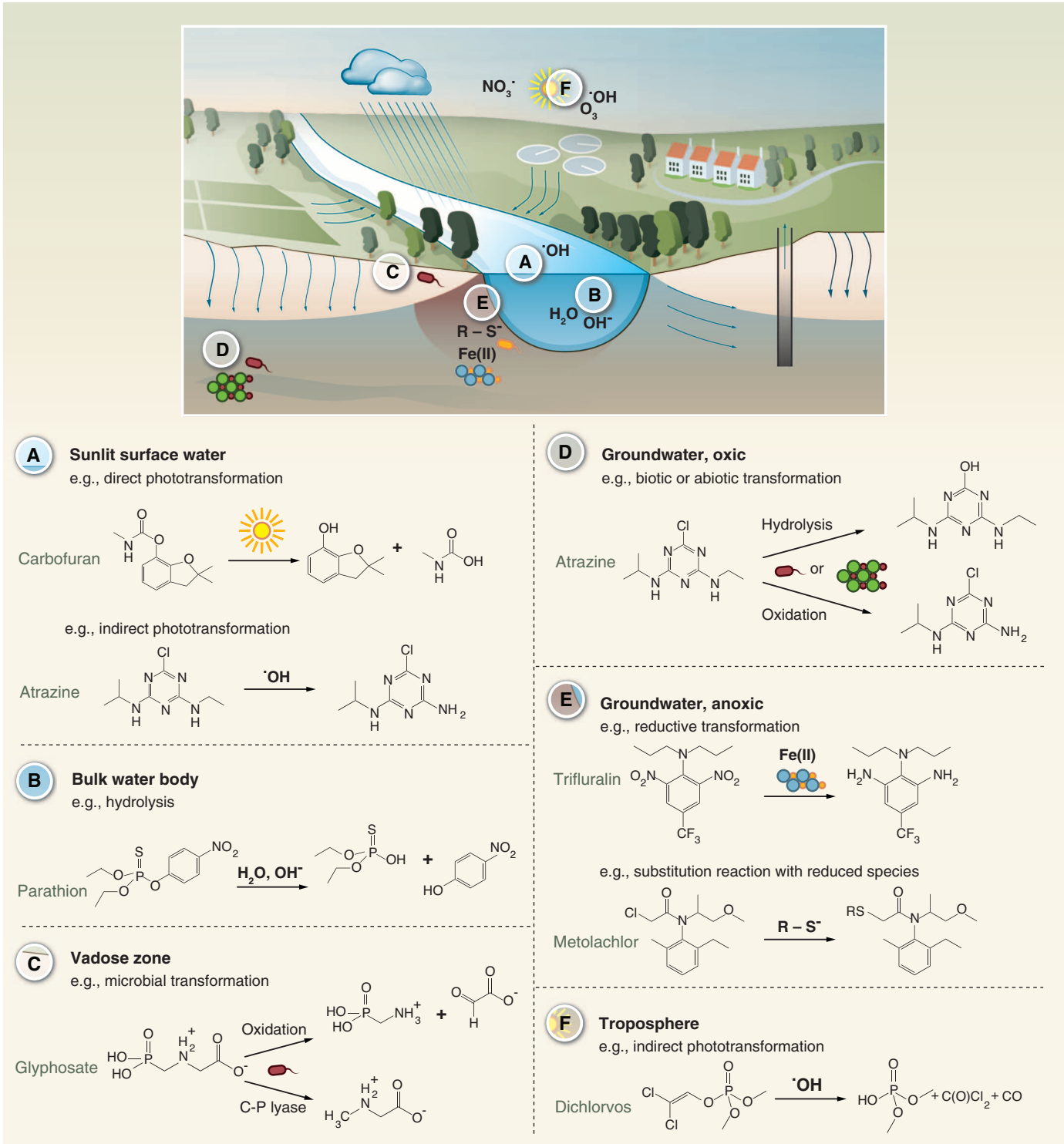

Fig. 1. Overview of pesticide degradation in the environment. (Upper) Main compartments and reaction partners for pesticide degradation. (Lower) Examples of relevant reactions in each compartment, including example reactions for important pesticide representatives [i.e., (**A**) carbofuran (direct phototransformation), atrazine (indirect phototransformation), (**B**) parathion, (**C**) glyphosate, (**D**) atrazine, (**E**) trifluralin (reductive transformation), metolachlor (substitution reaction), (**F**) dichlorvos].

Table 1. Main environmental degradation routes and environmental occurrence in secondary compartments for top 10 pesticide classes. Values are based on amounts used relative to total global pesticide consumption in 2009/2010 (*1*). AMPA, aminomethylphosphonic acid; DEA, desethylatrazine; NDMA, *N*-nitrosodimethylamin.

Pesticide class	Major representative active substance and structural motif	Major use category	Percent of global pesticide use	Main environmental degradation route	Environmental occurrence in secondary compartments (remote regions surface water, groundwater, etc.)
Dithiocarbamates	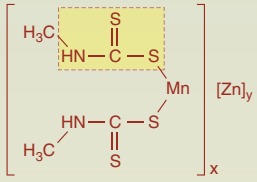 Mancozeb	Fungicides	7.1	Acid-catalyzed hydrolysis; formation of potential NDMA precursors (*49*)	Rarely observed
Organophosphates	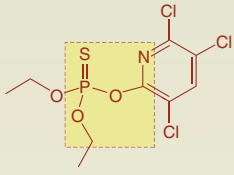 Chlorpyrifos	Insecticides	6.7	Microbial transformation (oxidation and hydrolysis)	Glyphosate and AMPA frequently detected in groundwater (*3*, *50*); chlorpyrifos, diazinon, disulfuton detected in rainwater and remote lake waters (*6*, *51*)
Phenoxy alkanoic acids	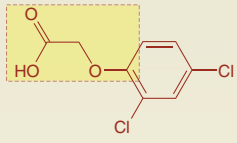 2,4-D	Herbicides	4.7	Microbial transformation (oxidative dealkylation and aromatic ring cleavage)	Parent compounds frequently detected in groundwater (*3*, *52*)
Amides	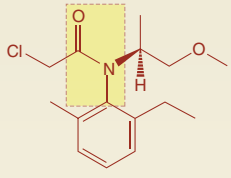 S-Metolachlor	Herbicides	4.2	Microbial transformation (hydrolysis and glutathione coupling)	Chloroacetanilides and their transformation products oxanilic (OXA) and ethanesulfonic acid (ESA) frequently detected in groundwater (*4*); metolachlor and alachlor detected in remote lake waters (*6*, *51*)
Bipyridyls	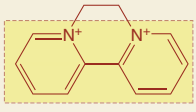 Diquat	Herbicides	3.2	Only very slowly biotransformed due to strong sorption to soil matrix	Rarely observed; mainly sorbed to sediments and soils
Triazines	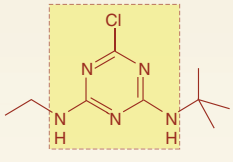 Terbuthylazine	Herbicides	2.3	Microbial transformation (oxidative dealkylation and hydrolysis)	Parent compounds and hydroxy- and dealkylated transformation products frequently detected in groundwater (significantly beyond phase-out period); atrazine and DEA detected in remote lake waters (*6*, *51*)

Triazoles, diazoles	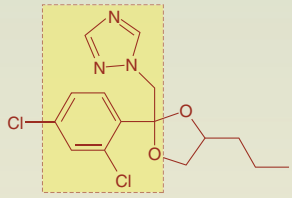 Propiconazole	Fungicides	2.0	Slow microbial transformation (oxidation); photo-transformation of specific representatives	Flutriafol detected in remote lake waters (*51*)
Carbamates	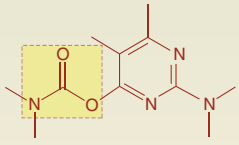 Pirimicarb	Insecticides/ herbicides	2.0	Ready microbial or base-catalyzed transformation (hydrolysis of ester bond); photo-transformation of specific representatives	Rarely observed
Urea derivatives	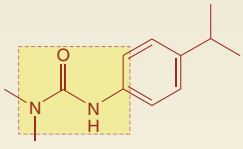 Isoproturon	Herbicides	1.7	Microbial transformation (oxidative dealkylation and hydrolysis)	Parent compounds frequently detected in groundwater (*3*)
Pyrethroids	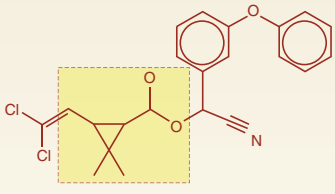 Cypermethrin	Insecticides	1.3	Microbial transformation (hydrolysis, oxidation); photo-transformation (direct and indirect)	Rarely observed; mainly sorbed to sediments and soils

metabolize glyphosate (Fig. 1C). The difficult nature of the reaction is underscored by the observation that C-P lyase, the enzyme system catalyzing C-P bond cleavage, is encoded by a 14-gene operon (*11*).

Given that biotic processes are often dominant and prokaryotes typically degrade pesticides completely, one may ask why transformation products of biotic processes are observed at all. This is sometimes attributed to "cometabolism," but the term itself does not provide insight into the numerous reasons why biotransformation products may accumulate. In atrazine metabolism, for example, many bacteria produce hydroxyatrazine and further metabolize it to carbon dioxide and ammonia. However, both whole cell (*12*) and purified enzyme studies (*13*) indicate that the enzyme producing hydroxyatrazine acts faster than the enzyme consuming it, so a substantial steady-state level of hydroxyatrazine accumulates. Therefore, the hydroxyatrazine that is observed in soil fate studies is not an end product of metabolism, but a metabolic intermediate that nonetheless can accumulate to substantial levels. In other situations (e.g., in wastewater treatment), microorganisms mostly grow on other, more readily assimilable carbon substrates, whereas pesticides present at trace concentrations are transformed through fortuitous metabolism, producing potentially recalcitrant intermediates.

An even more puzzling question is why pesticides are observed to persist over decades in groundwater although bacteria are in principle abundant and a potential for microbial pesticide degradation can therefore be detected even in groundwater (*14*). This paradox is closely related to the question of threshold concentrations [i.e., pesticide concentrations below which microbial degradation appears to stall (*15*)] in low-nutrient environments such as groundwater. As yet, very little is known about pesticide biodegradation under such conditions. Most prominently, methods have been lacking to follow biodegradation in groundwater over the relevant long time scales and to isolate relevant degraders from such environments.

Under Which Conditions Can Abiotic Pesticide Transformation Become Important?

In surface waters, phototransformation can substantially contribute to pesticide transformation (*5*, *16*). Environmental photochemistry distinguishes between direct and indirect photolysis/phototransformation: "direct" meaning that photons are absorbed by the contaminant itself, and "indirect" denoting that reactive species are formed through photon absorption by other water constituents. Because the electronic absorption spectrum of most pesticides shows little overlap with the spectrum of terrestrial sunlight, only a few pesticides are affected by direct phototransformation (*17*) (e.g., trifluralin, a dinitroaniline derivative, which absorbs sunlight even in the visible spectral region). By contrast, indirect phototransformation processes are more likely, because various photochemically active light absorbers are present in surface waters. The most prominent among these absorbers is dissolved natural organic matter (DOM), which is the precursor of excited triplet states, singlet (molecular) oxygen, superoxide radical anions, and other DOM-derived radicals. Nitrate and nitrite ions are additional active absorbers that produce hydroxyl radicals under irradiation. Indirect phototransformation of a given pesticide can be considered as the result of parallel reactions

with all these reactive species (*18*). To assess the transformation rate of a pesticide in the environment, one therefore has to know the concentrations of all relevant reactive species, together with their corresponding second-order rate constants for this pesticide. For hydroxyl radical and singlet oxygen, a comprehensive compilation of experimentally determined rate constants for organic compounds is available (*19*). In the absence of such rate constants, quantitative structure-activity relationships (QSARs) may allow their estimation for a specific pesticide from its chemical structure (*20*).

The relevance of non–sunlight-mediated chemical ("dark abiotic") transformations can differ greatly between pesticides. Textbook reactions can directly be predicted for some compounds based on the presence of functional groups. For example, abiotic hydrolysis in aqueous solution is well established for organophosphates (Fig. 1B), carboxylic acid esters, carbamates, carbonates, some halides (methyl bromide, propargyl), and many more. By contrast, compounds lacking suitable reactive groups, are frequently recalcitrant to chemical transformation. For rates to compete with biodegradation, specific conditions such as high pH or low-redox environments may be required, combined with in situ formation of suitable abiotic catalysts [e.g., (poly)sulfides, surface-bound Fe(II), MnO_2]. The latter is actually often mediated by microorganisms, which blurs the strict distinction between abiotic and biotic transformations. Nonetheless, some chemical transformations may only be recognized when investigated under the respective relevant conditions. Examples are clay-catalyzed triazine hydrolysis (Fig. 1D) (*21*), chloroacetanilide (*22*) and nitroaromatics transformation (*23*) in sulfidic environments (Fig. 1E), or glyphosate oxidation by MnO_2 (*24*). Chemical reactions may also prevail in compartments such as groundwater or lake hypolimnions, which have hydraulic retention times on the order of years and where biomass densities are lower due to almost complete removal of assimilable organic carbon.

What Methods Are Available to Assess and Predict Pesticide Degradation in Nature?

Available strategies to directly identify transformation of pesticides in nature either rely on the detection of parent compound disappearance, detection of transformation products, or evidence of an intrinsic transformation potential in a given environment. Many of the existing methods, however, are only sensibly applicable on the micro- or mesocosm scale (Fig. 2). For instance, the common strategy of monitoring parent pesticide concentrations by gas chromatography–mass spectrometry (GC-MS) or liquid chromatography–tandem mass spectrometry (LC-MS/MS) does not allow distinguishing transformation from other processes such as dilution or sorption unless combined with stringent mass balance modeling of the environmental system in question. Although the use of ^{14}C-labeled pesticides does enable mass balances, investigations with radioactively labeled substrates cannot be conducted in the field.

Detection of transformation products may provide evidence of degradation in the field. This approach is straightforward if products are known and standards are available (target analysis), and becomes more challenging otherwise (suspect or nontarget analysis). Here, the availability of high-resolution mass spectrometry has facilitated not only the development of multicomponent analytical methods for several hundred target

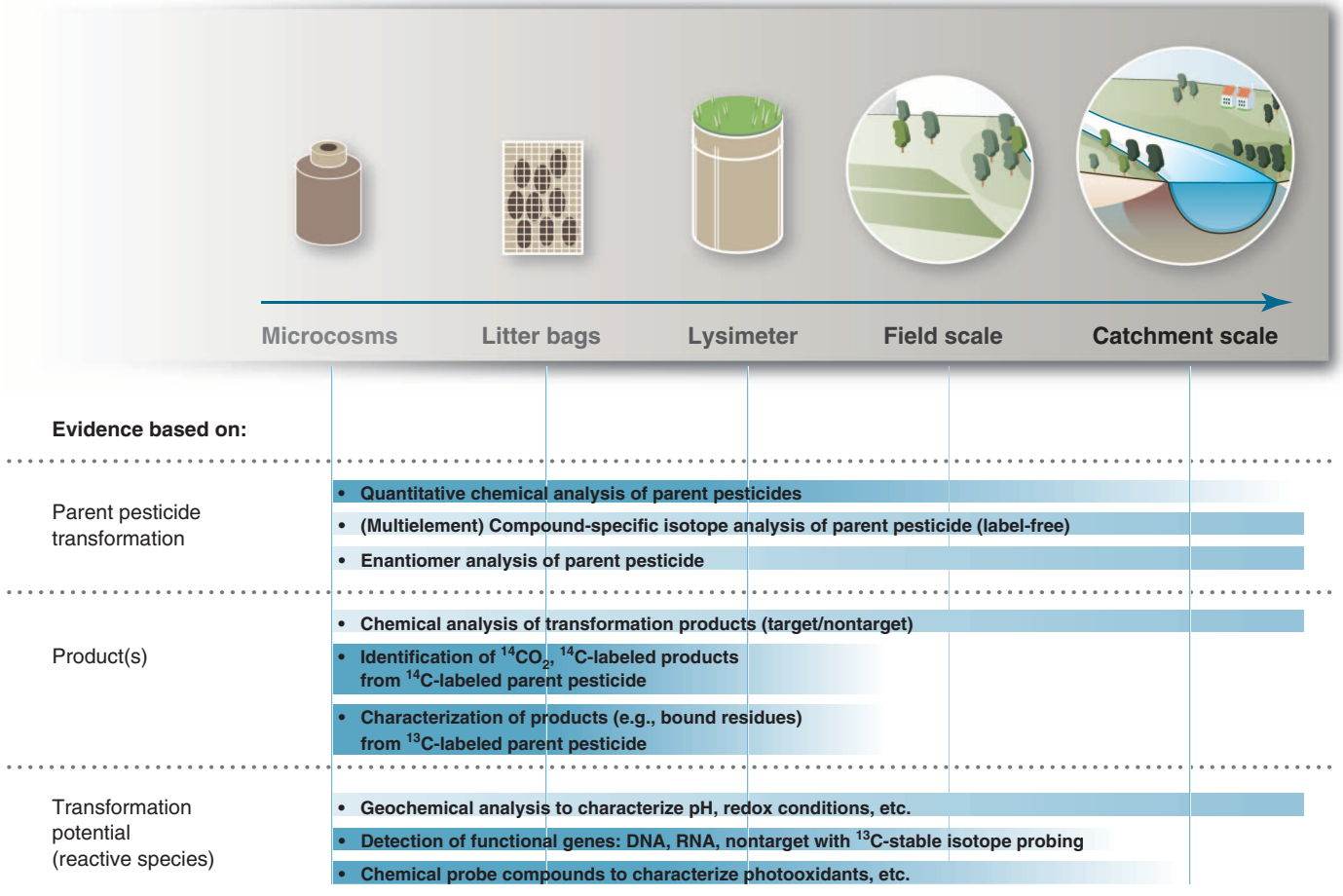

Fig. 2. Available analytical approaches to identify pesticide transformation in natural environments. For each approach, shading indicates the spatial scales at which it can best be applied.

analytes, as was recently done for 150 pesticide transformation products (*25*), but also the screening for suspected transformation products. Particularly in combination with models that predict likely transformation product structures, this latter option allows a more comprehensive assessment of the presence of pesticide transformation products in the environment, independent of the outcome from degradation studies carried out under specific conditions (*26*).

Compound-specific isotope analysis may provide yet a complementary line of evidence because it can detect degradation even if no metabolites are found and has the potential to cover sufficiently long time scales to study transformation in groundwater. Degradation-related information is derived from analysis of isotope ratios (e.g., $^{13}C/^{12}C$, $^{15}N/^{14}N$) of the parent pesticide in the absence of any label (natural isotopic abundance). Because kinetic isotope effects typically favor transformation of light isotopes (e.g., ^{12}C), heavy isotopes (^{13}C) become enriched in the remaining pesticide. Increasing $^{13}C/^{12}C$ isotope ratios in a parent compound thus provide direct evidence of its degradation. Therefore, if repeated pesticide analyses in groundwater over time—or spatially resolved measurements in combination with groundwater dating—show increasing $^{13}C/^{12}C$ isotope ratios in a parent pesticide, this provides direct evidence of its degradation, even if the pesticide was released long in the past. As demonstrated for the pesticide atrazine (*27*), even different transformation pathways can be elucidated provided that isotope effects of multiple elements are analyzed. In such a case, transformation mechanisms are identifiable from plots of $^{13}C/^{12}C$ versus $^{15}N/^{14}N$ parent compound data, reflecting different underlying carbon- and nitrogen-isotope effects. A challenge of the approach is the currently relatively high amount of substance needed for gas chromatography–isotope ratio mass spectrometry (GC-IRMS) or LC-IRMS analysis (100 ng to 1 μg), which, for instance, requires extraction of 10 liters of groundwater at pesticide concentrations of 100 ng/liter (*28*). For the special case of chiral pesticides, enantiomer analysis may provide yet another line of evidence based on a similar principle: enrichment of enantiomers (rather than isotopes) as a result of stereoselective biotransformation (*29*). Strongest insights can be expected when both approaches are combined in the field (*30*).

Methods detecting an intrinsic transformation potential are generally suited for field-scale investigations. Geochemical analysis of pH, redox potential, dissolved ions, and so forth is routinely applied to detect conditions that are conducive to certain biotic and abiotic pesticide transformations (Fig. 1). Chemical probe compounds are an elegant way to characterize the occurrence of abiotic reactive species in natural systems, but their use to estimate transformation rates in the field may be challenging. A first problem area is given when the reactive species are defined as a category and not as a single, well-defined chemical species. This is, for instance, the case with indirect photochemical reactions in surface waters, where excited triplet states of the DOM are formed as a manifold displaying a wide range of reactivities. 2,4,6-Trimethylphenol (TMP) has been used as a probe compound to measure DOM excited triplet states capable of undergoing oxidation reactions (*31*). Depending on the ability of the target pesticide to be transformed by such reactions, it will "feel" more or less triplet states than determined by TMP. Thus, the development of methods using additional probe compounds that better match target pesticide reactivity is essential to improve transformation rate predictions. A second critical question concerns the selectivity of probe compounds to detect individual reactive species when a mixture of reactive species is present. In general, a probe compound will react with more reactive species than with the one it is mainly intended for. To overcome these limitations, methods relying on the combined use of selective probe compounds and scavengers or quenchers appear most promising (*32*). An illustrative case from recent research is *N*,*N*-dimethylaniline. Used as probe compound for the carbonate radical (*33*), it also reacts very quickly with DOM excited triplet states, and its oxidation is partly hampered by DOM (*34*). Consequently, more selective and suitable probe compounds to detect carbonate radicals are urgently needed

To demonstrate a biotransformation potential in soil and sediment samples, nontarget analysis of degraders by stable isotope probing (SIP), where the use of ^{13}C-labeled parent pesticides facilitates ^{13}C labeling, isolation, and subsequent amplification of degrader DNA, is increasingly used (*35*). A complementary, potentially more quantitative, emerging technique is to directly study the potential of a community for pesticide biodegradation through enumeration of the biodegradative gene(s) via quantitative polymerase chain reaction (QPCR), high-throughput gene sequencing, or use of functional gene microarrays, as all of these methodologies have become easily accessible. A prerequisite for gene-based approaches, however, is that the involved genes are known and can be clearly attributed to a given transformation reaction. For instance, the *atzD* gene encoding cyanuric acid hydrolase has been found to correlate with atrazine biodegradation in the surface layers of an agricultural soil (*36*), consistent with the knowledge that AtzD cleaves the *s*-triazine ring during the course of bacterial atrazine metabolism. AtzD met the requirement of being unambiguously identifiable and hence quantifiable, as it belongs to a small protein family that largely consists of biodegradative enzymes. However, this situation is rare. Most pesticide biodegradative proteins studied to date are members of very large protein superfamilies, with as many as 600,000 individual members, the vast majority of which have different functions than the target enzyme. Another factor confounding gene-based approaches is that biodegradative functions can arise independently in evolution, such that genes with completely different sequences may catalyze the same reaction. It is well known that organophosphate esterases that differ markedly in their protein fold and mechanism can nonetheless act on the same organophosphate pesticide (*37*). This likely explains why PCR amplification failed to detect a target gene encoding an organophosphate esterase in soils containing bacteria that were later shown to express organophosphate esterase activity (*38*).

In the future, the broad-based applicability of gene-based methods for demonstrating biodegradation will be improved by new developments in bioinformatics that seek to better assign biological function to proteins when only their sequence is known (*39*). Moreover, it is also advisable to couple sequence-based methods with other independent methods whenever possible. If certain genes are implicated by nucleic acid–based methods, one can potentially use computational tools or protein functional databases to infer possible transformation products of a pesticide and then use sensitive mass spectrometric methods to identify the products as discussed above.

Are Transformation Products an Issue of Concern?

Even though their original effect is typically lowered (*40*), pesticide transformation products may still be highly relevant. First, certain transformations leave the active moiety intact—for instance, oxidation of thioethers to sulfones and sulfoxides (*41*). Mixtures of parent compound and transformation products may therefore have additive effects (*42*). Second, (eco-)toxicologically more potent structures may be generated. For instance, a recent debate centers on phenolic degradates of such diverse chemical classes as pyrethroids and aryloxyphenoxypropionic herbicides and whether they can act on estrogen receptors (*43*, *44*). Such transformation products with a potential for endocrine disruption or other chronic effects should receive particular attention because they are often smaller and more polar than their respective parent compounds. This increases their potential to reach drinking water resources such as groundwater and surface waters, where polar transformation products are found at fairly constant concentrations throughout the year (*5*). Pesticide transformation products in drinking water resources may also cause unexpected new problems such as the recently discovered formation of carcinogenic *N*-nitroso-dimethylamine from dimethylsulfamide, a microbial transformation product of the fungicides tolylfluanide and dichlofluanide, during drinking water treatment with ozone (*45*).

The issue of transformation product formation is specifically addressed in major regulatory frameworks. In Europe, for instance, "nonrelevant"

metabolites are distinguished from metabolites that are "relevant for groundwater resources" or even "ecotoxicologically relevant" (*46*). Ecotoxicologically relevant metabolites are those that pose a comparable or higher risk to soil or aquatic biota than the parent compound, and are therefore subject to the same level of risk assessment. Metabolites relevant for groundwater are those likely to reach groundwater in concentrations above 0.1 μg/liter and to display the same toxicity as the parent compound (target toxicity or severe other toxicity such as genotoxicity, reproductive toxicity, or carcinogenicity). Despite these regulatory provisions, however, it remains unclear how complete our current understanding of the occurrence and effects of pesticide transformation products really is. The past has shown that findings of particularly prevalent or toxicologically relevant transformation products typically emerged only 20 to 30 years after their market introduction. Examples are the detection of chloridazon transformation products (first marketed in 1964) in surface and groundwater (*47*), or the above-mentioned formation of carcinogenic *N*-nitroso-dimethylamine from tolylfluanid (first marketed in 1971). That these substances have been overlooked for so long may partially be attributable to limited analytical capabilities in the past. However, it also seems that the distinction between relevant and nonrelevant metabolites may have resulted in mobile and persistent transformation products receiving little attention because they were generally not considered toxicologically relevant.

A more complete picture of pesticide transformation products in environmental resources is expected to emerge over the next years thanks to advances in mass spectrometry as outlined above. This will confront society with questions on how to deal with the occurrence of certain transformation products in water resources, and on how to weigh human and environmental health against the benefits of the respective pesticides. Specifically, the decision to tolerate up to 10 μg/liter of "nonrelevant" metabolites in groundwater and drinking water is politically highly contentious in Europe. Some consider the higher limit acceptable as no imminent health risk can be proven, whereas others regard it as a fundamental deviation from the precautionary principle (*48*).

Outlook

As global pesticide use can be anticipated to continue to increase, the question of what residual pesticide concentrations are environmentally and socially acceptable will remain important. The new pesticide legislation in Europe puts more emphasis on hazard assessment, source control measures, and substitution. Substitution, however, also bears risks when substituting a well-investigated pesticide with one whose actual environmental fate is yet to be explored. Therefore, it is imminently important for scientist to improve their ability to predict the long-term fate, and in particular degradation, of pesticides in the environment beyond what is known from regulatory testing.

Future research in that field should particularly address the blind spots with respect to pesticide degradation at low concentrations and in low-nutrient situations encountered in groundwater, lake hypolimnions, or seawater. The development of such a system-oriented understanding of natural pesticide attenuation will require innovative tools for characterizing the transformation potential in those environments such as using combinations of advanced analytical approaches (e.g., compound-specific isotope analysis, enantiomer analysis, and mass spectrometry–based screening for transformation products). Also, developments in bioinformatics to assign biological functions to proteins on the basis of their sequences alone, in combination with inferring and screening for potential transformation products, are expected to play a crucial role. With these and other innovative tools at hand, questions on the extent of biodegradation at low pesticide concentrations, the underlying limitations ("bottlenecks of degradation") at such threshold concentrations, and the relative importance of biodegradation versus chemical processes in low-nutrient situations will become increasingly addressable.

References and Notes

1. Food and Agriculture Organization of the United Nations (FAO), FAOSTAT, 2012 (faostat.fao.org).
2. U.S. Environmental Protection Agency (U.S. EPA), "Pesticides Industry Sales and Usage" (Washington, DC, 2011).
3. H. Bartel *et al.*, "Wasserwirtschaft in Deutschland. Teil 1, Grundlagen" [Umweltbundesamt (UBA), Dessau-Rosslau, Germany, 2010].
4. R. J. Gilliom *et al.*, in *The Quality of Our Nation's Waters—Pesticides in the Nation's Streams and Ground Water, 1992–2001*, U. S. Department of the Interior, U.S. Geological Survey, Eds. (Reston, VA, 2006).
5. S. Huntscha, H. Singer, S. Canonica, R. P. Schwarzenbach, K. Fenner, *Environ. Sci. Technol.* **42**, 5507–5513 (2008).
6. P. B. Kurt-Karakus, C. Teixeira, J. Small, D. Muir, T. F. Bidleman, *Environ. Toxicol. Chem.* **30**, 1539–1548 (2011).
7. R. Atkinson *et al.*, *Water Air Soil Pollut.* **115**, 219–243 (1999).
8. S. D. Copley, *Nat. Chem. Biol.* **5**, 559–566 (2009).
9. M. L. de Souza, J. Seffernick, B. Martinez, M. J. Sadowsky, L. P. Wackett, *J. Bacteriol.* **180**, 1951–1954 (1998).
10. L. P. Wackett, M. Sadowsky, B. Martinez, N. Shapir, *Appl. Microbiol. Biotechnol.* **58**, 39–45 (2002).
11. B. Jochimsen *et al.*, *Proc. Natl. Acad. Sci. U.S.A.* **108**, 11393–11398 (2011).
12. M. Devers, N. Rouard, F. Martin-Laurent, *Environ. Microbiol.* **10**, 676–684 (2008).
13. J. L. Seffernick *et al.*, *J. Bacteriol.* **189**, 6989–6997 (2007).
14. G. S. Janniche, H. Spliid, H.-J. Albrechtsen, *J. Contam. Hydrol.* **140–141**, 45–55 (2012).
15. T. Egli, *Water Res.* **44**, 4826–4837 (2010).
16. A. C. Gerecke, S. Canonica, S. R. Müller, M. Schärer, R. P. Schwarzenbach, *Environ. Sci. Technol.* **35**, 3915–3923 (2001).
17. H. D. Burrows, M. Canle L, J. A. Santaballa, S. Steenken, *J. Photochem. Photobiol. B* **67**, 71–108 (2002).
18. J. Hoigné, in *Aquatic Chemical Kinetics: Reaction Rates of Processes in Natural Waters,* W. Stumm, Ed. (Wiley-Interscience, New York, 1990), pp. 43–70.
19. National Institute of Standards and Technology (NIST), NDRL/NIST Solution Kinetics Database on the Web. NIST Standard Reference Database 40, 2002 (http://kinetics.nist.gov/solution/).
20. S. Canonica, P. G. Tratnyek, *Environ. Toxicol. Chem.* **22**, 1743–1754 (2003).
21. J. C. Xu, J. W. Stucki, J. Wu, J. E. Kostka, G. K. Sims, *Environ. Toxicol. Chem.* **20**, 2717–2724 (2001).
22. A. R. Loch *et al.*, *Environ. Sci. Technol.* **36**, 4065–4073 (2002).
23. T. Zeng, Y.-P. Chin, W. A. Arnold, *Environ. Sci. Technol.* **46**, 3177–3187 (2012).
24. K. A. Barrett, M. B. McBride, *Environ. Sci. Technol.* **39**, 9223–9228 (2005).
25. T. Reemtsma, L. Alder, U. Banasiak, *J. Chromatogr. A* **1271**, 95–104 (2013).
26. S. Kern, K. Fenner, H. P. Singer, R. P. Schwarzenbach, J. Hollender, *Environ. Sci. Technol.* **43**, 7039–7046 (2009).
27. T. B. Hofstetter, M. Berg, *TrAC-Trends Anal. Chem.* **30**, 618–627 (2011).
28. K. Schreglmann, M. Hoeche, S. Steinbeiss, S. Reinnicke, M. Elsner, *Anal. Bioanal. Chem.* **405**, 2857–2867 (2013).
29. H. R. Buser, M. D. Muller, *Environ. Sci. Technol.* **32**, 626–633 (1998).
30. N. Milosevic *et al.*, *Water Res.* **47**, 637–649 (2013).
31. S. Halladja, A. Ter Halle, J. F. Pilichowski, A. Boulkamh, C. Richard, *Photochem. Photobiol. Sci.* **8**, 1066–1071 (2009).
32. E. De Laurentiis *et al.*, *Environ. Sci. Technol.* **46**, 8164–8173 (2012).
33. T. Zeng, W. A. Arnold, *Environ. Sci. Technol.* **47**, 6735–6745 (2013).
34. S. Canonica, H. U. Laubscher, *Photochem. Photobiol. Sci.* **7**, 547–551 (2008).
35. A. M. Cupples, G. K. Sims, *Soil Biol. Biochem.* **39**, 232–238 (2007).
36. C. Monard, F. Martin-Laurent, O. Lima, M. Devers-Lamrani, F. Binet, *Biodegradation* **24**, 203–213 (2013).
37. A. N. Bigley, F. M. Raushel, *BBA-Proteins Proteomics* **1834**, 443–453 (2013).
38. M. K. Choi *et al.*, *J. Microbiol. Biotechnol.* **19**, 1679–1687 (2009).
39. P. Radivojac *et al.*, *Nat. Methods* **10**, 221–227 (2013).
40. A. B. A. Boxall, C. J. Sinclair, K. Fenner, D. Kolpin, S. J. Maund, *Environ. Sci. Technol.* **38**, 368A–375A (2004).
41. C. B. Choung, R. V. Hyne, M. M. Stevens, G. C. Hose, *Arch. Environ. Contam. Toxicol.* **60**, 417–425 (2011).
42. S. Pesce *et al.*, *Aquat. Toxicol.* **99**, 492–499 (2010).
43. M. Q. Jin, L. Li, C. Xu, Y. Z. Wen, M. R. Zhao, *J. Environ. Sci. (China)* **22**, 290–296 (2010).
44. B. Laffin, M. Chavez, M. Pine, *Toxicology* **267**, 39–44 (2010).
45. C. K. Schmidt, H. J. Brauch, *Environ. Sci. Technol.* **42**, 6340–6346 (2008).
46. European Union, Regulation (EC) No. 1107/2009 of the European Parliament and of the Council of 21 October, *Off. J. Eur. Union L* **309**, 1 (2009).
47. G. Buttiglieri *et al.*, *Water Res.* **43**, 2865–2873 (2009).
48. H. H. Dieter, *Regul. Toxicol. Pharmacol.* **56**, 121–125 (2010).
49. L. P. Padhye, J. H. Kim, C. H. Huang, *Water Res.* **47**, 725–736 (2013).
50. S. Kilchmann, M. Reinhardt, M. Schürch, D. Traber, "Ergebnisse der Grundwasserbeobachtung Schweiz (NAQUA). Zustand und Entwicklung 2004-2006" [Bundesamt für Umwelt (BAFU), Bern, 2009].
51. D. C. G. Muir, C. Teixeira, F. Wania, *Environ. Toxicol. Chem.* **23**, 2421–2432 (2004).
52. F. Malaguerra, H.-J. Albrechtsen, L. Thorling, P. J. Binning, *Sci. Total Environ.* **414**, 433–444 (2012).

Acknowledgments: We thank R. Schwarzenbach, K. Lanz, and C. Stamm for helpful comments on the manuscript and the Swiss National Science Foundation (SNSF), Eawag, the Federal Office for the Environment (FOEN), the German National Science Foundation (DFG, SPP-1315), the Helmholtz Association, and the U.S. NSF (Partnerships for Innovation grant 1237754) for continuous support of our work.

10.1126/science.1236281

REVIEW

Wildlife Ecotoxicology of Pesticides: Can We Track Effects to the Population Level and Beyond?

Heinz-R. Köhler[1]* and Rita Triebskorn[1,2]

During the past 50 years, the human population has more than doubled and global agricultural production has similarly risen. However, the productive arable area has increased by just 10%; thus the increased use of pesticides has been a consequence of the demands of human population growth, and its impact has reached global significance. Although we often know a pesticide´s mode of action in the target species, we still largely do not understand the full impact of unintended side effects on wildlife, particularly at higher levels of biological organization: populations, communities, and ecosystems. In these times of regional and global species declines, we are challenged with the task of causally linking knowledge about the molecular actions of pesticides to their possible interference with biological processes, in order to develop reliable predictions about the consequences of pesticide use, and misuse, in a rapidly changing world.

Wildlife ecotoxicology has its roots in acute poisoning events in the late 19th century; however, public concern over the undesirable environmental effects of chemicals arose in the early 1960s with the publication of Rachel Carson´s *Silent Spring*, which publicly broached the issue of the environmental risks of pesticide use for the first time. Shortly thereafter, DDT and its metabolites were found to be responsible for population-level effects in raptorial birds and, with the realization of the global nature of organochlorine pesticide contamination, long-range studies on wildlife exposure, mainly on the basis of environmental analytical chemistry, were launched (*1*). At that time, in industrialized countries, attention was focused on acute mortality effects in wildlife after pesticide use, abuse, or misuse, mostly involving birds or fish. Currently, pesticide use is widespread in agriculture all over the world, but still only very few countries have established wildlife poisoning surveillance programs (*2*). As a result, many data on pesticides remain scattered and/or not publicly available (*3*). Even 15 years ago, incident registration was already considered an insufficient approach for understanding the side effects of pesticide use in agriculture (*4*). Further shortcomings that are inevitably associated with research on incidents are the difficulties in discriminating between poisoning and other causes of death and the limitations of the analytical detection of pesticides in carcasses (*2*).

Consequently, in the past 25 years, research interest has shifted from documenting incidents, and exclusively quantifying chemical exposure, to effect studies aimed at linking laboratory, mesocosm, and field experiments. Since the early 1990s, the proportion of effect-related publications has continuously increased, even though a large number of mechanistically oriented studies have been conducted on laboratory or domestic species, particularly mammals. In terms of sheer numbers of publications, most research on wildlife ecotoxicology deals with fish, insects, and, to a lesser extent, birds, amphibians, and arachnids (Fig. 1A). Effect-related research, which has addressed insecticides, herbicides, and fungicides in a rather constant proportion of published papers for more than 20 years, does not reflect the actual proportions of active ingredients applied in the United States or Europe, but rather overemphasizes the effects of insecticides (Fig. 1, C and D). Within the literature on pesticide effects, increasing numbers of publications have been recorded for some distinct insecticide classes in recent years, which is indicative of the importance of these currently dominating active ingredients (Fig. 1B). In this context, the past 5 years have revealed a particular progression of interest in the effects of organophosphates, pyrethroids, and the rather "new" class of neonicotinoids. However, there remains ongoing interest in first-generation organochlorine pesticides, such as DDT, which is still in use in many developing countries (*5*). Even though the banning of highly persistent organochlorines in developed countries has shifted pesticide use toward a vast diversity of readily biodegradable ingredients, the explosiveness of organochlorines on a global scale cannot be ignored. The Food and Agriculture Organization of the United Nations estimates that half a million tons of "old" obsolete pesticides have been scattered throughout developing regions in Asia, Latin America, and Africa.

[1]Animal Physiological Ecology, Institute of Evolution and Ecology, University of Tübingen, Konrad-Adenauer-Strasse 20, 72072 Tübingen, Germany. [2]Transfer Center for Ecotoxicology and Ecophysiology, Blumenstrasse 13, 72108 Rottenburg, Germany.

*Corresponding author. E-mail: heinz-r.koehler@uni-tuebingen.de

Regulatory programs have considerably changed the array of pesticides used in agriculture. Since 1993, both the United States and the European Union have implemented programs to update risk assessments for pesticides in use, which made manufacturers pull highly acutely toxic organophosphate and carbamate insecticides from these markets voluntarily. Current-use pesticides are mainly designed on the basis of their desired mode of action, which is aimed at displaying optimal efficiency in target, and minimum side effects in nontarget, organisms. Because of the frequently close phylogenetic relationships of beneficial and pest species, however, it is ambitious to both target and protect. One of the major challenges in wildlife ecotoxicology, therefore, is to trace the effects and side effects of chemicals, from their cellular targets through levels of increasing complexity to communities of species and the function of ecosystems. Here we provide an integrated view of the existing knowledge regarding pesticides of the past and present. This includes synthetic chemicals and biological compounds [such as spinosyns, azadirachtin, and *Bacillus thuringiensis* (Bt) δ-endotoxin] applied in agriculture but excludes nonagricultural biocides used as antifouling or fracking compounds, parasiticides, or antibiotics.

Individuals and Populations

As events of acute poisoning in wildlife have decreased in number during recent decades, at least in developed countries, the problem of chronic pesticide toxicity has moved into the focus of scientific interest. Wherever pesticide application is spatially restricted and buffer zones (such as riparian buffers) are respected, wildlife vertebrates currently are considered unlikely to be exposed to pesticide levels that are acutely toxic, with the exception of some examples of exceedances of acute toxicity values in aquatic systems (*6*, *7*) and anticholinesterase poisoning of birds (*8*). Chronic toxicity, however, has to be taken into account for all pesticides that are applied at regular intervals, particularly those that are highly persistent, such as organochlorines. In addition to their acute toxicity, which has occasionally led to mass deaths in the past, this group of insecticides (including DDT and its metabolite DDE, an androgen receptor antagonist) is known to chronically act as endocrine disruptors (*9*), exerting estrogenic and/or androgenic effects in rats, birds, and fish (*10*). DDT itself is carcinogenic (*9*). To date, more than 120 endocrine-disruptive pesticides are known, covering numerous chemical classes (*11*). Organochlorines, organophosphates, carbamates, pyrethroids, thiocarbamates, triazines, and triazoles furthermore exhibit thyroid disruption properties in rodents, birds, amphibians, and fish (*10*). Immunotoxicity, which is primarily caused by the inhibition of serine hydrolases or esterases, oxidative damage, and the modulation of signal transduction pathways

Fig. 1. Trends in research on pesticide effects and pesticide use. (**A**) Steadily increasing proportion of effect-related research among publications on pesticides in the past 28 years. (**B**) Journal publication numbers on effects related to pesticide classes. During the most recent years, the most substantial increase in the rate of publication was recorded for organophosphates, pyrethroids, and neonicotinoids. (**C**) The proportions of effect-related publications on herbicides, fungicides, and insecticides remained rather constant throughout the past 23 years but did not reflect the proportions of these pesticide classes used in the United States and Europe. (**D**) Effect-related research shows a bias toward domestic and lab model species (in red; including human cell lines) in relation to wildlife animals (in yellow) [calculated from data obtained from the Web of Science (March 2013), the U.S. Environmental Protection Agency, the European Crop Protection Association, and (*88*)].

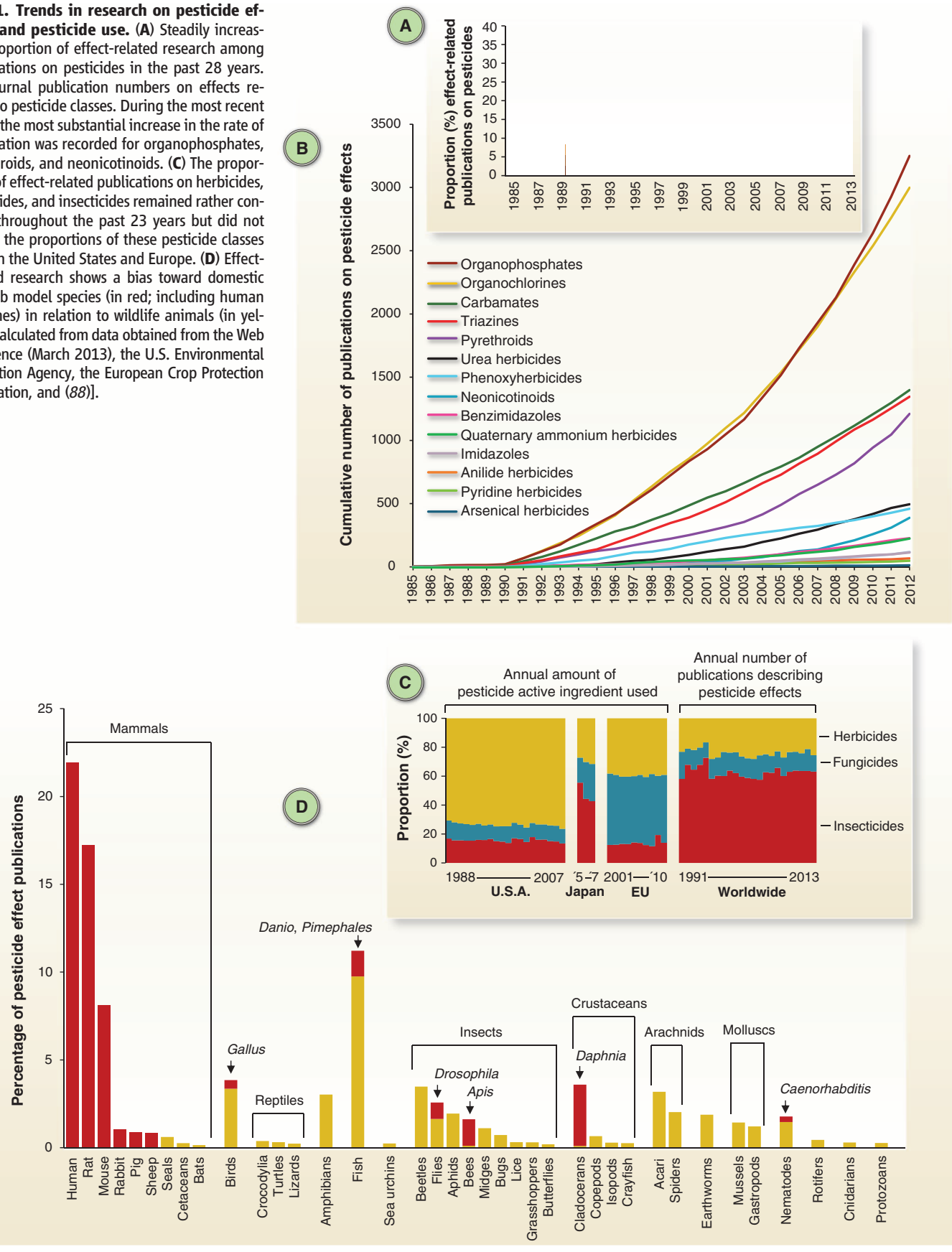

has been reported for organophosphates (*12*). The organochlorine chlordane, carbamates, the phenoxy herbicide 2,4-D, and atrazine were found to interact with the immune system of vertebrates (*13*). Organophosphates and carbamates impair metabolic functions such as thermoregulation, water and/or food intake, and behavior (activity, foraging time, learning ability) in vertebrates. Further consequences are weight loss, impaired development, and reduced reproduction and hatching success (*14*). Particularly in aquatic biota, a plethora of studies have revealed a broad range of pesticides representing a variety of chemical classes to induce embryotoxicity and teratogenicity in nontarget fish, amphibia, and invertebrates, which result in organ malformations, delayed hatching, growth suppression, and embryonic mortality (*15*). Some of these pesticide effects at the sub-individual or individual levels have been causally or plausibly linked to their consequences in populations (Fig. 2).

In general, information on the hazards of pesticides to wildlife is based on the knowledge of their environmental fate, persistence, application rate, and toxicity (*14*); the latter have been largely gained from laboratory experiments predominantly conducted on vertebrates, including mammalian model organisms. Although modern insecticides such as neonicotinoids previously were expected to exert only low toxicity on mammals, birds, and fish, because these compounds have a low affinity for vertebrates relative to insect nicotinic receptors (*16*), current research has provided evidence for respiratory, cardiovascular, neurological, and immunological toxicity in rats and humans (*17*, *18*). However, information about many endangered mammalian species, particularly arctic marine biota, is scarce and is limited to measurements of compounds and a few selected biomarkers, such as CyPIA1 activity (*19*). Effects indicative of endocrine disruption were reported for river otters, bears, seals, sea lions,

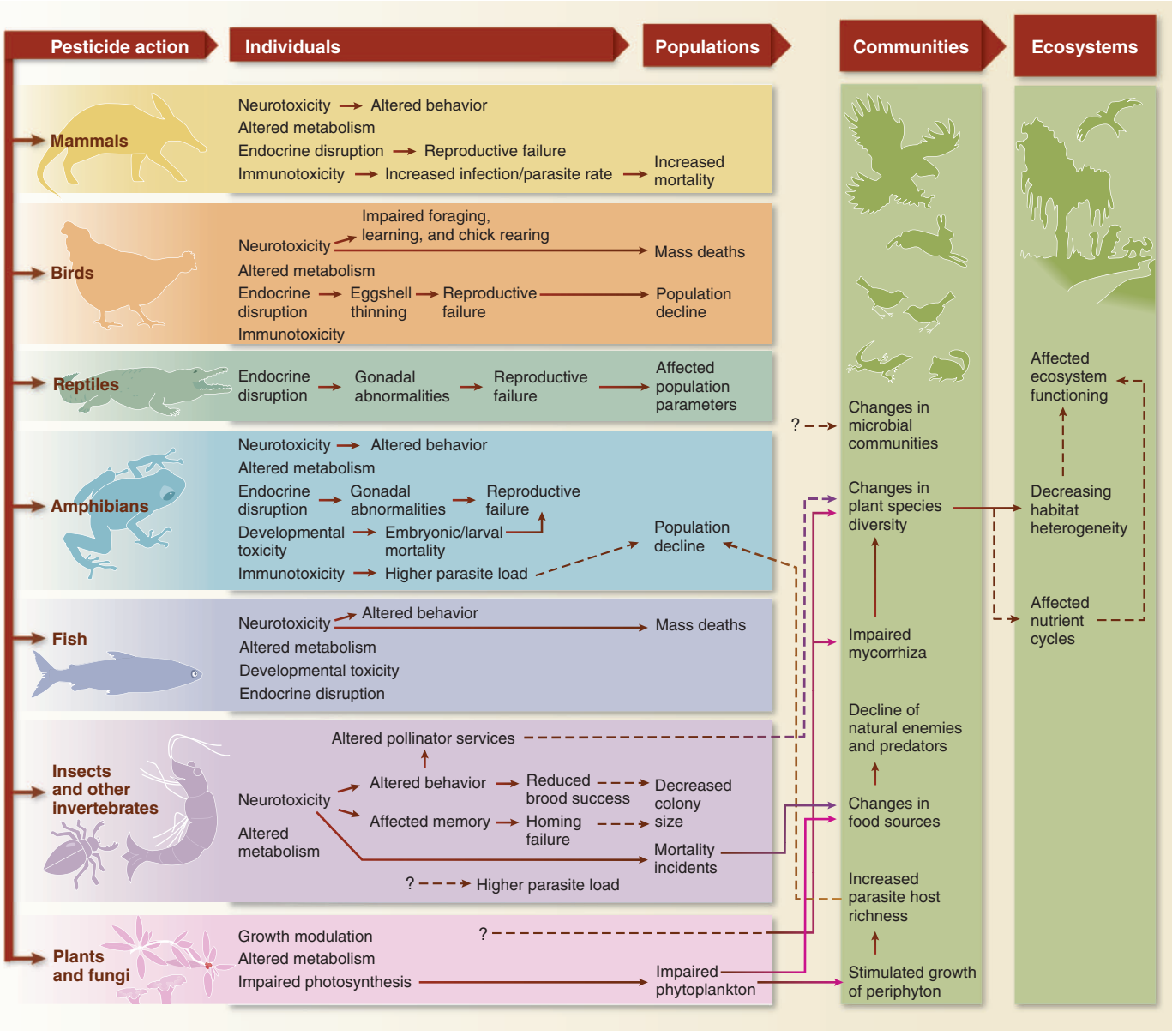

Fig. 2. Documented pesticide effects on wildlife at different levels of biological organization and known (solid arrows) or evidence-supported, anticipated (dashed arrows) interrelations among them. Research remains to be conducted wherever plausibly interrelated effects are not connected by arrows. Most of the sub-individual data for mammals are derived from non-wildlife studies.

and beluga whales from organochlorine-polluted environments, but it was impossible to separate the effects of DDT from those of sympatrically present nonpesticide organochlorines (*20*).

In birds, population effects of pesticides have been linked to neurotoxicity and endocrine disruption. Although acute mortality could be attributed to inhibition of acetylcholine esterase activity exerted by organochlorines, organophosphates, and carbamates (*8*, *21*), chronic exposure via oral uptake to organochlorines and organophosphates in particular, but also to carbamates and a variety of herbicides and fungicides, resulted in disturbances of the endocrine and reproductive system. DDT and its metabolite DDE had a devastating effect on many Laurentian Great Lakes bird species due to a reduction of eggshell thickness of up to 90% and, consequently, cracking, and even have affected migrating eagles that had consumed fish from the Great Lakes 2 years previously (*5*, *22*). Similar effects of organochlorines were detected in ducks and herons from the Ebro Delta in Spain (*21*). It is commonly accepted that these endocrine effects have caused the observed population declines. However, behavioral effects, including impaired incubation and chick-rearing behavior (*23*), which have been detected in captive birds after chronic exposure to all neurotoxic pesticide classes, have as yet not been linked to population declines (*24*).

The spill of highly persistent organochlorines (DDT and its metabolites, diclofol, dieldrin, and toxaphene) in Lake Apopka, Florida, in 1980 is well known as the only example linking the endocrine effects of pesticides to juvenile population densities and unexpected adult mortality in wildlife reptiles (*25*). The population parameters of American alligators were impaired by disrupted steroidogenesis, reduced testosterone levels and penis lengths in males, and elevated 17β-estradiol levels in juvenile females (*5*). Worldwide, amphibians have also been suffering alarming population declines. Signs of endocrine disruption, such as gonadal abnormalities and the feminization of males (*5*, *26*, *27*), interference with metamorphosis (*28*), changing behavior (*5*, *28*), and retarded development (*26*), have been frequently found in wildlife frogs and toads, but it has been difficult to relate these pesticide effects directly to population parameters, gene frequencies, or sex ratios (*28*). A recent meta-analysis revealed overall environmental pollution to have large effects on abnormality frequencies but only medium effects on survival and no effects on time of development (*29*). A key to mechanistically link pesticide impact and population declines in amphibians may lie in an impaired immune function and, consequently, in increased infection rates (*28*). Whether high acute mortality recently observed in European common frogs after direct dermal application of recommended rates of four fungicides, two herbicides, and the insecticide dimethoate (*30*) is field-relevant remains to be investigated.

Fish ecotoxicology faces similar challenges. Although literature on laboratory studies provides rich detail for sub-individual pesticide effects, attempts to link these to fish populations are rare. Apart from obvious relations in cases where pesticide runoff from orchards reached streams and caused fish kills (*31*), the difficulty in separating pesticide action from potentially interacting parameters in freshwater ecosystems in industrialized regions has hampered causality analysis. There is compelling global evidence that exposure to endocrine-disruptive chemicals is compromising the physiology and sexual behavior of fish, including effecting permanent alterations of sexual differentiation and impairment of fertility; however, it is thus far impossible to quantify the specific contribution of pesticides to these impairments (*20*). Whereas pesticide-induced neurological, endocrine, and olfactory dysfunction after cholinesterase inhibition have been correlated with fish behavior (*32*), effects at the population level associated with exposure to mixtures of pesticides and other chemicals have at most been plausibly linked to sub-individual effects by the application of Bradford-Hill´s criteria of causation (*33*, *34*). Generally, single-chemical risk assessment will probably underestimate the actual risks of pesticide mixtures to fish, as combinations of organophosphates and carbamates were shown to exert synergistic neurotoxicity and unpredicted mortality in Pacific salmon (*35*).

Research on interrelations between individual and population effects of pesticides on invertebrates is dominated by studies on insects, particularly bees. Honey bee poisoning incidents in developed countries such as the United Kingdom or Germany declined from the mid 1990s onward, in parallel to a decline in organophosphate incidents (*36*). The phenomenon of colony collapse disorder (CCD) and the suspicion that neonicotinoids and formamidines could be involved (*37*), however, has stimulated much recent research. There is evidence that neonicotinoid pesticides disrupt biogenic amine signaling and cause subsequent olfactory dysfunction, as well as affecting foraging behavior, learning, and memory abilities (*3*, *37*, *38*), but it is still unclear whether bee societies can buffer individual effects at field-realistic dosages (*3*, *39*). Two recent studies found that bumblebees exposed to field-realistic concentrations of imidacloprid suffer from impaired foraging, brood development, and colony success in terms of growth rate and new queen production, particularly in combinatorial exposure to the pyrethroid λ-cyhalothrin (*39*, *40*). In honey bees, thiamethoxam caused high worker mortality due to homing failure (*41*), but possible risks for colony collapse remain controversial (*41*, *42*). Alternative approaches designed to reduce impact on beneficial insects, such as bees, favor compounds of microbial origin such as spinosyns or the Bt δ-endotoxin *Cry*. Spinosyns, however, affect various physiological and behavioral traits of beneficial arthropods, particularly hymenopterans (*43*), whereas transgenic crops expressing *Cry* were shown to cause negative effects on the abundance of some insect taxa, predominantly on susceptible lepidopteran herbivores as well as their predators and parasitoids (*44*–*46*). So, despite all efforts to increase the specificity of insecticides, there is as yet no compound that both targets insect pests and leaves nontarget insects unaffected.

Across the Levels of Biological Organization

For the most part, pesticide research remains a scattered assemblage of data recorded at the molecular, cellular, physiological, or individual levels for different species on the one hand, and records of population declines or altered community structure in areas with high pesticide input or persistence on the other hand. Evidence for causal links across the levels is still scarce and restricted to the mentioned examples. At present, two strategies are favored to move from one level of biological organization to the next, more complex one. First, a multi-tiered approach combining controlled lab experiments, mesocosms, and field studies is needed to provide the basis for the application of Hill´s criteria of causation (*33*, *47*). Second, computational methods either relating observed population effects to underlying parameters [a top-down strategy (*20*)] or translating toxicity data derived from individuals to the level of wild populations and beyond (a bottom-up strategy) are increasingly being developed and refined (*48*). Refinement includes criteria quantifying the "best" model selection (*49*) and the adoption of population dynamics and food web modeling from ecology, accepting that a sophisticated understanding of species interactions is essential to detect and explain indirect pesticide effects (*50*). New approaches in population modeling include population-level measures of toxicant effects (such as those on population growth rate or age structure) and different sensitivities of life-history traits, and aim to determine the probability of extirpation or recovery of populations after pesticide exposure (*51*–*53*). Despite recent promising achievements (*54*, *55*), however, population modeling is still considered a relatively new subdiscipline in ecotoxicology (*48*) and is not yet developed well enough to fully assess pesticide impacts on endangered species (*56*).

Biotic Interactions and Communities: Indirect Effects

The current scarcity of incidents in developed countries, the shift from long-lived to mostly less-persistent compounds (except for sulfonylurea herbicides and neonicotinoids), and the awareness of long-term sublethal effects of pesticides have turned the attention of scientists and administrators toward the indirect consequences of

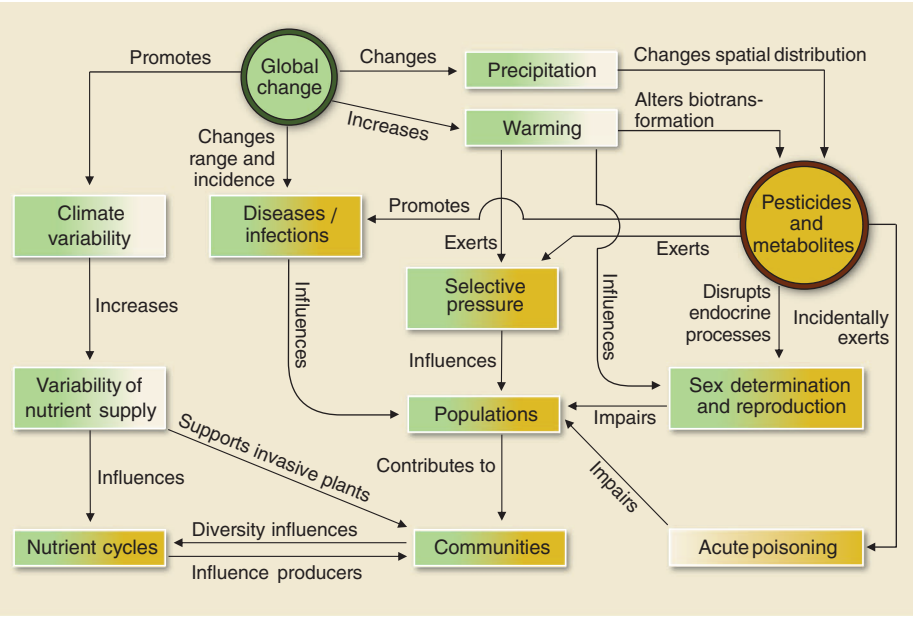

Fig. 3. Anticipated interactions of global change and pesticide effects on the physiology and ecology of wildlife species. The presumed impact of pesticides is depicted in yellow, and the presumed global climate change impact is in green.

pesticide use, which address changes in biotic interactions. Here, three main aspects have moved into focus: parasite-host interactions, predator-prey relationships, and pollination.

A number of pesticide compounds have been proven to affect immune parameters, and some cases of immunosuppression (exerted by organochlorine pesticides, organophosphates, carbamates, atrazine, and 2,4-D) were correlated to higher susceptibility of organisms to infection and parasite-caused diseases. For example, oysters exposed to DDT, toxaphene, and parathion were shown to be susceptible to fungal infection, and earthworms from triazine-treated orchards became infected with monocystid gregarines (*13*, *57*). In mammals, the use of anticholinesterase agents in agriculture can pose a threat of infections, disease outbreaks, and higher mortality, such as by tularemia in hares (*58*). Work on seals showed that organochlorine pollutants, including pesticides, have immunotoxic properties, impairing resistance to phocine distemper virus (*59*). Particularly in view of the global loss of amphibian populations, which has resulted in nearly one-third of the world's species being threatened, this subject seems to be crucial. Laboratory exposure experiments and field studies have shown an association between atrazine, malathion, esfenvalerate, or glyphosate exposure and increased infection of tadpoles with trematodes (*60*, *61*). A field survey of the northern leopard frog, *Rana pipiens*, revealed that atrazine pollution and inorganic phosphate accounted for 74% of the variation in the abundance of trematodes (*62*). Further mesocosm studies in ponds showed that atrazine killed the phytoplankton, thus allowing light to penetrate the water column and periphyton to assimilate the nutrients, including inorganic phosphate, released from the plankton. Presumably, periphyton growth provided more food to grazers and thus increased the richness of snails, which act as trematode intermediate hosts (*62*).

Other prominent indirect pesticide effects act on food webs and species competition through the removal of prey or competing species. Herbicides, which reduce the plant cover of soil and change plant species diversity, were found to be responsible for reduced food availability and thus adverse secondary effects on soil invertebrates and butterflies (*63*). The fungicide benomyl, which suppresses arbuscular mycorrhizal fungi, altered the patch-level floral display and resulted, after 3 years of fungal repression, in a two-thirds reduction of the total number of floral visits and in a shift in the community of floral visitors from large-bodied bees to small-bodied bees and flies (*64*). Indirect herbicide effects have also been reported for many vertebrate species, because weed and many noncrop plants are important components of their diet. Pesticide-induced diet shifts decreased species abundance and diversity in small mammals (*63*), reduced survival and reproductive rates in seed-eating or carnivorous birds (*65*, *66*), and resulted in declines of bird populations and species diversity (*63*). However, declining bird species are not found to be associated with particular plants but rather with reductions in overall diversity and the abundance of food plants in intensely managed arable land. Concomitantly, in these areas, a loss of insects and spiders, important sources of food for chicks of a wide range of bird species, was observed (*67*). Accompanying the trend toward monoculture on a large scale in the United States and parts of the developing world, herbicide use—particularly in combination with the cultivation of herbicide-tolerant crops—has frequently contributed to an overall reduction in habitat heterogeneity in agricultural landscapes and degraded their suitability as habitat for wildlife, including pollinators (*63*). Also, the biological pesticide spinosad has a wide variety of sublethal effects on natural enemies of pests and can drastically affect demographic traits in parasitoids and predators (*43*). Bt-transgenic crops, as an alternative to conventional insecticide use, did not impair the function and abundance of natural pest enemies in a 6–year study, but secondary effects by sublethally poisoned prey and diminished food quality for predators cannot be excluded for this kind of pest control (*45*). In aquatic systems, the most detrimental effects of herbicides address the reduction of the complexity and structure of the plankton and the submerged vegetation, including periphyton, all acting as food sources and refuges for phytophagous species such as waterbirds and amphibian tadpoles (*21*, *68*). In this regard, structural alterations in the planktonic community can result from direct herbicide effects on microalgae, from indirect consequences of pesticides on filter feeders (*69*), or from changes in competitive interactions [for example, small zooplankton (rotifers) were found to increase after larger zooplankton (cladocerans) were selectively decimated (*70*)]. Species of higher trophic levels, such as salmon, are most likely to be affected in population growth and productivity by indirect pesticide effects (*71*). Fleeger and co-workers list 56 cases of indirect pesticide effects on competition or predation in aquatic biota, identified in studies across trophic levels (*50*). It has to be concluded that, at least in aquatic systems, pesticides exert strong selection on invertebrates. Freshwater habitats are best-studied in this respect, whereas marine and estuarine systems are underrepresented. Furthermore, it is noteworthy that not only modulations in the population structure of prey or predator species, but also pesticide effects on interspecific behavior, may change predator-prey interactions, as shown for glyphosate in tiger salamanders (*72*) or imidacloprid in zebrafish (*73*) and their respective prey.

Probably the most meaningful example of indirect pesticide effects, however, does not address the aquatic environment but insect pollination. In bumblebee (*Bombus terrestris*) workers chronically exposed to realistic concentrations of imidacloprid and λ-cyhalothrin, pesticide-altered behavior was found to be associated with a declined pollen-collecting efficiency (*39*). For these insecticides, as well as for spinosad impact on

bees, it is likely that diminished foraging efficiency affects overall pollination services (*43*).

Can Microevolution Catch Up?

The selection of resistant phenotypes after multigeneration exposure can be a problem in pest control and, perhaps, a chance for nontarget species with high reproductive output and short generation time. As a matter of principle, the elucidation of long-term pesticide effects in communities of animals and plants is often hampered by the long generation times of the species involved and thus the inevitable inertia of these systems. In contrast, microbial communities display microevolutionary responses within a rather short time period. Transient effects of herbicides, including diuron and simazine, the dithiocarbamate fungicide mancozeb, and DDT, on microbial populations and communities and their function in ecosystems (as, for example, their role in nitrification) are regularly measurable, but studies have congruently revealed their high capacity to recover and to develop tolerance to these pesticides (*68*). Quite often, these tolerant bacteria benefit from pesticide application and use the compound itself as a carbon source (*74*). Similarly, insect and pathogen pests were found to benefit from elevated protein levels in 2,4-D–treated corn plants (*75*), whose yields on a per-hectare basis may thus equal those from organically managed corn (*76*). Studies also report at least partial restoration of community functions despite structural changes after pesticide treatment in communities of freshwater microalgae (*77*). It is, however, unclear to what extent the selection of resistance traits and/or a functional resilience of the community can be generalized throughout ecosystems, because studies on metazoans are rare. Recent field experiments revealed λ-cyhalodrin treatment to select 10-fold higher resistance against this pyrethroid in lady beetles (*Eriopsis connexa*) after 55 generations (*78*). Furthermore, the selection of resistance against deltamethrin was reported for the common green lacewing *Chrysoperla carnea* (*79*) but, up to now, there has been no indication regarding pesticide-tolerant bees, probably because the queens are not directly exposed to the toxin (*38*). However, the scarcity of information about nontarget species does not allow the degree to which resistance contributes to the regeneration of populations to be judged. Independent from evolutionary processes, however, ecological networks often allow for restoration by means of recruitment from the filial generation or immigrating individuals. Microcrustacean populations in stagnant waters, for example, usually recover from pesticide effects within a few weeks, provided that the compound is not persistent, the physicochemical environment remains intact, generation times are short, and immigration from the residual population is possible (*80*). There is also evidence that the reversal of intense pesticide use in arable systems can result in the rapid recovery of food sources for birds (*67*). In a review of the ecological consequences of insecticide use, Devine and Furlong listed a variety of cases in which terrestrial and aquatic insect, crustacean, lumbricid, and fish populations recovered within months when the pesticide treatment stopped (*81*). In this context, multilevel modeling allows situations in which reduced pesticide application will have the most benefit on restoring biodiversity to be detected (*54*).

Future Challenges in a Changing World

It is to be assumed that the global changes we are going to experience during the coming decades pose larger questions regarding pesticide impact on wildlife than we have been accustomed to. We cannot predict the consequences of a possible release of the bulk of obsolete pesticides that remain in developing countries. Shifts from the use of "old" and highly persistent pesticides to modern compounds may surely improve the situation in many countries of the world but, as outlined, they are also far from being unproblematic. As far as we know, even the latest generation of biopesticides poses problems for wildlife; perhaps not directly by receptor interaction in nontarget species, but at least indirectly via the impairment of species interactions.

Climate change will surely interact with the spatial distribution and effects of pesticides in nature (Fig. 3). Currently, it is possible to identify reasonable points of expected interactions, even though the magnitude of interference remains unclear. Elevated water temperatures may change the metabolite pattern of pesticides via alterations in biotransformation processes, and changes in precipitation may result in changes in volatilization and deposition (*82*). Global warming is decisively expected to affect the ecotoxicological potency of pesticides, because 83% of ecotoxicological studies on the combined effects of elevated temperature and pesticide exposure have revealed the synergistic action of these factors (*83*). Experimental evidence for this expectation has been provided by a study on the fungicide pyrimethanil, applied under thermally realistic global change summer conditions simulated for central Europe. In comparison to current temperatures, responses to the conditions in this study predict increased mortality, a declining population growth rate, and considerably reduced genetic diversity in the midge *Chironomus riparius* (*84*). Pesticide interactions with global warming will probably influence the direction in which selection acts upon biota, a factor that will be particularly problematic for populations or species living at the edge of their physiological tolerance (*82*). Further problems in a warming world may result from temperature interactions with the metabolic rates of heterothermic organisms and, with respect to endocrine-disruptive compounds, with physiological processes involved in temperature-dependent sex determination, as is known for reptile species (*25*). In addition, changes in the geographic range and incidence of many infectious diseases that may be fostered by pesticide-exerted immunotoxicity have been predicted (*60*). Higher-level pesticide effects, such as changes in plant communities, will probably interfere with the effects of global change on biodiversity and thus affect ecosystem function. Increased heterogeneity of nutrient supply associated with global change was shown to strongly promote plant invasion and thus to alter plant communities (*85*). In turn, plant diversity is known to influence biomass production (*86*) and nitrogen cycling (*87*).

In the coming years, there will be a paramount need to causally link both direct and indirect pesticide effects across levels of increasing biological complexity. Specifically, it will be essential to detect and quantify confounding factors that act synergistically with pesticide exposure, and to identify processes of particular vulnerability to interactions of pesticide impact and climate change.

References and Notes

1. B. A. Rattner, *Ecotoxicology* **18**, 773–783 (2009).
2. P. Berny, *J. Vet. Pharmacol. Ther.* **30**, 93–100 (2007).
3. T. Blacquière, G. Smagghe, C. A. M. van Gestel, V. Mommaerts, *Ecotoxicology* **21**, 973–992 (2012).
4. G. R. de Snoo, N. M. I. Scheidegger, F. M. W. de Jong, *Pestic. Sci.* **55**, 47–54 (1999).
5. H. J. Hamlin, L. J. Guillette Jr., *Syst. Biol. Reprod. Med.* **56**, 113–121 (2010).
6. K. Starner, *Pesticides in Surface Water from Agricultural Regions of California 2007-2008* (Report 248, California Environmental Protection Agency, Sacramento, CA, 2011); www.cdpr.ca.gov/docs/emon/pubs/ehapreps/report248final.pdf.
7. K. Starner, K. S. Goh, *Bull. Environ. Contam. Toxicol.* **88**, 316–321 (2012).
8. M. A. Fleischli, J. C. Franson, N. J. Thomas, D. L. Finley, W. Riley Jr., *Arch. Environ. Contam. Toxicol.* **46**, 542–550 (2004).
9. V. Turusov, V. Rakitsky, L. Tomatis, *Environ. Health Perspect.* **110**, 125–128 (2002).
10. F. Brucker-Davis, *Thyroid* **8**, 827–856 (1998).
11. R. McKinlay, J. A. Plant, J. N. B. Bell, N. Voulvoulis, *Environ. Int.* **34**, 168–183 (2008).
12. T. Galloway, R. Handy, *Ecotoxicology* **12**, 345–363 (2003).
13. T. S. Galloway, M. H. Depledge, *Ecotoxicology* **10**, 5–23 (2001).
14. P. Story, M. Cox, *Wildl. Res.* **28**, 179–193 (2001).
15. V. Pašková, K. Hilscherová, L. Bláha, *Rev. Environ. Contam. Toxicol.* **211**, 25–61 (2011).
16. M. Tomizawa, J. E. Casida, *Annu. Rev. Pharmacol. Toxicol.* **45**, 247–268 (2005).
17. L. Gawade, S. S. Dadarkar, R. Husain, M. Gatne, *Food Chem. Toxicol.* **51**, 61–70 (2013).
18. P. C. Lin, H. J. Lin, Y. Y. Liao, H. R. Guo, K. T. Chen, *Basic Clin. Pharmacol. Toxicol.* **112**, 282–286 (2013).
19. D. Muir *et al.*, *Sci. Total Environ.* **230**, 83–144 (1999).
20. J. Bernanke, H.-R. Köhler, *Rev. Environ. Contam. Toxicol.* **198**, 1–47 (2009).
21. S. Mañosa, R. Mateo, R. Guitart, *Environ. Monit. Assess.* **71**, 187–205 (2001).
22. T. Colborn, F. S. vom Saal, A. M. Soto, *Environ. Health Perspect.* **101**, 378–384 (1993).
23. D. M. Fry, *Environ. Health Perspect.* **103**, 165–171 (1995).

24. C. H. Walker, *Ecotoxicology* **12**, 307–316 (2003).
25. D. A. Crain, L. J. Guillette Jr., *Anim. Reprod. Sci.* **53**, 77–86 (1998).
26. T. Hayes *et al*., *Nature* **419**, 895–896 (2002).
27. T. B. Hayes *et al*., *Proc. Natl. Acad. Sci. U.S.A.* **107**, 4612–4617 (2010).
28. J. R. Rohr, K. A. McCoy, *Environ. Health Perspect.* **118**, 20–32 (2010).
29. A. Egea-Serrano, R. A. Relyea, M. Tejedo, M. Torralva, *Ecol. Evol.* **2**, 1382–1397 (2012).
30. C. A. Brühl, T. Schmidt, S. Pieper, A. Alscher, *Sci. Rep.* **3**, 1135 (2013).
31. D. M. Trotter, R. A. Kent, M. P. Wong, *Crit. Rev. Environ. Control* **21**, 137–176 (1991).
32. G. R. Scott, K. A. Sloman, *Aquat. Toxicol.* **68**, 369–392 (2004).
33. R. Triebskorn *et al*., *Hum. Ecol. Risk Assess.* **9**, 171–194 (2003).
34. S. M. Adams, Ed., *Biological Indicators of Aquatic Ecosystem Stress* (American Fisheries Society, Bethesda, MD, 2002).
35. C. A. Laetz *et al*., *Environ. Health Perspect.* **117**, 348–353 (2009).
36. E. A. Barnett, A. J. Charlton, M. R. Fletcher, *Pest Manag. Sci.* **63**, 1051–1057 (2007).
37. T. Farooqui, *Neurochem. Int.* **62**, 122–136 (2013).
38. L. P. Belzunces, S. Tchamitchian, J.-L. Brunet, *Apidologie (Celle)* **43**, 348–370 (2012).
39. R. J. Gill, O. Ramos-Rodriguez, N. E. Raine, *Nature* **491**, 105–108 (2012).
40. P. R. Whitehorn, S. O'Connor, F. L. Wackers, D. Goulson, *Science* **336**, 351–352 (2012).
41. M. Henry *et al*., *Science* **336**, 348–350 (2012).
42. J. E. Cresswell, H. M. Thompson, *Science* **337**, 1453, author reply 1453 (2012).
43. A. Biondi *et al*., *Pest Manag. Sci.* **68**, 1523–1536 (2012).
44. B. W. Clark, T. A. Phillips, J. R. Coats, *J. Agric. Food Chem.* **53**, 4643–4653 (2005).
45. J. Romeis, M. Meissle, F. Bigler, *Nat. Biotechnol.* **24**, 63–71 (2006).
46. M. Marvier, C. McCreedy, J. Regetz, P. Kareiva, *Science* **316**, 1475–1477 (2007).
47. R. M. Mann, R. V. Hyne, C. B. Choung, S. P. Wilson, *Environ. Pollut.* **157**, 2903–2927 (2009).
48. N. L. Scholz *et al*., *Bioscience* **62**, 428–434 (2012).
49. K. P. Burnham, D. R. Anderson, *Sociol. Methods Res.* **33**, 261–304 (2004).
50. J. W. Fleeger, K. R. Carman, R. M. Nisbet, *Sci. Total Environ.* **317**, 207–233 (2003).
51. U. Wennergren, J. Stark, *Ecol. Appl.* **10**, 295–302 (2000).
52. J. D. Stark, J. E. Banks, *Annu. Rev. Entomol.* **48**, 505–519 (2003).
53. J. D. Stark, in *Pesticide Regulation and the Endangered Species Act*, K. D. Racke *et al*., Eds. (ACS Symposium Series, American Chemical Society, Washington, DC, 2012), vol. 1111, pp. 259–270.
54. T. Amano *et al*., *Ecol. Lett.* **14**, 1263–1272 (2011).
55. C. A. Engelman, W. E. Grant, M. A. Mora, M. Woodin, *Ecol. Model.* **224**, 90–102 (2012).
56. Committee on Ecological Risk Assessment Under FIFRA and ESA; Board on Environmental Studies and Toxicology, Division on Earth and Life Studies; National Research Council, *Assessing Risks to Endangered and Threatened Species from Pesticides* (National Academies Press, Washington, DC, 2013).
57. V. Pizl, *Pedobiologia (Jena)* **28**, 399–402 (1985).
58. H. Bandouchova *et al*., *Neuroendocrinol. Lett.* **32**, 77–83 (2011).
59. M. D. Kendall, B. Safieh, J. Harwood, P. P. Pomeroy, *Sci. Total Environ.* **115**, 133–144 (1992).
60. J. M. Kiesecker, *Ecol. Res.* **26**, 897–908 (2011).
61. J. Koprivnikar, J. C. Redfern, *J. Wildl. Dis.* **48**, 925–936 (2012).
62. J. R. Rohr *et al*., *Nature* **455**, 1235–1239 (2008).
63. K. Freemark, C. Boutin, *Agric. Ecosyst. Environ.* **52**, 67–91 (1995).
64. J. F. Cahill Jr., E. Elle, G. R. Smith, B. H. Shore, *Ecology* **89**, 1791–1801 (2008).
65. I. Newton, *Ibis* **146**, 579–600 (2004).
66. J. A. Bright, A. J. Morris, R. Winspear, *A Review of Indirect Effects of Pesticides on Birds and Mitigating Land-Management Practices* (RSPB Research Report No. 28, The Royal Society for the Protection of Birds, UK, 2008); www.rspb.org.uk/ourwork/projects/details/192699-a-review-of-indirect-effects-of-pesticides-on-birds-and-mitigating-landmanagement-practices.
67. J. D. Wilson, A. J. Morris, B. E. Arroyo, S. C. Clark, R. B. Bradbury, *Agric. Ecosyst. Environ.* **75**, 13–30 (1999).
68. S. Lew, M. Lew, J. Szarek, T. Mieszczyński, *Fresenius Environ. Bull.* **18**, 1390–1395 (2009).
69. M. E. DeLorenzo, G. I. Scott, P. E. Ross, *Environ. Toxicol. Chem.* **20**, 84–98 (2001).
70. T. Hanazato, *Environ. Pollut.* **101**, 361–373 (1998).
71. K. H. Macneale, P. M. Kiffney, N. L. Scholz, *Front. Ecol. Environ* **8**, 475–482 (2010).
72. R. Brodman, W. D. Newman, K. Laurie, S. Osterfeld, N. Lenzo, *J. Herpetol.* **44**, 69–82 (2010).
73. M. Langer-Jaesrich, C. Kienle, H.-R. Köhler, A. Gerhardt, *Ecotoxicology* **19**, 1294–1301 (2010).
74. S. Lew, M. Lew, A. Biedunkiewicz, J. Szarek, *Arch. Environ. Contam. Toxicol.* **64**, 399–409 (2013).
75. I. N. Oka, D. Pimentel, *Science* **193**, 239–240 (1976).
76. D. Pimentel, P. Hepperly, J. Hanson, D. Douds, R. Seidel, *Bioscience* **55**, 573–582 (2005).
77. S. Pesce, A. Bouchez, B. Montuelle, *Rev. Environ. Contam. Toxicol.* **214**, 87–124 (2011).
78. A. R. S. Rodrigues, J. B. Torres, H. A. A. Siqueira, D. P. A. Lacerda, *Biol. Control* **64**, 217–224 (2013).
79. A. H. Sayyed, A. K. Pathan, U. Faheem, *Pestic. Biochem. Physiol.* **98**, 325–332 (2010).
80. R. P. A. Van Wijngaarden, T. C. M. Brock, P. J. Van den Brink, *Ecotoxicology* **14**, 355–380 (2005).
81. G. J. Devine, M. J. Furlong, *Agric. Human Values* **24**, 281–306 (2007).
82. P. D. Noyes *et al*., *Environ. Int.* **35**, 971–986 (2009).
83. M. Holmstrup *et al*., *Sci. Total Environ.* **408**, 3746–3762 (2010).
84. R. Müller *et al*., *Ecol. Evol.* **2**, 196–210 (2012).
85. M. Parepa, M. Fischer, O. Bossdorf, *Nat. Commun.* **4**, 1604 (2013).
86. P. B. Reich *et al*., *Science* **336**, 589–592 (2012).
87. Y. Oelmann *et al*., *Global Biogeochem. Cyc*. **25**, GB2014 (2011).
88. W. Zhang, F. Jiang, J. Ou, *P. Int. Acad. Ecol. Environ. Sci.* **1**, 125–144 (2011).

Acknowledgments: We thank S. Schwarz for help with literature research.

10.1126/science.1237591

The Xist lncRNA Exploits Three-Dimensional Genome Architecture to Spread Across the X Chromosome

Jesse M. Engreitz,[1,2] Amy Pandya-Jones,[3] Patrick McDonel,[1] Alexander Shishkin,[1] Klara Sirokman,[1] Christine Surka,[1] Sabah Kadri,[1] Jeffrey Xing,[1] Alon Goren,[1] Eric S. Lander,[1,4,5]* Kathrin Plath,[3]* Mitchell Guttman[1]*†

Many large noncoding RNAs (lncRNAs) regulate chromatin, but the mechanisms by which they localize to genomic targets remain unexplored. We investigated the localization mechanisms of the Xist lncRNA during X-chromosome inactivation (XCI), a paradigm of lncRNA-mediated chromatin regulation. During the maintenance of XCI, Xist binds broadly across the X chromosome. During initiation of XCI, Xist initially transfers to distal regions across the X chromosome that are not defined by specific sequences. Instead, Xist identifies these regions by exploiting the three-dimensional conformation of the X chromosome. Xist requires its silencing domain to spread across actively transcribed regions and thereby access the entire chromosome. These findings suggest a model in which Xist coats the X chromosome by searching in three dimensions, modifying chromosome structure, and spreading to newly accessible locations.

Mammalian genomes encode thousands of large noncoding RNAs (lncRNAs) (*1*–*5*), many of which play key functional roles in the cell (*6*–*9*). One emerging paradigm is that many lncRNAs can regulate gene expression (*6*, *8*–*11*) by interacting with chromatin regulatory complexes (*6*, *12*–*14*) and localizing these complexes to genomic target sites (*15*–*17*). Despite the central role of RNA-chromatin interactions, the mechanisms by which lncRNAs identify their genomic targets remain unexplored.

The Xist ncRNA provides a model to investigate the mechanisms of lncRNA localization (*11*, *18*, *19*). Xist initiates X-chromosome inactivation (XCI) by spreading in cis across the future inactive X chromosome (*20*, *21*), recruiting polycomb repressive complex 2 (PRC2) (*14*, *22*, *23*), and forming a transcriptionally silent nuclear compartment (*24*, *25*) enriched for repressive chromatin modifications including trimethylation of histone 3 lysine 27 (H3K27me3) (*22*, *23*). These functions of Xist—localization to chromatin and silencing of gene expression—are mediated by distinct RNA domains (*26*): Transcriptional silencing requires the A-repeat domain (*26*), which interacts with the PRC2 chromatin regulatory complex (*14*), whereas localization to chromatin requires several distinct domains (*26*–*28*) and interactions with proteins associated with the nuclear matrix (*29*–*31*). Despite these advances in our understanding of Xist, we still do not understand the process by which Xist localizes to chromatin and spreads across the X chromosome.

We present a biochemical method that enables high-resolution mapping of lncRNA localization. Using this method, we explored Xist localization during initiation and maintenance of XCI. During maintenance, Xist localized broadly across the entire X chromosome, lacking focal binding sites. During initiation of XCI, Xist transferred directly from its transcription locus to distal sites across the X chromosome that are defined not by specific sequences but by their spatial proximity in the nucleus to the Xist transcription locus. Furthermore, we show that Xist initially localized to the periphery of actively transcribed regions but gradually spread across them through a mechanism dependent on the A-repeat domain. Together, these results suggest that Xist initially localizes to distal sites across the chromosome by exploiting chromosome conformation, and may spread to new sites through its ability to modify chromatin structure.

Results and Discussion

RNA Antisense Purification (RAP): A Method to Map lncRNA Interactions with Chromatin

To determine the genomic localization of lncRNAs, we developed a method termed RAP, which is conceptually similar to previous methods (*32*–*34*) in that it uses biotinylated antisense probes that hybridize to a target RNA to purify the endogenous RNA and its associated genomic DNA from cross-linked cell lysate (Fig. 1A) (*35*). We designed RAP to enable specific purification of chromatin associated with a target lncRNA, achieve high-resolution mapping of the associated DNA target sites upon sequencing of the captured DNA, and robustly capture any lncRNA with minimal optimization. To achieve high specificity, RAP uses 120-nucleotide antisense RNA probes to form extremely strong hybrids with the target RNA, thereby enabling purification using denaturing conditions that disrupt nonspecific RNA-protein interactions and nonspecific hybridization with RNAs or genomic DNA. RAP uses deoxyribonuclease I (DNase I) to digest genomic DNA to ~150–base pair (bp) fragments, which provides high-resolution mapping of binding sites. To robustly capture a lncRNA, RAP uses a pool of overlapping probes tiled across the entire length of the target RNA to ensure capture even in the case of extensive protein-RNA interactions, RNA secondary structure, or partial RNA degradation (supplementary text).

To test our method, we used RAP to purify the Xist RNA and associated DNA from female mouse lung fibroblasts (MLFs), a differentiated cell line in which Xist is expressed from and coats the inactive X chromosome. We designed antisense probes tiled every 15 nucleotides across the 17-kb Xist transcript, excluding those that showed any complementarity to other RNAs or genomic DNA regions (*35*). This yielded a pool of 1054 unique probes. We performed RAP and observed an enrichment of the Xist RNA by more than a factor of 100 relative to either input or a control purification using "sense" probes from the same strand as Xist itself (Fig. 1B). When we sequenced all RNAs in the purified fraction, we found that the Xist RNA constituted ~70% of alignable reads despite representing <0.1% of the polyadenylated input RNA. The remaining reads were broadly distributed across ~7500 expressed transcripts, with no single transcript exceeding 2% of the total purified RNA (Fig. 1C). We sequenced the genomic DNA that copurified with the Xist RNA and observed a strong enrichment, with >70% of the DNA sequencing reads from the Xist purification originating from the X chromosome, versus ~5% from the input DNA samples (Fig. 1D).

To ensure that the DNA purified by Xist RAP reflected the endogenous localization of Xist, we performed three control experiments (fig. S1) (*35*): (i) To confirm that captured chromatin reflected preexisting interactions occurring in vivo, we purified Xist from non–cross-linked cellular extracts. In this condition, we did not obtain any detectable DNA signal by quantitative polymerase chain reaction (qPCR) despite obtaining comparable enrichments of the Xist RNA (*35*). (ii) To rule out the possibility that RAP captured genomic DNA through nonspecific hybridization with the probes or the target RNA, we tested

[1]Broad Institute of Harvard and MIT, Cambridge, MA 02142, USA. [2]Division of Health Sciences and Technology, Massachusetts Institute of Technology, Cambridge, MA 02139, USA. [3]Department of Biological Chemistry, Jonsson Comprehensive Cancer Center, Molecular Biology Institute, and Eli and Edythe Broad Center of Regenerative Medicine and Stem Cell Research, David Geffen School of Medicine, University of California, Los Angeles, CA 90095, USA. [4]Department of Biology, Massachusetts Institute of Technology, Cambridge, MA 02139, USA. [5]Department of Systems Biology, Harvard Medical School, Boston, MA 02114, USA.

*Corresponding author. E-mail: mguttman@caltech.edu (M.G.); kplath@mednet.ucla.edu (K.P.); lander@broadinstitute.org (E.S.L.)

†Present address: Division of Biology and Biological Engineering, California Institute of Technology, Pasadena, CA 91125, USA.

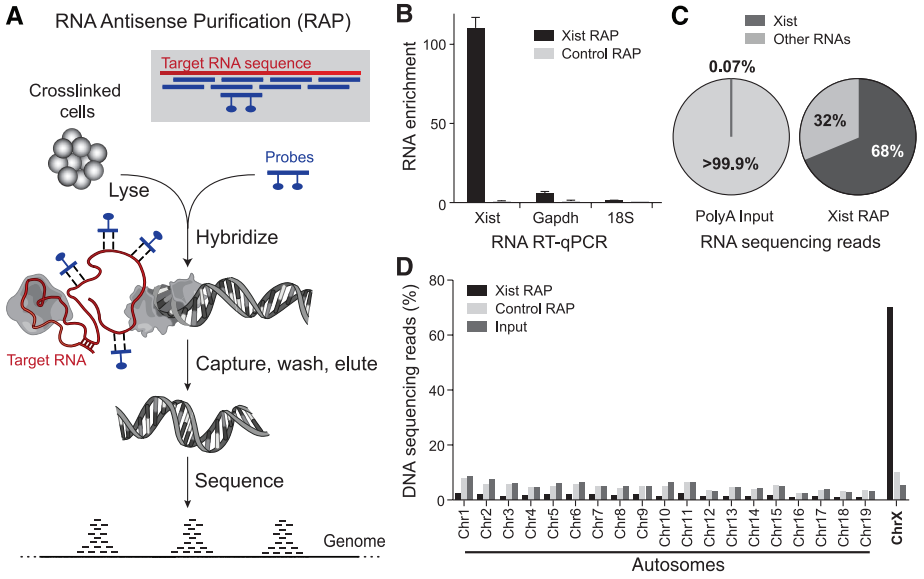

Fig. 1. RNA antisense purification (RAP) accurately purifies lncRNA-chromatin interactions. (A) Schematic diagram of RAP. Biotinylated probes (blue) are hybridized to the target RNA (red) cross-linked to proteins and DNA. Gray inset: 120-nucleotide antisense capture probes are designed to tile across the entire target RNA. **(B)** Reverse transcription qPCR of the RNA captured using antisense probes to Xist (Xist RAP, black) or sense probes to Xist (control RAP, gray) in MLFs. Enrichments represent means ± SEM (N = 3 replicate experiments) and are normalized to the mean of the sense control experiments. Note that Tsix, an antisense transcript overlapping Xist, is not expressed in MLFs. **(C)** RNA sequencing reads originating from the Xist transcript (dark gray) and all other cellular RNAs (light gray) for polyA-selected RNA (left) and RNA captured using antisense probes for the Xist RNA (right) (*35*). **(D)** DNA sequencing reads aligning to each chromosome after purification with antisense probes (Xist RAP, black), sense probes (control RAP, light gray), and input genomic DNA (dark gray) in MLFs.

whether sites with higher enrichment in Xist RAP showed complementarity to sequences present in the probes or Xist RNA sequence (*35*). We observed no relationship between sequence homology and RNA localization either on the X chromosome or on autosomes (fig. S2). (iii) To further exclude the possibility of direct probe-DNA interactions, we examined DNA captured in a control purification with sense probes that should capture double-stranded DNA with the same efficiency but will not hybridize to the target RNA. Using the sense probes, we observed no enriched regions across the entire genome (Fig. 1D) with the sole exception of a low-level enrichment at the *Xist* locus itself (*35*), likely reflecting perfect hybridization with the RNA probes. However, the amount of Xist genomic DNA purified in the control was <5% of the amount in the Xist purification, which suggests that most of the signal in Xist RAP resulted from RNA-mediated interactions (supplementary text).

Together, these results demonstrate the specificity of the RAP method to capture RNA interactions with chromatin.

Xist Binds Across the Inactive X in Differentiated Female Cells

Using RAP, we explored the localization of Xist in MLFs. We found that Xist showed enrichment over the entire X chromosome as opposed to showing punctate enrichment at specific locations (Fig. 2, A to C, and fig. S3). Indeed, >95% of 10-kb windows on the X chromosome were enriched by more than a factor of 10 relative to the input. In comparison, not a single window on an autosome reached this enrichment level (Fig. 2C). This broad localization pattern contrasts sharply with the roX2 ncRNA in *Drosophila*, which, despite its similar function of regulating gene expression across an entire chromosome, binds at discrete sites (*32*, *33*).

Although Xist showed enrichment across the entire X chromosome (factor of 23 average enrichment), we observed differences in the precise levels of enrichment across the chromosome (Fig. 2A), which were highly reproducible between replicates (Pearson correlation = 0.94; fig. S4) (*35*). To characterize this variation, we correlated Xist enrichment with other genomic features (table S1). We found that Xist enrichment strongly correlated with H3K27me3 across the entire chromosome (Pearson correlation = 0.69; Fig. 2, A and B), consistent with the known role for Xist in the recruitment of PRC2 (*14*, *22*, *23*). Xist levels also showed a strong correlation with gene density (Pearson correlation = 0.44) and a negative correlation with the density of long interspersed nuclear element (LINE) repeats (Pearson correlation = –0.25), which tend to reside in gene-poor regions.

To further explore this variation, we examined the most enriched (by a factor of >30) and least enriched (by a factor of <15) regions of the X chromosome (Fig. 2C) (*35*). The most enriched regions showed higher H3K27me3 occupancy in MLFs (factor of 1.7) and higher gene density (factor of 3) relative to the chromosome average, consistent with the chromosome-wide correlations. The least enriched regions contained genes known to escape XCI (*36*). Consistent with their preferential positioning outside of the Xist domain (*37*, *38*), escape genes displayed a ~50% reduction in Xist occupancy relative to silenced X-chromosome genes, with the level of Xist enrichment roughly reflecting the previously reported ratio of expression from the inactive versus active X chromosome (Pearson correlation = –0.66; Fig. 2D) (*35*, *39*). Closer examination of Xist localization at some escape genes revealed sharp boundaries separating escaped and non-escaped domains (Fig. 2E). One of the least enriched regions resided immediately distal to the *Xist* locus and included the lncRNA genes *Jpx* and *Ftx*, both of which have been previously reported to escape XCI and act as positive regulators of Xist (*40*, *41*) (Fig. 2F).

Together, the least enriched regions contained 53 genes with more than 40% depletion for Xist relative to the chromosome average (table S2). Twenty-four of these genes have been previously reported to partially escape inactivation, including 10 microRNA genes (*42*) and three lncRNAs (table S2). Three of these genes represent novel candidate escape genes in MLF, displaying on average 50% depletion of Xist relative to other genes on the X chromosome. The remaining genes are not expressed in MLF or are located within 300 kb of a known escape gene and thus likely do not escape XCI in this cell type.

Thus, the Xist RNA localizes broadly across the entire inactive X chromosome in differentiated cells, preferentially localizing at gene-rich regions (*43*, *44*) but excluding genes that are expressed on the inactive X chromosome. This broad localization pattern suggests that Xist localizes to chromatin in a degenerate fashion, possibly through interactions with the nuclear matrix (*29*, *30*, *44*).

Xist Initially Localizes to Defined Regions Across the X Chromosome

To gain insight into how Xist establishes this broad localization pattern during the initiation of XCI, we examined Xist localization upon activation in mouse embryonic stem (ES) cells (*20*). In the pluripotent state, Xist is not expressed and both X chromosomes are active (*20*, *21*, *45*, *46*). Induction of differentiation triggers Xist activation on one allele, leading to the silencing of the X chromosome in cis (*20*, *21*, *45*). To synchronize the initiation of XCI, we engineered a tetracycline-inducible promoter to drive Xist expression from its endogenous locus in a male mouse ES cell line (Fig. 3A and fig. S5) (*35*). Upon induction with doxycycline, these cells increased Xist expression by a factor of ~120 over a period of 6 hours (fig. S6). RNA fluorescence in situ hybridization

(FISH) showed that after 1 hour of induction, Xist appeared as a strong focal point and grew to a characteristic cloud over time (Fig. 3B and fig. S6), accompanied by exclusion of RNA polymerase II and accumulation of PRC2 and H3K27me3 over the Xist RNA compartment (fig. S6). Cells expressing Xist concurrently silenced expression of the Tsix RNA, which negatively regulates Xist in ES cells (fig. S6) (*47*).

To observe the process by which Xist initially spreads across the X chromosome, we used RAP to generate high-resolution maps of Xist localization across five time points from 0 to 6 hours after Xist induction (Fig. 3C and fig. S7). After 1 hour of Xist induction, we observed a strong ~5-Mb peak centered at the *Xist* transcription locus, corresponding to the spot of Xist localization observed using RNA FISH (Fig. 3B and fig. S6). Over the time course, this peak declined while Xist levels across the chromosome increased. These patterns mirrored the emergence of the

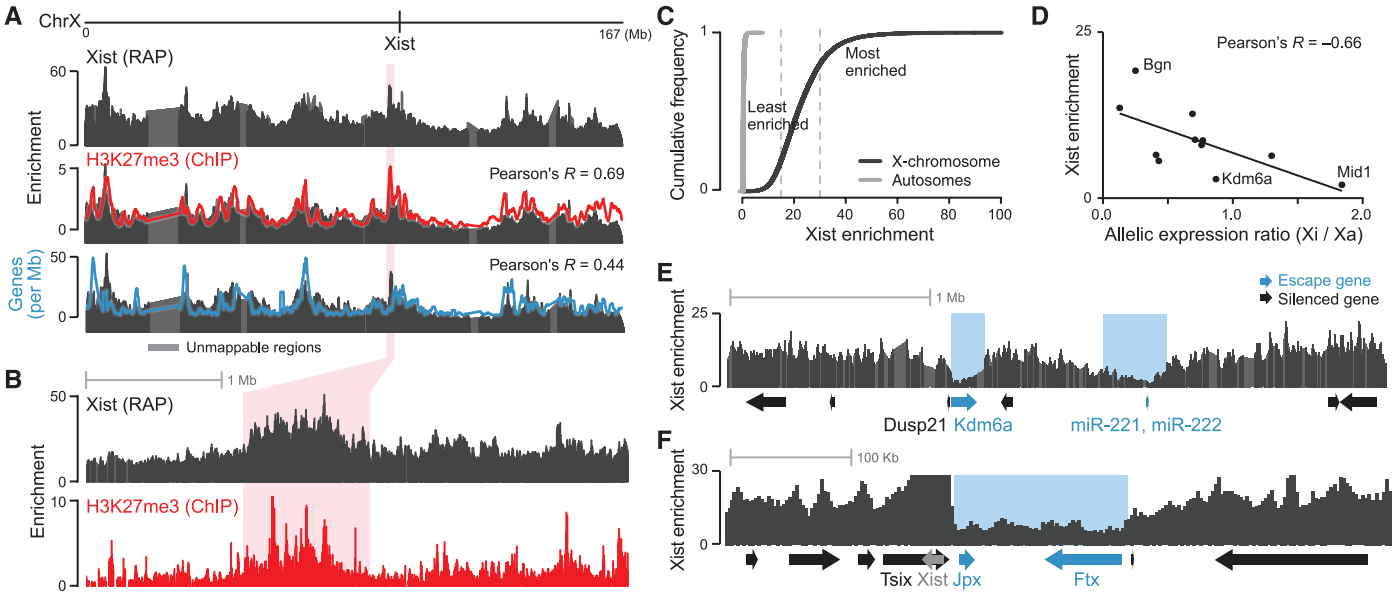

Fig. 2. High-resolution mapping of Xist localization on the inactive X chromosome in differentiated female cells. (**A**) Xist enrichment over input (dark gray), H3K27me3 enrichment over input (red line), and gene density (blue line) (*35*) across the entire X chromosome in female MLFs. (**B**) Zoom in on a highly enriched Xist region (light red box, chrX:95,000,000–99,000,000) shows Xist (black) and H3K27me3 (red) enrichments. (**C**) Cumulative distribution plot comparing Xist enrichment across all 10-kb windows on the X chromosome (black) and on autosomes (gray). Dashed lines demarcate the least and most highly enriched regions on the X chromosome. (**D**) Correlation between Xist enrichment and the ratio of expression from the inactive X (Xi) and active X (Xa) for known escape genes (*39*). (**E**) Xist enrichment (chrX:17,031,000–19,901,000) across two of the least enriched regions (blue boxes). (**F**) Xist enrichment around the *Xist* genomic locus including one of the least enriched regions (blue box). Xist enrichment at the *Xist* locus (gray arrow) extends above the *y*-axis maximum.

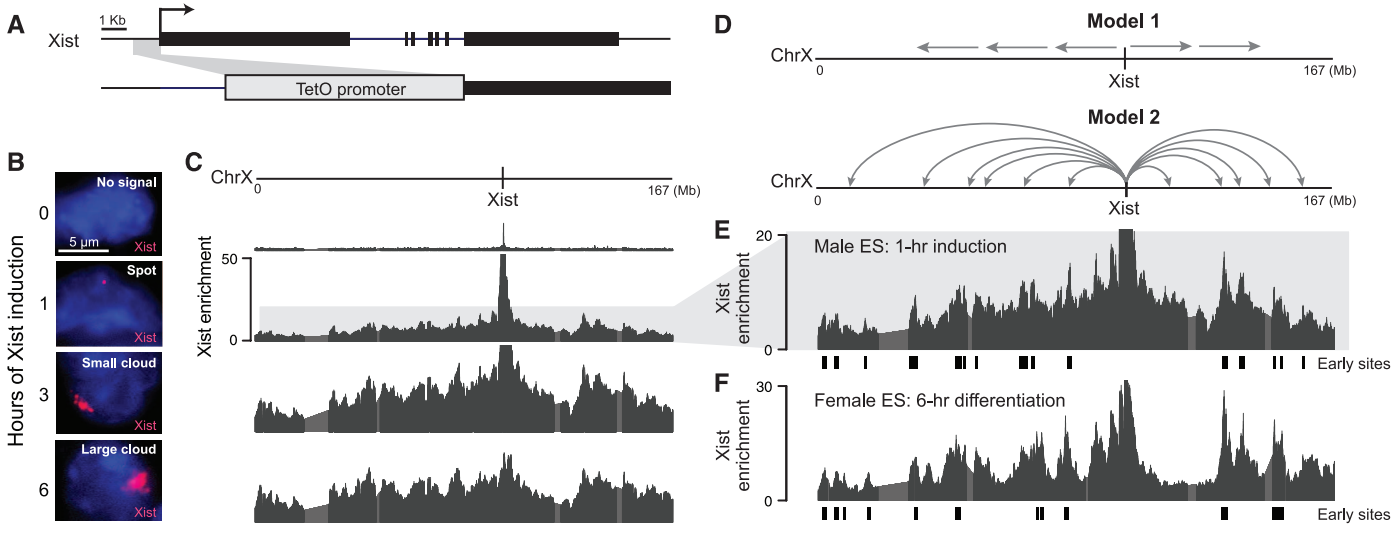

Fig. 3. High-resolution view of Xist spreading during initiation of XCI. (**A**) We replaced the 1027 bases upstream of Xist with a tetracycline-responsive (TetO) promoter in male mouse ES cells (*35*). (**B**) Representative FISH images for the Xist RNA (red) and (DAPI) staining of the nucleus (blue) after Xist induction with doxycycline. Xist FISH signals were classified into categories—including no signal, spot, small cloud, and large cloud—at each time point (*35*). (**C**) Xist RAP enrichments over input across the X chromosome for the same time points as in (B). The *y*-axis scale (0 to 50) is the same for all time points. Xist enrichment at the *Xist* locus extends above *y*-axis maximum. (**D**) Two proposed models for Xist spreading (gray arrows) from its transcription locus (tick mark) across the chromosome. (**E**) A zoom in on the *y* axis of Xist enrichment after 1 hour of Xist induction. (**F**) Xist enrichments from RAP in wild-type female ES cells after 6 hours of differentiation. Early sites are defined by significant deviations ($P < 0.05$) above the local (10-Mb) average (*35*).

large Xist cloud observable by FISH at these time points. By 6 hours, the pattern of Xist localization began to resemble stable XCI in MLFs, where Xist localizes broadly across the X chromosome and is preferentially enriched at gene-dense regions (fig. S7).

Two models have been proposed to explain how Xist accomplishes this rapid spreading across the entire X chromosome (Fig. 3D) (*44*, *48*): Either Xist spreads uniformly from its transcription site until it coats the entire chromosome, or Xist first localizes to "early" sites that are far from the Xist transcription locus (*44*). To distinguish between these models, we examined Xist localization by RAP after 1 hour of Xist induction. We identified 28 distal sites of Xist occupancy across the chromosome ($P < 0.05$; Fig. 3E) (*35*). These sites comprised broad domains (average size 367 kb) that were concentrated in 15 regions spaced across the entire X chromosome. These sites initially showed an approximate doubling of enrichment relative to neighboring regions, but this enrichment decreased over time (Fig. 3C), which suggests that Xist preferentially localizes to these sites early during the initiation of XCI. We also performed the RAP experiment across a differentiation time course in wild-type female ES cells (fig. S8) (*35*). We found that Xist localized to these same distal sites across the X chromosome in female ES cells (Fig. 3F and figs. S7 and S9), demonstrating that Xist also targets these early sites in a normal developmental context. Thus, Xist initially transfers from its transcription locus to distal early localization sites to initiate spreading across the X chromosome.

Three-Dimensional Chromosome Conformation Guides Xist to Early Localization Sites

To determine how Xist identifies and targets these early localization sites, we considered two possible explanations (Fig. 4A): (i) Early sites may have higher affinity for the Xist RNA, enabling them to recruit Xist as it diffuses away from its transcription locus ("affinity transfer") (*48*–*51*). (ii) Alternatively, early sites may be defined not by affinity for Xist RNA but by spatial proximity to the site of Xist transcription ("proximity transfer") (*44*, *49*).

We first explored the affinity transfer model. Early sites were not enriched for specific sequence motifs that could play a role in recruiting Xist (*35*). We further compared Xist enrichment to >250 genomic annotations, including features such as repeat element density and chromatin immunoprecipitation sequencing experiments in ES cells (table S1) (*35*). We did not observe a significant relationship between Xist localization and LINE1 repeat elements (Pearson correlation = –0.17) (supplementary text). Instead, Xist early localization sites displayed modest enrichments (factor of <2) for gene density (table S3). Yet the chromosome-wide correlation between Xist localization and gene density was relatively modest (Pearson correlation = 0.34) (*35*), which suggests that gene density alone does not explain early Xist localization patterns.

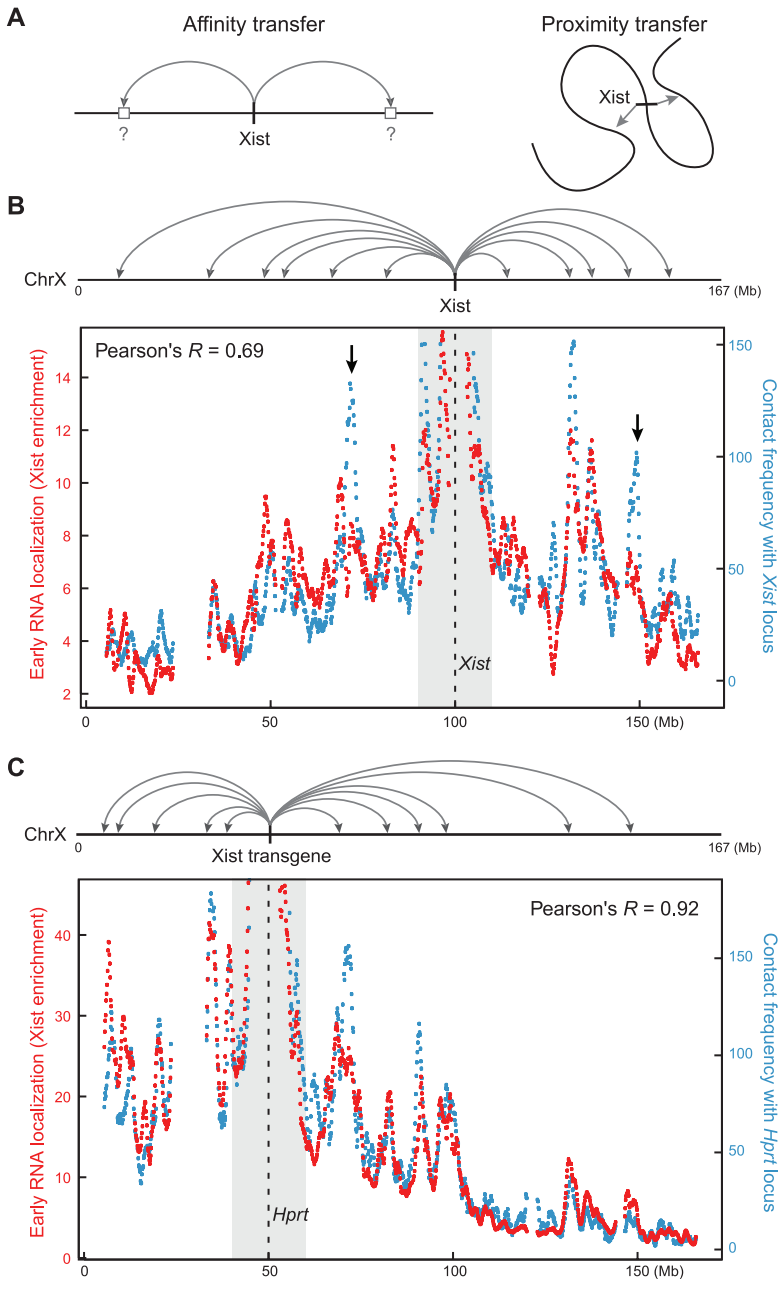

Fig. 4. Early Xist localization correlates with the three-dimensional proximity contacts of the Xist transcription locus. (**A**) Two models for how Xist spreads to early initiation sites (marked by gray arrows in all panels). Gray boxes on the left model represent hypothetical high-affinity interaction sites. (**B**) Correlation between Xist RNA localization (red) after 1 hour of Xist induction and Hi-C contact frequencies (blue) between distal sites and the *Xist* genomic locus (dashed line). Black arrows point to selected regions with lower Xist RNA enrichments than would be expected from the Hi-C contact frequencies. (**C**) Correlation between Xist transgene RNA localization (red) after 3 hours of induction of the Xist cDNA transgene in the *Hprt* locus and Hi-C contact frequencies (blue) between distal sites and the *Hprt* integration locus (dashed line). Correlation calculations exclude the shaded gray regions (10 Mb on each side). Contact frequencies represent normalized Hi-C interaction counts in male ES cells between each window and the window containing the *Xist* or *Hprt* locus (*35*).

In the proximity transfer model (Fig. 4A), the early Xist localization sites would be in close spatial proximity to the *Xist* transcription locus before Xist RNA induction, allowing direct transfer upon transcription of Xist RNA from its genomic locus to linearly distant chromosomal regions. To test this hypothesis, we examined the conformation of the X chromosome using a previously published male mouse ES cell data set (*52*) generated by genome-wide chromosome

conformation capture [Hi-C (*53*)]. Because of the sparseness of the Hi-C contact maps, we binned the data into 1-Mb regions based on the distance from the *Xist* genomic locus (*35*). We found a strong correlation between Xist RNA localization across the X chromosome and the frequency at which distal sites contact the *Xist* genomic locus (Pearson correlation = 0.69; Fig. 4B). We note that this correlation is not driven by the strong peak in both data sets centered at the *Xist* genomic locus because we considered only sites farther than 10 Mb from *Xist* itself (*35*). This strong correlation was also observed upon differentiation of female ES cells (Pearson correlation = 0.69; fig. S10A). These correlations exceeded that of any of the >250 genomic annotations that we tested in ES cells (table S1).

One possible explanation for this correlation is that RAP might be capturing distal sites because of their proximity-mediated contacts with the *Xist* DNA locus, rather than interactions with the Xist RNA. This is possible because in Xist RAP the *Xist* DNA locus is enriched by a factor of ~10 relative to the rest of the X chromosome (Fig. 4B). By capturing the *Xist* DNA locus through purification of Xist RNA, we might indirectly enrich other distal sites that are cross-linked to the *Xist* DNA locus, thereby yielding a pattern of enrichment similar to a standard chromosome conformation capture assay. However, if we observed a similar correlation between early Xist localization and chromosome conformation in the absence of a strong localization peak at the *Xist* genomic locus, then the pattern of Xist enrichment across the chromosome cannot be explained by proximity-induced cross-linking effects. To test this, we used our inducible system to turn off Xist transcription after 1 hour of induction and profiled Xist localization (*35*). We found that Xist RNA enrichment at its DNA locus declined from a factor of 102 to a factor of 14 over input, showing a level comparable to the rest of the X chromosome (fig. S10B). Xist remained enriched at the same distal regions (figs. S7 and S9) and showed a comparable correlation with proximity contacts to the *Xist* DNA locus (Pearson correlation = 0.59; fig. S10C). We conclude that the Xist RNA interacts directly with these spatially proximal sites.

Although these data show that early Xist localization correlates with spatial proximity, they do not demonstrate a causal relationship between Xist localization and chromosome conformation. If initial Xist localization is controlled by proximity-mediated contact with the *Xist* genomic locus, then altering the conformational context of the *Xist* transcription locus should lead to an early localization pattern defined by the proximity contacts of the new integration site. To test this directly, we used a male ES cell line that expresses an Xist cDNA from a Tet-inducible transgene incorporated at the *Hprt* locus, a genomic locus ~50 Mb proximal to the endogenous *Xist* locus (*26*) (figs. S7 and S10D). When we examined these cells at early time points after induction, we found that early Xist localization correlated strongly with proximity contacts at the *Hprt* integration site (Pearson correlation = 0.92; Fig. 4C) but not with those at the endogenous *Xist* locus (Pearson correlation = −0.02). Although these results do not exclude the possibility that additional chromatin features may be important for creating a permissive environment for Xist RNA localization, it is clear that chromosome conformation plays a dominant role in determining the early localization sites of the Xist RNA on the X chromosome.

Thus, spatial proximity to the Xist transcription locus guides early Xist RNA localization. This proximity-guided search may explain several of our other observations about Xist localization: (i) Because Xist is actively transcribed, it will be located within the "active compartment" of the nucleus (*53*). This may explain our observations that Xist preferentially localizes to gene-rich regions. (ii) Because chromosome conformation is heterogeneous in a cell population (*54*, *55*), the precise order by which Xist spreads to distal sites is likely to differ between individual cells. This may explain why Xist shows low-level early enrichment across the entire X chromosome, as all regions of the chromosome may contact the *Xist* genomic locus at some low frequency.

Xist Spreading to Active Genes Depends on Its Silencing Domain

Although early Xist localization correlated strongly with proximity contact frequency across the chromosome, we noticed several large chromosomal domains where Xist occupancy was lower than would be expected on the basis of observed proximity contacts (e.g., black arrows in Fig. 4B). These depleted regions contained many genes that are actively transcribed in ES cells; we termed these "active gene-dense regions." In contrast, the early-enriched Xist localization sites were also gene-dense but were enriched for genes that are inactive in ES cells. The depleted regions neighbored the early Xist localization sites such that Xist accumulated on the periphery of active gene-dense regions (fig. S11A).

To test whether actively transcribed genes generally showed reduced Xist occupancy, we explored Xist localization across all genes on the X chromosome 3 hours after Xist induction. Indeed, Xist showed on average a 15% focal depletion over active genes ($P = 0.006$, Mann-Whitney test), but was not depleted across inactive genes (Fig. 5, A and B). The level of Xist occupancy across active genes roughly reflected the level of expression in ES cells, with highly transcribed genes showing the lowest Xist occupancy (Pearson correlation = −0.33; fig. S11B). Furthermore, this focal depletion across active genes was temporary: Xist enrichment at genes expressed in ES cells increased over time and, upon stable inactivation in MLFs, was comparable to neighboring intergenic regions and inactive genes (fig. S11C). Together, these results suggest that the initial localization of Xist is hindered by some feature of actively transcribed genes but that Xist can eventually overcome this barrier to spread across these regions.

We hypothesized that the ability of Xist to spread across active genes is dependent on its ability to silence gene expression. Previous genetic studies have identified the A-repeat within Xist as an RNA domain that is necessary for silencing gene expression but is not required for the formation of the Xist RNA compartment (*25*, *26*). We therefore repeated the RAP experiments using an Xist RNA in which the A-repeat had been deleted (ΔA Xist) (*26*). We found that the localization of ΔA Xist over the whole X chromosome looked broadly comparable to that of wild-type Xist (Fig. 5C and fig. S12), consistent with previous observations by FISH (*25*, *26*). However, at high resolution, we observed a factor of ~2 depletion for ΔA Xist occupancy relative to wild-type Xist over active gene-dense regions, with ΔA Xist instead accumulating on the edges of these regions (Fig. 5C and fig. S11, D and E). This depletion extended across the entire region including active and inactive genes as well as intergenic sequences; this finding suggests that active gene-dense regions may loop out of the ΔA Xist compartment such that even inactive genes remain physically inaccessible to ΔA Xist spreading (Fig. 5E).

These results demonstrate that Xist initially localizes to the periphery of active gene-dense regions through a mechanism independent of its A-repeat domain, but requires the A-repeat to efficiently spread across active genes and access these regions. Notably, the A-repeat domain interacts with the PRC2 chromatin-modifying complex (*14*) and enables the spatial repositioning of active genes into the Xist compartment (*25*). Together, these observations suggest that the A-repeat may allow Xist to access and spread across active gene-dense regions by modifying chromatin and altering chromosome architecture to reposition these regions into the Xist compartment (Fig. 5E).

A Model for How Xist Exploits and Alters Three-Dimensional Genome Architecture to Spread Across the X Chromosome

Our data suggest a model for how Xist can integrate its two functions—localization to DNA and silencing of gene expression—to exploit and alter nuclear architecture to spread across the X chromosome (Fig. 6). In this model, at the initiation XCI, Xist exploits the preexisting three-dimensional conformation of the X chromosome to search for target sites across the chromosome. Upon encountering a new site, Xist transfers to this region through a mechanism that allows it to localize to any region of the X chromosome, possibly through its interaction with proteins in the nuclear matrix (*29*–*31*). Initially, Xist accumulates at spatially proximal sites on the periphery of active gene-dense regions, positioning itself to silence neighboring genes. Through the A-repeat domain, Xist leads to transcriptional si-

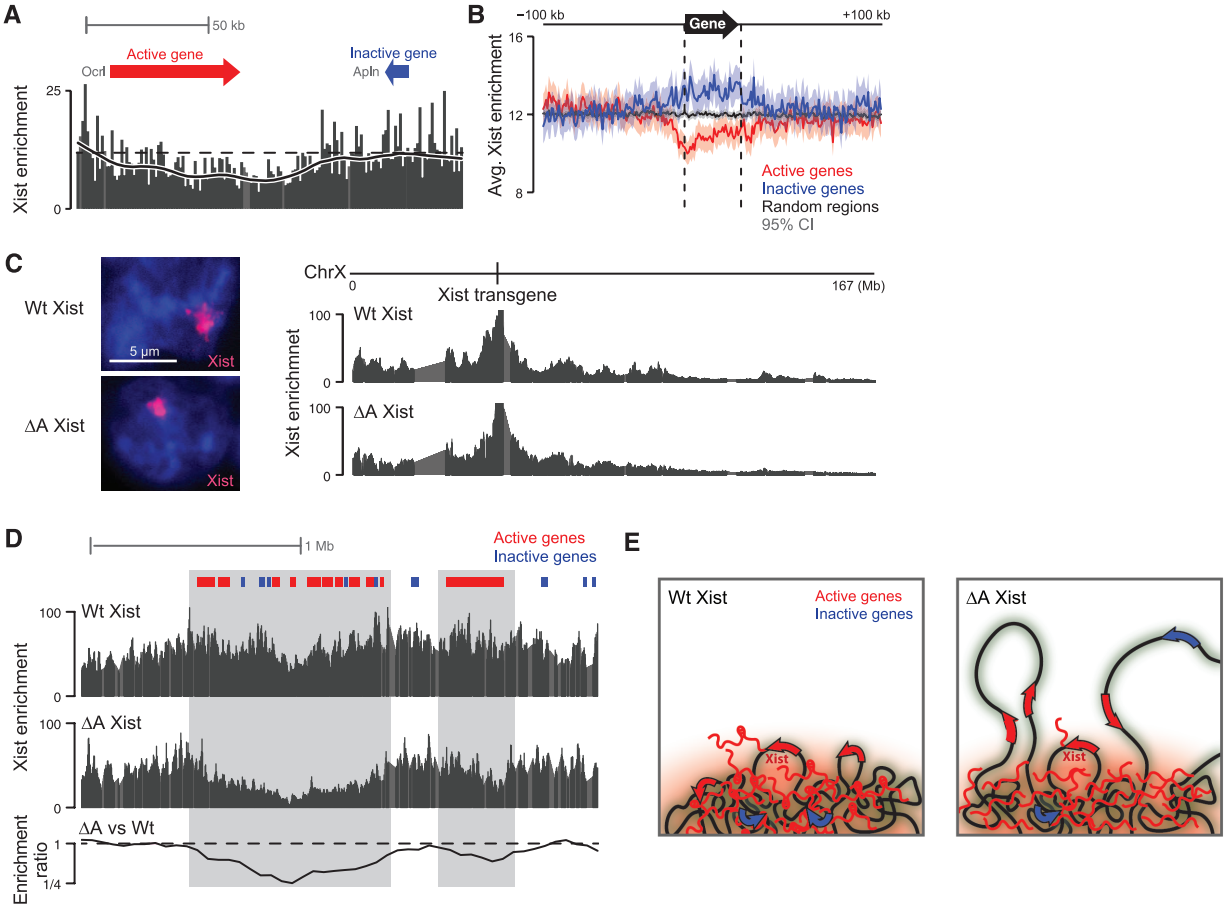

Fig. 5. The A-repeat deletion of Xist cannot spread over the active regions of the X chromosome. (**A**) Xist enrichment over representative genes at chrX:45,252,000–45,408,000. Dashed line denotes the average enrichment for the entire region. Solid line represents the smoothed enrichment in sliding windows across the region. (**B**) Xist enrichment averaged over all active genes (red line, N = 608), inactive genes (blue line, N = 595), and randomly permuted regions across the X chromosome (black line) (*35*). Shaded regions represent 95% confidence intervals for the average enrichment. (**C**) Localization of wild-type Xist (Wt Xist, top) and Xist lacking the A-repeat (ΔA Xist, bottom) by RNA FISH (left) and RAP (right) across the X chromosome. (**D**) Comparison of Wt and ΔA Xist enrichment across a representative region at chrX:44,600,000-47,100,000. Gray boxes mark regions that are depleted for Xist localization in ΔA versus Wt Xist. All panels present data from 3 hours after Xist induction in undifferentiated male ES cells, where Xist is expressed from its endogenous locus [(A) and (B)] or from the *Hprt* locus [(C) and (D)]. Genes were classified as active or inactive using RNA sequencing data from undifferentiated male ES cells (*35*). (**E**) Model: In the presence of the A-repeat (left), Xist localizes across the entire X chromosome (red cloud) but is initially excluded from active genes (red arrows). In the absence of the A-repeat (right), Xist accumulates on the periphery of active gene-dense regions but cannot spread to actively transcribed genes (red arrows) or inactive genes (blue arrows) that lie within these regions.

lencing (*26*) and repositioning of these genes into the growing Xist silenced compartment (*25*), possibly through recruitment of PRC2 (*14*) and other proteins (*56*) that lead to chromosomal compaction (*57*, *58*). By repositioning previously active regions into its growing compartment, Xist effectively pulls new regions of active chromatin closer to the *Xist* transcription locus, thus allowing Xist RNA to spread to new sites by proximity transfer. Because Xist is actively transcribed throughout XCI, it will remain spatially close to other actively transcribed genes (*59*), the precise targets required for propagating Xist-mediated silencing. This process—involving searching in three dimensions, modifying chromatin state and chromosome architecture, and spreading to newly accessible locations—would explain how Xist can silence the entire X chromosome reproducibly, such that silencing occurs in each cell, even though chromosome conformation (and thus the early Xist localization sites) may vary among individual cells in a population.

This coordinated interplay between lncRNA localization and chromosome conformation may have broader implications beyond Xist. Other lncRNAs may similarly take advantage of chromosome conformation to identify target sites in close spatial proximity (*9*, *17*, *60*), which could even reside on other chromosomes (*61*, *62*). This search strategy capitalizes on the ability of a lncRNA to act while tethered to its transcription locus (*63*), in contrast to an mRNA, which requires export and translation to carry out its function. Because chromosome conformation is nonrandom, a proximity-guided search strategy might explain how low-abundance lncRNAs can reliably identify their genomic targets. Upon binding these targets, lncRNAs may in turn alter chromosome conformation through their interactions with various chromatin regulatory complexes (*15*, *16*). These alterations would allow localization to and regulation of previously inaccessible chromatin domains, and might even establish local nuclear compartments that contain the co-regulated targets of lncRNA complexes.

Methods

RAP

We designed a set of 120-nucleotide oligos tiled every 15 nucleotides across the entire Xist RNA sequence, excluding sequences that originated from a repetitive region. We synthesized this pool of oligos using microarray-based DNA synthesis technology and incorporated T7 promoter sequences through PCR. We generated RNA probes by in vitro transcription in the presence of biotin–uridine triphosphate. We cross-linked cells with 2 mM disuccinimidyl glutarate for 45 min and 3% formaldehyde for 10 min. We lysed cells and digested chromatin to 100- to 300-bp frag-

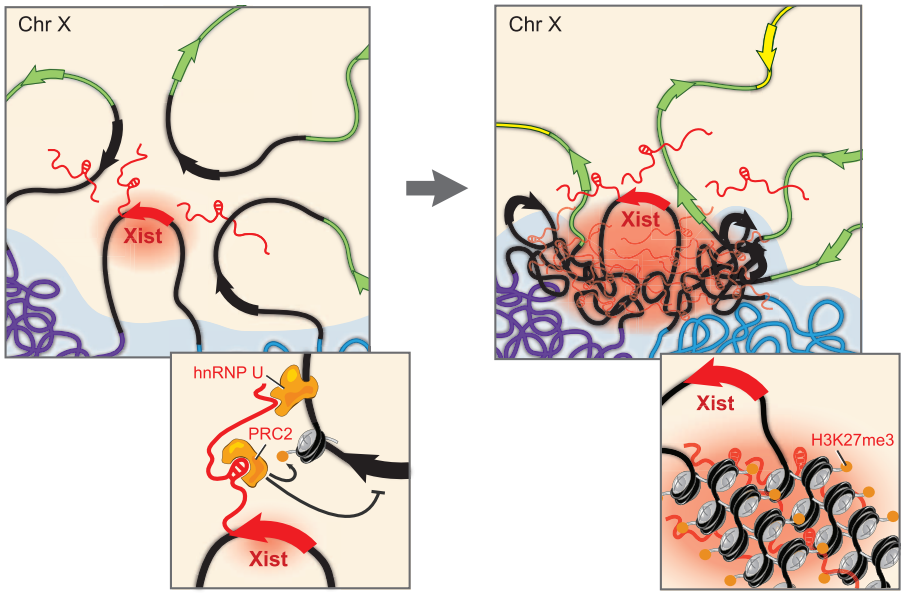

Fig. 6. A model for how Xist exploits and alters three-dimensional genome architecture to spread across the X chromosome. Upon induction of expression in ES cells (left), Xist (red) spreads to spatially proximal sites on the periphery of active gene-dense regions (black). Gene-poor regions (blue, purple) contact the *Xist* transcription locus infrequently, leading to slower spreading to these regions. When encountering a new region (left inset), Xist interacts with chromatin through a degenerate localization mechanism, possibly through the matrix protein hnRNP U (*30*, *34*), and uses its A-repeat domain to spread over active genes. Xist may then recruit PRC2 (*14*) and other proteins (*56*) to modify and compact chromatin, thereby repositioning nearby chromosomal regions into the Xist RNA compartment (red cloud, right inset). These structural changes may propagate Xist spreading (right) by pulling new regions (green, yellow) of the chromosome into closer proximity to the *Xist* genomic locus and the growing Xist compartment.

ments through a combination of sonication and treatment with TURBO DNase. We diluted the lysate to hybridization conditions containing 3 M guanidine thiocyanate. We precleared lysate preparations by adding streptavidin-coated magnetic beads for 20 min at 45°C. Biotin-labeled RNA capture probes were mixed with the heated lysate and incubated at 45°C for 2 hours. We captured the probe-RNA complexes with streptavidin-coated beads and washed six times at 45°C. We eluted captured chromatin complexes and reversed cross links by adding proteinase K to the probe-bead complexes and incubating overnight at 65°C. We generated standard Illumina sequencing libraries and obtained >5 million 25-bp paired-end reads per sample.

Inducible Xist Cell Lines

For the time course, we used a male ES cell line in which the wild-type *Xist* promoter was replaced with a Tet-inducible promoter. For chromosome conformation and A-repeat deletion experiments, we used male ES cell lines carrying a wild-type or ΔA Xist cDNA transgene in the *Hprt* locus under control of a Tet-inducible promoter. To induce Xist expression, we added doxycycline to a final concentration of 2 μg/ml at a defined time before fixing cells.

Data Analysis

Sequencing reads were aligned to the *Mus musculus* genome (mm9). We calculated enrichment ratios between read counts in the RAP experiment and the input in overlapping windows across the chromosome. To identify early sites in the time-course experiments, we looked for 100-kb windows with enrichments that exceeded the local mean ($P < 0.05$). We correlated Xist enrichment across the chromosome with normalized Hi-C interaction counts measured in male mouse ES cells at 1-Mb resolution (*52*). For Hi-C correlation analysis, we excluded all bins within 10 Mb on either side of the *Xist* transcription locus, which would otherwise dominate the correlation calculation because of the strong local peaks in both the Hi-C and RAP data sets. To define active and inactive genes, we analyzed RNA sequencing data from embryonic stem cells and defined "active" genes as those expressed with $P < 0.001$.

Complete materials and methods are available as supplementary materials.

References and Notes

1. T. Derrien *et al.*, The GENCODE v7 catalog of human long noncoding RNAs: Analysis of their gene structure, evolution, and expression. *Genome Res.* **22**, 1775–1789 (2012). doi: 10.1101/gr.132159.111; pmid: 22955988
2. FANTOM Consortium, RIKEN Genome Exploration Research Group and Genome Science Group (Genome Network Project Core Group), The transcriptional landscape of the mammalian genome. *Science* **309**, 1559–1563 (2005). doi: 10.1126/science.1112014; pmid: 16141072
3. M. Guttman *et al.*, Ab initio reconstruction of cell type-specific transcriptomes in mouse reveals the conserved multi-exonic structure of lincRNAs. *Nat. Biotechnol.* **28**, 503–510 (2010). doi: 10.1038/nbt.1633; pmid: 20436462
4. M. Guttman *et al.*, Chromatin signature reveals over a thousand highly conserved large non-coding RNAs in mammals. *Nature* **458**, 223–227 (2009). doi: 10.1038/nature07672; pmid: 19182780
5. M. N. Cabili *et al.*, Integrative annotation of human large intergenic noncoding RNAs reveals global properties and specific subclasses. *Genes Dev.* **25**, 1915–1927 (2011). doi: 10.1101/gad.17446611; pmid: 21890647
6. M. Guttman *et al.*, lincRNAs act in the circuitry controlling pluripotency and differentiation. *Nature* **477**, 295–300 (2011). doi: 10.1038/nature10398; pmid: 21874018
7. I. Ulitsky, A. Shkumatava, C. H. Jan, H. Sive, D. P. Bartel, Conserved function of lincRNAs in vertebrate embryonic development despite rapid sequence evolution. *Cell* **147**, 1537–1550 (2011). doi: 10.1016/j.cell.2011.11.055; pmid: 22196729
8. U. A. Ørom *et al.*, Long noncoding RNAs with enhancer-like function in human cells. *Cell* **143**, 46–58 (2010). doi: 10.1016/j.cell.2010.09.001; pmid: 20887892
9. K. C. Wang *et al.*, A long noncoding RNA maintains active chromatin to coordinate homeotic gene expression. *Nature* **472**, 120–124 (2011). doi: 10.1038/nature09819; pmid: 21423168
10. J. L. Rinn *et al.*, Functional demarcation of active and silent chromatin domains in human HOX loci by noncoding RNAs. *Cell* **129**, 1311–1323 (2007). doi: 10.1016/j.cell.2007.05.022; pmid: 17604720
11. J. T. Lee, Epigenetic regulation by long noncoding RNAs. *Science* **338**, 1435–1439 (2012). doi: 10.1126/science.1231776; pmid: 23239728
12. M. C. Tsai *et al.*, Long noncoding RNA as modular scaffold of histone modification complexes. *Science* **329**, 689–693 (2010). doi: 10.1126/science.1192002; pmid: 20616235
13. T. Nagano *et al.*, The Air noncoding RNA epigenetically silences transcription by targeting G9a to chromatin. *Science* **322**, 1717–1720 (2008). doi: 10.1126/science.1163802; pmid: 18988810
14. J. Zhao, B. K. Sun, J. A. Erwin, J. J. Song, J. T. Lee, Polycomb proteins targeted by a short repeat RNA to the mouse X chromosome. *Science* **322**, 750–756 (2008). doi: 10.1126/science.1163045; pmid: 18974356
15. M. Guttman, J. L. Rinn, Modular regulatory principles of large non-coding RNAs. *Nature* **482**, 339–346 (2012). doi: 10.1038/nature10887; pmid: 22337053
16. J. L. Rinn, H. Y. Chang, Genome regulation by long noncoding RNAs. *Annu. Rev. Biochem.* **81**, 145–166 (2012). doi: 10.1146/annurev-biochem-051410-092902; pmid: 22663078
17. A. Kanhere, R. G. Jenner, Noncoding RNA localisation mechanisms in chromatin regulation. *Silence* **3**, 2 (2012). doi: 10.1186/1758-907X-3-2; pmid: 22292981
18. C. Gontan, I. Jonkers, J. Gribnau, Long noncoding RNAs and X chromosome inactivation. *Prog. Mol. Subcell. Biol.* **51**, 43–64 (2011). doi: 10.1007/978-3-642-16502-3_3; pmid: 21287133
19. D. Umlauf, P. Fraser, T. Nagano, The role of long non-coding RNAs in chromatin structure and gene regulation: Variations on a theme. *Biol. Chem.* **389**, 323–331 (2008). doi: 10.1515/BC.2008.047; pmid: 18225988
20. K. Plath, S. Mlynarczyk-Evans, D. A. Nusinow, B. Panning, Xist RNA and the mechanism of X chromosome inactivation. *Annu. Rev. Genet.* **36**, 233–278 (2002). doi: 10.1146/annurev.genet.36.042902.092433; pmid: 12429693
21. P. Avner, E. Heard, X-chromosome inactivation: Counting, choice and initiation. *Nat. Rev. Genet.* **2**, 59–67 (2001). doi: 10.1038/35047580; pmid: 11253071
22. K. Plath *et al.*, Role of histone H3 lysine 27 methylation in X inactivation. *Science* **300**, 131–135 (2003). doi: 10.1126/science.1084274; pmid: 12649488
23. J. Silva *et al.*, Establishment of histone h3 methylation on the inactive X chromosome requires transient recruitment of Eed-Enx1 polycomb group complexes. *Dev. Cell* **4**, 481–495 (2003). doi: 10.1016/S1534-5807(03)00068-6; pmid: 12689588

24. C. M. Clemson, J. A. McNeil, H. F. Willard, J. B. Lawrence, XIST RNA paints the inactive X chromosome at interphase: Evidence for a novel RNA involved in nuclear/chromosome structure. *J. Cell Biol.* **132**, 259–275 (1996). doi: 10.1083/jcb.132.3.259; pmid: 8636206
25. J. Chaumeil, P. Le Baccon, A. Wutz, E. Heard, A novel role for Xist RNA in the formation of a repressive nuclear compartment into which genes are recruited when silenced. *Genes Dev.* **20**, 2223–2237 (2006). doi: 10.1101/gad.380906; pmid: 16912274
26. A. Wutz, T. P. Rasmussen, R. Jaenisch, Chromosomal silencing and localization are mediated by different domains of Xist RNA. *Nat. Genet.* **30**, 167–174 (2002). doi: 10.1038/ng820; pmid: 11780141
27. C. E. Senner *et al.*, Disruption of a conserved region of Xist exon 1 impairs Xist RNA localisation and X-linked gene silencing during random and imprinted X chromosome inactivation. *Development* **138**, 1541–1550 (2011). doi: 10.1242/dev.056812; pmid: 21389056
28. A. Beletskii, Y. K. Hong, J. Pehrson, M. Egholm, W. M. Strauss, PNA interference mapping demonstrates functional domains in the noncoding RNA Xist. *Proc. Natl. Acad. Sci. U.S.A.* **98**, 9215–9220 (2001). doi: 10.1073/pnas.161173098; pmid: 11481485
29. Y. Hasegawa *et al.*, The matrix protein hnRNP U is required for chromosomal localization of Xist RNA. *Dev. Cell* **19**, 469–476 (2010). doi: 10.1016/j.devcel.2010.08.006; pmid: 20833368
30. D. Pullirsch *et al.*, The Trithorax group protein Ash2l and Saf-A are recruited to the inactive X chromosome at the onset of stable X inactivation. *Development* **137**, 935–943 (2010). doi: 10.1242/dev.035956; pmid: 20150277
31. R. Agrelo *et al.*, SATB1 defines the developmental context for gene silencing by Xist in lymphoma and embryonic cells. *Dev. Cell* **16**, 507–516 (2009). doi: 10.1016/j.devcel.2009.03.006; pmid: 19386260
32. C. Chu, K. Qu, F. L. Zhong, S. E. Artandi, H. Y. Chang, Genomic maps of long noncoding RNA occupancy reveal principles of RNA-chromatin interactions. *Mol. Cell* **44**, 667–678 (2011). doi: 10.1016/j.molcel.2011.08.027; pmid: 21963238
33. M. D. Simon *et al.*, The genomic binding sites of a noncoding RNA. *Proc. Natl. Acad. Sci. U.S.A.* **108**, 20497–20502 (2011). doi: 10.1073/pnas.1113536108; pmid: 22143764
34. P. D. Mariner *et al.*, Human Alu RNA is a modular transacting repressor of mRNA transcription during heat shock. *Mol. Cell* **29**, 499–509 (2008). doi: 10.1016/j.molcel.2007.12.013; pmid: 18313387
35. See supplementary materials on *Science* Online.
36. J. B. Berletch, F. Yang, J. Xu, L. Carrel, C. M. Disteche, Genes that escape from X inactivation. *Hum. Genet.* **130**, 237–245 (2011). doi: 10.1007/s00439-011-1011-z; pmid: 21614513
37. S. Dietzel *et al.*, The 3D positioning of ANT2 and ANT3 genes within female X chromosome territories correlates with gene activity. *Exp. Cell Res.* **252**, 363–375 (1999). doi: 10.1006/excr.1999.4635; pmid: 10527626
38. G. N. Filippova *et al.*, Boundaries between chromosomal domains of X inactivation and escape bind CTCF and lack CpG methylation during early development. *Dev. Cell* **8**, 31–42 (2005). doi: 10.1016/j.devcel.2004.10.018; pmid: 15669143
39. F. Yang, T. Babak, J. Shendure, C. M. Disteche, Global survey of escape from X inactivation by RNA-sequencing in mouse. *Genome Res.* **20**, 614–622 (2010). doi: 10.1101/gr.103200.109; pmid: 20363980
40. D. Tian, S. Sun, J. T. Lee, The long noncoding RNA, Jpx, is a molecular switch for X chromosome inactivation. *Cell* **143**, 390–403 (2010). doi: 10.1016/j.cell.2010.09.049; pmid: 21029862
41. C. Chureau *et al.*, Ftx is a non-coding RNA which affects Xist expression and chromatin structure within the X-inactivation center region. *Hum. Mol. Genet.* **20**, 705–718 (2011). doi: 10.1093/hmg/ddq516; pmid: 21118898
42. R. Song *et al.*, Many X-linked microRNAs escape meiotic sex chromosome inactivation. *Nat. Genet.* **41**, 488–493 (2009). doi: 10.1038/ng.338; pmid: 19305411
43. S. M. Duthie *et al.*, Xist RNA exhibits a banded localization on the inactive X chromosome and is excluded from autosomal material in cis. *Hum. Mol. Genet.* **8**, 195–204 (1999). doi: 10.1093/hmg/8.2.195; pmid: 9931327
44. A. Tattermusch, N. Brockdorff, A scaffold for X chromosome inactivation. *Hum. Genet.* **130**, 247–253 (2011). doi: 10.1007/s00439-011-1027-4; pmid: 21660507
45. S. Arthold, A. Kurowski, A. Wutz, Mechanistic insights into chromosome-wide silencing in X inactivation. *Hum. Genet.* **130**, 295–305 (2011). doi: 10.1007/s00439-011-1002-0; pmid: 21567178
46. D. H. Kim, Y. Jeon, M. C. Anguera, J. T. Lee, X-chromosome epigenetic reprogramming in pluripotent stem cells via noncoding genes. *Semin. Cell Dev. Biol.* **22**, 336–342 (2011). doi: 10.1016/j.semcdb.2011.02.025; pmid: 21376830
47. J. T. Lee, N. Lu, Targeted mutagenesis of Tsix leads to nonrandom X inactivation. *Cell* **99**, 47–57 (1999). doi: 10.1016/S0092-8674(00)80061-6; pmid: 10520993
48. S. F. Pinter *et al.*, Spreading of X chromosome inactivation via a hierarchy of defined Polycomb stations. *Genome Res.* **22**, 1864–1876 (2012). doi: 10.1101/gr.133751.111; pmid: 22948768
49. H. Marks *et al.*, High-resolution analysis of epigenetic changes associated with X inactivation. *Genome Res.* **19**, 1361–1373 (2009). doi: 10.1101/gr.092643.109; pmid: 19581487
50. Y. Jeon, J. T. Lee, YY1 tethers Xist RNA to the inactive X nucleation center. *Cell* **146**, 119–133 (2011). doi: 10.1016/j.cell.2011.06.026; pmid: 21729784
51. E. Heard *et al.*, Methylation of histone H3 at Lys-9 is an early mark on the X chromosome during X inactivation. *Cell* **107**, 727–738 (2001). doi: 10.1016/S0092-8674(01)00598-0; pmid: 11747809
52. J. R. Dixon *et al.*, Topological domains in mammalian genomes identified by analysis of chromatin interactions. *Nature* **485**, 376–380 (2012). doi: 10.1038/nature11082; pmid: 22495300
53. E. Lieberman-Aiden *et al.*, Comprehensive mapping of long-range interactions reveals folding principles of the human genome. *Science* **326**, 289–293 (2009). doi: 10.1126/science.1181369; pmid: 19815776
54. J. Dekker, M. A. Marti-Renom, L. A. Mirny, Exploring the three-dimensional organization of genomes: Interpreting chromatin interaction data. *Nat. Rev. Genet.* **14**, 390–403 (2013). doi: 10.1038/nrg3454; pmid: 23657480
55. T. Misteli, The concept of self-organization in cellular architecture. *J. Cell Biol.* **155**, 181–185 (2001). doi: 10.1083/jcb.200108110; pmid: 11604416
56. R. S. Nozawa *et al.*, Human inactive X chromosome is compacted through a PRC2-independent SMCHD1-HBiX1 pathway. *Nat. Struct. Mol. Biol.* **20**, 566–573 (2013). doi: 10.1038/nsmb.2532; pmid: 23542155
57. A. Rego, P. B. Sinclair, W. Tao, I. Kireev, A. S. Belmont, The facultative heterochromatin of the inactive X chromosome has a distinctive condensed ultrastructure. *J. Cell Sci.* **121**, 1119–1127 (2008). doi: 10.1242/jcs.026104; pmid: 18334550
58. C. Naughton, D. Sproul, C. Hamilton, N. Gilbert, Analysis of active and inactive X chromosome architecture reveals the independent organization of 30 nm and large-scale chromatin structures. *Mol. Cell* **40**, 397–409 (2010). doi: 10.1016/j.molcel.2010.10.013; pmid: 21070966
59. E. Splinter *et al.*, The inactive X chromosome adopts a unique three-dimensional conformation that is dependent on Xist RNA. *Genes Dev.* **25**, 1371–1383 (2011). doi: 10.1101/gad.633311; pmid: 21690198
60. P. G. Maass *et al.*, A misplaced lncRNA causes brachydactyly in humans. *J. Clin. Invest.* **122**, 3990–4002 (2012). doi: 10.1172/JCI65508; pmid: 23093776
61. A. Williams, C. G. Spilianakis, R. A. Flavell, Interchromosomal association and gene regulation in trans. *Trends Genet.* **26**, 188–197 (2010). doi: 10.1016/j.tig.2010.01.007; pmid: 20236724
62. C. G. Spilianakis, M. D. Lalioti, T. Town, G. R. Lee, R. A. Flavell, Interchromosomal associations between alternatively expressed loci. *Nature* **435**, 637–645 (2005). doi: 10.1038/nature03574; pmid: 15880101
63. J. T. Lee, Lessons from X-chromosome inactivation: Long ncRNA as guides and tethers to the epigenome. *Genes Dev.* **23**, 1831–1842 (2009). doi: 10.1101/gad.1811209; pmid: 19684108

Acknowledgments: We thank A. Gnirke for initial discussions about the RAP method; T. Mikkelsen for assistance with oligonucleotide synthesis; M. Garber and J. Rinn for helpful discussions and ideas; A. Wutz for generously providing Xist transgenic cell lines; S. Rao, N. Cherniavsky, and E. Lieberman-Aiden for analytical help and discussions; P. Russell, M. Cabili, E. Hacisuleyman, and L. Goff for critical reading of the manuscript; L. Gaffney for assistance with figures; and S. Knemeyer for illustrations. Supported by the Fannie and John Hertz Foundation and National Defense Science and Engineering Graduate Fellowship (J.M.E.); an NIH postdoctoral fellowship (1F32GM103139-01) (A.P.-J.); NIH Director's Early Independence Award DP5OD012190 (M.G.), National Human Genome Research Institute Center for Excellence for Genomic Sciences grant P50HG006193 (M.G.); National Institute of General Medical Sciences grant P01GM099134 (K.P.); California Institute for Regenerative Medicine grants RN1-00564, RB3-05080, and RB4-06133 (K.P.); the Broad Institute of MIT and Harvard (M.G. and E.S.L.); and the Eli and Edythe Broad Center of Regenerative Medicine and Stem Cell Research at UCLA (K.P.). Sequencing data are available online from the NCBI Gene Expression Omnibus (accession no. GSE46918, www.ncbi.nlm.nih.gov/geo/) and additional data and information is available at www.lncRNA.caltech.edu/RAP/. J.M.E., E.S.L., and M.G. are inventors on a patent application from the Broad Institute that covers the selective purification of RNA-bound molecular complexes in cells.

Supplementary Materials

www.sciencemag.org/cgi/content/full/science.1237973/DC1
Materials and Methods
Supplementary Text
Figs. S1 to S14
Tables S1 to S6
References (*64*–*79*)

18 March 2013; accepted 20 June 2013
Published online 4 July 2013;
10.1126/science.1237973

All-Optical Switch and Transistor Gated by One Stored Photon

Wenlan Chen,[1] Kristin M. Beck,[1] Robert Bücker,[1,2] Michael Gullans,[3] Mikhail D. Lukin,[3] Haruka Tanji-Suzuki,[1,3,4] Vladan Vuletić[1]*

The realization of an all-optical transistor, in which one "gate" photon controls a "source" light beam, is a long-standing goal in optics. By stopping a light pulse in an atomic ensemble contained inside an optical resonator, we realized a device in which one stored gate photon controls the resonator transmission of subsequently applied source photons. A weak gate pulse induces bimodal transmission distribution, corresponding to zero and one gate photons. One stored gate photon produces fivefold source attenuation and can be retrieved from the atomic ensemble after switching more than one source photon. Without retrieval, one stored gate photon can switch several hundred source photons. With improved storage and retrieval efficiency, our work may enable various new applications, including photonic quantum gates and deterministic multiphoton entanglement.

Photons are excellent carriers of quantum information, but it is difficult to induce the strong interactions between individual photons that are required for, for example, all-optical quantum information processing. Nevertheless, advances toward such interactions have been made in cavity quantum electrodynamics (QED) systems with atoms (*1*–*6*) or artificial atoms (*7*–*11*) and in a cavity-free system by using atomic Rydberg states (*12*, *13*) or dye molecules (*14*). All-optical switching of one beam by another (*15*) and cross-phase modulation (*16*) have been demonstrated at the level of a few hundred photons by means of electromagnetically induced transparency (EIT) (*17*–*21*). At the few-photon level, nonclassical light has been generated (*1*, *4*, *6*–*9*, *11*–*13*, *22*), and optical nonlinearities of 16° in phase shift (*23*) and up to ~20% in two-photon attenuation (*5*, *9*, *10*) have been observed in cavity QED systems. Although switching of the cavity transmission by a single atom has also been achieved (*24*), the realization of an optical transistor exhibiting gain with gate signals at the few- or one-photon level (*25*) remains a challenge.

We demonstrate a cavity QED version (*18*) of an optical switch (*25*) based on EIT in a four-level system (*17*–*19*) in which the collective atomic excitation associated with the storage of one gate photon (*20*, *26*, *27*) blocks the resonator transmission. Our system (*5*) consists of an ensemble of laser-cooled cesium atoms optically trapped inside a high-finesse optical cavity (Fig. 1A) operating in the strong-coupling regime (*1*–*6*) of cavity QED. Each atom has a four-state *N*-type level structure $|g\rangle \leftrightarrow |d\rangle \leftrightarrow |s\rangle \leftrightarrow |e\rangle$ with two stable ground states, $|g\rangle$ and $|s\rangle$, and two electronic excited states, $|d\rangle$ and $|e\rangle$ (Fig. 1B). For atoms prepared in state $|g\rangle$, this atomic structure mediates an effective interaction between free-space photons (photons resonant with the $|g\rangle \rightarrow |d\rangle$ transition serving as gate photons) and cavity photons (photons resonant with the $|s\rangle \rightarrow |e\rangle$ transition serving as the source) (*17*–*19*). These two transitions are connected via a control laser that addresses the $|d\rangle \rightarrow |s\rangle$ transition and induces transparency (EIT) for the gate photons. By ramping the control laser power down to zero, we stored a weak gate pulse inside the atomic ensemble (Fig. 1B) and retrieved it at a later time by adiabatically reapplying the control beam (Fig. 1D) (*20*, *26*, *27*). In between storage and retrieval, we applied a source beam (Fig. 1C). The atomic population in state $|s\rangle$ associated with the stored gate pulse can block the transmission of the source pulse through the cavity (*24*). Because of the finite optical depth (OD) of the ensemble (OD $\leq$ 0.9) and suboptimal control waveform (*28*), 1 out of 5 to 10 incident gate photons is stored.

We first characterized the cavity transmission without gate photon retrieval. To this end, we measured the average cavity transmission spectrum for different mean stored gate photon numbers $\langle n_g \rangle$ (Fig. 2). Because the gate pulses are weak classical pulses (coherent states), they are associated with Poissonian distributions in photon number n_g, and there is a finite probability $p(0) = e^{-\langle n_g \rangle}$ that the stored gate pulse does not contain any photons. Therefore, even if one photon were to perfectly switch off the source beam, there is a maximum average switching contrast $1-e^{-\langle n_g \rangle}$ for measurements with coherent states of gate photons (Fig. 2, inset, solid line). The measured data points lie close to the maximum possible switching contrast and within the theoretically expected range (Fig. 2, gray area).

The photon number quantization of the gate pulse and the cavity blocking by just one gate photon are evident when we plot histograms of transmission spectra (Fig. 3) instead of the average transmission. The histogram shows two clearly separated components (Fig. 3B), where the high-transmission component corresponds to $n_g = 0$, whereas the low-transmission component corresponds to $n_g \geq 1$ (mostly $n_g = 1$ gate photons). The high-to-low peak transmission ratio gives an extinction factor for one stored gate photon of $T^{-1} = 11 \pm 1$.

In order to characterize the optical gain of the system, we measured the distribution of the

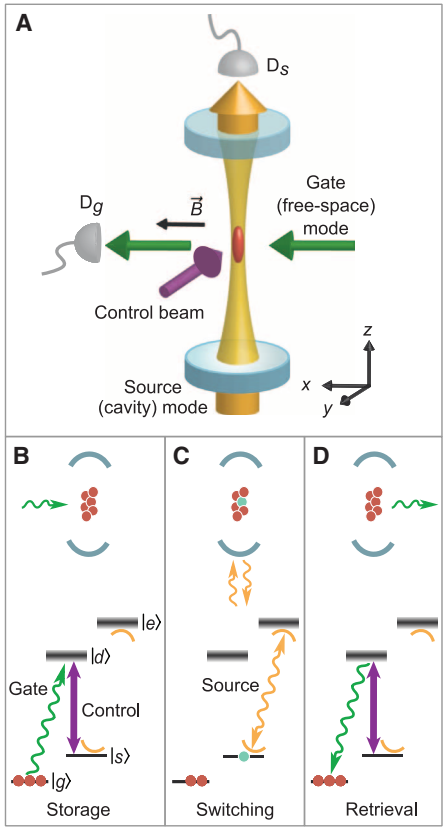

Fig. 1. All-optical switch and transistor. (**A**) Setup and (**B** to **D**) atomic level scheme with experimental sequence. An ensemble of laser-cooled atoms is trapped inside an optical resonator operating in the single-atom strong-coupling regime on the $|s\rangle \rightarrow |e\rangle$ transition. (B) We first stored a gate photon in the medium, which corresponds to a collective atomic excitation to state $|s\rangle$. (C) This collective excitation blocks the transmission of source photons through the cavity and (D) can be retrieved. Retrieved gate and transmitted source photons are measured with photon counters D_g and D_s, respectively. The atomic states of ^{133}Cs used in this experiment are $|g\rangle = |6S_{1/2},F = 3, m_F = 3\rangle$, $|d\rangle = |6P_{3/2},4,4\rangle$, $|s\rangle = |6S_{1/2},4,4\rangle$, and $|e\rangle = |6P_{3/2},5,5\rangle$, where F and m_F denote the hyperfine and magnetic sublevels, respectively.

[1]Department of Physics and Research Laboratory of Electronics, Massachusetts Institute of Technology, Cambridge, MA 02139, USA. [2]Vienna Center for Quantum Science and Technology, Atominstitut, Technische Universität Wien, Stadionallee 2, 1020 Vienna, Austria. [3]Department of Physics, Harvard University, Cambridge, MA 02138, USA. [4]Photon Science Center, School of Engineering, University of Tokyo, 2-11-16 Yayoi, Bunkyo-ku, Tokyo 113-8656, Japan.

*Corresponding author. E-mail: vuletic@mit.edu

transmitted source photon number, $M_s = \frac{\mathcal{T}}{\mathcal{T}+\mathcal{L}}\int dt\, m_c(t)\,\kappa$, on cavity resonance. Here, $m_c(t)$ is the intracavity photon number at time t, κ is the cavity linewidth, and $\frac{\mathcal{T}}{\mathcal{T}+\mathcal{L}} = 0.66$ (with cavity mirror transmission $\mathcal{T}$ and mirror loss $\mathcal{L}$) accounts for the outcoupling efficiency of an intracavity photon. M_s can be determined from the detected photon number and the independently measured detection-path efficiency (*29*). As shown in Fig. 4A, the distribution is double peaked, with the high-transmission peak with average source photon number $\langle M_s\rangle|_{n_g=0}$ corresponding no gate photon, whereas the gray area of low transmission $\langle M_s\rangle|_{n_g\geq 1}$ corresponds to the blocking by one or more gate photons. The optical gain per stored gate photon can then be defined as the gate-photon–induced change in source transmission, $G = \langle M_s\rangle|_{n_g=0} - \langle M_s\rangle|_{n_g\geq 1}$, which is directly determined from the measured histogram. The measured gain as a function of the applied source photon number is shown in Fig. 4B, in which the gain saturation occurring around 1000 source photons is likely due to optical pumping of the atom into magnetic sublevels with weaker cavity coupling. One stored gate photon can block more than ~600 source photons, of which ~400 are available outside the cavity.

In order to operate the device with gate retrieval in which the stored photon is recovered in the original optical mode after switching the source light, the source integration time was reduced to 1 μs, which is less than the measured lifetime $\tau = (2.1 \pm 0.1)$ μs of the collective spin excitation. In this case, we can directly measure the cavity transmission probability conditioned on the detection of a gate photon, given by the gate-source cross-correlation function $g^{(2)}_{gs} = \langle n_g n_s\rangle/(\langle n_g\rangle\langle n_s\rangle)$ in the limit $\langle n_g\rangle, \langle n_s\rangle \ll 1$. On cavity resonance, we measured $g^{(2)}_{gs} = 0.29^{+0.09}_{-0.08}$ for 0.2 average retrieved gate photons and 0.1 average source photons transmitted. These average photon values were chosen so as to minimize the two-photon probability in each beam while ensuring that the signal-to-background ratio remains sufficiently high. If we subtract independently measured detector backgrounds (*29*), we find a corrected value of $g^{(2)}_{gs} = 0.17^{+0.08}_{-0.06}$. This substantial anticorrelation, arising from the effective interaction between two initially uncorrelated photons of different wavelengths, is in good agreement with the value $T = 0.09 \pm 0.01$ deduced from Fig. 3B and the value $T = 0.16 \pm 0.06$ expected from first principles.

Last, we determined the available gain G_r in retrieval mode by measuring the retrieval reduction as a function of source photon number and display the result in Fig. 4E. In the process, it is only the scattering of a source photon into free space that reveals the location of the excited atom, collapsing the collective state into a single-atom state and preventing the retrieval. This scattering is suppressed in the strong-coupling limit of cavity QED, and the observed dependence of retrieval on source photon number agrees well with the theoretical model. The physical gain of the device operated at $1/e$ retrieval reduction is $G_r = 2.2 \pm 0.2$, and the available gain outside the cavity is 1.4 ± 0.1 (lower owing to the 0.66 outcoupling efficiency). This demonstrates a gain exceeding unity in transistor operation in which the gate photon is preserved.

Our observations can be quantitatively understood in a simple cavity QED model: One atom in state $|s\rangle$ reduces the cavity transmission (*1*, *4*) by a factor of $T = (1+\eta)^{-2}$, where η is the single-atom cooperativity (*30*). In the strong-coupling regime of cavity QED, $\eta \gg 1$, already one stored gate photon can thus switch the source beam from transmission to reflection with high contrast. The cooperativity parameter η also governs the number of source photons that can be switched: The destruction probability for the collective excitation is given by the probability of scattering a photon into free space on the $|s\rangle \rightarrow |e\rangle$ transition. Such scattering probability is suppressed by cavity to $2\eta/(1+\eta)^2$ in the regime of continuous cavity excitation (*30*). For $\eta \gg 1$, high transistor

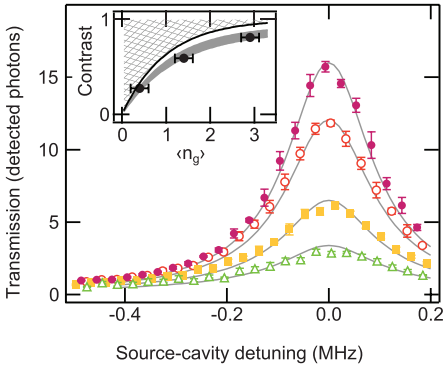

Fig. 2. Cavity transmission in the presence of stored gate photons. Average transmission spectra of a source beam applied for 24 μs for mean stored gate photon numbers $\langle n_g\rangle$ = 0, 0.4, 1.4, and 2.9 (top to bottom). The solid lines are theoretical curves (*29*). Error bars are SEM. (**Inset**) The relative transmission on cavity resonance (switching contrast) versus $\langle n_g\rangle$. The gray area indicates the theoretical prediction. The solid black line corresponds to the maximum average switching contrast that can be observed with coherent states of gate photons.

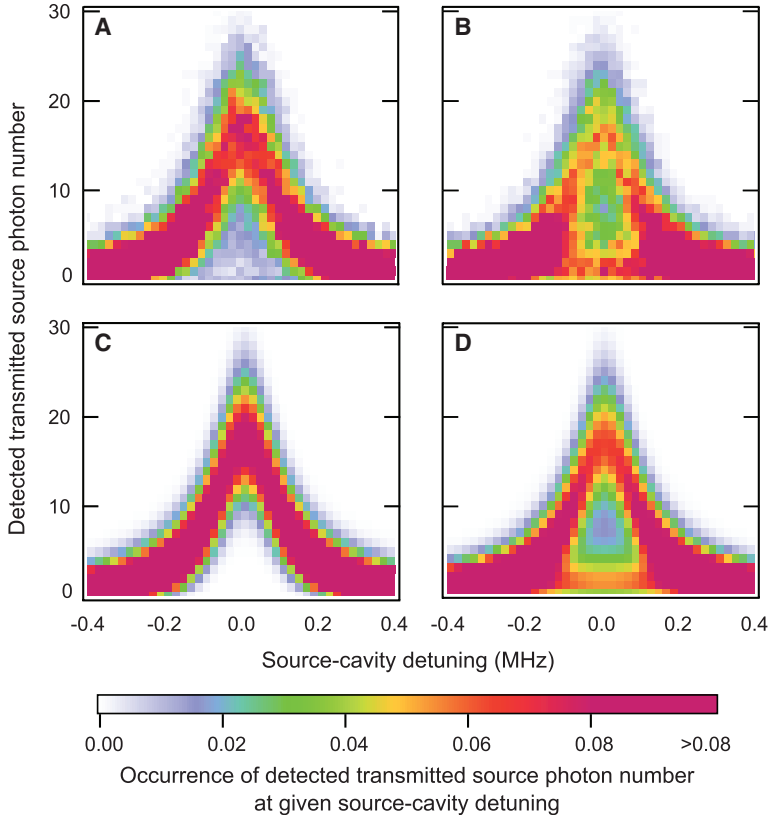

Fig. 3. Histogram of cavity transmission spectra. Cavity transmission (**A**) without and (**B**) with $\langle n_g\rangle$ = 0.5 gate photons. The horizontal axis indicates the detuning of the source beam from the cavity resonance, and the vertical axis indicates the number of detected transmitted source photons in a 24-μs detection window. The color indicates the occurrence rate of a particular detected transmitted source photon number for a given source-cavity detuning. The histogram displays a clear separation between the zero-gate-photon component $n_g = 0$ with high cavity transmission (17 detected source photons), and the component $n_g \geq 1$ ($n_g = 1$ with probability 0.8, $n_g > 1$ with 0.2) leading to cavity blocking (1.5 detected photons). (**C** and **D**) The corresponding theoretically expected histograms. The extinction factor 17/1.5 for one gate photon is $T^{-1} = 11 \pm 1$.

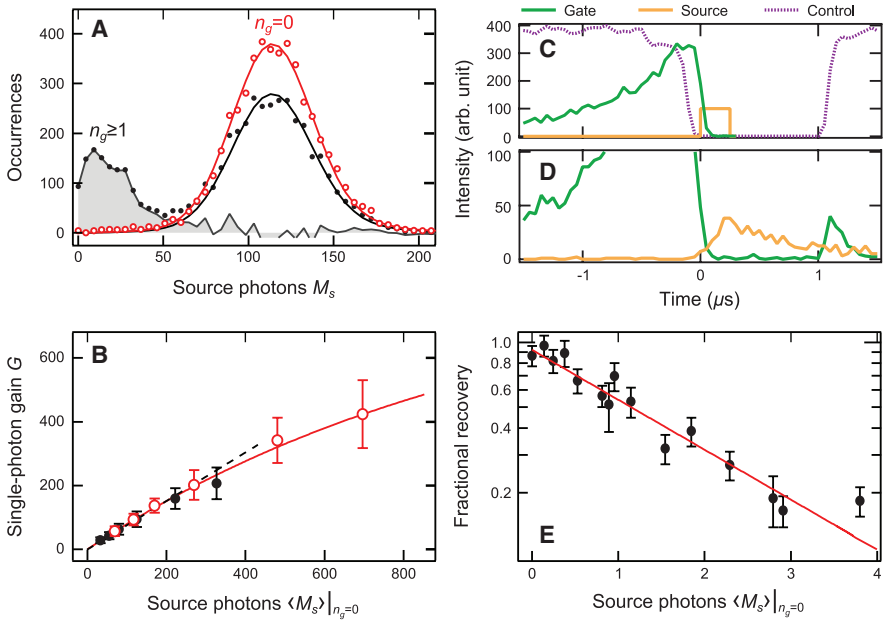

Fig. 4. Measurement of transistor gain. (**A**) Histogram of the integrated source photon number M_s in a 50-μs window. The graph shows M_s for no applied gate photon (n_g = 0, open red circles) with a Poissonian fit and for a coherent state with $\langle n_g \rangle$ = 0.4 stored gate photons (solid black circles). The gray area indicates the contribution from events with $n_g \geq 1$, with average value denoted by $\langle M_s \rangle|_{n_g \geq 1}$. (**B**) Transistor gain $G = \langle M_s \rangle|_{n_g} = 0 - \langle M_s \rangle|_{n_g \geq 1}$ as a function of source strength $\langle M_s \rangle|_{n_g} = 0$ for integration times of 25 μs (solid black circles) and 50 μs (open red circles), with a linear fit to the first nine data points (black dashed line) and with exponential fit for gain saturation (red line). (**C** and **D**) Timing sequence for retrieval operation with (C) input pulses and (D) output pulses. (The actual gate, control, and source beam waveforms are shown, but relative powers are not to scale.) First, the control beam is adiabatically ramped down at t = 0 in order to store a gate photon in the atomic medium. Then, a source pulse is sent onto the cavity, and its transmission is measured. Subsequently, the control beam is adiabatically ramped up in order to retrieve and detect the gate photon. The combined storage and retrieval efficiency in the absence of source light after a storage time of 1 μs is (3.0 ± 0.1)%. (**E**) Measurement of transistor gain in retrieval mode. The average fractional retrieval efficiency of the gate photon after 1 μs is plotted versus $\langle M_s \rangle|_{n_g} = 0$ with an exponential fit. The fitted source photon number resulting in e^{-1} reduction is M_{s0} = 1.9 ± 0.1 outside of the cavity (M_{s0} = 2.8 ± 0.2 before outcoupling losses, which is in good agreement with the theoretical value 2.8 ± 0.1).

gain can be achieved, and the gate photon can be still retrieved from the atomic ensemble afterward. Because the cavity-blocking mechanism does not rely on the collective nature of the atomic excitation, even when the latter is destroyed, the remaining atom in state $|s\rangle$ continues to switch the source beam, leading to high gain $G >> 1$ in the incoherent regime.

For the present system (*5*), the cooperativity for a two-level atom at an antinode is $\eta_0 = 8.6 \pm 0.4$. Averaging over polarization factors, the cavity standing wave, and the gate beam reduces the available cooperativity. The directly averaged cooperativity value is $\langle \eta \rangle = 2.8$, whereas the effective cooperativities for the transmission extinction and the attenuation photon number are $\eta_T = 1.5$ and $\eta_a = 3.3$, respectively (*29*). The theoretical model is in agreement with our measurements of the transmission reduction induced by one gate photon and with the measured dependence of gate-photon retrieval efficiency on source photon number, as displayed in Fig. 4E. The theoretical model, after including optical pumping into other magnetic sublevels (*29*), also reproduces the measured cavity transmission histogram, as shown in Fig. 3D.

Our system constitutes a testbed in which we have explored the physical principles relevant to an all-optical transistor based on cavity QED with an atomic ensemble. Before it can be used as a practical device, it will be necessary to improve the input and output coupling efficiencies for the gate and source photons, which limit the usable gain in the system. The combined storage and retrieval efficiency of 3% for the gate photon is limited primarily by the optical density. The latter could be improved by using a deeper trap, in combination with further cooling of the atomic ensemble, which would also increase the gate-photon storage time that is currently limited by Doppler broadening. The cavity outcoupling efficiency for the source photons of 0.66 could be improved to 0.97 by using state-of-the-art mirrors (*1*, *2*, *4*).

The present work opens up new perspectives for all-optical information processing with strong deterministic interactions between initially uncorrelated, distinguishable photons. The gain $G_r > 1$ in operation with gate photon retrieval may enable not only hitherto unexplored all-optical quantum circuits with feedback and gain, but also the nondestructive detection of the gate photon—a feat that has so far only been accomplished for microwave photons confined in a cavity (*31*). The correlations between one gate and multiple source photons produced by the effective photon-photon interaction can be used to create two-mode entangled states of many photons. Last, cavities with larger cooperativity (*1*–*4*) may enable high-fidelity deterministic photonic quantum gates.

References and Notes

1. K. M. Birnbaum *et al.*, *Nature* **436**, 87–90 (2005).
2. F. Brennecke *et al.*, *Nature* **450**, 268–271 (2007).
3. Y. Colombe *et al.*, *Nature* **450**, 272–276 (2007).
4. A. Kubanek *et al.*, *Phys. Rev. Lett.* **101**, 203602 (2008).
5. H. Tanji-Suzuki, W. Chen, R. Landig, J. Simon, V. Vuletić, *Science* **333**, 1266 (2011).
6. D. W. Brooks *et al.*, *Nature* **488**, 476–480 (2012).
7. P. Michler *et al.*, *Science* **290**, 2282–2285 (2000).
8. D. Press *et al.*, *Phys. Rev. Lett.* **98**, 117402 (2007).
9. I. Fushman *et al.*, *Science* **320**, 769–772 (2008).
10. T. Volz *et al.*, *Nat. Photonics* **6**, 605–609 (2012).
11. R. Bose, D. Sridharan, H. Kim, G. S. Solomon, E. Waks, *Phys. Rev. Lett.* **108**, 227402 (2012).
12. Y. O. Dudin, A. Kuzmich, *Science* **336**, 887–889 (2012).
13. T. Peyronel *et al.*, *Nature* **488**, 57–60 (2012).
14. J. Hwang *et al.*, *Nature* **460**, 76–80 (2009).
15. M. Bajcsy *et al.*, *Phys. Rev. Lett.* **102**, 203902 (2009).
16. H.-Y. Lo *et al.*, *Phys. Rev. A* **83**, 041804(R) (2011).
17. H. Schmidt, A. Imamogdlu, *Opt. Lett.* **21**, 1936–1938 (1996).
18. A. Imamoğlu, H. Schmidt, G. Woods, M. Deutsch, *Phys. Rev. Lett.* **79**, 1467–1470 (1997).
19. S. Harris, Y. Yamamoto, *Phys. Rev. Lett.* **81**, 3611–3614 (1998).
20. M. Fleischhauer, M. D. Lukin, *Phys. Rev. Lett.* **84**, 5094–5097 (2000).
21. M. Fleischhauer, A. Imamoglu, J. P. Marangos, *Rev. Mod. Phys.* **77**, 633–673 (2005).
22. B. Dayan *et al.*, *Science* **319**, 1062–1065 (2008).
23. Q. A. Turchette, C. J. Hood, W. Lange, H. Mabuchi, H. J. Kimble, *Phys. Rev. Lett.* **75**, 4710–4713 (1995).
24. R. J. Thompson, G. Rempe, H. J. Kimble, *Phys. Rev. Lett.* **68**, 1132–1135 (1992).
25. D. E. Chang, A. S. Sørensen, E. A. Demler, M. D. Lukin, *Nat. Phys.* **3**, 807–812 (2007).
26. C. Liu, Z. Dutton, C. H. Behroozi, L. V. Hau, *Nature* **409**, 490–493 (2001).
27. D. F. Phillips, A. Fleischhauer, A. Mair, R. L. Walsworth, M. D. Lukin, *Phys. Rev. Lett.* **86**, 783–786 (2001).
28. A. V. Gorshkov, A. André, M. Fleischhauer, A. S. Sørensen, M. D. Lukin, *Phys. Rev. Lett.* **98**, 123601 (2007).
29. Materials and methods are available as supplementary materials on *Science* Online.
30. H. Tanji-Suzuki *et al.*, *Adv. At. Mol. Opt.* **60**, 201–237 (2011).
31. C. Guerlin *et al.*, *Nature* **448**, 889–893 (2007).

Acknowledgments: This work was supported by NSF and the Air Force Office of Scientific Research. K.M.B. gratefully acknowledges support from NSF through the Graduate Research Fellowship (0645960). R.B. gratefully acknowledges support from the Fonds zur Förderung der wissenschaftlichen Forschung through the doctoral program CoQuS (W1210).

Supplementary Materials

www.sciencemag.org/cgi/content/full/science.1238169/DC1
Materials and Methods
Supplementary Text
Fig. S1
Table S1
References and Notes

22 March 2013; accepted 24 June 2013
Published online 4 July 2013;
10.1126/science.1238169

Control of Metal Nanocrystal Size Reveals Metal-Support Interface Role for Ceria Catalysts

Matteo Cargnello,[1,2] Vicky V. T. Doan-Nguyen,[2] Thomas R. Gordon,[3] Rosa E. Diaz,[4] Eric A. Stach,[4] Raymond J. Gorte,[5] Paolo Fornasiero,[1]* Christopher B. Murray[2,3]*

Interactions between ceria (CeO_2) and supported metals greatly enhance rates for a number of important reactions. However, direct relationships between structure and function in these catalysts have been difficult to extract because the samples studied either were heterogeneous or were model systems dissimilar to working catalysts. We report rate measurements on samples in which the length of the ceria-metal interface was tailored by the use of monodisperse nickel, palladium, and platinum nanocrystals. We found that carbon monoxide oxidation in ceria-based catalysts is greatly enhanced at the ceria-metal interface sites for a range of group VIII metal catalysts, clarifying the pivotal role played by the support.

The properties of heterogeneous catalysts are often determined by the synergy between support (typically metal oxides) and supported phases (typically metal nanoparticles). Ceria (CeO_2) is an example of an "active support" that can greatly increase rates for reactions involving redox steps, such as CO oxidation and the water-gas shift (WGS) reaction (*1*, *2*), by comparison to "inert," nonreducible supports such as alumina (*3*, *4*). The observed enhancement is assumed to result from active sites at the metal-ceria interface, because rates can be much greater than the sum of the rates over ceria and the metal individually (*1*). Evidence that the oxygen atoms migrate from the support to the metal particles has come only from model systems (*5*, *6*) not operating under industrially relevant reaction conditions. Understanding size-activity relations for ceria-based catalysts is important for improving catalyst performance. The turnover rate for CO oxidation is thought to be independent of metal particle size (*7*, *8*), so this reaction is an ideal probe for studying the role that the metal-support interface plays by measuring changes in rates upon varying the concentration of interfacial sites. Chemical methods for preparing metal nanoparticles on high-surface-area supports typically lead to large or asymmetric metal particle size distributions, which prevent definitive correlation between particle size and activity (for example, subsets of particles could be completely inactive or disproportionately more active). Monodisperse metal particles tested under realistic reaction conditions are critical for understanding the relation between catalytic activity and specific particle size (*9*, *10*).

Here, we used monodisperse, size-tunable metal nanocrystals (NCs) of Ni, Pd, and Pt to demonstrate the role of the metal-support interface in ceria-based systems. The relative fraction of interfacial sites was varied for both ceria and alumina supports, and the role of ceria in enhancing CO oxidation rates under realistic conditions was revealed (scheme S1) (*11*).

We prepared monodisperse Ni, Pd, and Pt NCs by thermally decomposing metal(II) acetylacetonates in a benzyl ether solution in the presence of oleylamine (OLAM), trioctylphosphine (TOP), and, in some samples, oleic acid (OLAC) (table S1) (*11*). By varying the surfactant concentration and reaction temperature, various NC sizes for each metal (small, medium, and large) were obtained. Figure S1 shows transmission electron microscopy (TEM) images of Ni (4 to 12 nm), Pd (2.5 to 6.3 nm), and Pt NCs (1.6 to 2.9 nm) that were quantitatively obtained with particle size distributions below 6%, without any post-synthetic size-selective precipitation processes. The uniformity in size of the NCs was confirmed by small-angle x-ray scattering (fig. S2) (*11*) and by the fact that they formed large areas of three-dimensional (3D) hexagonal close-packed superlattices with single domains exceeding several micrometers (*12*, *13*) (Fig. 1). High-resolution TEM (HRTEM) studies (Fig. 1, G to I) provided evidence of the overall crystallinity of the samples, although x-ray diffraction patterns showed that the presence of defects (visible in, e.g., Fig. 1G) broadened the diffraction peaks (fig. S2) (*11*), in agreement with previous studies (*14*).

The monodisperse Ni, Pd, and Pt NCs were adsorbed from toluene solutions onto both alumina and ceria supports, and heating the materials in air at 300°C completely removed the organic capping agents. Low metal loadings (0.5 weight percent) and high-surface-area supports (~100 $m^2\ g^{-1}$ for alumina and ~60 $m^2\ g^{-1}$ for ceria) mimicked real catalyst formulations and ensured that the NCs were well separated and resistant to particle sintering. We examined these samples by means of TEM and CO chemisorption. Because the high electron density of ceria makes the determination of size distributions by TEM particularly difficult (especially in the case of Ni and Pd) (*15*), the particle sizes and distributions were initially determined by analyzing the alumina-based systems (fig. S3). We confirmed that particle sizes and distributions obtained on the alumina samples were also representative of the ceria-based counterparts through TEM analysis of the Pt/CeO_2 samples (fig. S3, L to N). Strong Z-contrast between Pt and ceria in high-angle annular dark-field scanning TEM (HAADF-STEM) images let us confirm that the particle size and shape did not change upon deposition and calcinations of the particles on this support. The Z-contrast for the Ni/CeO_2 and Pd/CeO_2 samples was less strong, and thus we also used electron energy loss spectroscopy (EELS) to map the individual Ni and Pd NCs (fig. S4) (*11*) to measure size distributions. For Pd and Pt catalysts, there was little change in the NC sizes after deposition and calcination (fig. S5) (*11*). For Ni, we observed the formation of hollow spheres, likely caused by the Kirkendall effect (fig. S3, A to C) (*11*, *16*). Nonetheless, even in this case, the very narrow size dispersion was maintained and there was no Ni metal loss during this process (fig. S5) (*11*). Furthermore, it is apparent from the particle size distribution measurements [histograms in fig. S5 (*11*)] that the particles

[1]Department of Chemical and Pharmaceutical Sciences, ICCOM-CNR, Consortium INSTM, University of Trieste, 34127 Trieste, Italy. [2]Department of Materials Science and Engineering, University of Pennsylvania, Philadelphia, PA 19104, USA. [3]Department of Chemistry, University of Pennsylvania, Philadelphia, PA 19104, USA. [4]Center for Functional Nanomaterials, Brookhaven National Laboratory, Upton, NY 11973, USA. [5]Department of Chemical and Biomolecular Engineering, University of Pennsylvania, Philadelphia, PA 19104, USA.

*Corresponding author. E-mail: pfornasiero@units.it (P.F.); cbmurray@sas.upenn.edu (C.B.M.)

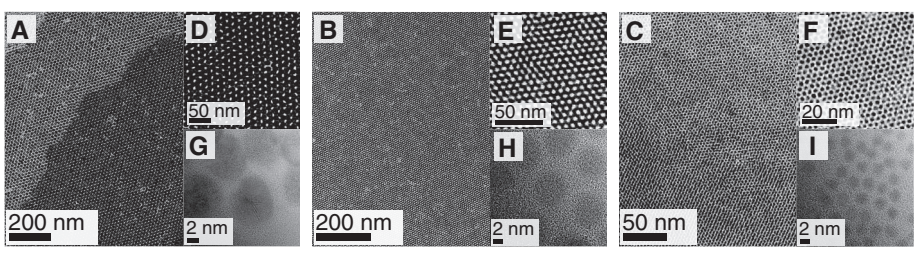

Fig. 1. As-prepared nanocrystals. (**A** to **C**) TEM images of hexagonal close-packed 3D assemblies of (A) Ni NCs, (B) Pd NCs, and (C) Pt NCs. (**D** to **F**) Magnified images. (**G** to **I**) High-resolution TEM images showing distinct NCs.

supported on ceria had a slightly wider size distribution: The distributions for the small, medium, and large sizes were completely separated for the Pt/Al_2O_3, whereas there was a slight overlap in the distributions for the Pt/CeO_2. There was no overlap in the particle size distributions for the Pd and Ni samples. We also conducted environmental TEM (ETEM) experiments by heating the samples in situ in air to 300°C under conditions otherwise similar to the calcination process (fig. S6) (*11*). The images show restructuring at the metal-ceria interface with the particles adhering to the ceria surface, but this neither changes the overall particle size nor the particle shape used for the calculation of the fraction of particular sites (see below). We also took into account the slight variability of the metal-ceria interface in our calculations by performing careful HRTEM studies (fig. S7) (*11*). The CO chemisorption experiments provided information on the total population of accessible metal sites (table S2) (*11*) and confirmed that the trends in metal particle size are retained after deposition and calcination. All of the above data confirm that particle sizes and distributions are maintained in the final catalysts (Fig. 2). HRTEM analysis indicates that the larger particles maintained their original cuboctahedral morphology, and suggests that smaller particles spread over both supports into shapes that resemble a cubo-octahedron truncated along the {100} direction.

The data obtained by conventional and aberration-corrected TEM and by CO chemisorption were used to prepare a physical model of the particles. In the case of Pd, the modeled particles are shown in Fig. 2D. The models were used to quantify the number of atoms with particular coordination environments, such as corner and perimeter sites at the interface with CeO_2 and surface atoms that are not in direct contact with the support. Previous reports made use of the entire size distribution to develop a physical model of the particles (*17*, *18*), but in our case, extremely narrow distribution of NC sizes and shapes allowed the use of average values.

The different particle sizes and shapes differ in terms of length of the metal-support interface, so we could directly analyze the impact of this parameter for CO oxidation. For the catalytic tests, the metallic phase of the NCs was ensured by a mild prereduction (fig. S8) (*11*), and TEM characterization of the catalysts after reaction did not show any change in size or shape of the particles. To ensure that neither mass nor thermal diffusion limitations affected the results, we used high space velocities and diluted each catalyst with inert support materials (*8*, *11*, *19*) (fig. S9). Reaction orders for CO and O_2 were measured on the series of small Pt samples that gave the highest volumetric CO oxidation rates (fig. S10) (*11*). On the alumina-supported Pt, in excess CO, the reaction orders were ~ –1 in CO and ~1 in O_2, in agreement with the previous values (*3*); hence, O_2 activation is inhibited by adsorbed CO on the

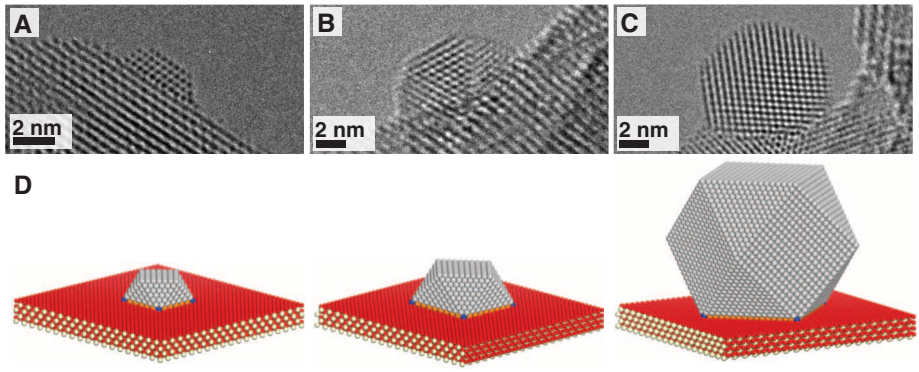

Fig. 2. Heat-treated nanocrystals. (**A** to **C**) HRTEM images of Pd/CeO_2 catalysts after calcination at 300°C and reduction at 150°C: small (A), medium (B), and large (C) samples. (**D**) Physical models prepared to describe the particles. Blue, orange, and gray colors indicate corner, perimeter, and surface atoms, respectively; red and white are oxygen and cerium atoms of the ceria support.

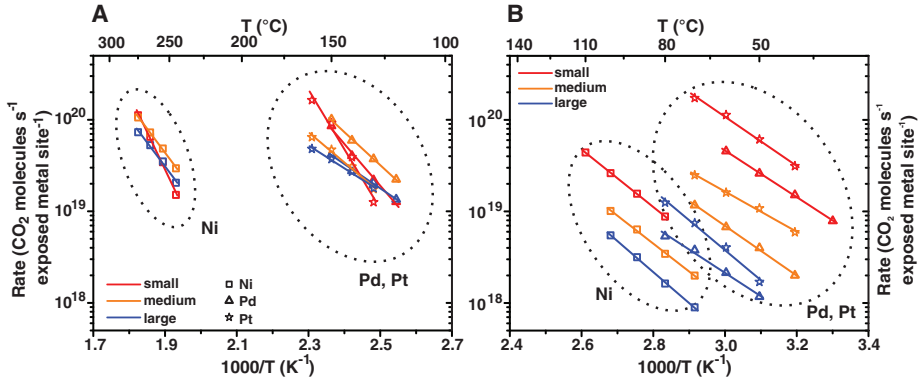

Fig. 3. Kinetic data. (**A** and **B**) Arrhenius-type plots for CO oxidation over (A) Al_2O_3 and (B) CeO_2 samples, where a difference in the 1000/T scale should be noted.

metal particle surface (*8*). In the case of the ceria sample, the reaction orders were ~0 in CO and slightly positive in O_2, implying that a second reaction mechanism must be active (*20*). The results of CO oxidation on ceria- and alumina-supported metals under lean conditions (excess oxygen; see supplementary materials) are reported as kinetic plots in Fig. 3 and light-off curves in fig. S11 (*11*).

The metals deposited on ceria had higher catalytic rates than their alumina-supported counterparts, as evidenced by the much lower temperatures needed to completely oxidize CO (fig. S11) (*11*). The apparent activation energies (E_a) for the ceria-based catalysts (fig. S12) (*11*) were in the range of 40 to 70 kJ mol^{-1}. Alumina-supported samples showed higher apparent E_a values of 50 to 150 kJ mol^{-1}. These values are in agreement with results from other studies (*3*). Notably, we found similar activation energies for all ceria-supported catalysts, implying that a similar mechanism must be operative regardless of the metal.

The alumina-based catalysts exhibited rates that were independent of metal particle size when normalized to the metal surface area (Fig. 3A), as determined by CO chemisorption (*8*). However, the ceria-based catalysts displayed a strong size-dependent activity, with normalized reaction rates decreasing with increasing NCs size for all three metals studied (Fig. 3B) (*11*). The alumina-supported NCs were essentially saturated by CO, which likely limited any effects of these intrinsically different sites on the alumina-supported metals. By contrast, the zero-order rate in CO observed for ceria-based catalysts is a result of reaction between CO adsorbed on the metal and O_2 provided by the ceria, so that the CO on the metal is unable to suppress the rate of O_2 adsorption onto ceria (*21*, *22*). Despite the large number of elegant theoretical and experimental studies of oxygen spillover from ceria to Pt on model single crystals under low pressures (*6*), no reports have overcome the so-called "material and pressure gap" (*23*, *24*) by experimentally demonstrating—under realistic working conditions—the involvement of ceria lattice oxygen in the oxidation of CO, and thus addressing the role of the metal-ceria interface.

HRTEM allows us to build a model of the shape of the supported NCs as they form faceted solids on the support interface. To determine whether the important variable that is altered by particle size is the surface-to-volume ratio or

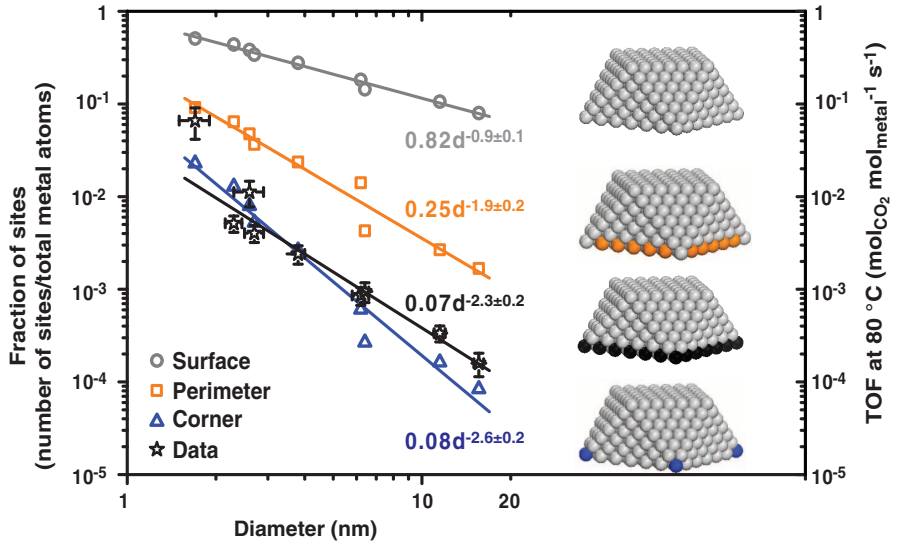

Fig. 4. Model analysis. Calculated number of sites with a particular geometry (surface and perimeter or corner atoms in contact with the support) as a function of diameter and TOF at 80°C of the nine ceria-based samples.

the perimeter-to-surface ratio in the metal NCs, we used the model described above to calculate the fraction of atoms located at the various surface sites (surface atoms not in contact with ceria, and perimeter or corner atoms at the metal-support interface; see Fig. 2D) (*17*, *18*, *25*, *26*). We analyzed the scaling relation in this framework with the use of the particle shapes obtained by HRTEM (Fig. 2). For any regular solid other than a sphere, the number of surface sites per volume is proportional to the diameter (d) as $\sim d^{-1}$, that of the edge sites to $\sim d^{-2}$, and that of the vertices to $\sim d^{-3}$. For this reason, the model was robust, in that the relations did not drastically change when particles of slightly different geometries were used. We then plotted in the same graph the fraction of sites with a particular position as a function of particle size for all nine ceria-based samples (Fig. 4). The slight scatter in the graph arose because we compared metals with dissimilar lattice constants and slightly different shapes. These results showed a scaling of $d^{-0.9 \pm 0.1}$ for the surface atoms, and of $d^{-1.9 \pm 0.2}$ and $d^{-2.6 \pm 0.1}$ for perimeter and corner atoms in direct contact with the support, respectively. We then collected the turnover frequency (TOF) values of the CeO_2-based catalysts at 80°C (a convenient temperature to test all the catalysts under kinetic conditions) and plotted the data on the same graph. The TOFs for all nine samples showed a dependence of the diameter as $d^{-2.3 \pm 0.2}$, implying that the metal atoms at the nexus of the metal, support, and atmosphere were the active sites for this reaction and that the larger surface-to-volume ratio of small particles translates to an increased boundary length and higher activity. The value of the slope implies that the corner atoms were the most active sites overall, most likely because of their lower coordination number compared to the other perimeter atoms, as observed in other systems (*17*, *18*). The slight deviation from the expected trend for the small and medium Pt samples might be an effect from some very small particles that were detected by high-resolution STEM (fig. S3) (*11*) that contributed more to the observed reactivity. Nonetheless, we conclude that the perimeter atoms were the active sites for CO oxidation on ceria-based catalysts. It may be fortuitous, but the TOF for our Pt small sample ($\sim$0.2 s^{-1} at 80°C) is similar to that reported for single-site Pt/FeO_x catalysts (0.3 s^{-1} at the same temperature) (*27*). Despite the different nature of the systems, this further corroborates the validity of our approach.

The trend in catalytic activity (size dependence) was not influenced by the reaction environment. Similar results were obtained from stoichiometric, lean (excess of oxygen), or rich (excess of CO) conditions (figs. S13 and S14) (*11*). The apparent activation energies are in the range of 40 to 70 kJ mol^{-1} for all the samples and conditions (fig. S15) (*11*). This experiment conclusively shows that CO oxidation by group VIII metals deposited on CeO_2 is size-dependent, with a direct participation in the reaction of metal atoms at the perimeter and ceria surface oxygen, and that Ni in contact with ceria exhibits rates similar to those of Pd or Pt. Our results demonstrate a robust method to explore the role of interfacial sites in catalysis, and demonstrate that the use of size-selected nanoparticles can successfully identify catalytically active sites.

References and Notes

1. T. Bunluesin, R. J. Gorte, G. W. Graham, *Appl. Catal. B* **15**, 107–114 (1998).
2. Q. Fu, H. Saltsburg, M. Flytzani-Stephanopoulos, *Science* **301**, 935–938 (2003).
3. T. Bunluesin, E. S. Putna, R. J. Gorte, *Catal. Lett.* **41**, 1–5 (1996).
4. A. Trovarelli, *Catal. Rev. Sci. Eng.* **38**, 439–520 (1996).
5. G. S. Zafiris, R. J. Gorte, *J. Catal.* **139**, 561–567 (1993).
6. G. N. Vayssilov *et al.*, *Nat. Mater.* **10**, 310–315 (2011).
7. H. J. Freund, G. Meijer, M. Scheffler, R. Schlögl, M. Wolf, *Angew. Chem. Int. Ed.* **50**, 10064–10094 (2011).
8. A. D. Allian *et al.*, *J. Am. Chem. Soc.* **133**, 4498–4517 (2011).
9. M. Che, C. O. Bennett, *Adv. Catal.* **36**, 55–172 (1989).
10. A. A. Herzing, C. J. Kiely, A. F. Carley, P. Landon, G. J. Hutchings, *Science* **321**, 1331–1335 (2008).
11. See supplementary materials on *Science* Online.
12. S. Sun, C. B. Murray, D. Weller, L. Folks, A. Moser, *Science* **287**, 1989–1992 (2000).
13. A. Dong, J. Chen, P. M. Vora, J. M. Kikkawa, C. B. Murray, *Nature* **466**, 474–477 (2010).
14. S. W. Kim *et al.*, *Nano Lett.* **3**, 1289–1291 (2003).
15. J. C. González *et al.*, *Angew. Chem. Int. Ed.* **48**, 5313–5315 (2009).
16. Y. Yin *et al.*, *Science* **304**, 711–714 (2004).
17. M. Shekhar *et al.*, *J. Am. Chem. Soc.* **134**, 4700–4708 (2012).
18. W. D. Williams *et al.*, *J. Am. Chem. Soc.* **132**, 14018–14020 (2010).
19. R. M. Koros, E. J. Nowak, *Chem. Eng. Sci.* **22**, 470 (1967).
20. G. S. Zafiris, R. J. Gorte, *J. Catal.* **143**, 86–91 (1993).
21. S. H. Oh, C. C. Eickel, *J. Catal.* **112**, 543–555 (1988).
22. T. Bunluesin, H. Cordatos, R. J. Gorte, *J. Catal.* **157**, 222–226 (1995).
23. H. Oosterbeek, *Phys. Chem. Chem. Phys.* **9**, 3570–3576 (2007).
24. G. A. Somorjai, R. L. York, D. Butcher, J. Y. Park, *Phys. Chem. Chem. Phys.* **9**, 3500–3513 (2007).
25. A. Carlsson, A. Puig-Molina, T. V. W. Janssens, *J. Phys. Chem. B* **110**, 5286–5293 (2006).
26. T. Janssens *et al.*, *Top. Catal.* **44**, 15–26 (2007).
27. B. Qiao *et al.*, *Nat. Chem.* **3**, 634–641 (2011).

Acknowledgments: We thank M. Graziani, T. Montini (University of Trieste), B. Diroll, and K. Bakhmutsky (University of Pennsylvania) for discussions and help. Supported by University of Trieste through FRA project and COST Action CM1104 (M.C. and P.F.); the U.S. Department of Energy's Advanced Research Projects Agency, Energy (ARPA-E) grant DE-AR0000123 (V.V.T.D.-N.); NSF through the Nano/Bio Interface Center at the University of Pennsylvania, grant DMR08-32802 (T.R.G.); Air Force Office of Scientific Research Multidisciplinary University Initiative grant FA9550-08-1-0309 (R.J.G.); and a Richard Perry University Professorship (C.B.M.). Aberration-corrected EM (R.E.D. and E.A.S.) was carried out at the Center for Functional Nanomaterials, Brookhaven National Laboratory, which is supported by the U.S. Department of Energy, Office of Basic Energy Sciences, under contract DE-AC02-98CH10886. M.C. conceived the idea for the study. M.C. and V.V.T.D.-N. synthesized the metal NCs. M.C. prepared the catalysts and collected the catalytic data. R.E.D. performed TEM, STEM, and ETEM characterization with help from V.V.T.D.-N. and T.R.G. E.A.S. coordinated all TEM studies. T.R.G. prepared the physical model of the NCs. R.J.G., P.F., and C.B.M. supervised the project. M.C. wrote the draft and all authors commented on the data and the manuscript.

Supplementary Materials

www.sciencemag.org/cgi/content/full/science.1240148/DC1
Materials and Methods
Scheme S1
Figs. S1 to S15
Tables S1 and S2

6 May 2013; accepted 24 June 2013
Published online 18 July 2013;
10.1126/science.1240148

Incision into the Eastern Andean Plateau During Pliocene Cooling

Richard O. Lease*† and Todd A. Ehlers

Canyon incision into mountain topography is commonly used as a proxy for surface uplift driven by tectonic or geodynamic processes, but climatic changes can also instigate incision. The ~1250-kilometer (km)–long eastern margin of the Andean Plateau hosts a series of 1.5- to 2.5-km-deep canyons that cross major deformation zones. Using (U-Th)/He thermochronology, we document a transition from Miocene faulting to Pliocene canyon incision across the northeastern plateau margin. Regionally, widespread Pliocene incision into the eastern plateau margin is concurrent with a shift in global climate from early Pliocene warmth to late Pliocene cooling. Enhanced moisture transport onto the Andean Plateau driven by sea surface temperature changes during cooling is the likely pacemaker for canyon incision.

Defining the role of tectonic and climate processes in shaping mountain topography is often limited by an inability to discern among different exhumation mechanisms. Deep canyons have been carved into high-elevation, low-relief terrain along both flanks of the Andean Plateau (Fig. 1). Reconstructing the space-time pattern of incision across the plateau can illuminate the ultimate causes for incision. On the western plateau margin, the onset of canyon incision ~9 million years ago (Ma) (*1*, *2*) has been interpreted as a consequence of plateau-wide surface uplift driven by geodynamic processes (*3*), although this view has been challenged (*4*). A close look at the eastern plateau margin suggests that headward canyon incision into high-elevation terrain accelerated in the past few million years (My) (*5*, *6*).

The humid northeastern plateau margin is a well-constrained tectonic and geomorphic boundary where the timing of incision is unknown. The physiography and geology of the northeastern plateau margin reveals large magnitudes of both river incision and faulting in southern Peru (Fig. 2). In this area, deformation is concentrated along the Eastern Cordillera reverse fault zone (Fig. 2A), which thrusts Paleozoic over Triassic sediments with 5 to 7 km of vertical offset (*7*, *8*) (fig. S1). In addition, several canyons dissect the plateau margin in this region, incising into the low-relief plateau surface presently at elevations of >4 km (Fig. 2, B and C). Minimal net glacial erosion of the plateau is suggested by the preservation of 6 Ma volcanics (*9*) beneath the Quelccaya ice cap (*10*) and the lack of a systematic correlation between topography and glacier equilibrium line altitudes (*11*) (Fig. 2D). Locally, the Eastern Cordillera reverse fault is exposed at the midpoint of the 2.5-km-deep Rio San Gaban canyon (Fig. 2D).

We examined the cooling history of the upper crust in the Rio San Gaban canyon to determine when erosion accelerated in response to faulting versus incision. We used (U-Th)/He thermochronology for the minerals apatite (AHe) and zircon (ZHe), with effective closure temperatures (T_c) of ~60°C and ~180°C, respectively (*12*). We collected a single suite of samples within a dual reference frame: (i) on either side of a major crustal fault and (ii) within an incised canyon (Fig. 2D). Of 11 samples collected, 7 (5) yielded apatite (zircon) suitable for dating, primarily from Triassic and Jurassic plutons (tables S1 to S3). Our three lowest-elevation sample sites had been previously analyzed for biotite K/Ar thermochronology (BAr) (*13*), with a T_c of ~350°C (*12*).

ZHe ages exhibit a sharp discontinuity across the fault that reveals differential Miocene erosion (Fig. 3A). On the hanging-wall, samples from a 1560- to 2060-m range of elevations have identical 15 Ma ZHe cooling ages. This consistency suggests that rapid thrust-induced rock uplift and erosion of the hanging-wall was ongoing by middle Miocene time, with 4 to 6.4 km of exhumation since then (assuming a geothermal gradient range of 25° to 40°C/km). In contrast, samples on the footwall have a wider 76- to 94-Ma range of ZHe ages that define a period of older, slower cooling. Overall, this pattern indicates that rapid Miocene erosion was limited to the hanging-wall, with fault-related deformation imposing a fundamental control.

Pronounced differential erosion across the fault is also evident with higher temperature chronometers. On the hanging-wall, BAr ages (*13*) increase linearly from 87 to 125 Ma with increasing elevation and indicate slow cooling within a partial retention zone (Fig. 3A). These late Cretaceous BAr ages (T_c = 350°C) on the hanging-wall are now juxtaposed against a wide range of late Cretaceous ZHe ages (T_c = 180°C) on the footwall. Thermal histories derived from inverse modeling of thermochronometer ages (*14*) corroborate disparate late Cretaceous-Miocene cooling for hanging-wall versus footwall samples (Fig. 3C). The ~150°C difference in cooling/erosion magnitude across the fault demonstrates large reverse fault displacement that initiated at or before ~20 Ma.

In contrast to discontinuous ZHe and BAr ages, AHe ages are identical on either side of the fault and suggest that Pliocene erosion was independent of deformation patterns (Fig. 3, A and B). Samples from a wide 1700-m range of elevation within an incised canyon have a narrow 4.1- to 2.8-Ma range of AHe ages, reflecting rapid, synchronous erosion of both hanging-wall and footwall blocks by this time. Modeled thermal histories of individual sam-

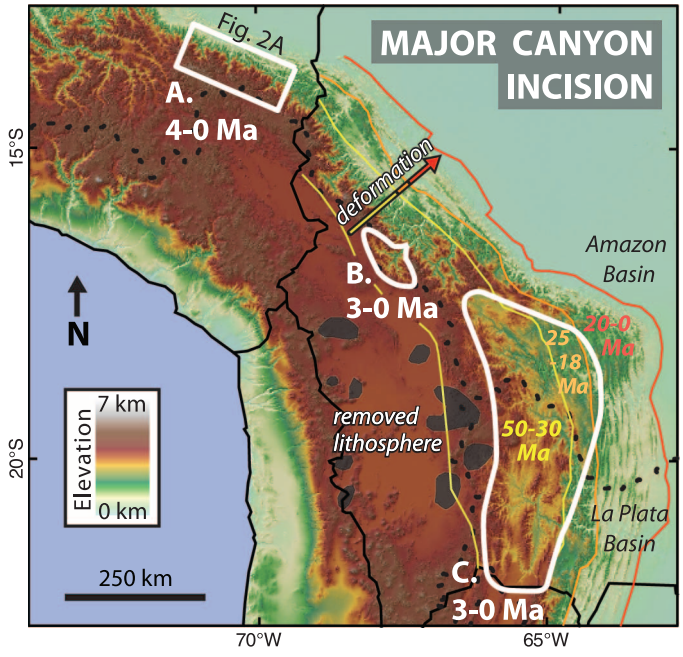

Fig. 1. Pliocene canyon incision into the eastern margin of the Andean Plateau. Study areas for (**A**) Rio San Gaban, (**B**) Rio La Paz (*6*, *16*), and (**C**) San Juan del Oro (*5*). Eastern Andes deformation fronts and timing are denoted by colored lines: yellow, Eastern Cordillera; orange, Interandean; red, Subandean (*16*–*18*). Removed mantle lithosphere is denoted by black polygons (*19*). Amazon and La Plata watersheds are outlined with black dashed line.

Department of Geosciences, University of Tübingen, Tübingen 72074, Germany.

*Present address: U.S. Geological Survey, Anchorage, AK 99508, USA.

†Corresponding author. E-mail: rlease@usgs.gov

ples corroborate this finding of rapid Pliocene erosion (Fig. 3C), and we estimate at least 1 to 1.6 km of exhumation for each sample (geothermal gradient range of 25° to 40°C/km). The low-relief plateau surface capping the canyon, on the other hand, displays only minor Pliocene exhumation: One footwall sample exhibits scattered single-grain ages suggestive of slow Miocene-Pliocene cooling, which is consistent with minimal erosion of the 6 Ma volcanic deposits upstream. Beneath the low-relief plateau surface, 4- to 3-Ma cooling ages present at incision depths of 1.9 to 2.4 km in the canyon suggest that rapid incision of the modern canyon began in Pliocene time without displacement on the fault (Fig. 3B). Although AHe ages do not correlate with distance along the transect, we estimate a vertical incision rate of 0.6 km/My and a headward incision rate ≥ 9 km/My since 4 Ma, which are comparable to rates estimated for the northwestern margin of the Andean Plateau (*15*). We interpret Pliocene erosion to reflect a fundamental shift, when rivers began incising rapidly into the northeastern plateau margin and across an inactive major fault (fig. S2).

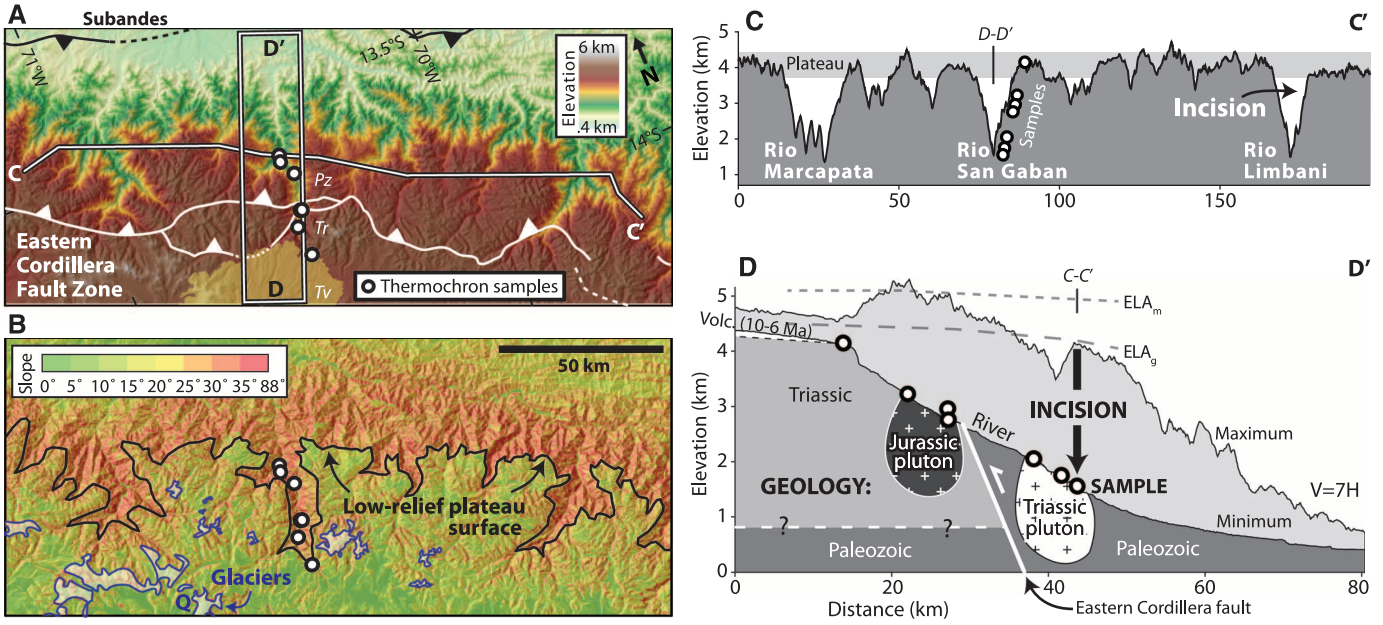

Fig. 2. Tectonic and geomorphic setting of canyons on the northeastern Andean Plateau margin. (**A**) Tectonic context: topography and major geology. Tertiary deformation was concentrated along the Eastern Cordillera reverse fault zone (5 to 7 km of vertical offset) (*7*). Tv, Tertiary volcanics (*9*); Tr, Triassic Mitu Group; Pz, Paleozoic sedimentary rocks. (**B**) Geomorphic context: Slope map showing extent of low-relief plateau surface, modern glaciers, and high-relief plateau margin. Threshold hillslopes adjacent to incised canyons erode primarily by landsliding. Q, Quelccaya ice cap (*10*). (**C**) Topographic profile C-C′ (parallel to plateau margin) showing 2.5-km-deep canyons incised into low-relief plateau surface at elevations >4 km. Sample locations projected onto profile. (**D**) Swath topographic profile D-D′ (perpendicular to plateau margin) showing structural and geomorphic context of thermochronology sampling transect. ELA, glacier equilibrium line altitude: m, modern; g, glacial (*11*).

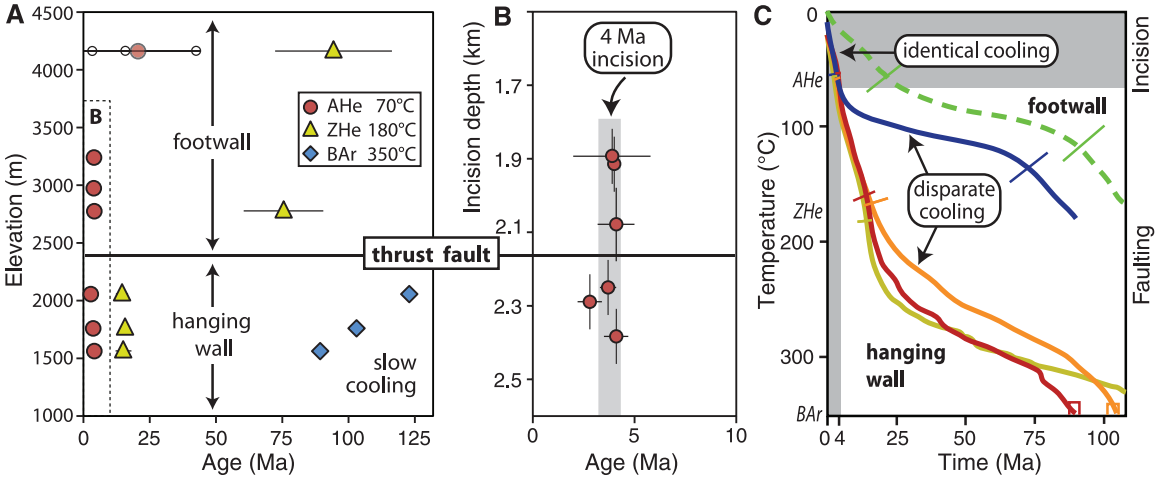

Fig. 3. Thermochronological results from the San Gaban Canyon, northeastern Andean Plateau margin. (**A**) Cooling ages versus elevation. AHe, apatite (U-Th)/He; ZHe, zircon (U-Th)/He; and BAr, biotite K/Ar. He age error at ± 2σ standard error. (**B**) AHe cooling ages versus incision depth. Age error at ± 2σ standard error. Incision depth = maximum swath elevation − sample elevation (see Fig. 2D). (**C**) Thermal histories of individual samples with paired AHe-ZHe (-BAr) cooling ages. Lines are weighted mean cooling paths from inverse modeling (*14*). Colored error bars delimit extent of all "good" model fits in the vicinity of thermochronometer analyses and are drawn orthogonal to the cooling path. Weighted mean cooling paths predict observed ages either exactly or within 0.3 My. Range of model solutions reported in fig. S3.

Pliocene incision into the eastern margin of the Andean Plateau is widespread (Fig. 1). Volcanic chronostratigraphy from basins on the plateau margin indicate deposition until ~3 Ma and incision thereafter. On the southeastern margin, major incision of 1-km-deep canyons into the extensive San Juan del Oro erosion surface did not occur until after ~3 Ma, several million years after the erosion surface formed between 12 and 9 Ma (*5*). Similar in timing, breaching of the central portion of the internally drained Altiplano basin occurred since ~3 Ma via incision of the Rio La Paz through the Eastern Cordillera (*6*, *16*). On the northeastern plateau margin, our results indicate the onset of bedrock cooling due to rapid canyon incision by 4 to 3 Ma (Fig. 3). Over >1250-km distances, regional incision into the eastern margin of the Andean Plateau has accelerated since 4 to 3 Ma (*5*, *6*, *16*) (Figs. 1 and 3).

Pliocene incision into the eastern Andean Plateau occurred across different tectonic, geodynamic, and catchment boundaries, suggesting that a mechanism unrelated to these fields was responsible for incision. Several examples support this. First, the >1250 km along-strike extent of Pliocene incision crosses areas with wide-ranging deformation histories (20 to 50 Ma) and exhumation magnitudes (4 to 10 km) (*17*) that suggest that Pliocene incision was decoupled from active deformation (Fig. 1). Furthermore, movement on basement megathrust faults that could drive hinterland surface uplift above crustal ramps had ceased by 20 to 25 Ma (*16*, *18*) in the incised areas. To the east of our canyon transect, limited deformation in the Subandes has occurred since 15 Ma [<30% shortening (*8*)], suggesting that crustal thickening and isostatic compensation alone did not drive surface uplift and erosion in the past 4 My. Second, geodynamic mechanisms are limited to small areas and are thus unable to drive regional surface uplift and rapid Pliocene incision over >1250 km. For example, piecemeal removal of lithospheric mantle has only been documented for isolated areas <150 km wide (Fig. 1) (*19*). Likewise, other geodynamic mechanisms such as lower crustal flow, flat slab subduction, or an increase in the taper angle of the fold and thrust belt are geographically limited and/or incremental processes. Third, drainage capture is unable to drive the 1.5- to 2.5-km-deep incision observed because incised catchments persistently graded to near sea level close to the mountain front (*20*), and the catchments span a broad area in both the Amazon and La Plata watersheds. Thus, the lack of a correlation between regional incision and localized tectonic, geodynamic, or drainage reorganization phenomena suggests that a regional mechanism such as climate change triggered incision and that surface uplift and canyon incision are temporally decoupled.

Large magnitudes of climate change were coeval with the Pliocene onset of rapid river incision documented here. Tropical precipitation patterns were fundamentally affected by sea surface temperature (SST) changes during the global transition from early Pliocene warmth to late Pliocene cooling (*21*). First, the late Pliocene strengthening of both zonal and meridional SST gradients in the equatorial Pacific, together with shoaling of the thermocline (*21*), heralds the transition from early Pliocene "permanent" El Niño–like conditions to the late Pliocene onset of the El Niño–Southern Oscillation (ENSO) (*22*). Altiplano precipitation on interannual time scales is particularly sensitive to ENSO phase. A precipitation increase occurs during La Niña when upper-level easterlies transport convective Amazon rainfall onto the plateau (*23*), whereas a precipitation decrease occurs during El Niño when westerlies dominate. Second, the late Pliocene marks the onset of protracted north Atlantic cooling (*21*, *24*). Amazon moisture flux is enhanced (*25*) when a strengthened Atlantic meridional SST gradient displaces the Intertropical Convergence Zone southward (*26*). Intensified Altiplano precipitation on millennial time scales is linked to North Atlantic cold events (*27*). In contrast to orographic rainfall established at lower elevations along the eastern Cordillera since 15 to 11 Ma (*17*, *28*), moisture flux into the high elevation Altiplano was not favored until Pacific and Atlantic SST gradients changed at 4 to 3 Ma (*21*).

We propose that enhanced moisture flux into the Altiplano drove rapid incision (*29*) of its eastern margin starting at 4 to 3 Ma (Fig. 1). During modern La Niña, a fourfold increase in heavy storm events and twofold increase in specific stream power drives both vigorous Andean incision (*30*) upstream and episodic sedimentation in the Amazon (*31*) downstream. Furthermore, Quaternary glacier growth and lake expansion on the Altiplano were driven both by periods of La Niña–like conditions (*10*, *32*, *33*) and periods of Northern Hemisphere cooling (*25*, *27*, *34*, *35*), with up to threefold increases in precipitation (*36*). On million-year time scales, the 4- to 3-Ma onset of eastern Andean Plateau dissection (Fig. 1), glaciation (*37*), and plateau lakes (*38*) suggest that enhanced Altiplano precipitation began in the late Pliocene. Given this consistency and the lack of plausible tectonic drivers for incision, we conclude that SST-driven precipitation changes during global cooling regulated late Pliocene incision into the eastern Andean Plateau.

References and Notes

1. T. F. Schildgen, K. V. Hodges, K. X. Whipple, P. W. Reiners, M. S. Pringle, *Geology* **35**, 523–526 (2007).
2. G. D. Hoke *et al.*, *Tectonics* **26**, TC5021 (2007).
3. C. N. Garzione *et al.*, *Science* **320**, 1304–1307 (2008).
4. T. A. Ehlers, C. J. Poulsen, *Earth Planet. Sci. Lett.* **281**, 238–248 (2009).
5. L. Kennan, S. H. Lamb, L. Hoke, *Geol. Soc. London Spec. Publ.* **120**, 307–323 (1997).
6. G. Zeilinger, F. Schlunegger, *Terra Nova* **19**, 373–380 (2007).
7. V. Carlotto, *Bol. Soc. Geol. Peru* **101**, 91–119 (2006).
8. N. Gotberg, N. McQuarrie, V. C. Caillaux, *Geol. Soc. Am. Bull.* **122**, 727–742 (2010).
9. A. Cheilletz *et al.*, *Tectonophysics* **205**, 307–327 (1992).
10. L. G. Thompson, E. Mosley-Thompson, B. M. Arnao, *Science* **226**, 50–53 (1984).
11. A. G. Klein, G. O. Seltzer, B. L. Isacks, *Quat. Sci. Rev.* **18**, 63–84 (1999).
12. P. W. Reiners, M. T. Brandon, *Annu. Rev. Earth Planet. Sci.* **34**, 419–466 (2006).
13. D. J. Kontak, E. Farrar, A. H. Clark, D. A. Archibald, *J. S. Am. Earth Sci.* **3**, 231–246 (1990).
14. R. A. Ketcham, *Rev. Mineral.* **58**, 275–314 (2005).
15. T. F. Schildgen, G. Balco, D. L. Shuster, *Earth Planet. Sci. Lett.* **293**, 377–387 (2010).
16. N. McQuarrie, J. B. Barnes, T. A. Ehlers, *Tectonics* **27**, TC3007 (2008).
17. J. B. Barnes, T. A. Ehlers, N. Insel, N. McQuarrie, C. J. Poulsen, *Geology* **40**, 1135–1138 (2012).
18. B. K. Horton, *Tectonics* **24**, TC3011 (2005).
19. S. L. Beck, G. Zandt, *J. Geophys. Res.* **107**, 2230 (2002).
20. C. Hoorn *et al.*, *Science* **330**, 927–931 (2010).
21. A. V. Fedorov *et al.*, *Nature* **496**, 43–49 (2013).
22. A. V. Fedorov *et al.*, *Science* **312**, 1485–1489 (2006).
23. R. Garreaud, M. Vuille, A. C. Clement, *Palaeogeogr. Palaeoclimatol. Palaeoecol.* **194**, 5–22 (2003).
24. M. Mudelsee, M. E. Raymo, *Paleoceanography* **20**, PA4022 (2005).
25. L. G. Thompson *et al.*, *Science* **340**, 945–950 (2013).
26. J. C. Chiang, M. Biasutti, D. S. Battisti, *Paleoceanography* **18**, 1094 (2003).
27. P. A. Baker *et al.*, *Science* **291**, 640–643 (2001).
28. C. J. Poulsen, T. A. Ehlers, N. Insel, *Science* **328**, 490–493 (2010).
29. K. L. Ferrier, K. L. Huppert, J. T. Perron, *Nature* **496**, 206–209 (2013).
30. B. Bookhagen, M. R. Strecker, in *Amazonia: Landscape and Species Evolution*, C. Hoorn, F. P. Wesselingh, Eds. (Wiley-Blackwell Publishing Ltd., Oxford, UK, 2010), pp. 223–241.
31. R. Aalto *et al.*, *Nature* **425**, 493–497 (2003).
32. R. S. Bradley, M. Vuille, D. Hardy, L. G. Thompson, *Geophys. Res. Lett.* **30**, 1174 (2003).
33. C. J. Placzek, J. Quade, P. J. Patchett, *Geol. Soc. Am. Bull.* **118**, 515–532 (2006).
34. L. G. Thompson *et al.*, *Science* **282**, 1858–1864 (1998).
35. S. C. Fritz *et al.*, *Quat. Res.* **68**, 410–420 (2007).
36. C. J. Placzek, J. Quade, P. J. Patchett, *Earth Planet. Sci. Lett.* **363**, 97–108 (2013).
37. C. M. Clapperton, *Nature* **277**, 375–377 (1979).
38. R. Gaupp, A. Kött, G. Wörner, *Palaeogeogr. Palaeoclimatol. Palaeoecol.* **151**, 79–100 (1999).

Acknowledgments: We thank E. Enkelmann and P. Reiners for laboratory assistance, N. Eichelberger for field assistance, and the NSF Continental Dynamics program for support (EAR-0907817 to T.A.E.). The data reported in this paper are available in the supplementary materials.

Supplementary Materials

www.sciencemag.org/cgi/content/full/341/6147/774/DC1
Materials and Methods
Figs. S1 to S3
Tables S1 to S3
References (*39*–*42*)

15 April 2013; accepted 15 July 2013
10.1126/science.1239132

Basal Drainage System Response to Increasing Surface Melt on the Greenland Ice Sheet

T. Meierbachtol,[1]* J. Harper,[1] N. Humphrey[2]

Surface meltwater reaching the bed of the Greenland ice sheet imparts a fundamental control on basal motion. Sliding speed depends on ice/bed coupling, dictated by the configuration and pressure of the hydrologic drainage system. In situ observations in a four-site transect containing 23 boreholes drilled to Greenland's bed reveal basal water pressures unfavorable to water-draining conduit development extending inland beneath deep ice. This finding is supported by numerical analysis based on realistic ice sheet geometry. Slow meltback of ice walls limits conduit growth, inhibiting their capacity to transport increased discharge. Key aspects of current conceptual models for Greenland basal hydrology, derived primarily from the study of mountain glaciers, appear to be limited to a portion of the ablation zone near the ice sheet margin.

Measurements on the Greenland ice sheet (GIS) show widespread meltwater forcing on velocity, affecting marine (*1*, *2*) and terrestrially terminating regions (*2*–*10*) many tens of kilometers inland from the margin (*4*, *5*, *10*). During the summer melt season, velocities commonly increase up to 100% or more above winter averages (*2*, *3*, *5*–*10*) and can exceed 300% (*4*, *10*). However, the future response of the ice sheet to enhanced surface melt intensity, longer melt seasons, extended melt zones, and increasing high-melt or -rainfall events is unclear, with apparently conflicting possibilities. Positive feedbacks may be limited. Observations show that velocity peaks in the melt season and diminishes later in the summer as ablation increases (*3*, *10*). Further, years with high ablation display smaller average seasonal speedups near the ice sheet margin (*6*). Alternatively, longer surface melt seasons in a warmer climate enhance ice sheet motion due to more short-term accelerations from melt pulses repeatedly overwhelming the subglacial system (*4*, *11*). The nature of changes in sliding motion affects sea level by dictating the extent to which ice is drawn to lower elevations where melt rates are high and ice is discharged through calving termini.

The degree to which meltwater input influences sliding dynamics is driven by the disparity between the rate of change of water input and the capacity of the subglacial drainage network (*4*, *11*, *12*). Observations on the GIS show the basal network evolves through the melt season, with enhanced efficiency extending upward of 50 km inland from the ice sheet margin (*13*, *14*). The mechanism driving evolution is commonly interpreted to follow the smaller mountain glacier conceptual model, whereby an inefficient network of linked cavities switches to a system of efficient channels by melting of the overlying ice roof. The sensitivity to sustained meltwater input is reduced as the inefficient network evolves to a high-capacity channelized system, but short-term perturbations still overwhelm even these efficient drainage features. Basal pressure measurements, which are restricted in time and space (*15*–*18*), and dye-tracing experiments along the ablation zone (*14*) provide the only direct measurements of subglacial hydrologic conditions to date. Whereas basal pressure observations have proven indispensable for elucidating hydrologic processes in the mountain glacier setting, scarce observational data sets from the GIS so far have limited the extension of these processes to the ice sheet scale with confidence. Using in situ water pressure measurements in boreholes drilled along a 34–km transect in the western GIS and modeling, we tested the hypothesis that basal conduit melt processes drive the formation of a channelized network across the drainage regime.

During the summers of 2010–2012, we used hot-water methods to drill 23 boreholes to the ice sheet bed at sites along an E-W transect in western Greenland (Fig. 1). Borehole sites extend inland from the margin of terrestrially terminating Isunnguata Sermia and represent a range of settings, from shallow marginal conditions with ice depth of 100 to 150 m (hereafter referred to as S1) to 34 km deep in the interior, where ice thickness is >800 m (S4) (*19*). Sites also sample a bedrock trough (S3) and an adjacent shallow area located 17 km inland (S2). Before borehole refreezing, we performed hydrological impulse tests (*19*) and instrumented boreholes with basal water pressure sensors for long-term (up to >1 year) monitoring.

We measured distinctive spatial variability in borehole water pressure behavior at the ice sheet margin (S1) as compared to deeper in the interior (S2 to S4). Of the 13 holes drilled at S1, 6 immediately connected to the active subglacial system as evidenced by rapid water level drops when the drill intersected the bed (fig. S1). Basal water pressures in these holes suggest a mix of distributed and channelized drainage during the summer melt season. Daily water pressure swings exceeding 70% of ice overburden (OB) (Fig. 2) indicate borehole connection to a highly efficient, channelized system (*20*). In other holes, small-amplitude variations superimposed on steady high pressure suggest limited drainage capacity (Fig. 2), which is corroborated by the slow accommodation of water introduced to holes during impulse testing. Similar variability over high mean pressures has been interpreted to reflect a distributed drainage configuration (*21*, *22*).

All 10 boreholes located 17 to 34 km from the margin experienced 50- to 125-m water level drops [12 to 17% OB equivalent (fig. S1)] when the drill intersected the bed, indicating connection to an active drainage system. At S2 and S4, pressure records are similar to those at boreholes near the ice sheet edge interpreted to be connected to a linked cavity network. Water pressures 34 km inland at S4 remained between 88 and 94% OB during the late melt season (days of year 200 to 240), with diurnal variations limited to 4% OB or less. Pressures at S2 were steadily between 82 and 92% OB with small variations of similar magnitude as those at S4 (Fig. 2). In the adjacent trough (S3), hydraulic connections between boreholes were evident over 20-m length scales, but long-term connectivity to a broader drainage system appears to be transient. Water level behavior at S3 periodically switched from steadily near or above 100% OB, to exhibiting diurnal variations up to 14% OB. We interpret this behavior to reflect temporary establishment and loss of connections along the bed.

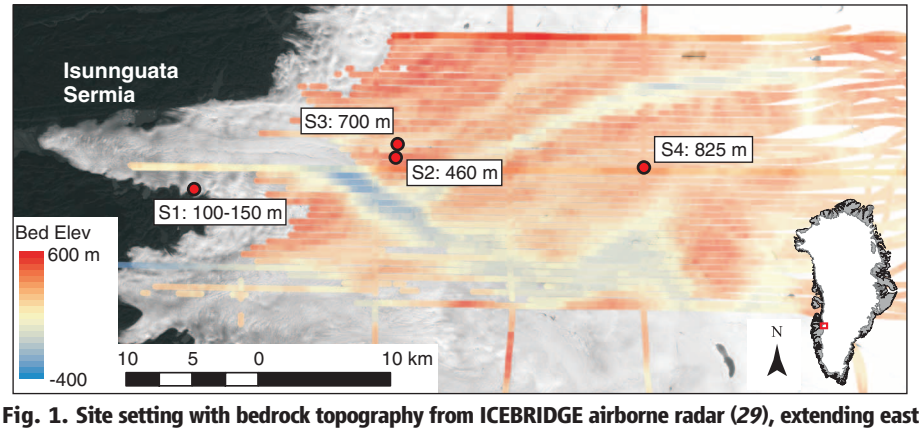

Fig. 1. Site setting with bedrock topography from ICEBRIDGE airborne radar (*29*), extending east from Isunnguata Sermia. Drill sites are denoted by red dots, with site number and ice thickness for reference.

[1]Department of Geosciences, the University of Montana, 32 Campus Drive, Missoula, MT 59812, USA. [2]Department of Geology and Geophysics, University of Wyoming, 1000 University Avenue, Laramie, WY 82071, USA.

*Corresponding author. E-mail: toby.meierbachtol@umontana.edu

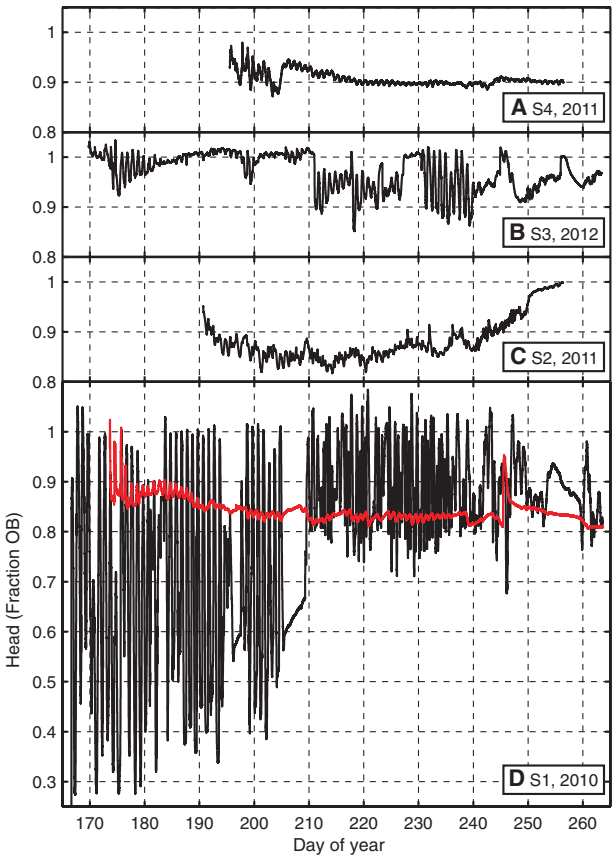

Fig. 2. (A to D) Characteristic long-term water pressure records at S1 to S4 as a fraction of OB. S1 (D) showed significant spatial variability, with some holes showing large diurnal variations (black line), whereas others showed small-amplitude variations at high pressure (red line). The slow increase in water level during days of year 205 to 210 at S1 (black line) may represent the slow closure of an efficient connection or advection of the borehole away from such a hydrologic feature. Boreholes were drilled over the course of three field seasons, thus presented pressure records do not all span the same time period (the drill year is shown in the boxes). Head as fraction of OB pressure (h_{ob}) is calculated as $h_{ob} = \frac{h_w \rho_w}{h_i \rho_i}$, where h_w is head equivalent of water pressure measured in the borehole, h_i is ice thickness, and ρ_w and ρ_i are water and ice densities, respectively.

Consistent with existing observations to the north near Jakobshavn Isbræ (*17*, *18*), we see no direct evidence of high-capacity basal melt channels in our inland (17 and 34 km from the ice sheet margin) boreholes, as manifested by reduced mean pressures and large-amplitude diurnal pressure variations. However, limited sample locations do not preclude the existence of such basal pathways, motivating comparison of basal pressure conditions through numerical analysis. Following previous theoretical development of steady-state conduit dynamics (*23*), we modeled conduit conditions on the ice sheet domain under a range of constant discharge values (*19*). We find that steady conduit pressures less than 70% OB are limited to <10 km from the margin and increase toward OB further inland (Fig. 3). Near the ice sheet margin, expected conduit pressures lower than our distributed measurements reinforce the previous theory that water is driven into these low-pressure features, enhancing their stability (*11*). The reverse is true away from the margin. Pressure differentials between our inland measurements and conduit theory are diminished, and measured pressures at S4 are lower than expected in conduits. In this interior setting, water driven away from high-pressure conduits would feed the distributed network represented by our measurements, resulting in conduit instability and collapse.

Steady-state analysis neglects variable input as surface meltwater routed to the bed through

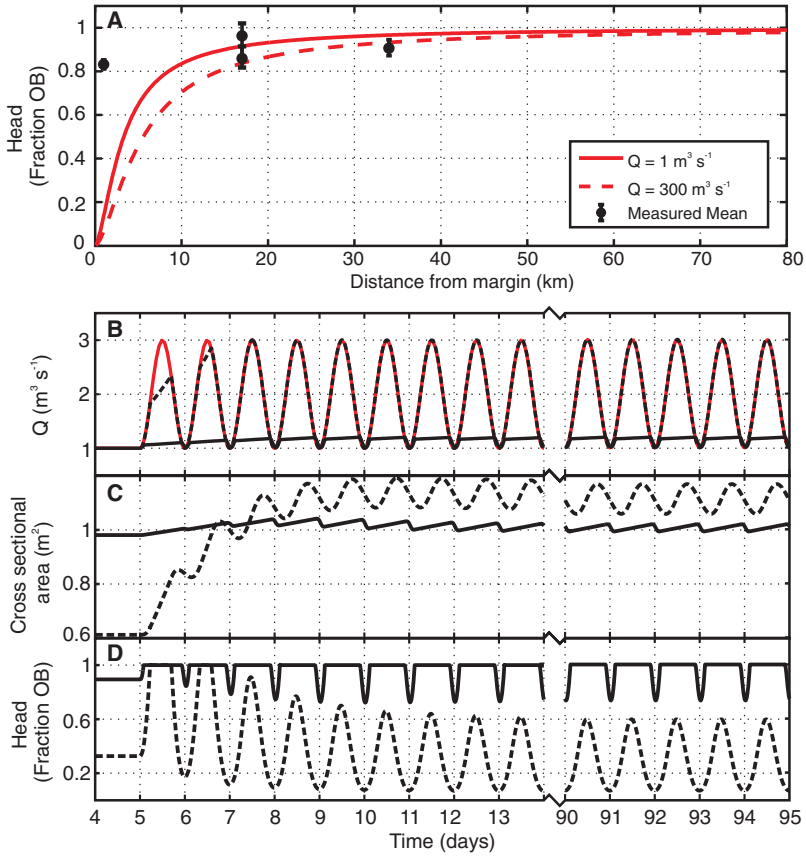

Fig. 3. Simulation results from steady-state conduit analysis (A) and transient experiments (B to D). Steady-state conduit simulations were performed for an envelope of discharges (Q) ranging from a low of 1 $m^3\ s^{-1}$ [solid red line in (A)] to an upper limit of 300 $m^3\ s^{-1}$ (dashed red line), guided by proglacial measurements (*4*). Mean pressures encompassing days of year 200 to 240 from distributed network measurements are shown by black dots; vertical bars denote maximum and minimum pressures during the time period. Transient experiments were forced with diurnally varying input [red line in (B)]. Conduit discharge (B), cross-sectional area (C), and head as fraction of OB (D) are displayed at 3 and 40 km for the margin (dashed line) and inland (solid black line) scenarios, respectively. Margin and inland scenarios are assumed to be representative of conditions expected near S1 and S4.

discrete moulins undergoes seasonal (*24*) and diurnal (*25*) change. We therefore extended our analysis to include transient forcing by implementing a conduit melt-closure model (*19*). Creep closure from ice deformation and opening from meltback of conduit walls determined cross-sectional area, and turbulent flow was simulated through the semicircular conduit. We focus here on two test cases representing a conduit near the margin (with a length of 3 km) and extending to the drainage interior (40 km) to illustrate geometric effects on conduit growth via melting. We assume a preexisting conduit and force the system with diurnally varying discharge. Meltback of the ice walls near the ice sheet margin promotes basal conduit growth (Fig. 3), so that changes in input are rapidly accommodated, thereby preventing elevated pressures. In contrast, interior conduit melt rates are >95% slower than creep closure. Stunted conduit geometry from slow growth can only accommodate a fraction of the imposed input and at pressures largely constrained to 100% OB. The imposed input range (1 to 3 $m^3 s^{-1}$) requires a period of variation that is unreasonably long (90 days) to be fully accommodated by the conduit (supplementary text).

Enhanced conduit closure under thicker ice has been highlighted as a driving difference between alpine and ice sheet subglacial hydraulics (*10*, *12*). However, our pressure records imply that maximum closure rates are similar at marginal sites and in the interior. This is supported by our numerical test cases, despite ice thickness at the inland setting that is three times that at the margin. Instead, low basal conduit melt rates limit channel evolution at inland areas of the ice sheet. The melting of conduit walls is a function of discharge and hydraulic gradient. Steep surface slopes are common in both alpine glaciers and near the ice sheet margin, leading to large hydraulic gradients at the glacier bed and hence to high basal conduit melt rates. In contrast, much of the ice sheet ablation zone away from the margin is characterized by muted surface slopes, which limit conduit growth through dissipative heating effects.

Asymmetry between conduit meltback and closure rates dictates that basal conduits can only be sustained by generally steady discharge conditions. Despite variable surface input, it is possible that the modulation of discharge through basal or englacial water storage and release could facilitate near-steady basal flow. Other work suggests that reversing hydraulic gradients enable an adjacent network to temporarily store water driven out of conduits during periods of high flux and return it during times of low flow (*20*, *26*). However, that model assumes preexisting basal conduits. Our results suggest basal melt rates are too slow to fully establish a channelized network during a single summer season (supplementary text). Further, our measurements of the basal pressure regime question interior conduit stability under steady flow conditions.

Our data and numerical experiments do not support the widespread growth of a conduit network in the drainage interior by ice-wall melt processes alone. Nevertheless, velocity interpretations (*10*), proglacial stream measurements (*13*), and dye-tracing experiments (*14*) provide evidence for seasonally increasing drainage efficiency away from the margin. This implies that other physical processes at the bed are more important than previously recognized in regions where gradient-driven basal melting is muted. We surmise that, toward the ice sheet interior, a network of efficient distributed pathways develops in contrast to large melt channels. Accelerated sliding through the melt season may increase pathway discharge by enlarging space on the lee sides of bed asperities, allowing such a network to transport significant quantities of water (supplementary text). Regardless, any working model of GIS subglacial hydrology must reconcile observations of both pressure and drainage efficiency under relaxed gradient regimes atypical of mountain glaciers.

Accurate representation of processes driving the behavior of ice/water interactions at the ice sheet bed is crucial to understanding drainage system evolution and our ability to quantify the impact of surface meltwater input on ice sheet acceleration. Our results caution against the direct transfer of processes from the alpine setting to the ice sheet interior, where geometric differences are accentuated. Future efforts to assess drainage dynamics away from the ice sheet margin should focus on developing additional mechanisms for growing drainage system efficiency, such as sliding over bedrock. The importance of processes in this interior regime is paramount, considering that surface melt extent and intensity have increased over the GIS during the observational era (*27*, *28*), and future warming is projected to expand melt intensity toward the ice sheet interior.

References and Notes

1. A. J. Sole *et al.*, *J. Geophys. Res.* **116**, 1–11 (2011).
2. I. Joughin *et al.*, *Science* **320**, 781–783 (2008).
3. I. Bartholomew *et al.*, *Nat. Geosci.* **3**, 408–411 (2010).
4. I. Bartholomew *et al.*, *J. Geophys. Res.* **117**, 1–17 (2012).
5. S. Palmer, A. Shepherd, P. Nienow, I. Joughin, *Earth Planet. Sci. Lett.* **302**, 423–428 (2011).
6. A. V. Sundal *et al.*, *Nature* **469**, 521–524 (2011).
7. A. Shepherd *et al.*, *Geophys. Res. Lett.* **36**, 2–5 (2009).
8. H. J. Zwally *et al.*, *Science* **297**, 218–222 (2002).
9. R. S. W. van de Wal *et al.*, *Science* **321**, 111–113 (2008).
10. M. J. Hoffman, G. A. Catania, T. A. Neumann, L. C. Andrews, J. A. Rumrill, *J. Geophys. Res.* **116**, 1–16 (2011).
11. C. Schoof, *Nature* **468**, 803–806 (2010).
12. T. C. Bartholomaus, R. S. Anderson, S. P. Anderson, *Nat. Geosci.* **1**, 33–37 (2008).
13. I. Bartholomew *et al.*, *Geophys. Res. Lett.* **38**, 1–5 (2011).
14. D. M. Chandler *et al.*, *Nat. Geosci.* **6**, 195–198 (2013).
15. H. H. Thomsen, O. B. Olesen, *Rapport Grønlands Geologiske Undersogelse* **152**, 36–38 (1991).
16. H. H. Thomsen, O. B. Olesen, R. J. Braithwaite, C. E. Boggild, *Rapport Grønlands Geologiske Undersogelse* **152**, 80–84 (1991).
17. A. Iken, K. Echelmeyer, W. Harrison, M. Funk, *J. Glaciol.* **39**, 15–25 (1993).
18. M. Lüthi, M. Funk, A. Iken, S. Gogineni, M. Truffer, *J. Glaciol.* **48**, 369–385 (2002).
19. Materials and methods are available as supplementary materials on *Science* Online.
20. B. Hubbard, M. Sharp, I. Willis, M. Nielsen, C. Smart, *J. Glaciol.* **41**, 572–583 (1995).
21. A. Iken, R. A. Bindschadler, *J. Glaciol.* **32**, 101–119 (1986).
22. B. Kamb, *J. Geophys. Res.* **92**, 9083–9100 (1987).
23. H. Röthlisberger, *J. Glaciol.* **11**, 177–203 (1972).
24. D. van As *et al.*, *Cryosphere* **6**, 199–209 (2012).
25. D. McGrath, W. Colgan, K. Steffen, P. Lauffenburger, J. Balog, *J. Glaciol.* **57**, 954–964 (2011).
26. R. B. Alley, *Hydrol. Processes* **10**, 649–660 (1996).
27. T. L. Mote, *Geophys. Res. Lett.* **34**, L22507 (2007).
28. M. Tedesco, *Geophys. Res. Lett.* **34**, 1–6 (2007).
29. C. Allen, IceBridge MCoRDS L2 Ice Thickness. Greenland 2010-2011 (NASA DAAC at the National Snow and Ice Data Center, Boulder, CO, 2010).

Acknowledgments: We thank J. Johnson for his thoughtful review and comments that improved this manuscript. Many thanks to all those who provided field assistance. This work is funded by SKB-Posiva-NWMO through the Greenland Analogue Project and NSF (Office of Polar Programs–Arctic Natural Sciences grant no. 0909495).

Supplementary Materials

www.sciencemag.org/cgi/content/full/341/6147/777/DC1
Materials and Methods
Supplementary Text
Figs. S1 to S6
Tables S1 to S3
References (*30*–*43*)

31 January 2013; accepted 2 July 2013
10.1126/science.1235905

Earliest Evolution of Multituberculate Mammals Revealed by a New Jurassic Fossil

Chong-Xi Yuan,[1] Qiang Ji,[1] Qing-Jin Meng,[2] Alan R. Tabrum,[3] Zhe-Xi Luo[4]*

Multituberculates were successful herbivorous mammals and were more diverse and numerically abundant than any other mammal groups in Mesozoic ecosystems. The clade also developed diverse locomotor adaptations in the Cretaceous and Paleogene. We report a new fossil skeleton from the Late Jurassic of China that belongs to the basalmost multituberculate family. Dental features of this new Jurassic multituberculate show omnivorous adaptation, and its well-preserved skeleton sheds light on ancestral skeletal features of all multituberculates, especially the highly mobile joints of the ankle, crucial for later evolutionary success of multituberculates in the Cretaceous and Paleogene.

Multituberculates are one of the most long-lived mammalian clades, existing from the Middle Jurassic to the Paleogene (*1*–*6*). With the unique teeth adapted for omnivorous-herbivorous feeding (*2*–*4*), and versatile locomotor adaptations to many habitats

(*7*–*10*), multituberculates dominated the Late Cretaceous mammalian faunas and thrived in the Paleocene on Laurasian continents (*1*, *2*, *6*).

Here, we report on a newly discovered multituberculate, *Rugosodon eurasiaticus* gen. et sp. nov. (Figs. 1 and 2 and figs. S1 to S5) (*11*), from the Jurassic Tiaojishan Formation of China, dated to be 160 million years old (*11*, *12*), in a fauna with other Jurassic mammals (*13*, *14*). *Rugosodon eurasiaticus* has a dental formula of I3/i1, C1/c0, P5/p4, M2/m2, with all diagnostic features for the Multituberculata (*1*), such as bladelike ultimate lower premolar (p4), lingually offset cusp rows of upper M2 from M1, and masseteric fossa extending anteriorly on the mandibular body below m1 (Fig. 2). Analyses of craniodental features of *Rugosodon*, based on a matrix of major Mesozoic and Paleogene multituberculate taxa and their outgroups (*4*, *11*, *15*, *16*), have placed it in the Paulchoffatiidae (fig. S6, A and B), a diverse family previously known only by skull fragments, disassociated jaws, and teeth from the Late Jurassic of Portugal (*3*, *17*), plus one tooth from the Cretaceous of North America (*18*). Analyses of craniodental and skeletal features among all mammaliaform clades also corroborate the close affinities of *Rugosodon* to paulchoffatiids, and nested them within Multituberculata (fig. S6C) (*11*). By cusps and ornamentation of molars, *Rugosodon* is

[1]Institute of Geology, Chinese Academy of Geological Sciences, Beijing 100037, China. [2]Beijing Museum of Natural History, Beijing 100050, China. [3]Section of Vertebrate Paleontology, Carnegie Museum of Natural History, Pittsburgh, PA 15213, USA. [4]Department of Organismal Biology and Anatomy, University of Chicago, Chicago, IL 60637, USA.

*Corresponding author. E-mail: zxluo@uchicago.edu

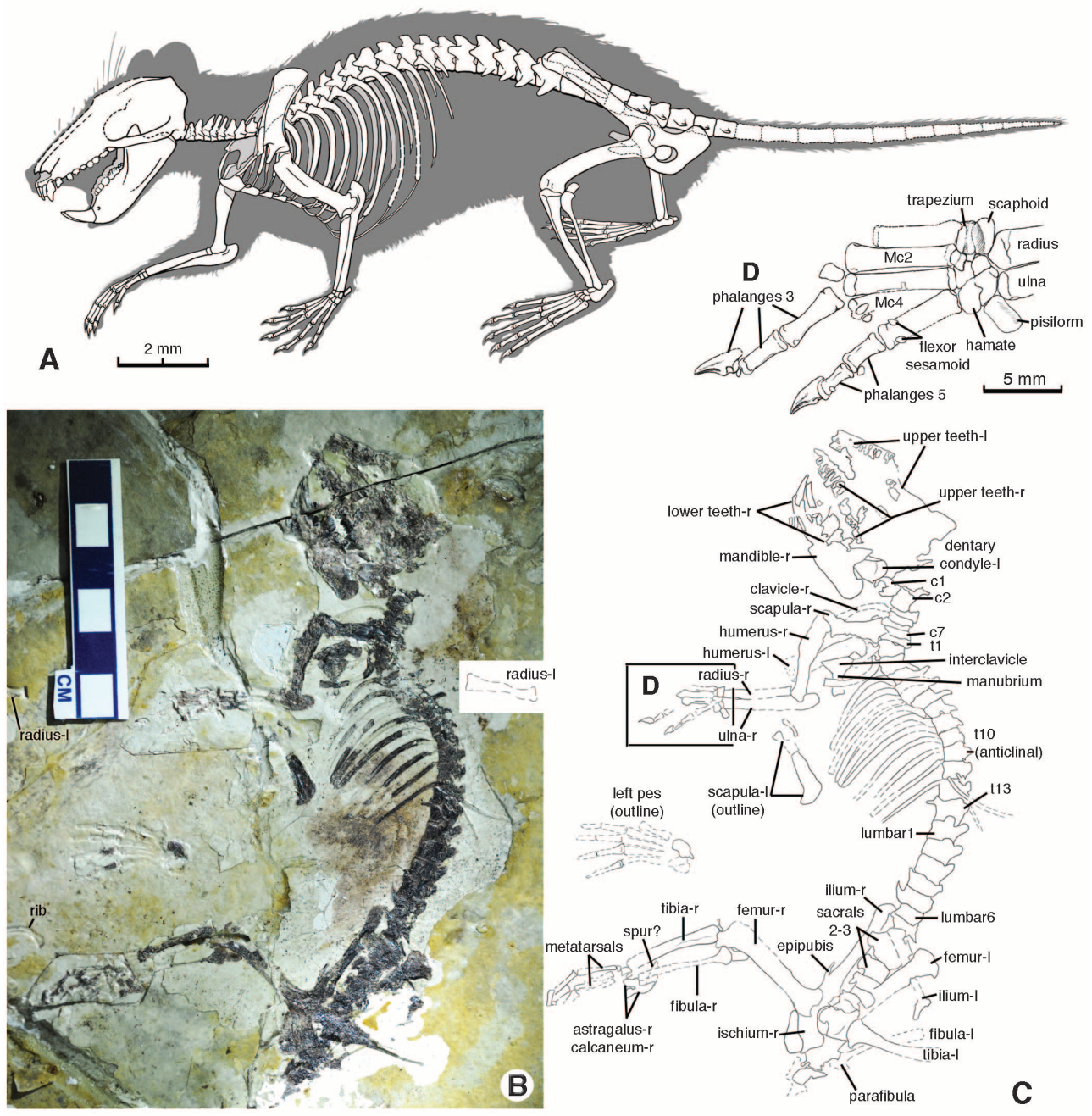

Fig. 1. New Jurassic mammal *Rugosodon eurasiaticus* gen. et sp. nov. (Multituberculata, Paulchoffatiidae). (**A**) Reconstruction of *Rugosodon* as a terrestrial omnivore. (**B** and **C**) The holotype [Beijing Museum of Natural History (BMNH) 1142B (counterpart); BMNH1142A (main part) in fig. S1 in (*11*)]. (**D**) Right manus (composite from BMNH1142A and B). Left versus right sides designated on BMNH 1142A: -l, left; -r, right; c1, c2, and c7, cervical vertebrae 1, 2, and 7; Mc, metacarpals; t1 to t13, thoracic vertebrae 1 to 13.

distinguishable from the family Pinheirodontidae, known from western Europe and considered to be related to paulchoffatiids (*1*, *3*, *19*), and also from the Eobaataridae (including *Sinobaatar*) with extensive distribution in the Early Cretaceous of Asia (*1*, *20*).

The m1-2 of *Rugosodon* are ornamented with ridges and grooves (Fig. 2); m2 has a main basin rimmed by a crenulated margin and a tall, trenchant anterolingual cusp. Upper M1-2 are also rugose, with M2 densely pitted (the etymology of the new genus) (Fig. 2). In these otherwise unique occlusal features, *Rugosodon* closely resembles the paulchoffatiid *Plesiochoffatia* (*17*) and other unnamed multituberculates assignable to *Plesiochoffatia* from the Jurassic of Portugal (figs. S3 and S4). The discovery of *Rugosodon* extends the distribution of this family from Europe to Asia during the Late Jurassic, suggesting a major mammalian faunal exchange within Eurasia in the Jurassic (thus the etymology of the species) (*21*).

Rugosodon has a body mass of 65 to 80 g as estimated from mandibular (28 mm) and skull (34 mm) lengths (*11*). The holotype is a late-stage subadult, indicated by alternating tooth replacements at P2 and P4 positions (Fig. 2A and fig. S4), known for most multituberculates (*20*, *22*) through stem eutherians (*1*). We interpret its diet as omnivorous. The bladelike p4 and the trenchant anterolingual cusps of m1-2 are respectively capable of cutting and puncturing arthropods or worms, whereas the multicusp rows of M1/m1 are for shearing plant matter. Among the best analogs of extant mammals with comparable body-mass range, the African dormouse *Graphiurus* has similar molars with rimmed basins and is a frugivore-granivore, supplemented with feeding on arthropods, worms, and small vertebrates (*23*). A recent analysis (*2*) on a full range of tooth types of diverse taxa hypothesized that multituberculates had an animal-dominated omnivorous diet during the Jurassic and Early Cretaceous and only diversified during the Late Cretaceous into plant-dominated omnivorous and herbivorous feeding guilds. The uneven cusps in the lingual cusp row of m1 and the trenchant cusp of m2, for puncturing, and the m2 basin occluding with the large posterior cusp of M2 suggest that *Rugosodon*, and likely paulchoffatiids as a group, had a mixed diet of plants and invertebrates, as previously suggested (*3*). Thus, the new fossil is consistent with the hypothesis on dietary evolution of multituberculates from the Jurassic to the Paleogene (*2*).

Rugosodon was inferred here to be a terrestrial mammal from its hand and finger bones (*11*). The terminal phalanx is dorsoventrally low and laterally wide (Fig. 1D) (*9*, *24*, *25*). By hand-bone proportion, *Rugosodon* was more likely to be terrestrial than arboreal. Its phalangeal index [(proximal + intermediate phalangeal lengths)/metacarpal length] (*26*) at 117% would indicate preference to a terrestrial substrate when compared with sciuromorph rodents with similar values (*26*). By comparison to diprotodontian marsupials, which include both extant terrestrial and arboreal species, the phalangeal slenderness index (*27*) of *Rugosodon* would place it among terrestrial species, well below the value range of arborealists. Overall morphometric comparison suggests that it is more likely a terrestrial mammal (*11*).

Rugosodon provides the only information on skeletal characters for the Paulchoffatiidae, the basalmost multituberculate family, for assessing the condition of the common ancestor of all multituberculates (Figs. 3 and 4 and fig. S6C). *Rugosodon* is therian-like in the vertebral column (*28*), with a distinctive thoraco-lumbar boundary and an anticlinal vertebra at thoracic 10 (Fig. 1, A to C), as in Cretaceous multituberculates (*9*, *29*) and most trechnotherians (*28*).

The calcaneus ("heel bone") is mediolaterally compressed at midlength and elongates to a swelling tubercle (Fig. 3, B, E, and K), for increasing the in-lever of muscles of the Achilles tendon, for plantarflexion of the foot at the ankle (Fig. 3, node 4) in multituberculates, as in the clade of spalacotherioids through therians (*30*, *31*) (Fig. 3, node 2). By contrast, elongation of the calcaneus is either absent or underdeveloped in more plesiomorphic mammaliaforms (Fig. 3, F to H) (*10*, *30*). It is noteworthy that the "peroneal" groove for the peroneus longus tendon evolved in the subclade of cimolodontans (Fig. 3, node 5) within multituberculates (node 4) and convergently in *Zhangheotherium* within spalacotherioids (Fig. 3, node 3) (*31*).

Rugosodon shows that the Jurassic paulchoffatiids are strikingly similar to later multituberculates in four major tarsal joints (Figs. 3 and 4 and fig. S5) (*7*–*10*): (i) At the upper ankle joint of *Rugosodon* (Fig. 3, A to D), the distal tibia has a peglike medial condyle and a spiral lateral condyle, exactly as in the Paleogene *Eucosmodon* and *Ptilodus* (*7*, *8*) and Late Cretaceous forms (*9*, *10*). The medial astragalar facet pivots on the medial tibial condyle, and the lateral astragalar facet glides along the curved lateral tibial condyle (Fig. 4, A and B, curved arrow), facilitating easy rotation of the upper ankle joint, for a wide abduction and eversion of the hind foot [figure 1 in (*7*)]. (ii) At the lower ankle joint (Fig. 3B), the calcaneus and the astragalus are slightly dislocated, exposing the calcaneo-astragalar contact, which was interpreted to be capable of translational movement for the calcaneus relative to the astragalus,

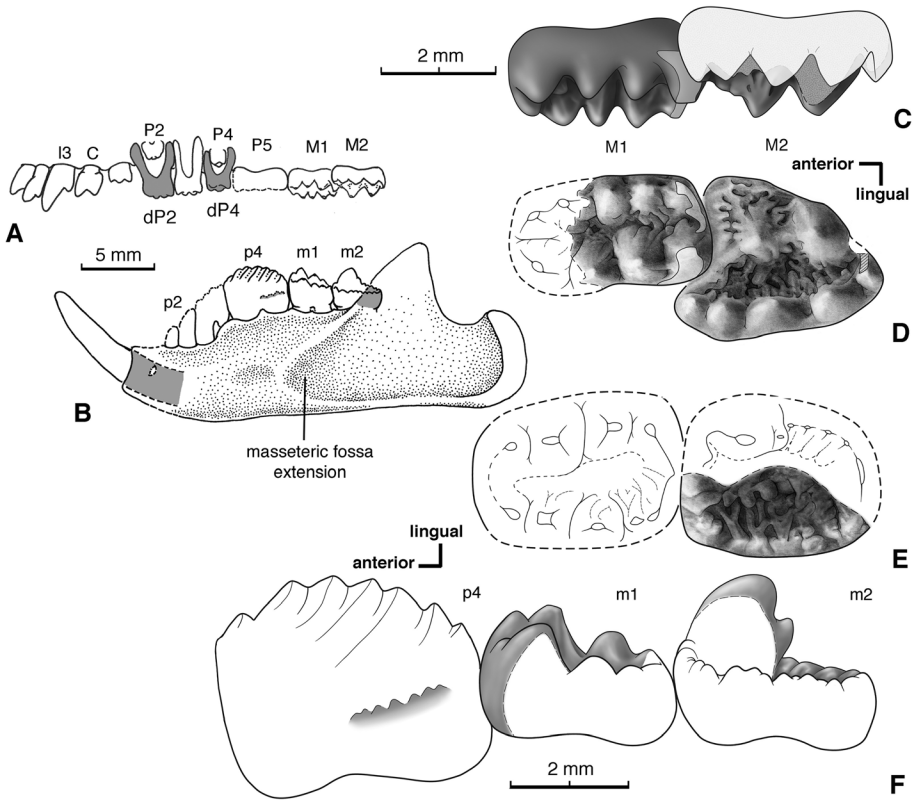

Fig. 2. Mandible and dentition of *Rugosodon eurasiaticus*. (**A**) Upper dentition with alternating replacement of premolars (composite, lateral view; details in figs. S2 to S4). (**B**) Mandible and lower dentition (composite, lateral view). (**C** and **D**) Right upper M1 and M2 lingual and occlusal views. (**E**) Left lower m1 and m2 occlusal view. (**F**) Labial view of lower premolar p4 (labial cingulid cuspules are conjectural, indicated by shading) and m1 and m2. I/i, upper and lower incisors; C, upper canine; P/p, upper and lower premolars; M/m, upper and lower molars; dP2, dP4, deciduous premolars 2 and 4. Carbon-shading: tooth surface directly photographed in the same view as illustrated. White surface: based on camera lucida drawing in the same view. Dashed line: estimate of molar width because m1s and m2s are split lengthwise between BMNH1143A and B and could not be measured directly (*11*).

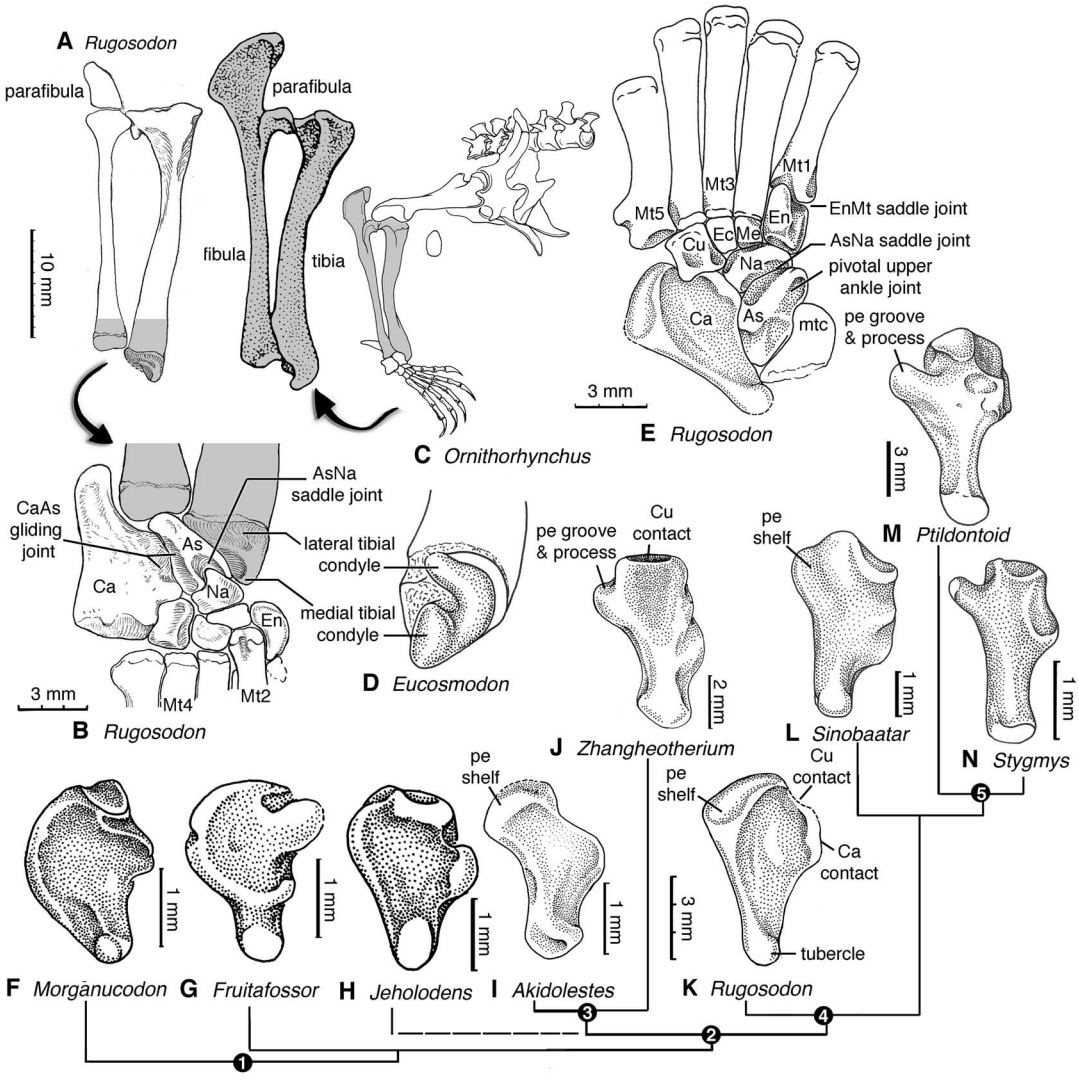

Fig. 3. Evolution of multituberculate pedal features (see also fig. S5). (**A** and **B**) Paulchoffatiid *Rugosodon*, lower hind limb (anterior view) and tarsals (dorsal view) as preserved. (**C**) Monotreme *Ornithorhynchus*, for orienting tibia and fibula with full parafibula. (**D**) Paleocene *Eucosmodon* [after (*8*)], tibial distal end (epiphysis) showing a peg-like medial tibial condyle and a spiral lateral tibial condyle. (**E**) *Rugosodon*, ventral (plantar) view of tarsals and metatarsals, for orienting the calcanei in (**F** to **N**). Evolution of the calcaneus among mammaliaforms (node 1) through theriiforms [node 2, ancestor of (multituberculates + trechnotherians)]. The peroneal groove and its process evolved from shelf by convergence, in cimolodontan subclade (node 5) within multituberculates (node 4) and separately in spalacotherioid mammals (node 3) (*31*). As, astragalus; Ca, calcaneus; CaAs joint, calcaneo-astragalar contact; Cu, cuboid; Cu-contact, calcaneal facet for receiving cuboid; Ec, ectocuneiform; En, entocuneiform; Me, mesocuneiform; Mt1 to 5, metatarsals 1 to 5; mtc, medial tibial condyle (on the distal tibia); Na, navicular; pe-shelf, broader peroneal shelf; pe-groove and process, groove for tendon of peroneus longus and its related peroneal process. [Redrawn from (*8*, *10*, *30*, *31*)]

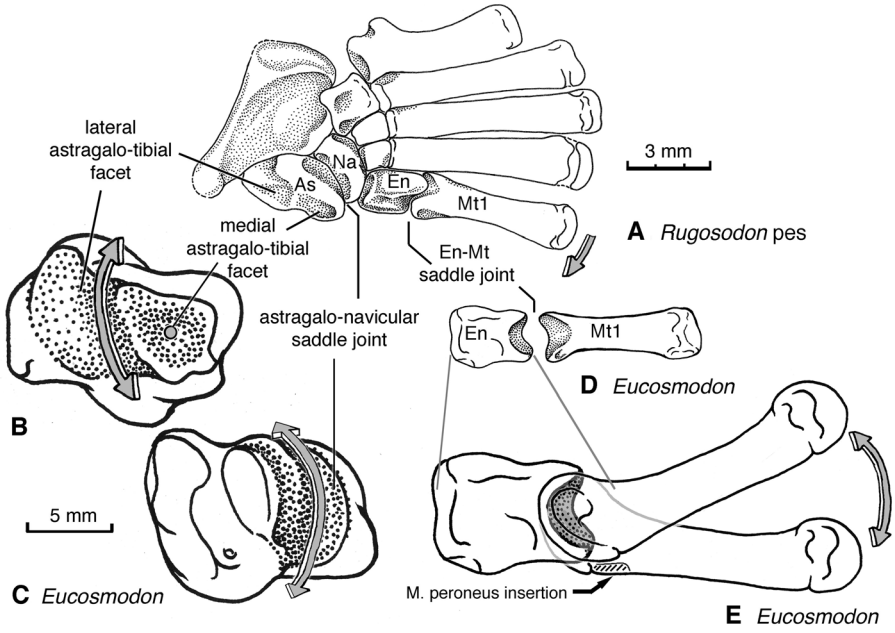

Fig. 4. Function of the hind foot of multituberculates. Hyperabduction and eversion of the foot by pivotal rotation at the upper ankle joint; inversion-eversion and dorsi- and plantarflexion at the saddle joint of the navicular and the astragulus; dorsiflexion and planterflexion; also abduction of metatarsal 1 to the entocuneiform. (**A**) *Rugosodon* (ventral view); metatarsal 1 capable of abduction (arrow). (**B**) Typical multituberculate astragalus and upper ankle joint. The medial tibial condyle pivots on the medial astragalotibial facet, and the lateral tibial condyle glides (curved arrow) on the lateral astragalotibial facet [after (*7*)]. (**C**) Ventral view of astragalus; curved groove on the astragalus forming a saddle joint with the navicular, allowing side-ways movement (curved arrow). (**D** and **E**) Entocuneiform-metatarsal saddle joint facilitating greater dorsi- and plantarflexion of the metatarsal of pedal digit 1; tendon insertion of peroneus longus after (*9*). (B) to (E) based on *Eucosmodon*.

facilitating plantarflexion and inversion of the foot (*7*, *8*). (iii) The astragalus and the navicular have a saddle joint, as well characterized for Cretaceous and Paleogene multituberculates (*7*–*10*), permitting not only side-to-side but also dorsi- and plantarflexion of the navicular to the astragalus (Fig. 4C, curved arrow), enhancing mobility of the midtarsal joint of the hind foot in general (*7*–*10*). (iv) The entocuneiform-metatarsal joint (Fig. 4A) is formed by a deep saddle of the entocuneiform, reciprocated by a curved groove on metatarsal 1 (Fig. 4D), identical in the Jurassic *Rugosodon* as in all later multituberculates (*8*, *10*). This joint facilitates rotation of metatarsal 1 to the entocuneiform (Fig. 4E), amplifying to an even greater dorsoventral excursion for phalanges of the hallux (pedal digit 1), as pulled by the peroneus longus and the extensor digitorium hallucis, both originating near the enlarged parafibula at the knee joint (Fig. 3A). The saddle on the entocuneiform allowed abduction of metatarsal 1, although that element is not habitually abducted as preserved in situ in *Rugosodon* (Fig. 3, B and D). The mobility of metatarsal 1 in multituberculates is a unique condition not seen in other Mesozoic mammals.

Despite a great taxonomic diversity and a wide range of feeding adaptations over the long history of multituberculates (*1*, *2*), the morphology of their ankles is remarkably conserved (*7*). The highly mobile tarsal joints are well suited for foot functions on uneven substrates (including arboreality) (*7*) and are apparently versatile enough to be retained in fossorial (*1*) and saltatorial forms (*9*). Major diversifications of multituberculates in the Cretaceous and Paleogene have a structural underpinning in ankle bones of their common ancestor of the Jurassic, for which *Rugosodon* provides fresh fossil evidence.

References and Notes

1. Z. Kielan-Jaworowska *et al*., *Mammals from the Age of Dinosaurs; Origins, Evolution, and Structure* (Columbia Univ. Press, New York, 2004).
2. G. P. Wilson *et al*., *Nature* **483**, 457–460 (2012).
3. G. Hahn, R. Hahn, in *Guimarota: A Jurassic Ecosystem*, T. Martin, B. Krebs, Eds. (Verlag Dr. Friedrich Pfeil, Munich, 2000), pp. 97–108.
4. P. M. Butler, *Acta Palaeontol. Pol.* **45**, 317–342 (2000).
5. P. M. Butler, J. J. Hooker, *Acta Palaeontol. Pol.* **50**, 185–207 (2005).
6. K. D. Rose, *The Beginning of the Age of Mammals* (Johns Hopkins Univ. Press, Baltimore, MD, 2006).
7. F. A. Jenkins Jr., D. W. Krause, *Science* **220**, 712–715 (1983).
8. D. W. Krause, F. A. Jenkins, *Bull. Mus. Compar. Zool.* **150**, 199–246 (1983).
9. Z. Kielan-Jaworowska, P. P. Gambaryan, *Postcranial Anatomy and Habits of Asian Multituberculate Mammals: Fossils and Strata no. 36* (Scandinavian Univ. Press, Oslo, Copenhagen, Stockholm, 1994).
10. F. S. Szalay, *Evolutionary History of the Marsupials and an Analysis of Osteological Characters* (Cambridge Univ. Press, Cambridge, 1994).
11. Materials and methods are available as supplementary materials on *Science* Online.
12. Y.-Q. Liu *et al*., *Palaeogeogr. Palaeoclimatol. Palaeoecol.* **323–325**, 1–12 (2012);
13. Z.-X. Luo, C. X. Yuan, Q. J. Meng, Q. Ji, *Nature* **476**, 442–445 (2011).
14. Z.-X. Luo, Q. Ji, C. X. Yuan, *Nature* **450**, 93–97 (2007).
15. G. W. Rougier *et al*., *Am. Mus. Novit.* **3193**, 1–12 (1997).
16. Z. Kielan-Jaworowska, J. H. Hurum, *Palaeontology* **44**, 389–429 (2001).
17. G. Hahn, R. Hahn, *Berliner Geowissen. Abhand. E* **28**, 39–84 (1998).
18. R. L. Cifelli, C. L. Gordon, T. R. Lipka, C. S. Scott, *Can. J. Earth Sci.* **50**, 315–323 (2013).
19. A. Badiola, J. I. Canudo, G. Cuenca-Bescós, *Cretac. Res.* **32**, 45–57 (2011).
20. N. Kusuhashi, Y. Hu, Y. Wang, T. Setoguchi, H. Matsuoka, *J. Vertebr. Paleontol.* **29**, 1264–1288 (2009).
21. T. Martin, A. O. Averianov, H.-U. Pfretzschner, *Palaeodiversity Palaeoenviron.* **90**, 295–319 (2010).
22. N. S. Greenwald, *J. Vertebr. Paleontol.* **8**, 265–277 (1988).
23. R. M. Nowak, *Walker's Mammals of the World: Vol. II (6th Edition)* (Johns Hopkins Univ. Press, Baltimore, MD, 1999).
24. N. MacLeod, K. D. Rose, *Am. J. Sci.* **293**, (A), 300–355 (1993).
25. F. S. Szalay, E. J. Sargis, *Geodiversitas* **23**, 139–302 (2001).
26. E. C. Kirk, P. Lemelin, M. W. Hamrick, D. M. Boyer, J. I. Bloch, *J. Hum. Evol.* **55**, 278–299 (2008).
27. V. Weisbecker, D. I. Warton, *J. Morphol.* **267**, 1469–1485 (2006).
28. Q. Ji, Z. X. Luo, X. Zhang, C. X. Yuan, L. Xu, *Science* **326**, 278–281 (2009).
29. P. C. Sereno, in *Amniote Paleobiology: Perspectives on the Evolution of Mammals, Birds, and Reptiles*, M. T. Carrano *et al*., Eds. (Univ. of Chicago Press, Chicago, 2006) 315–370.
30. Z.-X. Luo, J. R. Wible, *Science* **308**, 103–107 (2005).
31. M. Chen, Z.-X. Luo, *J. Mamm. Evol.* **20**, 159–189 (2013).

Acknowledgments: We thank Z. Zeng, D. Liu, X. Xia (BMNH), M. A. Klingler, and A. M. Isch for assistance for research and graphics, and J. R. Wible and M. R. Dawson for improving the manuscript. Authors benefited from discussion with R. L. Cifelli, W. A. Clemens, M. R. Dawson, G. Hahn, J. A. Hopson, Y.-Q. Liu, T. Martin, P. C. Sereno, and J. R. Wible. Support was received from Ministry of Land Resources and Ministry of Science and Technology of China 973 Project Funding (C.-X.Y. and Q.J.), Scientific Commission of Beijing and Beijing Museum of Natural History (Q.-J.M.), NSF, Carnegie Museum, and University of Chicago (Z.-X.L.).

Supplementary Materials

www.sciencemag.org/cgi/content/full/341/6147/779/DC1
Supplementary Text
Figs. S1 to S7
References (*32*–*59*)

18 March 2013; accepted 9 July 2013
10.1126/science.1237970

Identification of Wheat Gene *Sr35* That Confers Resistance to Ug99 Stem Rust Race Group

Cyrille Saintenac,[1]*† Wenjun Zhang,[2]† Andres Salcedo,[1] Matthew N. Rouse,[3] Harold N. Trick,[1] Eduard Akhunov,[1]‡§ Jorge Dubcovsky[2,4]‡§

Wheat stem rust, caused by *Puccinia graminis* f. sp. *tritici* (*Pgt*), is a devastating disease that can cause severe yield losses. A previously uncharacterized *Pgt* race, designated Ug99, has overcome most of the widely used resistance genes and is threatening major wheat production areas. Here, we demonstrate that the *Sr35* gene from *Triticum monococcum* is a coiled-coil, nucleotide-binding, leucine-rich repeat gene that confers near immunity to Ug99 and related races. This gene is absent in the A-genome diploid donor and in polyploid wheat but is effective when transferred from *T. monococcum* to polyploid wheat. The cloning of *Sr35* opens the door to the use of biotechnological approaches to control this devastating disease and to analyses of the molecular interactions that define the wheat-rust pathosystem.

The fungus *Puccinia graminis* f. sp. *tritici* (henceforth *Pgt*) is the causal agent of wheat stem rust, a devastating disease responsible for major outbreaks and large losses of wheat yields in the past. The deployment of *Pgt* resistance genes, combined with the eradication of the alternative host (barberry), provided an effective control of this disease for the past 50 years (*1*). However, the widely deployed *Pgt* resistance gene *Sr31* was overcome by a previously uncharacterized race of *Pgt* identified in Uganda in 1999 and designated Ug99 (or TTKSK, according to the North American system for *Pgt* race nomenclature) (*2*). A decade later, six previously unidentified Ug99-related *Pgt* races, some showing a broader virulence spectrum, have been detected and have spread to the wheat-growing regions of Africa, Yemen, and Iran (*3*). Roughly 90% of the wheat varieties grown worldwide are susceptible to Ug99 and related races, representing a serious threat to global food security (*3*). The Borlaug Global Rust Initiative was launched in 2005 to coordinate international efforts to fight Ug99 (www.globalrust.org). The identification and characterization of Ug99-resistance genes *Sr35* (in this

[1]Department of Plant Pathology, Kansas State University, Manhattan, KS 66506, USA. [2]Department of Plant Sciences, University of California, Davis, CA 95616, USA. [3]Cereal Disease Laboratory, U.S. Department of Agriculture (USDA)–Agricultural Research Service, St. Paul, MN 55108, USA. [4]Howard Hughes Medical Institute (HHMI), Chevy Chase, MD 20815, USA.

*Present address: Genetics Diversity and Ecophysiology of Cereals, Institut National de la Recherche Agronomique–Université Blaise Pascal, UMR1095, 5 Chemin de Beaulieu, 63039 Clermont-Ferrand, France.
†These authors contributed equally to this work.
‡These authors contributed equally to this work.
§Corresponding author. E-mail: eakhunov@ksu.edu (E.A.); jdubcovsky@ucdavis.edu (J.D.)

study) and *Sr33* [in a companion paper (*4*)] are part of these efforts.

The stem rust resistance gene *Sr35* was identified in previous screens for resistance to *Pgt* in the diploid wheat species *Triticum monococcum* (*5*, *6*). The genome of *T. monococcum*, designated A^m, is closely related to the genome of *T. urartu*, the diploid donor of the A genome in tetraploid (*T. turgidum*, pasta wheat) and hexaploid wheat (*T. aestivum*, bread wheat) (*7*). *Sr35* was prioritized for cloning because it confers near immunity against Ug99, Ug99-related races, and the TRTTF group of races from Africa, Yemen, and Pakistan; the TRTTF group has a broad but different virulence profile from the Ug99 race group (*3*, *8*). *Sr35* was also selected because previous studies have confirmed that this gene is effective against the same virulent races when it is transferred to hexaploid wheat by crossing and recombination (*5*, *8*).

The gene *Sr35* was previously mapped on the long arm of chromosome $3A^m$ in *T. monococcum* (*8*). In this study, we used 4575 recombinant gametes (1925 F_2 and 725 BC_1F_1 plants) and seven molecular markers derived from the colinear region in *Brachypodium distachyon* (Fig. 1A) to map *Sr35* between markers *AK331487* [0.02 centimorgans (cM)] and *AK332451* (0.98 cM) (Fig. 1B). We then used the closest proximal markers *AK331487* and *SFGH* (*S-formylglutathione hydrolase-like*) to screen a *T. monococcum* bacterial artificial chromosome (BAC) library of the *Sr35*-resistant accession DV92 (*9*). The 23 selected BAC clones were assembled by fingerprinting into a single contig that spanned the *Sr35* locus (Fig. 1, C and D; fig. S1; and table S1).

We sequenced three overlapping BACs covering the *Sr35* region (*10*) and annotated the 307,519–base pair (bp) sequence (KC573058). This sequence includes a cluster of coiled-coil, nucleotide-binding, leucine-rich repeat (LRR) (henceforth, CNL) disease resistance genes, including five intact genes (*CNL1*, *CNL2*, *CNL4*, *CNL6*, and *CNL9*), two pseudogenes (*pCNL3* and *pCNL10*), and three small gene fragments (*pCNL5*, *pCNL7*, and *pCNL8*) (Fig. 1E). A phylogenetic tree of the complete *CNL* genes showed that *CNL4* and *CNL9* are the most closely related members of this cluster (fig. S2). The annotated sequence also includes two unrelated genes (*SFGH* and *APGG1*) and two pseudogenes (*pABC* and *pAP2*) (Fig. 1E). Additional markers developed from this sequence were used to delimit the *Sr35* candidate region to a 213-kb segment including candidate genes *APGG1*, *CNL4*, *CNL6*, and *CNL9* (Fig. 1E and table S1).

We sequenced these four candidate genes in a *T. monococcum* collection including 24 Ug99-resistant accessions carrying *Sr35* and 25 susceptible accessions without *Sr35*. We identified two resistant (R1 and R2) and six susceptible haplotypes (S1 to S6, table S2, primers in tables S3 to S5). The two resistant haplotypes differ in a short *CNL4* region with a 6-bp deletion and four single-nucleotide polymorphisms (SNPs) but show no differences in *APGG1*, *CNL6*, and *CNL9*. All susceptible accessions have mutations in *CNL9*, and among them, five have mutations only in *CNL9*, which suggests that this gene is necessary to confer resistance to Ug99. Among these five susceptible accessions, three of them share three close SNPs that result in amino acid changes at positions 854, 856, and 858 [RLWFT to HLRFS (R, Arg; L, Leu; W, Trp; F, Phe; T, Thr; H, His; S, Ser)] in the C-terminal region of the LRR domain (Fig. 2A). The same three SNPs are present in the closely related *CNL4* gene, suggesting a conversion event.

To validate the previous results, we mutagenized the *Sr35*-resistant accession G2919 with ethylmethanesulfonate (*10*). Out of 1087 M_2 mutant families screened with race RKQQC, we identified two mutant families segregating for susceptibility, which were validated with races Ug99 and TRTTF (Fig. 2B). Sequencing of the four candidate genes in these susceptible plants confirmed the presence of mutations only in *CNL9*. The first mutant ($cnl9^{1296}$) contained a G-to-A mutation that resulted in a premature stop codon at position 856 (Fig. 2A) and truncated the last 64 amino acids. In the progeny of a cross between $cnl9^{1296}$ and the resistant parental line G2919 (33 F_2 plants), homozygocity for the mutation cosegregated with susceptibility to Ug99.

The second susceptible mutant ($cnl9^{1120}$) showed the same three SNPs detected in accession PI428167-2 (RLWFT to HLRFS) (table S2). To test if this was the result of seed contamination or cross-pollination, we used genotyping-by-sequencing (*11*) to estimate the level of polymorphisms among $cnl9^{1296}$, $cnl9^{1120}$, and the nonmutagenized line G2919 (table S6 and supplementary text). We show that $cnl9^{1120}$ has the level of mutations and the ratio of homozygous-to-heterozygous loci expected from a mutagenized plant. Therefore, a spontaneous gene conversion between *CNL4* and *CNL9* is the most parsimonious explanation for the three linked mutations in $cnl9^{1120}$. Two of these amino acid positions (856 and 858) overlap with 15 amino acids located in the C-terminal half of the LRR domain of CNL9 that show evidence of positive selection (fig. S3, A and B, and table S7). Concisely, mutants $cnl9^{1296}$ and $cnl9^{1120}$ confirmed that *CNL9* is necessary for the *Sr35*-mediated resistance and that the distal region of the LRR domain is critical for *Sr35* function.

To determine if *CNL9* is sufficient to confer resistance to Ug99, we generated transgenic hexaploid wheat plants expressing the *CNL9* gene under the control of its native promoter (*10*). Out of four putative T_0 transgenic plants, only one, designated #1123, showed consistent expression of the transgene (fig. S4) and cosegregation between the presence of the transgene and resist-

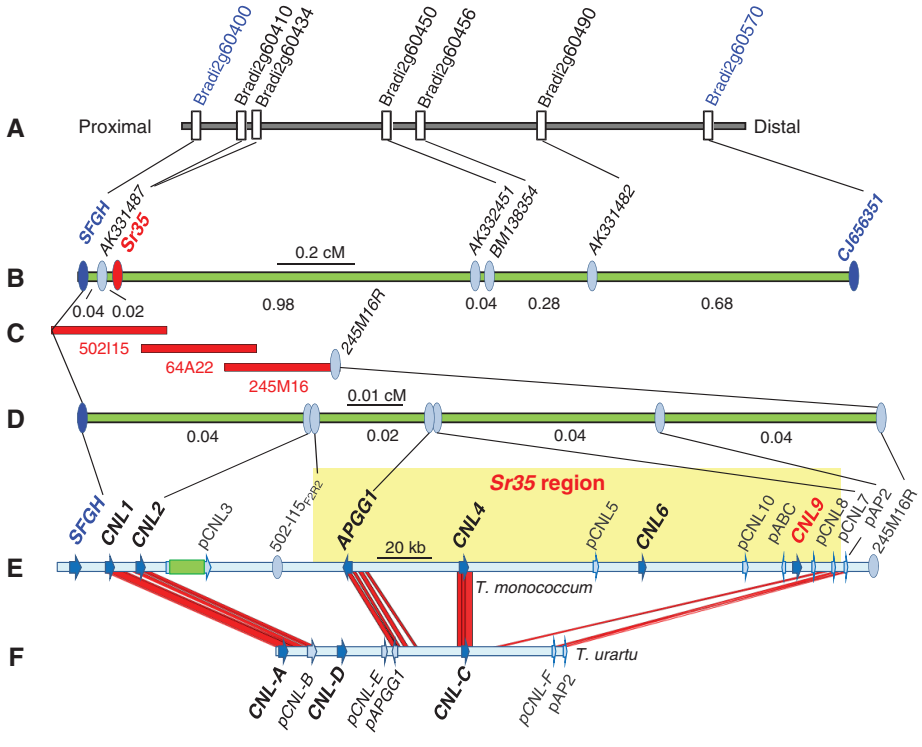

Fig. 1. Genetic and physical maps of *Sr35*. (**A**) A 174-kb colinear region of *Brachypodium* (*8*). Only genes for which a wheat orthologous gene was found in databases are represented here. (**B**) Genetic map of the *Sr35* locus. (**C**) Screening the DV92 BAC library with proximal markers *SFGH* and *AK331487* (only BACs from the minimum tilling path are shown). (**D**) High-density map. (**E**) Graphical representation of the *T. monococcum* annotated sequences (KC573058). The letter "p" before the gene name denotes a pseudogene (*pCNL3* has an inserted retroelement). The *Sr35* candidate gene region is highlighted in yellow. (**F**) Comparison of *T. monococcum* DV92 and *T. urartu* G1812 (KC816724) orthologous regions (92% identity threshold).

ance to Ug99 and RKQQC in the T_1 and T_2 progeny (Fig. 2C, fig. S5, and table S8). In contrast, all #1123 T_1 and T_2 plants were susceptible to the *Sr35*-virulent race QTHJC, regardless of the presence or absence of the transgene (Fig. 2C and fig. S5). This result suggests that the *CNL9* transgene has the same race specificity as *Sr35*. Taken together, the natural variation, mutant, and transgenic results demonstrate that *CNL9* is *Sr35*.

With the use of rapid amplification of cDNA ends (*10*), we found that the *CNL9* transcripts have a 196-bp 5′ untranslated region (UTR) and a 1526-bp 3′UTR that includes three introns (fig. S6A). The three introns in the 3′UTR were also detected in all *T. urartu*–, *T. turgidum* cv. *durum*–, and *T. aestivum*–related *CNL* genes for which we were able to obtain both genomic and transcript data (table S9). Both *CNL* homologs from *B. distachyon* (table S9) also have two introns in the 3′UTR, indicating that this structural feature is conserved in this disease resistance cluster. Exons 3 and 4 from the *B. distachyon CNL* genes correspond to exons 4 and 5 from the *T. monococcum CNL9* homolog.

Transcript levels of *CNL9* in leaves from G2919 plants inoculated with *Pgt* race RKQQC (*10*) were 40-, 81-, and 411-fold higher than those of candidate genes *APGG1*, *CNL4*, and *CNL6*, respectively (Fig. 2D), but did not significantly differ from mock-inoculated plants at different time points (Fig. 2E). With the use of isoform-specific primers (fig. S6B and table S5), we found that ~8% of the *T. monococcum CNL9* transcripts were represented by an alternative splicing variant that retained the second intron in the 3′UTR (Fig. 2E). We also detected transcripts with and without the same intron in *T. turgidum* (table S9). The ratio between the two *CNL9* transcript isoforms did not show changes in *T. monococcum* G2919 plants mock-inoculated and inoculated with *Pgt* race RKQQC (Fig. 2E). This finding suggests that the relative proportion of the two alternative splice forms is not affected by the presence of the pathogen. Previously reported alternative splicing events in *CNL* genes do not involve introns in the 3′UTR (*12*–*18*), which might be a distinctive feature of this particular group of *CNL* genes.

So far, *Sr35* has not been reported in *T. urartu* or polyploid wheat species. To better understand the reasons for this absence, we performed a comparative analysis of the *T. monococcum* (KC573058) and *T. urartu* (KC816724) colinear regions, which diverged less than 1 million years ago (*19*). The *T. monococcum* region encompassing genes *CNL6* and *CNL9* and pseudogenes *pCNL5*, *pCNL8*, *pCNL10*, and *pABC* is absent in *T. urartu* (Fig. 1F). Conversely, the *T. urartu* region including *TuCNL-D* and pseudogene *pCNL-E* is missing in *T. monococcum*. Large insertions and deletions have been found in other colinear intergenic regions of the *T. monococcum* and *T. urartu* genomes (*19*, *20*). The large and repetitive genomes of wheat show higher rates of insertion and deletions than the human genome (*19*).

A screen of 41 *T. urartu* accessions and 19 wild tetraploid wheat *T. turgidum* ssp. *dicoccoides* accessions (table S10) revealed no orthologs of *TmCNL9* (fig. S7). Gene *TuCNL-H* from *T. urartu* accession G1545 from Iran encoded the same RWT amino acids found in CNL9 at positions 854, 856, and 858, but the rest of the sequence was different and clustered with a separate set of *CNL* genes (fig. S7). Because *T. urartu* is the donor of the A genome to the polyploid wheat species (*7*), it is not surprising that *CNL9* homologs have not been detected in the genomic sequence of *T. aestivum* (www.wheatgenome.org/) or in the transcriptome of *T. turgidum* (wheat.pw.usda.gov/GG2/WheatTranscriptome/) (fig. S2).

The absence of *Sr35* in the tested pasta and bread wheat varieties highlights the value of wheat landraces and wild relatives as a reservoir of currently unknown resistance specificities. It also suggests that *Sr35* has the potential to improve stem rust resistance in a wide range of wheat germplasm. Our transgenic experiments additionally indicate that the transfer of *CNL9-Sr35* to hexaploid wheat is sufficient to confer effective

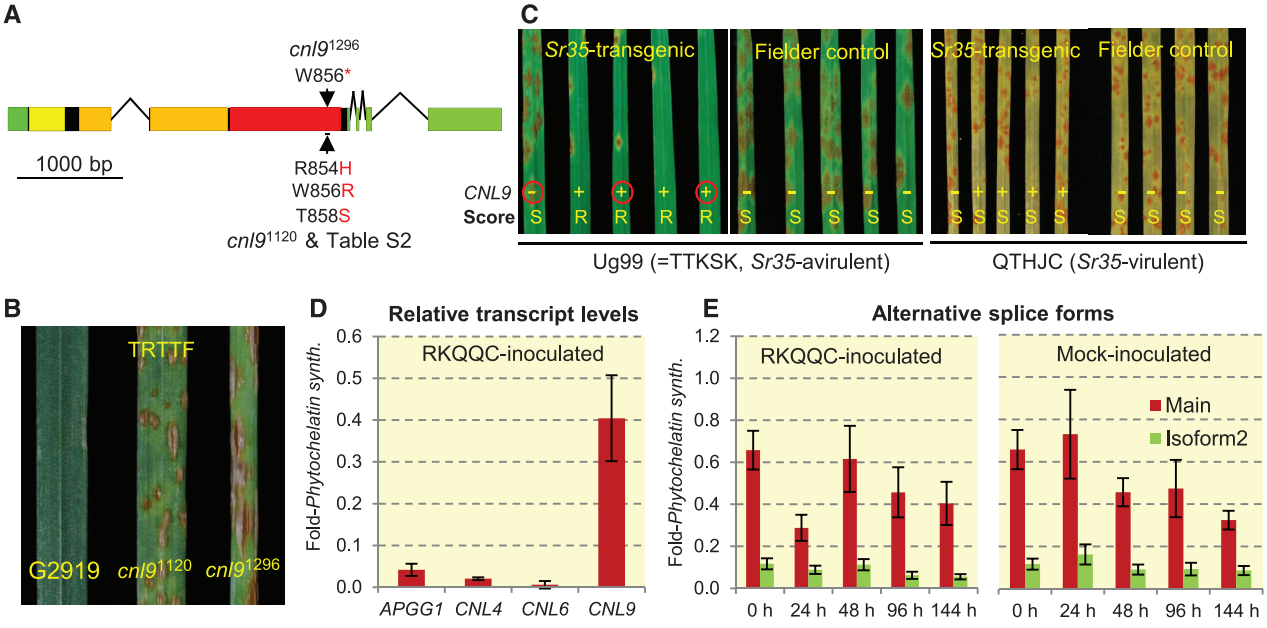

Fig. 2. Functional validation of the *CNL9* gene. (**A**) *CNL9* gene structure. Green, UTR; black, coding exons; yellow, coiled-coil domain; orange, nucleotide-binding domain; red, LRR domain; arrows, amino acid changes in susceptible induced mutants *cnl9*^{1296} (W856*) and *cnl9*^{1120} or natural mutants (table S2, RLWFT to HLRFS). (**B**) Infection types produced on *T. monococcum* G2919 and *CNL9* mutants *cnl9*^{1120} and *cnl9*^{1296} inoculated with *Pgt* race TRTTF. G2919 carries both *Sr35* and *Sr21* resistance genes, so we selected a race (TRTTF) that is virulent to *Sr21* and avirulent to *Sr35* to validate the mutations in *Sr35*. (**C**) Infection types on seedlings of T_1 lines from event #1123 segregating for the *CNL9* transgene. Plants carrying the *CNL9* transgene (+) were resistant to Ug99 (R), and plants without the transgene (-) were susceptible (S) (table S8). When inoculated with *Sr35*-virulent race QTHJC, all plants were susceptible, suggesting similar race specificity between the transgenic and natural *Sr35*. Red circles indicate available progeny tests in fig. S5. S, susceptible; R, resistant. (**D**) Relative transcript levels of candidate genes *APPG1*, *CNL4*, *CNL6*, and *CNL9* (main isoform) in G2919 6 days after inoculation with race RKQQC. (**E**) Transcript levels of the *CNL9* main isoform (red) and isoform two (green, retained intron) in mock- or race RKQQC–inoculated G2919 plants. Leaves were collected at 0, 24, 48, 96, and 144 hours after inoculation. Transcript levels are expressed relative to the *Phytochelatin synthase* internal control using the $2^{-\Delta Ct}$ method. Error bars in (D) and (E) denote SEM based on six biological and two technical replicates.

levels of resistance to Ug99. In contrast, some *CNL* genes (for example, wheat leaf rust resistance gene *Lr10*) require the presence of additional *CNL* genes to provide resistance (*21*).

CNL proteins mediate recognition of pathogen-derived effector molecules, as well as host proteins altered by the pathogen, and they subsequently activate host defenses. These proteins have an ancient origin and are encoded by one of the largest, most variable multigene families in plants (*22*). Members of this family confer resistance to a wide range of pathogens and pests. Remaining challenges are to identify which genes are responsible for resistance to a specific pathogen and to understand the signal transduction pathways involved in the plant resistance response. This information is particularly important in the case of Ug99, which now threatens the major wheat-producing areas in Asia (*3*).

The identification of *Sr35* and of *Sr33* in a companion paper (*4*) opens the door to transgenic approaches to control this devastating pathogen. *Sr35* shows a strong hypersensitive reaction to the TTKSK and TRTTF race groups when introgressed into hexaploid wheat but is susceptible to some *Pgt* races and, therefore, should not be deployed alone. In contrast, *Sr33* is resistant to all races tested so far (*23*, *24*) but confers only moderate resistance to the Ug99 race group when introgressed alone in hexaploid wheat. On the basis of these complementary characteristics, it might be beneficial to combine these two genes, by either crossing and recombination or transforming wheat with a cassette including both genes. The insertion of multiple resistance genes in a single locus can accelerate breeding efforts to pyramid multiple sources of resistance, which is a reasonable strategy to increase the durability of available resistance genes.

References and Notes

1. R. A. McIntosh, C. R. Wellings, R. F. Park, *Wheat Rusts, an Atlas of Resistance Genes*, K. Jean, Ed. (Commonwealth Scientific and Industrial Research Organisation, Melbourne, Australia, 1995).
2. Z. A. Pretorius, R. P. Singh, W. W. Wagoire, T. S. Payne, *Plant Dis.* **84**, 203 (2000).
3. R. P. Singh *et al.*, *Annu. Rev. Phytopathol.* **49**, 465–481 (2011).
4. S. Periyannan *et al.*, *Science* **341**, 786–789 (2013).
5. R. A. McIntosh, P. L. Dyck, T. T. The, J. Cusick, D. L. Milne, *Plant Breed.* **92**, 1–14 (1984).
6. M. N. Rouse, Y. Jin, *Plant Dis.* **95**, 941–944 (2011).
7. J. Dvorak, P. E. McGuire, B. Cassidy, *Genome* **30**, 680–689 (1988).
8. W. Zhang *et al.*, *Crop Sci.* **50**, 2464–2474 (2010).
9. D. Lijavetzky *et al.*, *Genome* **42**, 1176–1182 (1999).
10. Materials and methods are available as supplementary materials on *Science* Online.
11. C. Saintenac, D. Jiang, S. Wang, E. Akhunov, *G3* **3**, 1105–1114 (2013).
12. S. Costanzo, Y. L. Jia, *Plant Sci.* **177**, 468–478 (2009).
13. E. Ferrier-Cana *et al.*, *Theor. Appl. Genet.* **110**, 895–905 (2005).
14. X. P. Tan *et al.*, *BMC Plant Biol.* **7**, 56 (2007).
15. H. Sela *et al.*, *Mol. Plant Pathol.* **13**, 276–287 (2012).
16. D. A. Halterman, F. S. Wei, R. P. Wise, *Plant Physiol.* **131**, 558–567 (2003).
17. D. A. Halterman, R. P. Wise, *Mol. Plant Pathol.* **7**, 167–176 (2006).
18. W. Gassmann, in *Nuclear pre-mRNA Processing in Plants* (Springer, Heidelberg, 2008), vol. 326, pp. 219–233.
19. J. Dubcovsky, J. Dvorak, *Science* **316**, 1862–1866 (2007).
20. T. Wicker *et al.*, *Plant Cell* **15**, 1186–1197 (2003).
21. C. Loutre *et al.*, *Plant J.* **60**, 1043–1054 (2009).
22. J. X. Yue, B. C. Meyers, J. Q. Chen, D. C. Tian, S. H. Yang, *New Phytol.* **193**, 1049–1063 (2012).
23. J. Huerta-Espino, thesis, University of Minnesota, St. Paul, MN (1992).
24. M. N. Rouse, E. L. Olson, B. S. Gill, M. O. Pumphrey, Y. Jin, *Crop Sci.* **51**, 2074–2078 (2011).

Acknowledgments: This project was supported by Agricultural and Food Research Initiative grants 2011-68002-30029 (Triticeae-CAP) and 2012-67013-19401 from the USDA National Institute of Food and Agriculture, by the Borlaug Global Rust Initiative, and by support to J.D. from the HHMI and the Gordon and Betty Moore Foundation grant GBMF3031. We thank J. Nirmala, S. Sehgal, M. Padilla, S. Chao, K. Jordan, H. Lee, and D. Burdan for excellent technical support; B. Bowden and J. Dvorak for providing critical materials; K. Krasileva, A. Akhunova, and C. Li for valuable suggestions; and the University of California, Davis, and Kansas State University Genomic facilities. We also thank M. Pumphrey for his collaboration in the initial stages of the project, including design and initial development of the high-resolution mapping and TILLING populations. Sequences have been deposited in GenBank under accession numbers KC573058, KC816724, KF113354 to KF113357, and KC876115 to KC876121. Author contributions are listed in the supplementary materials.

Supplementary Materials

www.sciencemag.org/cgi/content/full/science.1239022/DC1
Materials and Methods
Supplementary Text
Figs. S1 to S7
Tables S1 to S10
References (*25*–*47*)

11 April 2013; accepted 10 June 2013
Published online 27 June 2013;
10.1126/science.1239022

The Gene *Sr33*, an Ortholog of Barley *Mla* Genes, Encodes Resistance to Wheat Stem Rust Race Ug99

Sambasivam Periyannan,[1] John Moore,[1] Michael Ayliffe,[1] Urmil Bansal,[2] Xiaojing Wang,[4,6] Li Huang,[4] Karin Deal,[3] Mingcheng Luo,[3] Xiuying Kong,[5] Harbans Bariana,[2] Rohit Mago,[1] Robert McIntosh,[2] Peter Dodds,[1] Jan Dvorak,[3] Evans Lagudah[1]*

Wheat stem rust, caused by the fungus *Puccinia graminis* f. sp. *tritici*, afflicts bread wheat (*Triticum aestivum*). New virulent races collectively referred to as "Ug99" have emerged, which threaten global wheat production. The wheat gene *Sr33*, introgressed from the wild relative *Aegilops tauschii* into bread wheat, confers resistance to diverse stem rust races, including the Ug99 race group. We cloned *Sr33*, which encodes a coiled-coil, nucleotide-binding, leucine-rich repeat protein. *Sr33* is orthologous to the barley (*Hordeum vulgare*) *Mla* mildew resistance genes that confer resistance to *Blumeria graminis* f. sp. *hordei*. The wheat *Sr33* gene functions independently of *RAR1*, *SGT1*, and *HSP90* chaperones. Haplotype analysis from diverse collections of *Ae. tauschii* placed the origin of *Sr33* resistance near the southern coast of the Caspian Sea.

Stem rust [*Puccinia graminis* f. sp. *tritici* (*Pgt*)] of wheat is a major threat to global food security. Continued adaptation of the pathogen necessitates continued development of new *Pgt*-resistant wheat varieties (*1*). A *Pgt* race, Ug99 or TTKSK, identified in Uganda in 1999, was virulent on 90% of wheat cultivars grown globally, including those carrying the stem rust resistance (*Sr*) *31* resistance gene, which hitherto had been widely deployed and effective for more than 30 years (*2*, *3*). Ug99 and subsequent mutational derivatives that overcame additional resistance genes raised concerns of a disease epidemic that could devastate wheat crops, which provide 20% of the world's caloric intake. More than 50 *Pgt* resistance (*R*) loci, including those introgressed from wild relatives such as *Aegilops tauschii*, have been cataloged in wheat.

The *Pgt R* gene, *Sr33*, discovered from *Ae. tauschii*, the diploid progenitor of the D genome in hexaploid wheat (*4*, *5*), was introgressed into common wheat (*Triticum aestivum*, genomes AABBDD). There, *Sr33* provides a valuable, intermediate level of resistance to diverse *Pgt* races, including the Ug99 lineage (*6*). To isolate the *Sr33* gene, we used a single-chromosome substitution genetic stock, CS1D5405, which has chromosome 1D of wheat cv Chinese Spring (CS) replaced by the corresponding chromosome bearing *Sr33*

[1]Commonwealth Scientific and Industrial Research Organization (CSIRO) Plant Industry, General Post Office Box 1600, Canberra, ACT 2601, Australia. [2]The University of Sydney Plant Breeding Institute–Cobbitty, PB4011, Narellan, NSW 2567, Australia. [3]Department of Plant Sciences, University of California, Davis, CA 95616, USA. [4]Department of Plant Sciences and Plant Pathology, Montana State University, Bozeman, MT 59717, USA. [5]Institute of Crop Science, Chinese Academy of Agricultural Sciences, Beijing 100081, China. [6]State Key Laboratory of Crop Stress Biology for Arid Areas and College of Life Sciences, Northwest Agriculture and Forestry University, Yangling, Shaanxi 712100, China.

*Corresponding author. E-mail: evans.lagudah@csiro.au

from *Ae. tauschii* accession RL5288, to generate a recombinant inbred family segregating for *Sr33* (*5*). We identified 30 progeny, from an estimated 2850 gametes of this family, that contained recombination events between expressed sequence tag markers BE405778 and BE499711, which flank the 1 cM region that contains *Sr33*.

We used an amplified fragment-length polymorphism (AFLP) marker derived from a dehydrin gene located 0.04 cM from *Sr33* to initiate the construction of a physical map of the *Sr33* locus by screening a bacterial artificial chromosome (BAC) library of *Ae. tauschii* accession AL8/78 (*7*). A BAC contig, ctg4713, was identified that contained several genes, including a coiled-coil nucleotide-binding leucine-rich repeat (*CNL*) gene designated as *Ae. tauschii* resistance gene analog 1a (*AetRGA1a*) (Fig. 1). We rescreened the BAC library with an *AetRGA1a* probe to identify contig ctg5455, which contained three additional *RGA1* members (designated as *AetRGA1b-d*) that cosegregate with *Sr33* (Fig. 1). We screened a second BAC library from *Ae. tauschii* accession AUS18913 (*8*) to identify two additional cosegregating *RGA1* members (*AetRGA1e* and *AetRGA1f*) and two other *RGAs* unrelated to the *RGA1* family (designated as *AetRGA2a* and *AetRGA3a).* The three *RGA* families (*RGA1* through *3*) present at the *Sr33* locus are syntenic and orthologous to three *CNL* genes (*RGH1* through *3*) present at the barley *Mla* locus. The *RGH1* family includes the *Mla* gene, which provides resistance to *Blumeria graminis* f. sp. *hordei* (*Bgh*), the causal agent of barley powdery mildew (*9*). More than 30 variants of the *Mla* gene exist, each conferring specific resistance to different races of *Bgt* (*10*). The cDNA of *AetRGA2a* carries an unusual C terminal, absent from the related barley gene (*RGH2a*), that has 80% identity to the Exo70 subunit of exocyst complex present in *T. urartu* (*11*) (fig. S1).

We mutagenized CS1D5405 with ethyl methane sulfonate (EMS) and identified nine mutants that had lost *Sr33* resistance to Ug99 (table S1). Five mutants (E1 to E5) contained deletions that removed *AetRGA1b*, *AetRGA1c*, *AetRGA1e*, *AetRGA2a*, and *AetRGA3a* (Fig. 2). We found no evidence for deletions of these five genes in the remaining four mutants (E6 to E9), but those four mutants did show nucleotide changes relative to the wild-type sequence in *AetRGA1e*. Mutants E6 and E7 had single, unique missense mutations in the P-loop domain of the predicted protein, whereas mutants E8 and E9 had missense mutations in RNBS-B and GLPL motifs of the nucleotide-binding site (NBS) domain, respectively (fig. S2). To further confirm that *AetRGA1e* is the *Sr33* gene, we produced 20 independent *AetRGA1e* transgenic lines in the Fielder wheat cultivar, which is susceptible to the Australian *Pgt* race 98-1,2,3,5,6 (Fig. 2). When challenged with *Pgt*, each transgenic line exhibited a partial-resistance phenotype characteristic of *Sr33.* In subsequent generations, this resistance phenotype cosegregated with the *AetRGA1e* transgene, which we hereafter refer to as the *Sr33* gene (Fig. 2).

RNA-based polymerase chain reaction analyses indicated that *Sr33* encodes six exons (fig. S2), and the predicted protein contains motifs that are conserved in barley and *T. monococcum* mildew A (MLA) proteins and other CNL proteins (*10*, *12*). The SR33 protein shows greatest similarity (86%) to the MLA-like protein present in *T. monococcum* (TmMLA) but shows little homology to previously characterized wheat leaf rust (*P. triticina*) resistance proteins leaf rust resistance (LR) 1, LR10 and LR21, which are also members of the CNL protein class (fig. S3). Among the barley MLA family, SR33 is most similar to MLA34 (80% similarity).

Some MLA proteins of barley require the chaperone proteins RAR1, SGT1, and HSP90 for function (*13*), as does the wheat LR21 protein (*14*). No compromised *Sr33* resistance was apparent when these three chaperone genes were each independently silenced in CS1D5405 using a viral-induced gene silencing (VIGS) assay (fig. S4) that reduced the transcript accumulation of these genes by 50 to 80% (table S2). In contrast, targeted degradation of *Sr33* transcripts by VIGS resulted in increased susceptibility to *Pgt* infection. In addition, no evidence of direct interaction between SR33 and these chaperones was observed by yeast two-hybrid assays (fig. S5), providing genetic and biochemical evidence that SR33 immunity function is independent of this chaperone complex. Yeast hybrid assays also showed that the coiled-coil (CC) domain of SR33, unlike MLA10, do not homodimerize and do not interact with the WRKY transcription factors that interact with both MLA10 and TmMLA1 (fig. S5). Thus, the apparent structural similarities between SR33 and MLA proteins do not predict functional requirements.

CNL proteins frequently induce cell death in response to infection with an avirulent pathogen, which can be observed microscopically as autofluorescence of dead cells. Our microscopic analysis, however, did not identify an extensive hypersensitive cell death response associated with the partial resistance conferred by *Sr33* compared with the response elicited by the more effective stem rust resistance gene *Sr45*. The majority of *Pgt* infection sites on the *Sr45*-containing genotype CS1D5406 were surrounded by autofluorescent cells, indicative of cell death, whereas very little autofluorescence was observed on the *Sr33*-containing genotype (fig. S6).

We used the *Sr33* sequence to search for similar sequences from a collection of 368 *Ae. tauschii* accessions from various geographical locations spanning the natural distribution of the species. Gene sequences were obtained from 36 accessions with no amplification product from the remaining 332 lines, which suggests that the latter accessions either encode highly divergent

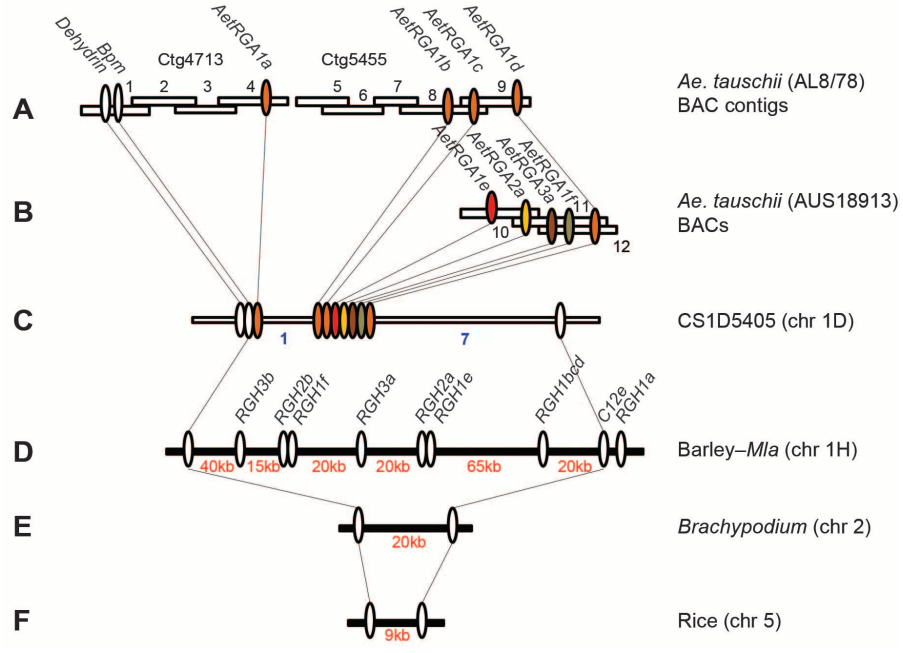

Fig. 1. Synteny between (C) wheat (CS1D5405) 1DS region carrying *Sr33* and (A) *Ae. tauschii* (AL8/78) BAC contigs, (B) *Ae. tauschii* (AUS18913) BACs, (D) barley, (E) *Brachypodium*, and (F) rice. The ovals in orange represent the members of *AetRGA1* class, in yellow for *AetRGA2*, and in brown and gray the pseudo genes *AetRGA3a* and *AetRGA1f*, respectively. The *Sr33* gene *AetRGA1e* is indicated by the red oval. Numbers in blue indicate the number of recombinants among 2850 gametes and in red the physical distance in kilobases. Numbers in black indicate the *Ae. tauschii* BACs. The order of *AetRGA1d* through *AetRGA1d* in CS1D5405 was inferred from the mapping information on the small interstitial deletion mutant E5 and BAC sequences from accessions AL8/78 and AUS18913.

variants or lack the gene. Of the 36 accessions, 7 contained sequences identical to the original *Sr33* source (sequence I). A second sequence variant, present in accession PI603225, differed from sequence I by a single amino acid at position 588. A third sequence variant, identified in 20 accessions, contained six amino acid substitutions in the leucine-rich repeat (LRR) region (fig. S7). A fourth variant, identified in three Russian accessions, contained several amino acid substitutions in both the NBS and LRR regions. A fifth sequence, present in five Iranian accessions, encoded a truncated protein. Sequence variants I to III were present in accessions collected in the southern coastal region of the Caspian Sea. Only sequences I and II out of the five variants conferred *Pgt* resistance against multiple races (tables S3 and S4). In allelism tests involving PI603225 and the original *Sr33* donor, no susceptible plants were obtained in the progeny, further indicating that sequence variants I and II constitute allelic forms (*15*).

The wheat *Sr33*, barley, and *T. monococcum Mla* genes are examples of orthologous *CNL* genes evolving to recognize divergent pathogen species. Previous genetic studies have mapped *Pgt R* genes *Sr31* and *SrR* (now designated *Sr50*) to a locus in rye chromosome 1S where a *Mla*-related gene family is also present. These rye chromosomal segments have been introgressed into wheat and serve as additional sources of *Pgt* resistance (*16*). It is possible that *Sr33*, *Sr31*, and *Sr50* constitute a homeologous set of *Mla*-like *Pgt R* genes. Ug99 inflicts heavy damage to plants with only *Sr31* but is avirulent on plants with *Sr33* and *Sr50.* Thus, the isolation of these *Pgt R* genes may lead to better understanding of how the plant immune response adapts to virulence changes in *Pgt*.

Combining resistance genes to develop durable resistance is the prevailing strategy for gene deployment in wheat. We have previously demonstrated additive resistance when *Sr33* was combined with *Sr2*, an adult plant, partial, race-nonspecific *Pgt* gene that has provided durable resistance for more than 70 years (*17*). Preferably, *Sr33* should be deployed together with genes like *Sr2* to maintain its longevity. No *Pgt* race is virulent on plants containing both *Sr33* and the *Sr35* gene identified in the companion paper (*18*), because collectively these two genes provide resistance to all known *Pgt* races when codeployed. This feature, coupled with the strong immune response of *Sr35* against the Ug99 group of races, makes it very attractive to combine *Sr33* and *Sr35* as cisgenes at a single locus, an approach greatly facilitated by recent advances in Agrobacterium-mediated transformation of this species, and transferred into a wheat background carrying the *Sr2* gene.

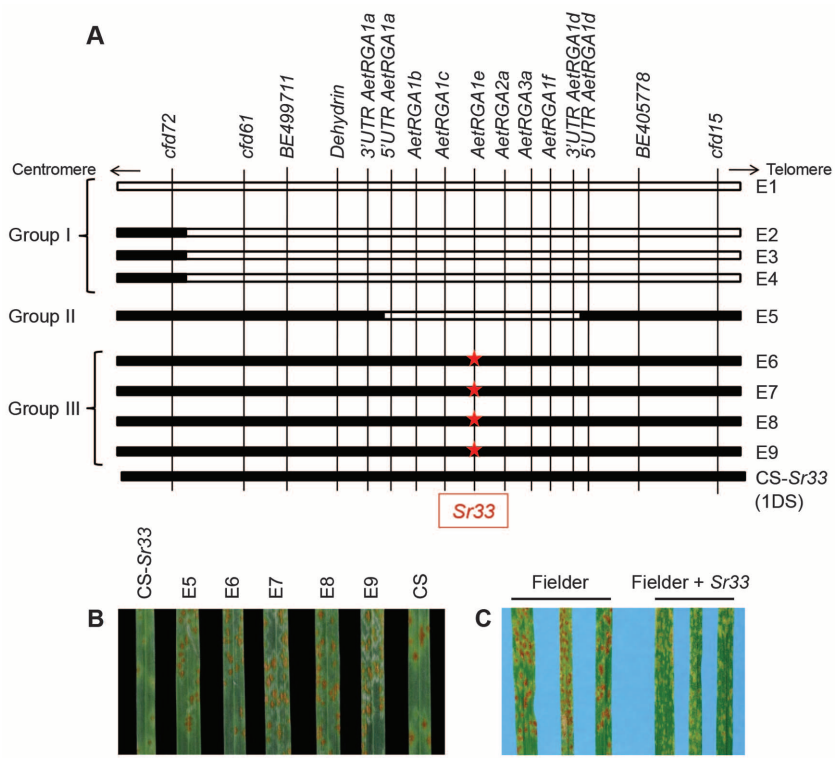

Fig. 2. (A) Groups of *Sr33*-susceptible mutants generated through EMS treatment. Open bars indicate the length of chromosome 1DS segment lost due to mutation, and the stars in red represent the single-nucleotide polymorphism (SNP) change. Group I consists of mutants with large chromosome segments; group II is mutants with a small interstitial deletion; and group III represents the four mutants carrying SNP changes. (**B**) Stem rust response of *Sr33* carrying line (CS1D5405, designated as CS-*Sr33*) and the EMS mutants against Ug99 (TTKSK). Mutant lines with the short interstitial deletion (E5) and with SNP changes (E6, E7, E8, and E9) show a clear susceptible reaction as seen on CS. (**C**) Rust infection response of transgenic wheat cv Fielder against the Australian stem rust race 98-1, 2, 3, 5, and 6. Fielder sib lines without *Sr33* show clear susceptibility, and lines carrying the *Sr33* genomic clone show the typical *Sr33*-mediated stem rust resistance.

References and Notes

1. P. G. Pardey *et al.*, *Science* **340**, 147–148 (2013).
2. Y. Jin, R. P. Singh, *Plant Dis.* **90**, 476–480 (2006).
3. R. P. Singh *et al.*, *Annu. Rev. Phytopathol.* **49**, 465–481 (2011).
4. E. R. Kerber, *Crop Sci.* **27**, 204–206 (1987).
5. S. S. Jones, J. Dvorak, D. R. Knott, C. O. Qualset, *Genome* **34**, 505–508 (1991).
6. M. N. Rouse, E. L. Olson, B. S. Gill, M. O. Pumphrey, Y. Jin, *Crop Sci.* **51**, 2074–2078 (2011).
7. M. C. Luo *et al.*, *Genomics* **82**, 378–389 (2003).
8. O. Moullet, H. B. Zhang, E. S. Lagudah, *Theor. Appl. Genet.* **99**, 305–313 (1999).
9. F. Wei, R. A. Wing, R. P. Wise, *Plant Cell* **14**, 1903–1917 (2002).
10. S. Seeholzer *et al.*, *Mol. Plant Microbe Interact.* **23**, 497–509 (2010).
11. H. Q. Ling *et al.*, *Nature* **496**, 87–90 (2013).
12. T. Jordan *et al.*, *Plant J.* **65**, 610–621 (2011).
13. K. Shirasu, *Annu. Rev. Plant Biol.* **60**, 139–164 (2009).
14. S. R. Scofield, L. Huang, A. S. Brandt, B. S. Gill, *Plant Physiol.* **138**, 2165–2173 (2005).
15. E. L. Olson *et al.*, *Theor. Appl. Genet.* **126**, 1179–1188 (2013).
16. R. Mago *et al.*, *Theor. Appl. Genet.* **104**, 1317–1324 (2002).
17. M. Ayliffe *et al.*, *Mol. Plant Microbe Interact.* **26**, 658–667 (2013).
18. C. Saintenac *et al.*, *Science* **341**, 783–786 (2013).

Acknowledgments: This work was supported in part by funds provided through a grant from the Borlaug Global Rust Initiative (BGRI) Durable Rust Resistance in Wheat (DRRW) Project (administered by Cornell University with a grant from the Bill & Melinda Gates Foundation and the UK Department for International Development); Office of the Chief Executive (OCE) Post Doctoral Fellowship of CSIRO, Australia; Grains Research and Development Corporation, Australia; Endeavor International Postgraduate Research Scholarship of Department of Education, Science and Training (DEST) and Sydney University, Australia; Australian Centre for International Agricultural Research project (CIM2007/084). X.W. acknowledges support from the Basic Research to Enable Agricultural Development Program of the National Science Foundation (NSF) of the United States (IOS-0965429) and partial support from NSF Plant Genome Research Program grant DBI-0701916 (J.D. is principal investigator). We are grateful to M. Rouse (USDA-ARS Cereal Disease Laboratory) for the tests with Ug99 and derived races. We thank N. Upadhyaya, A. Ashton, S. Chandramohan, L. Viccars, T. Richardson, K. Newell, H. Miah, and X. Xia for technical assistance. Sequences of Resistance Gene Analog (RGA) genes from *Ae. tauschii* and hexaploid wheats were deposited in GenBank under accession numbers KF031279 to KF031303.

Supplementary Materials

www.sciencemag.org/cgi/content/full/science.1239028/DC1
Materials and Methods
Figs. S1 to S7
Tables S1 to S6
References (*19*–*39*)

11 April 2013; accepted 7 June 2013
Published online 27 June 2013;
10.1126/science.1239028

A Long Noncoding RNA Mediates Both Activation and Repression of Immune Response Genes

Susan Carpenter,[1,2] Daniel Aiello,[1] Maninjay K. Atianand,[1] Emiliano P. Ricci,[3] Pallavi Gandhi,[1] Lisa L. Hall,[4] Meg Byron,[4] Brian Monks,[1] Meabh Henry-Bezy,[1] Jeanne B. Lawrence,[4] Luke A. J. O'Neill,[2] Melissa J. Moore,[3] Daniel R. Caffrey,[1]*† Katherine A. Fitzgerald[1]*†

An inducible program of inflammatory gene expression is central to antimicrobial defenses. This response is controlled by a collaboration involving signal-dependent activation of transcription factors, transcriptional co-regulators, and chromatin-modifying factors. We have identified a long noncoding RNA (lncRNA) that acts as a key regulator of this inflammatory response. Pattern recognition receptors such as the Toll-like receptors induce the expression of numerous lncRNAs. One of these, lincRNA-Cox2, mediates both the activation and repression of distinct classes of immune genes. Transcriptional repression of target genes is dependent on interactions of lincRNA-Cox2 with heterogeneous nuclear ribonucleoprotein A/B and A2/B1. Collectively, these studies unveil a central role of lincRNA-Cox2 as a broad-acting regulatory component of the circuit that controls the inflammatory response.

The innate immune system coordinates host defenses through germ line–encoded pattern recognition receptors [e.g., Toll-like receptors (TLRs)], which recognize microbial products and induce the expression of hundreds of proteins involved in antimicrobial defense and adaptive immunity (*1*–*3*). Recent studies have identified thousands of long noncoding RNAs (lncRNAs) in mammalian genomes (*4*–*9*) that regulate gene expression in different biological processes [reviewed in (*5*)]. lncRNAs are differentially regulated in virus-infected cells (*10*) and in dendritic cells after lipopolysaccharide (LPS) stimulation (*4*). Recently, the lncRNA NeST was shown to control susceptibility to Theiler's virus and *Salmonella* infection in mice through epigenetic regulation of the interferon-γ (IFN-γ) locus (*11*, *12*). Although lncRNAs can be induced in innate immune cells (*4*, *10*), whether lncRNAs act as regulators of gene expression in innate immunity is unknown.

To identify lncRNAs transcribed during the innate immune response, we conducted whole-transcriptome analysis (RNA-seq) (*6*) of mouse bone marrow–derived macrophages (BMDMs) stimulated with the synthetic bacterial lipopeptide Pam_3CSK_4, a Tlr2 ligand (Fig. 1A). Pam_3CSK_4 induced the transcription of numerous protein-coding genes involved in the immune response (Fig. 1A, inner track), as well as 62 lncRNAs (Fig. 1A, outer track, and table S1). The most significantly induced lncRNAs tended to occur in chromosomal regions where we also detected higher expression of immune genes, which suggests that these genes are co-regulated. lincRNA-Cox2 was among the most highly induced lncRNAs and is proximal to the prostaglandin-endoperoxide synthase 2 [*Ptgs2*(*Cox2*)] gene (Fig. 1A); lncRNA-Ehd1 and lncRNA-Lyn were also induced after Tlr2 and Tlr4 stimulation (fig. S1, A and B).

A previous study demonstrated that lincRNA-Cox2 was induced in dendritic cells after stimulation with LPS (*4*). However, whether lincRNA-Cox2 regulates the inflammatory response that is associated with TLR signaling is unknown. We identified three splice variants of lincRNA-Cox2 (Fig. 1B; GenBank accession numbers JX682706, JX682707, and JX682708). Variant 1 was the most abundant transcript containing exons 1 and 4, common to all splice variants. Consequently, we designed primers for quantitative PCR (qPCR) and short hairpin RNA (shRNA) that targeted these regions. Using qPCR, we confirmed that LPS induced similar temporal patterns of expression of both lincRNA-Cox2 and its neighboring *Ptgs2* (*Cox2*) gene in bone marrow–derived dendritic cells (BMDCs, Fig. 1, C and D). R848, a synthetic antiviral compound that activates Tlr7/8, induced lincRNA-Cox2 and *Ptgs2* (*Cox2*) in BMDCs, whereas polyinosinic-polycytidylic acid, a synthetic double-stranded RNA that activates Tlr3, had no effect (fig. S2, A to D). Both *Listeria monocytogenes*–infected BMDMs and splenocytes from *Listeria*-infected mice also had elevated levels

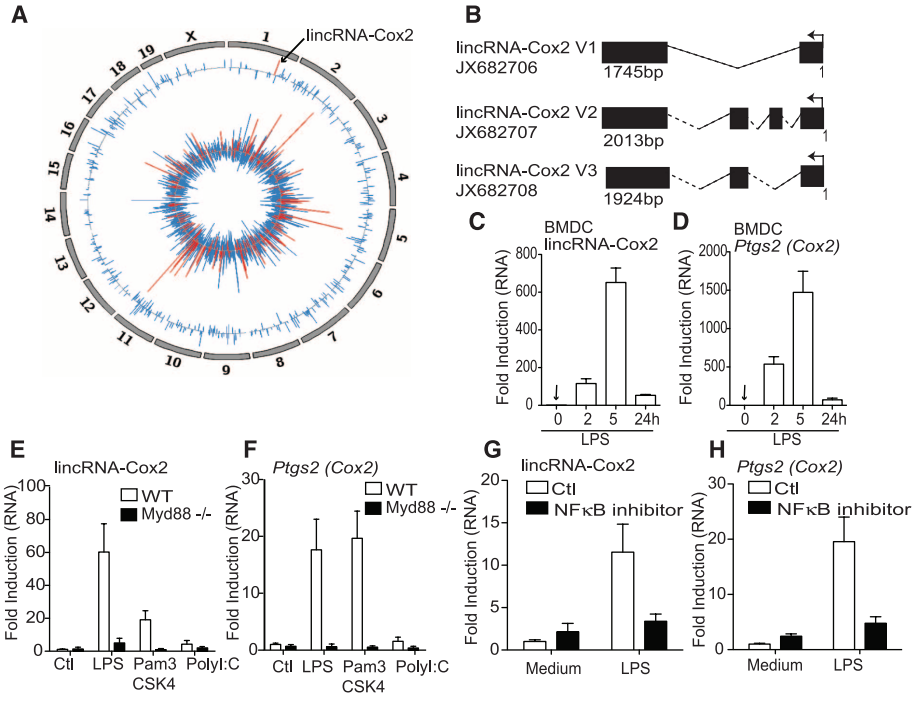

Fig. 1. lincRNA-Cox2 expression is induced by Tlr ligands in a MyD88- and NF-κB–dependent manner. (**A**) The Circos plot shows genome-wide differential expression (RNA-seq) between untreated and Pam_3CSK_4 (Tlr1/2)–stimulated (5 hours) BMDMs. The inner track shows $\log_2$ relative change for protein-coding genes that are classified into immune genes (red; see supplementary materials) and other genes (blue). The outer track shows $\log_2$ relative change for all lncRNAs. lincRNA-Cox2 is highlighted in red on chromosome 1 (arrow). (**B**) lincRNA-Cox2 encodes three splice variants. (**C** and **D**) RNA was extracted from primary BMDCs stimulated with LPS for 0, 2, 5, or 24 hours. Expression levels of lincRNA-Cox2 (C) and *Ptgs2* (*Cox2*) (D) were examined by qRT-PCR and expressed relative to time 0 hours (which was set to 1, indicated by arrow). (**E** and **F**) Induction of lincRNA-Cox2 and *Ptgs2* (*Cox2*) after qRT-PCR on BMDMs obtained from wild-type (WT) or *Myd88*$^{-/-}$ mice. (**G** and **H**) BMDMs were treated for 30 min with a NF-κB inhibitor (1 μg/ml), followed by stimulation with LPS (100 ng/ml); expression levels of lincRNA-Cox2 (G) and *Ptgs2* (*Cox2*) (H) were examined by qRT-PCR. Data represent means ± SD from three independent experiments.

[1]Division of Infectious Diseases and Immunology, Department of Medicine, University of Massachusetts Medical School, Worcester, MA 01605, USA. [2]School of Biochemistry and Immunology, Trinity College Dublin, Dublin 2, Ireland. [3]Howard Hughes Medical Institute, University of Massachusetts Medical School, Worcester, MA 01605, USA. [4]Department of Cell and Developmental Biology, University of Massachusetts Medical School, Worcester, MA 01605, USA.

*These authors contributed equally to this work.
†Corresponding author. E-mail: kate.fitzgerald@umassmed.edu (K.A.F.); daniel.caffrey@umassmed.edu (D.R.C.)

of lincRNA-Cox2 (fig. S3, A and B). Induction of lincRNA-Cox2 and its neighboring gene *Ptgs2* (*Cox2*) was dependent on the Tlr adaptor protein MyD88 (Fig. 1, E and F) and transcription factor NF-κB signaling (Fig. 1, G and H).

We next examined the protein-coding capacity of lincRNA-Cox2 by assessing its association with polysomes within cells. BMDMs were treated with cycloheximide to trap ribosomes on RNA molecules and either left untreated or pretreated with EDTA (disrupting all RNA-protein interactions) or with harringtonine (specifically disrupting translation). Cell lysates were fractionated and RNA analyzed by qPCR (*13*–*15*). We compared *Gapdh* mRNA with lincRNA-Cox2 and another lincRNA, lncRNA-Eps, which had previously been shown to be noncoding (*16*). As expected, *Gapdh* mRNA sedimented with a high velocity through the sucrose gradient because it was associated with polysomes. In contrast, lincRNA-Cox2 and lncRNA-Eps remained in lighter fractions (fig. S4). Treatment with EDTA or harringtonine resulted in a shift of *Gapdh* mRNA, but not lincRNA-Cox2 or lncRNA-Eps, from the higher-velocity to the lower-velocity fractions. Furthermore, most of the open reading frames identified in lincRNA-Cox2 were found to have poor Kozak strength (fig. S5). Collectively, these studies indicate that lincRNA-Cox2 is unlikely to encode a protein product.

We next generated BMDM cell lines in which lincRNA-Cox2 expression was silenced by shRNA (Fig. 2A). Silencing of lincRNA-Cox2 did not alter expression of *Ptgs2* (*Cox2*) (fig. S6). To identify potential targets of lincRNA-Cox2, we conducted RNA-seq in both control and lincRNA-Cox2–silenced cells before and after stimulation with Pam_3CSK_4. Silencing of lincRNA-Cox2 increased the expression of 787 genes by a factor of 3 or greater in unstimulated cells (table S2). A Gene Ontology (GO) enrichment analysis indicated that genes related to the immune response were significantly overrepresented in these up-regulated genes (Fig. 2B and table S3). This gene set included chemokines (*Ccl5*, *Cx3cl1*), chemokine receptors (*Ccrl*), and IFN-stimulated genes (ISGs) (*Irf7*, *Oas1a*, *Oas1l*, *Oas2*, *Ifi204*, and *Isg15*) (Fig. 2B). In the same cells stimulated with Pam_3CSK_4, silencing of lincRNA-Cox2 resulted in attenuated expression of 713 genes by a factor of 3 or greater (table S4). Examples of these genes include *Tlr1*, *Il6* (interleukin-6), and *Il23a*.

We confirmed these findings by means of an RNA profiling technology to simultaneously analyze mRNA expression levels of differentially regulated genes (nCounter; Nanostring, Seattle, WA). In unstimulated cells, silencing of lincRNA-Cox2 led to a marked increase in expression of *Irf7*, *Ccl5* (*Rantes*), and ISGs relative to control cells (Fig. 2C, columns 1 and 2, and fig. S7), whereas the Pam_3CSK_4-induced expression of *Tlr1* and *Il6* was attenuated (Fig. 2C, columns 3 and 4). We confirmed these findings in three independent shRNA lines by measuring protein levels for Ccl5 (Rantes) and Il6 (Fig. 2, D and

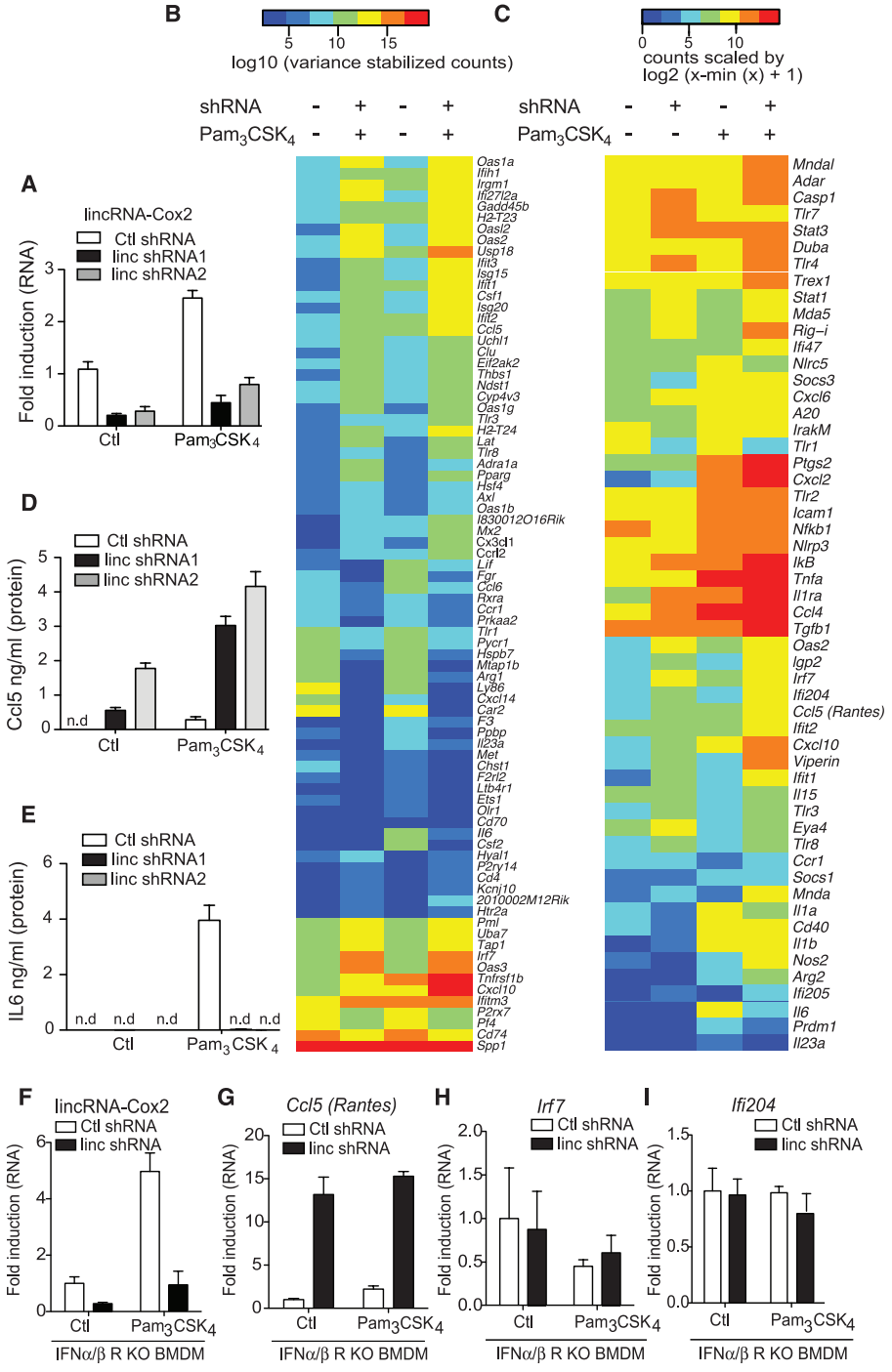

Fig. 2. lincRNA-Cox2 is a major regulator of immune genes. (**A**) qRT-PCR was carried out on BMDMs stably expressing lentiviral shRNA specific to lincRNA-Cox2 (shRNA) or a control shRNA. Expression of lincRNA-Cox2 was measured. (**B**) RNA-seq analysis on lincRNA-Cox2 knockdown or control shRNA BMDMs that were either stimulated with Pam_3CSK_4 or unstimulated. The heat map shows mRNA levels for genes annotated in GO as immune genes. These genes are among the top 50 up-regulated immune genes in unstimulated cells when lincRNA-Cox2 was silenced or the top 50 down-regulated immune genes in stimulated cells when lincRNA-Cox2 was silenced. The 100 genes were ranked according to absolute values of $\log_2$ relative change; the top 80 differentially expressed genes are displayed. (**C**) Heat map representation of differentially regulated genes performed on RNA extracted from control or lincRNA-Cox2 knockdown cells stimulated with Pam_3CSK_4 for 5 hours. (**D** and **E**) Cells were stimulated with Pam_3CSK_4 for 24 hours, and Ccl5 (D) and Il6 (E) levels were measured in lincRNA-Cox2 knockdown cells by enzyme-linked immunosorbent assay (ELISA) (n.d., not detected). (**F** to **I**) lincRNA-Cox2 was silenced in IFN α/β receptor (IFN α/β R) KO cells. Expression levels of lincRNA-Cox2 (F), *Ccl5* (G), *Irf7* (H), and *Ifi204* (I) were measured by qRT-PCR. Data represent means ± SD from three independent experiments.

E, and fig. S8). In contrast to these genes, the Tlr2-dependent induction of Il1β was unaffected in cells deficient in lincRNA-Cox2 (fig. S9). We also observed reduced Il6 in macrophages stimulated with R848 and Pam_2CSK_4 (a ligand that activates a Tlr2-Tlr6 heterodimer) (fig. S10). We next silenced lincRNA-Cox2 in macrophages lacking the type I IFN α/β receptor (IFN α/βR KO) in order to distinguish between IFN-dependent and IFN-independent targets of lincRNA-Cox2 (Fig. 2, F to I, and fig. S11, A and B). *Ccl5* was regulated by lincRNA-Cox2 independently of type I IFN signaling, whereas regulation of *Irf7* and *Ifi204* appeared to be secondary to type I IFN signaling. Despite the elevated expression of IFN pathway components, silencing of lincRNA-Cox2 did not render cells permissive to Tlr2-induced TBK1 activation, a measure of Irf3 signaling (fig. S12). Finally, because shRNA silencing of lincRNA-Cox2 led to decreased expression of Tlr1, we wanted to eliminate the possibility that we inadvertently impaired Pam_3CSK_4 signaling via the Tlr1-Tlr2 heterodimer. We restored expression of Tlr1 in lincRNA-Cox2–silenced cells and confirmed that the differential regulation of Ccl5 and Il6 was not due to impaired expression of Tlr1 (fig. S13). Taken together, these data indicate that lincRNA-Cox2 regulates distinct classes of immune genes both basally and after TLR stimulation.

We next conducted "gain-of-function" studies by generating macrophages that ectopically expressed lincRNA-Cox2 (Fig. 3A). Macrophages that ectopically expressed lincRNA-Cox2 had decreased levels of *Ccl5*, *Irf7*, and other ISGs (Fig. 3B). *Il6* was not detected when lincRNA-Cox2 was overexpressed in unstimulated cells. However, *Il6* levels were significantly enhanced when lincRNA-Cox2 was overexpressed in Pam_3CSK_4 stimulated cells (Fig. 3C). These results further demonstrate that lincRNA-Cox2 represses Ccl5 while simultaneously enhancing the expression of TLR-induced Il6.

lncRNAs can be found in the nucleus, cytoplasm, or both compartments (*17*–*19*). We examined the localization of lincRNA-Cox2 in macrophages by performing quantitative reverse

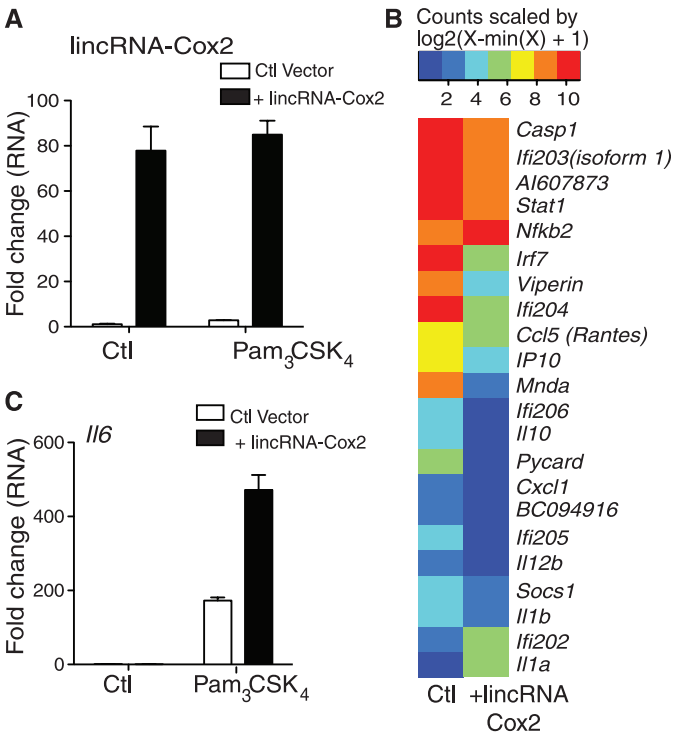

Fig. 3. Differential gene expression after overexpression of lincRNA-Cox2. (**A**) A BMDM cell line stably overexpressing lincRNA-Cox2 or a control vector was generated. qRT-PCR was carried out and overexpression of lincRNA-Cox2 was confirmed. (**B**) Heat map representation of differentially regulated genes from control or lincRNA-Cox2–overexpressing BMDMs. (**C**) qRT-PCR was carried out on control or lincRNA-Cox2–overexpressing cells stimulated with Pam_3CSK_4 for 5 hours. Data represent means ± SD from three independent experiments.

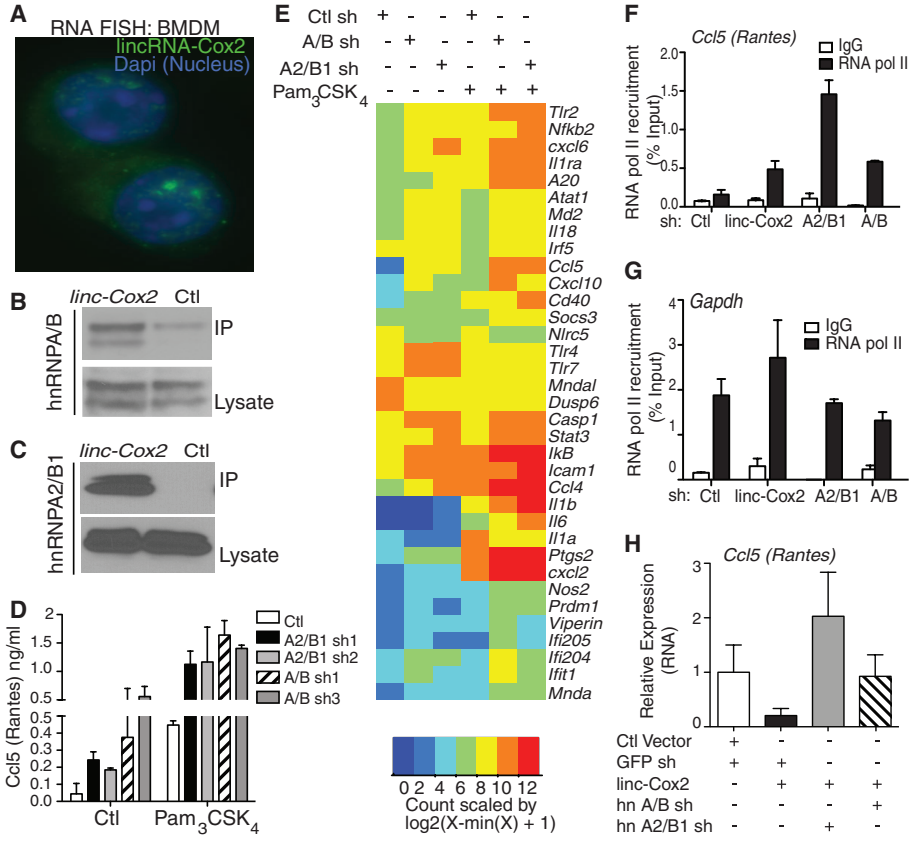

Fig. 4. lincRNA-Cox2 is localized to both the cytosolic and nuclear compartments and interacts with hnRNP-A/B and A2/B1 to regulate immune genes. (**A**) BMDMs were labeled with a lincRNA-Cox2 probe via RNA FISH and counterstained with 4′,6-diamidino-2-phenylindole (DNA to visualize the nucleus). (**B** and **C**) Biotinylated lincRNA-Cox2 or antisense RNA was incubated with nuclear extracts, and interaction with endogenous hnRNP-A/B (B) or hnRNP-A2/B1 (C) was assessed after immunoprecipitation and Western blot (upper panels). Expression levels of hnRNP-A/B (B) or hnRNP-A2/B1 (C) (lower panels) in input lysates were also examined. (**D**) Cell lines with shRNA targeting hnRNP-A/B or hnRNP-A2/B1 were stimulated with Pam_3CSK_4; Ccl5 production was measured in these cells by ELISA. (**E**) Heat map representation of differentially regulated genes of control shRNA–, hnRNP-A/B shRNA–, or hnRNP-A2/B1 shRNA–expressing BMDMs stimulated with Pam_3CSK_4 (100 nM) for 5 hours. (**F** and **G**) Recruitment of RNA Pol II to the Ccl5 promoter as determined by ChIP analysis in cells expressing shRNA targeting lincRNA-Cox2, hnRNP-A/B, or hnRNP-A2/B1. (**H**) hnRNP-A/B or hnRNP-A2/B1 was knocked down using lentiviral shRNA in lincRNA-Cox2–overexpressing BMDMs; *Ccl5* expression levels were measured using qRT-PCR. Data are representative of three separate experiments.

transcription PCR (qRT-PCR) on RNA isolated from nuclear or cytosolic fractions (fig. S14). Using RNA fluorescence in situ hybridization (FISH), substantial amounts of lincRNA-Cox2 were visible in both the nuclear and the cytosolic compartments of macrophages (Fig. 4A and fig. S15, A and B). Analysis of published RNA-seq data from nuclear and cytosolic fractions of macrophages (*20*) confirmed that lincRNA-Cox2 was present in both compartments, unlike Neat1, which was exclusively nuclear (fig. S16). RNA FISH analysis demonstrated efficient targeting of lincRNA-Cox2 in the nuclear fractions of our shRNA-silenced cells (fig. S15, C to F).

Many lncRNAs regulate transcription through their interactions with chromatin-modifying complexes or with heterogeneous nuclear ribonucleoproteins (hnRNPs) (*5*, *21*–*23*). To identify binding partners for lincRNA-Cox2, we incubated in vitro–transcribed biotinylated lincRNA-Cox2 as well as an antisense lincRNA-Cox2 control RNA with nuclear or cytosolic extracts of macrophages and subjected RNA binding proteins to mass spectrometry for identification. hnRNP-A/B and hnRNP-A2/B1 were identified as specific binding partners for lincRNA-Cox2 in both the nuclear and cytosolic fractions (fig. S17). The ability of hnRNP-A/B and hnRNP-A2/B1 to bind lincRNA-Cox2 was confirmed by Western blot analysis (Fig. 4, B and C).

hnRNPs are multifunctional nuclear RNA binding proteins involved in various aspects of RNA biology (*24*, *25*). hnRNPs also act as mediators of lncRNA-induced transcriptional repression (*22*, *23*). hnRNP-A/B has been linked to transcriptional repression of some genes (*26*, *27*), and hnRNP-A2/B1 and hnRNP-A/B have been shown to associate (*28*). Therefore, we hypothesized that lincRNA-Cox2 regulates the transcription of immune genes by associating with these hnRNPs. To test this directly, we generated macrophages lacking expression of hnRNP-A/B or hnRNP-A2/B1 by shRNA (fig. S18, A and B). Knockdown of hnRNP-A/B and hnRNP-A2/B1 did not modulate the levels of lincRNA-Cox2 itself (fig. S19) but did result in an enhancement of Ccl5 protein levels in both unstimulated and Pam_3CSK_4-stimulated cells (Fig. 4D). Multiplex RNA analysis also revealed elevated levels of *Ccl5*, *Stat1*, *Tlr7*, *Icam1*, and *IκB* in hnRNP-silenced macrophages (Fig. 4E). There was considerable overlap between genes that were regulated by lincRNA-Cox2 and these two hnRNP proteins (fig. S20 and table S5). We also examined the occupancy of RNA polymerase II at the promoters of the *Ccl5* and *Irf7* genes using chromatin immunoprecipitation (ChIP) and found increased levels of RNA polymerase II (Pol II) at the *Ccl5* and *Irf7* promoters when lincRNA-Cox2 or either of the hnRNPs were silenced in unstimulated cells (Fig. 4, F and G, and fig. S21). The occupancy of RNA Pol II on the promoter of *Il6* was reduced when lincRNA-Cox2 but not hnRNP-A/B or A2/B1 was knocked down in Pam_3CSK_4-stimulated cells (fig. S22); this effect was consistent with hnRNPs having no effect on Pam_3CSK_4-induced *Il6* mRNA levels (Fig. 4E). Silencing of hnRNP-A2/B1 or hnRNP-A/B in cells that overexpressed lincRNA-Cox2 also reversed the inhibitory effect of lincRNA-Cox2 on *Ccl5* expression (Fig. 4H and fig. S23). Taken together, these experiments confirm that hnRNP-A/B and hnRNP-A2/B1 form a complex with lincRNA-Cox2 to repress the transcription of immune genes. The identification of hnRNP-A/B and hnRNP-A2/B1 further underscores the importance of hnRNPs in lncRNA function (*21*–*23*).

Innate immune responses have the capacity to both combat infectious microbes and drive pathological inflammation, which contributes to diseases such as atherosclerosis, autoimmunity, and cancer. A multitude of regulatory checkpoints control TLR signaling and inflammatory responses. We propose a model whereby TLR signaling induces lncRNAs, such as lincRNA-Cox2, that serve as repressors and activators of genes through their physical interactions with various regulatory complexes. As such, lncRNAs represent a component of the innate immune response that can both restrain and promote aspects of inflammatory signaling. Further characterization of these regulatory networks is likely to reveal novel drug targets and opportunities for therapeutic intervention in infectious and inflammatory diseases.

References and Notes

1. T. Kawai, S. Akira, *Ann. N.Y. Acad. Sci.* **1143**, 1–20 (2008).
2. R. Medzhitov, T. Horng, *Nat. Rev. Immunol.* **9**, 692–703 (2009).
3. P. J. Murray, S. T. Smale, *Nat. Immunol.* **13**, 916–924 (2012).
4. M. Guttman *et al.*, *Nature* **458**, 223–227 (2009).
5. J. L. Rinn, H. Y. Chang, *Annu. Rev. Biochem.* **81**, 145–166 (2012).
6. A. Mortazavi, B. A. Williams, K. McCue, L. Schaeffer, B. Wold, *Nat. Methods* **5**, 621–628 (2008).
7. M. Guttman *et al.*, *Nat. Biotechnol.* **28**, 503–510 (2010).
8. M. Guttman, J. L. Rinn, *Nature* **482**, 339–346 (2012).
9. E. Birney *et al.*, *Nature* **447**, 799–816 (2007).
10. X. Peng *et al.*, *mBio* **1**, e00206 (2010).
11. S. P. Collier, P. L. Collins, C. L. Williams, M. R. Boothby, T. M. Aune, *J. Immunol.* **189**, 2084–2088 (2012).
12. J. A. Gomez *et al.*, *Cell* **152**, 743–754 (2013).
13. N. T. Ingolia, G. A. Brar, S. Rouskin, A. M. McGeachy, J. S. Weissman, *Nat. Protoc.* **7**, 1534–1550 (2012).
14. N. T. Ingolia, S. Ghaemmaghami, J. R. Newman, J. S. Weissman, *Science* **324**, 218–223 (2009).
15. N. T. Ingolia, L. F. Lareau, J. S. Weissman, *Cell* **147**, 789–802 (2011).
16. W. Hu, B. Yuan, J. Flygare, H. F. Lodish, *Genes Dev.* **25**, 2573–2578 (2011).
17. J. Cheng *et al.*, *Science* **308**, 1149–1154 (2005).
18. Q. Wu *et al.*, *PLoS ONE* **3**, e2803 (2008).
19. R. Louro, A. S. Smirnova, S. Verjovski-Almeida, *Genomics* **93**, 291–298 (2009).
20. D. M. Bhatt *et al.*, *Cell* **150**, 279–290 (2012).
21. A. M. Khalil *et al.*, *Proc. Natl. Acad. Sci. U.S.A.* **106**, 11667–11672 (2009).
22. M. Huarte *et al.*, *Cell* **142**, 409–419 (2010).
23. Y. Hasegawa *et al.*, *Dev. Cell* **19**, 469–476 (2010).
24. G. Dreyfuss, M. Hentze, A. I. Lamond, *Cell* **85**, 963–972 (1996).
25. A. M. Krecic, M. S. Swanson, *Curr. Opin. Cell Biol.* **11**, 363–371 (1999).
26. C. Gao *et al.*, *J. Biol. Chem.* **279**, 11236–11243 (2004).
27. C. Gao, H. Guo, Z. Mi, P. Y. Wai, P. C. Kuo, *J. Immunol.* **175**, 523–530 (2005).
28. C. S. Raju *et al.*, *Mol. Biol. Cell* **19**, 3008–3019 (2008).

Acknowledgments: We thank N. Singh for advice on RNA-seq, A. J. Crawford for help with quantification of RNA FISH, and K. Jeffrey, L. Stuart, N. Silverman, D. Golenbock, and E. Lien for critical reading of this manuscript. The data presented in this paper are tabulated in the main paper and in the supplementary materials. All RNA-seq data are available for download from NCBI Gene Expression Omnibus (www.ncbi.nlm.nih.gov/geo/) under accession number GSE40978. Supported by Ireland Health Research Board/Marie Curie Fellowship MCPD/2010/04 (S.C.) and by NIH grants AI067497 (K.A.F.) and GM053234 (J.B.L.).

Supplementary Materials

www.sciencemag.org/cgi/content/full/science.1240925/DC1
Materials and Methods
Figs. S1 to S23
Tables S1 to S5
References (*29*–*35*)

23 May 2013; accepted 24 July 2013
Published online 1 August 2013;
10.1126/science.1240925

Cleavage of Fibrinogen by Proteinases Elicits Allergic Responses Through Toll-Like Receptor 4

Valentine Ongeri Millien,[1] Wen Lu,[2] Joanne Shaw,[5] Xiaoyi Yuan,[2] Garbo Mak,[3] Luz Roberts,[3] Li-Zhen Song,[3] J. Morgan Knight,[2] Chad J. Creighton,[4] Amber Luong,[5] Farrah Kheradmand,[1,2,3,6,7]* David B. Corry[1,2,3,6,7]*

Proteinases and the innate immune receptor Toll-like receptor 4 (TLR4) are essential for expression of allergic inflammation and diseases such as asthma. A mechanism that links these inflammatory mediators is essential for explaining the fundamental basis of allergic disease but has been elusive. Here, we demonstrate that TLR4 is activated by airway proteinase activity to initiate both allergic airway disease and antifungal immunity. These outcomes were induced by proteinase cleavage of the clotting protein fibrinogen, yielding fibrinogen cleavage products that acted as TLR4 ligands on airway epithelial cells and macrophages. Thus, allergic airway inflammation represents an antifungal defensive strategy that is driven by fibrinogen cleavage and TLR4 activation. These findings clarify the molecular basis of allergic disease and suggest new therapeutic strategies.

Allergic asthma is a chronic inflammatory airway disease that is characterized by both airway obstruction and enhanced systemic and airway allergic inflammation marked by interleukin-4 (IL-4)–secreting T helper 2 (T_H2) cells, eosinophils, and serum immunoglobulin

E (IgE). Proteinases able to elicit T_H2 cell–driven allergic responses are secreted by fungi (*1*) and can be found in natural sources linked to allergic disease such as pollens (*2*) and dust mite antigens like Der p 1 (*3*, *4*). Nonetheless, nonproteinase allergens such as ovalbumin also possess allergenic activity. Prior studies have linked TLR4, a microbial pattern-recognition receptor, to both proteinase-dependent and -independent allergic responses in mice (*5*–*7*), but a mechanism that explains the importance of proteinases and TLR4 in diverse allergic contexts involving both proteinase-active and -inactive allergens remains unknown.

To study the role of TLR4 in the context of proteinase-dependent allergic inflammation, we assessed wild-type (WT) and *Tlr4*$^{-/-}$ mice after intranasal exposure to a fungal proteinase derived from *Aspergillus oryzae* (PAO) [endotoxin content: 1.7×10^{-3} endotoxin units (EU)/μg]. Consistent with our prior observations (*2*), WT mice challenged with PAO developed canonical features of asthma, including airway hyperresponsiveness, airway infiltration by eosinophils, enhanced production of the mucin gene transcript *Muc5ac*, goblet cell metaplasia of the airway, and enhanced production of transcripts for the proinflammatory cytokines IL-4, IL-5, and IL-13 (fig. S1, A to G). In contrast, all of these allergic parameters, with the exception of lung IL-4 transcripts, were either attenuated or abrogated in *Tlr4*$^{-/-}$ mice. Thus, TLR4 is essential for the expression of proteinase-dependent asthma-like disease in mice.

Quantification of IL-4–secreting cells from whole lungs of proteinase-challenged mice (fig. S1H) confirmed the equivalent presence of IL-4–producing cells in the lung regardless of mouse genotype, suggesting that T_H2 cell development and recruitment occurred independently of TLR4. We then immunized mice against ovalbumin and confirmed that ovalbumin-specific T_H2 cell development was equivalent or enhanced in *Tlr4*$^{-/-}$ mice compared with controls (fig. S1I). Induction of total IgE, an IL-4– and T_H2 cell–dependent process (*8*–*11*), was also identical between WT and *Tlr4*$^{-/-}$ mice (fig. S1J).

Both the fungus *A. niger* and proteinase-free ovalbumin (1.8×10^{-3} EU/μg) also induced TLR4-dependent allergic lung disease in controls compared with proteinase-challenged WT mice (fig. S2). The consistent defect in disease expression seen in *Tlr4*$^{-/-}$ mice was durable because identical reductions in allergic disease parameters were seen after 2 and 4 weeks of ovalbumin immunization (fig. S2). Thus, TLR4 was required for the development of allergic airway disease, regardless of allergen proteinase content, but was dispensable for T_H2 responses.

We confirmed the reduced IL-5 transcript production in *Tlr4*$^{-/-}$ mice by assessing secreted

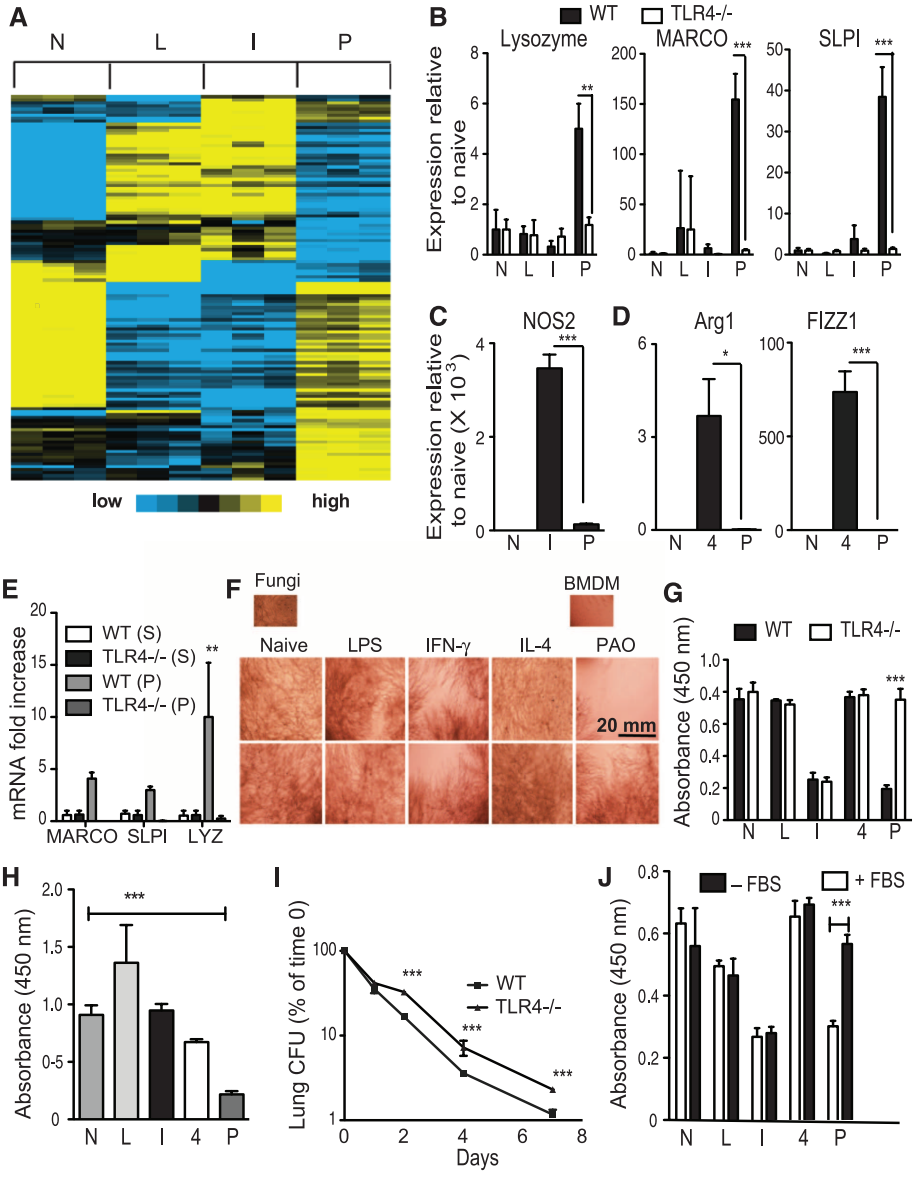

Fig. 1. PAO induces a distinct fungistatic macrophage phenotype through TLR4. (**A** to **D**) BMDMs from WT or *Tlr4*$^{-/-}$ mice were left unstimulated (N) or cultured in the presence of lipopolysaccharide (L), IFN-γ (I), PAO (P), or IL-4 (4) as indicated. (A) Heat map depicting the relative expression of 252 gene probes, as assessed by microarray ($P < 0.01$ and fold change >1.5, comparing PAO to each of the other groups) of WT BMDMs. (B) Polymerase chain reaction (PCR)–based analysis of lysozyme, MARCO, and SLPI. (C) NOS2 expression in IFN-γ– and PAO-activated WT macrophages. (D) Arg1 and Fizz1 expression in IL-4– and PAO-activated WT macrophages. (**E**) MARCO, SLPI, and lysozyme (LYZ) mRNA expression in alveolar macrophages derived from mice challenged with PBS (S) or PAO (P). (**F**) BMDMs from WT (top row) and *Tlr4*$^{-/-}$ (bottom row) mice were treated with IFN-γ, LPS, IL-4, or PAO for 24 hours and then cultured with *A. niger* conidia. Photomicrographs depict filamentous fungal growth. (**G**) Quantification of fungal growth in the same experiment, as assessed by XTT assay ($n = 3$ replicates per group). (**H**) PAO-treated human peripheral blood monocyte-derived macrophages were cultured under the same conditions as in (F) and assessed by XTT assay for their ability to restrain fungal growth ($n = 3$ patients). (**I**) WT and *Tlr4*$^{-/-}$ mice were intranasally challenged with 400,000 *A. niger* conidia, and lungs were harvested and fungal colony forming units (CFU) were determined over 7 days. (**J**) Fungistatic potential of BMDMs was determined as in (G), but in the presence (+) and absence (–) of fetal bovine serum (FBS). Data are presented as means ± SEM (error bars) from one of three comparable experiments. *$P < 0.05$; **$P < 0.01$; ***$P < 0.001$ by Mann-Whitney (two group comparisons) and Kruskal-Wallis (three or more group comparisons) tests.

[1]Translational Biology and Molecular Medicine Program, Baylor College of Medicine, Houston, TX, USA. [2]Department of Pathology and Immunology, Baylor College of Medicine, Houston, TX, USA. [3]Department of Medicine, Baylor College of Medicine, Houston, TX, USA. [4]Dan L. Duncan Cancer Center, Baylor College of Medicine, Houston, TX, USA. [5]Department of Otorhinolaryngology–Head and Neck Surgery, University of Texas Health Science Center at Houston, Houston, TX, USA. [6]Biology of Inflammation Center, Baylor College of Medicine, Houston, TX, USA. [7]Michael E. DeBakey VA Medical Center, Houston, TX, USA.

*Corresponding author. E-mail: dcorry@bcm.edu (D.B.C.); farrahk@bcm.edu (F.K.)

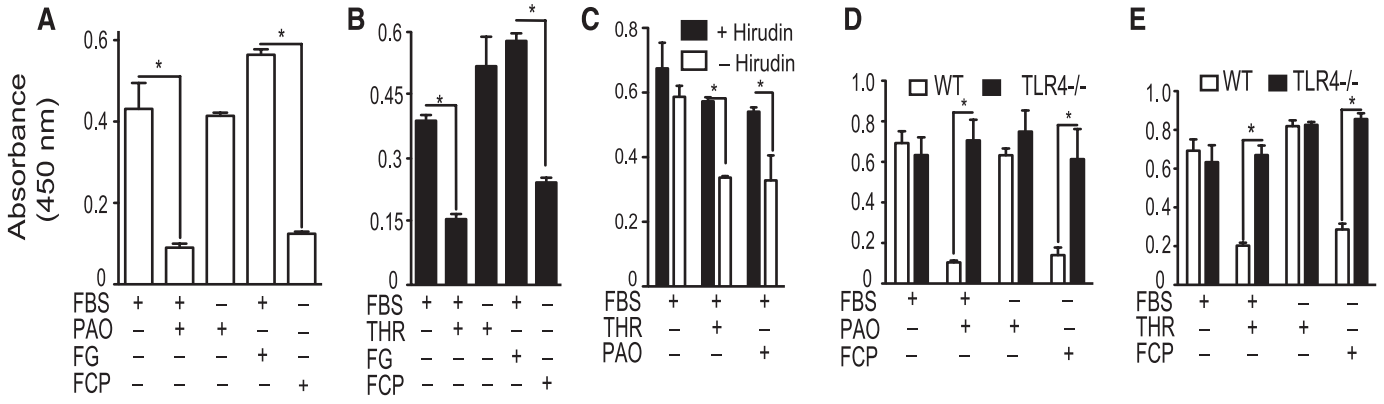

Fig. 2. Fibrinogen mediates PAO-dependent fungistasis through TLR4. BMDMs were cultured for 24 hours in the presence of FBS, PAO, fibrinogen (FG), FCP, or thrombin (THR), as indicated, and then inoculated with the conidia of *A. niger* for 24 hours, testing the requirement of (**A**) PAO and (**B**) thrombin for induction of fungistasis and (**C**) the effect of the thrombin inhibitor hirudin on PAO- and thrombin-dependent fungistasis, as assessed by XTT assay. (**D**) PAO and (**E**) thrombin were further compared with FCPs alone for their ability to induce fungistasis in the presence or absence of the *Tlr4* gene ($n = 3$ replicates per group). Data are presented as means ± SEM (error bars) from one of four comparable experiments. *$P < 0.05$ by Mann-Whitney test.

IL-5 levels in bronchoalveolar lavage fluid (fig. S3A). Type 2 innate lymphoid cells (ILCs) secrete IL-5 and IL-13, but not IL-4, in the setting of airway proteinase challenge (*12*), suggesting that these cells might be influenced by TLR4. Indeed, relative to vehicle-challenged animals, ILCs failed to be recruited as robustly into bronchoalveolar lavage fluid in *Tlr4*$^{-/-}$ mice relative to WT animals after proteinase challenge, potentially accounting in part for the reduced T_H2 cytokine production in *Tlr4*$^{-/-}$ mice (fig. S3, B and C).

We next considered whether other TLRs played a role in proteinase-dependent allergic lung disease. Most TLRs signal through one of two major adapter proteins, MyD88 and TRIF, whereas TLR4 signals through both adapters (*13*). Mice deficient in either MyD88 or TRIF showed an enhanced or identical disease phenotype as genotype matched control mice when challenged with *A. niger* spores (fig. S4). In contrast, mice deficient in both MyD88 and TRIF showed complete disease abrogation. Thus, proteinase-dependent allergic lung disease is mediated through TLR4 and not other TLRs.

Because TLR4 does not determine T_H2 responses, we turned to macrophages to further explore how TLR4 controls allergic disease. Relative to naïve cells, bone marrow–derived macrophages (BMDMs) expressed distinct transcriptional programs when activated by lipopolysaccharide (LPS), interferon-γ (IFN-γ), and PAO (Fig. 1A). Specific genes induced by PAO included lysozyme (*Lyz*), macrophage receptor with a collagenous structure (*Marco*), and secretory leukoproteinase inhibitor (*Slpi*), all of which have been linked to antifungal immunity (*14*–*16*), and their induction was dependent on TLR4 (Fig. 1B). PAO did not induce genes linked to previously characterized macrophage phenotypes, including IFN-γ–activated type 1 macrophages (M1) (nitric oxide synthase 2 (NOS2)] and IL-4–activated M2 (arginase 1 and FIZZ1) (*17*) (Fig. 1, C and D). Alveolar macrophages from mice treated with PAO similarly showed up-regulation of lysozyme, MARCO, and SLPI (Fig. 1E). Thus, PAO induced a macrophage phenotype marked by expression of a distinct transcriptional profile that included genes with antifungal properties.

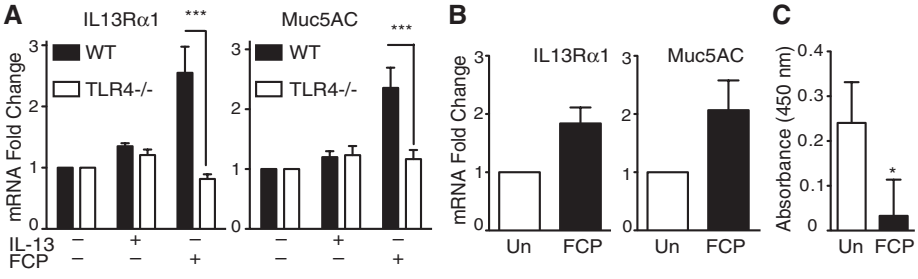

Fig. 3. FCPs up-regulate IL-13rα1 and Muc5AC on airway epithelium. (**A**) WT and *Tlr4*$^{-/-}$ mouse primary airway epithelial cells were cultured in the presence of IL-13 or FCPs for 24 hours, and *Il13ra1* and *Muc5ac* gene transcripts were analyzed by quantitative PCR ($n = 3$). (**B**) *Il13ra1* and *Muc5ac* transcripts were similarly analyzed from human primary airway epithelial cells 24 hours after treatment with FCPs or left unstimulated (Un) ($n = 4$). (**C**) Unstimulated and FCP-pretreated human airway epithelial cells were assessed for their ability to inhibit the growth of *A. niger* by XTT assay ($n = 3$ replicates per group.). Data are presented as means ± SEM (error bars) from one of three (murine) or two (human) comparable experiments. *$P < 0.05$; ***$P < 0.001$ by Mann-Whitney test.

We next determined if PAO-activated macrophages were capable of restraining fungal growth in vitro. Relative to naïve BMDMs, as assessed by both microscopy and colorimetric quantification, only IFN-γ– and PAO-activated macrophages efficiently controlled fungal growth when the conidia of *A. niger* were added to cultures (Fig. 1, F and G, and fig. S5). Human monocyte-derived macrophages were similarly responsive to PAO treatment, although less so to IFN-γ compared with mouse BMDMs (Fig. 1H). However, control of fungal growth through PAO, but not IFN-γ, required the presence of TLR4 (Fig. 1, F to H). Again, MyD88 and TRIF were individually dispensable for control of fungal growth in macrophages activated by PAO, but deletion of both adapters abrogated the ability of mouse macrophages to control fungal growth (fig. S6). These in vitro findings correlated with a reduced ability of *Tlr4*$^{-/-}$ mice to clear *A. niger* conidia from the airway after a single inhalational challenge (Fig. 1I).

Unlike other macrophage activators, PAO-dependent inhibition of fungal growth (fungistasis) required the presence of serum, suggesting that fungal proteinases acted through both a serum factor and TLR4 to induce macrophage antifungal immunity (Fig. 1J). Fibrinogen, a proposed TLR4 ligand (*18*), is the functional mammalian analog of the arthropod factors pro-Späetzle and coagulogen, which regulate antifungal immunity through Toll (*19*).

To determine if fibrinogen mediates proteinase-dependent fungistasis, we added it (1.8×10^{-5} EU/μg) to BMDM cultures, with and without fungal and endogenous proteinases, and the conidia of *A. niger*. Only when stimulated by PAO in the presence of serum did BMDMs exhibit robust fungistatic activity (Fig. 2A). Identical results were obtained in experiments in which PAO was substituted with the endogenous proteinase thrombin, which converts fibrinogen to fibrin as the terminal step in the clotting cascade while also creating additional cleavage products that do not

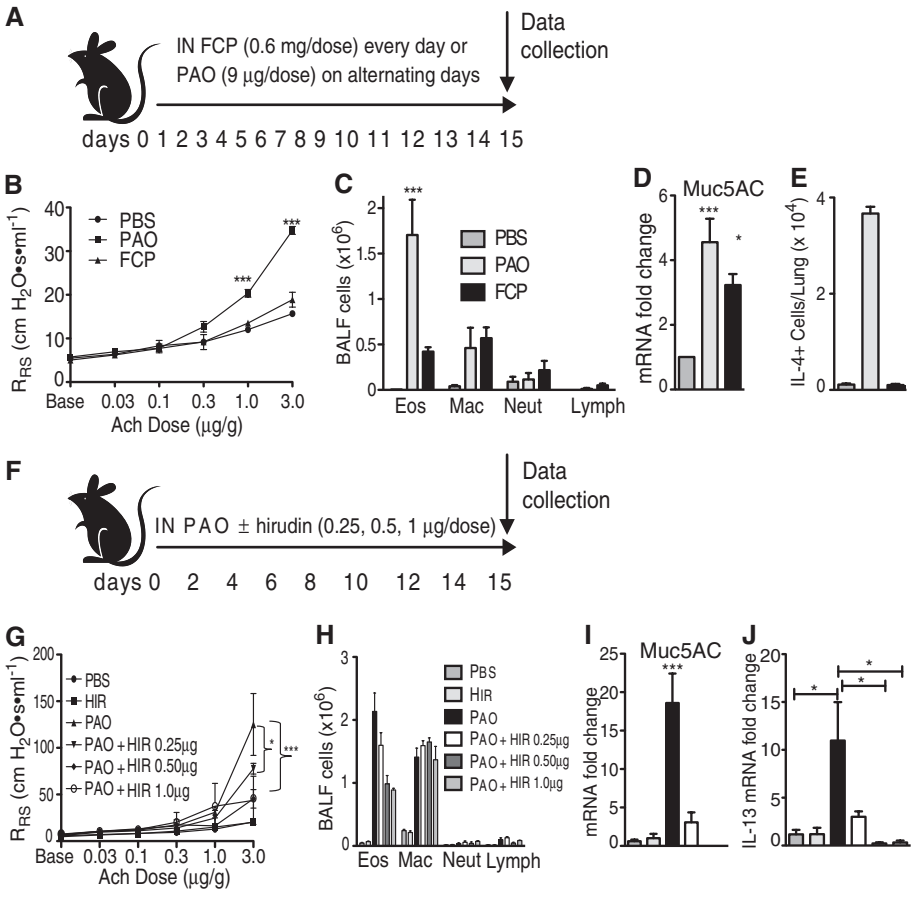

Fig. 4. Fibrinogenolysis is necessary but insufficient for expression of robust allergic airway disease. (**A**) C57BL/6 mice were challenged intranasally with PAO or FCPs as indicated, after which (**B**) airway hyperresponsiveness, (**C**) total bronchoalveolar lavage fluid (BALF) inflammatory cells, (**D**) lung Muc5AC transcripts, and (**E**) total lung IL-4–secreting cells were quantitated. (**F** to **J**) C57BL/6 mice were intranasally challenged with PAO without and with hirudin or hirudin alone on alternating days for 2 weeks, and the indicated parameters were assessed ($n \geq 3$ mice per group). Data are presented as means ± SEM (error bars) from one of three comparable experiments. Data are averages ± SEM. *$P <$ 0.05; ***$P <$ 0.001 by Kruskal-Wallis test. R_{RS}, respiratory system resistance.

participate in clot formation (Fig. 2B). These results suggested that rather than fibrinogen in per se, fibrinogen cleavage products (FCPs) were required to induce fungistasis. FCPs created by incubating fibrinogen with PAO or thrombin induced fungistasis to a comparable degree as whole serum and proteinase when added to BMDMs (Fig. 2, A and B). Moreover, the thrombin inhibitor hirudin (3.4×10^{-3} EU/μg) neutralized both PAO- and thrombin-dependent fungistasis that was induced in the presence of serum (Fig. 2C). Another abundant serum protein and putative TLR4 ligand, fibronectin (*20*), had no effect on macrophage fungistasis in either native or cleaved forms (fig. S7).

In addition to fungistasis (Fig. 2, D and E), FCPs also induced in BMDM the expression of mRNA for IL-13Rα1, a component of the IL-13 receptor that is required for expression of allergic airway disease (*21*), and the airway mucin gene *Muc5ac* through TLR4 (Fig. 3A). FCPs yielded similar findings and also induced fungistatic activity in human primary airway epithelial cells (Fig. 3, B and C).

Together, these findings support a model in which both endogenous and exogenous airway proteinase activities with allergenic potential produce alternate TLR4 ligands from fibrinogen that license innate immune cells to respond to T_H2 cells, as required for full expression of allergic airway disease. To test this model, we first administered intranasally to mice the maximum tolerated dose of FCPs, 0.6 mg per dose (Fig. 4A), which induced modest airway eosinophil recruitment and *Muc5ac* gene expression but failed to induce airway hyperresponsiveness and IL-4–secreting cells (Fig. 4, B to F). Thus, FCPs appeared to influence only innate immune cells and specifically did not induce T_H2 responses that are required for robust allergic lung disease.

We conducted additional studies to confirm that airway proteinase activity was required for allergic lung disease using the proteinase inhibitor hirudin. Our in vitro studies indicated that hirudin, a known thrombin antagonist, could also inhibit PAO-mediated fungistasis (Fig. 2C), suggesting that hirudin may possess broad-spectrum antiproteinase activity. In a dose-dependent manner, hirudin progressively and significantly attenuated PAO-dependent allergic lung disease while leaving unaffected robust lung IL-4 responses (Fig. 4, G to K), a phenotype that resembles that of *Tlr4*$^{-/-}$ mice challenged with diverse allergens (figs. S1 and S2). Hirudin further inhibited ovalbumin-dependent allergic airway disease, suggesting that ovalbumin challenge activates an endogenous proteinase, possibly thrombin, to achieve the fibrinogenolysis that is necessary for disease expression (fig. S8). Together, these studies confirm the importance of airway fibrinogenolysis for the expression of allergic lung disease, regardless of the proteinase content of the inhaled allergen.

Although previous studies have shown that TLR4 contributes to T_H2 responses (*5*, *22*, *23*), we have shown here that TLR4 is not required for T_H2 cell development but rather is required for responsiveness of innate airway cells to T_H2 cells. Our findings do not exclude the possibility that bacterial endotoxin, a canonical TLR4 ligand, could mediate T_H2 responses under some conditions, as shown previously (*5*), but additional studies are needed to determine the contribution of fibrinogenolysis to this observation. Although independent of TLR4, T_H2 cells nonetheless develop through a proteinase-dependent pathway (*24*), suggesting that proteinases coordinate both innate and adaptive allergic pathways that together lead to allergic inflammation and disease (fig. S9).

Ultimately, mammalian TLR4 preserves the crucial role of arthropod Toll by linking proteinase-dependent fibrinogenolysis to antifungal immunity. However, in addition to fungi, mammals must also defend against other proteinase-associated pathogens such as helminth parasites (*25*) and, potentially, viruses (*26*). Although highly effective, the ancient proteinase-Toll–based defensive strategy is also susceptible to aberrant activation in response to innocuous proteinase sources such as pollens and many allergens, both with and without intrinsic proteinase activity. Clarification of the contribution of true infections to common allergic airway disorders such as allergic rhinitis, asthma, and chronic rhinosinusitis will determine the usefulness of interrupting FCP-TLR4 signaling as a therapeutic strategy.

References and Notes

1. P. Porter *et al.*, *Mucosal Immunol.* **2**, 504–517 (2009).
2. F. Kheradmand *et al.*, *J. Immunol.* **169**, 5904–5911 (2002).
3. A. H. Clarke, W. R. Thomas, J. M. Rolland, C. Dow, R. M. O'Brien, *Int. Arch. Allergy Immunol.* **120**, 126–134 (1999).
4. S. N. Kelada *et al.*, *Am. J. Respir. Cell Mol. Biol.* **45**, 817–824 (2011).
5. S. C. Eisenbarth *et al.*, *J. Exp. Med.* **196**, 1645–1651 (2002).
6. H. Hammad *et al.*, *Nat. Med.* **15**, 410–416 (2009).
7. A. Trompette *et al.*, *Nature* **457**, 585–588 (2009).
8. F. D. Finkelman *et al.*, *J. Immunol.* **141**, 2335–2341 (1988).

9. J. Pène *et al.*, *Proc. Natl. Acad. Sci. U.S.A.* **85**, 6880–6884 (1988).
10. C. M. Snapper, F. D. Finkelman, W. E. Paul, *J. Exp. Med.* **167**, 183–196 (1988).
11. T. L. Stevens *et al.*, *Nature* **334**, 255–258 (1988).
12. T. Y. F. Halim, R. H. Krauß, A. C. Sun, F. Takei, *Immunity* **36**, 451–463 (2012).
13. J. L. Casanova, L. Abel, L. Quintana-Murci, *Annu. Rev. Immunol.* **29**, 447–491 (2011).
14. C. M. Woods, D. N. Hooper, E. H. Ooi, L. W. Tan, A. S. Carney, *Am. J. Rhinol. Allergy* **25**, 236–240 (2011).
15. S. Józefowski, Z. Yang, J. Marcinkiewicz, L. Kobzik, *Inflamm. Res.* **61**, 113–126 (2012).
16. J. F. Tomee, P. S. Hiemstra, R. Heinzel-Wieland, H. F. Kauffman, *J. Infect. Dis.* **176**, 740–747 (1997).
17. C. D. Mills, *Crit. Rev. Immunol.* **21**, 399–425 (2001).
18. C. P. Hodgkinson, K. Patel, S. Ye, *Thromb. Haemost.* **100**, 301–307 (2008).
19. N. J. Gay, F. J. Keith, *Biochim. Biophys. Acta* **1132**, 290–296 (1992).
20. Y. Okamura *et al.*, *J. Biol. Chem.* **276**, 10229–10233 (2001).
21. A. Munitz, E. B. Brandt, M. Mingler, F. D. Finkelman, M. E. Rothenberg, *Proc. Natl. Acad. Sci. U.S.A.* **105**, 7240–7245 (2008).
22. K. Dabbagh, M. E. Dahl, P. Stepick-Biek, D. B. Lewis, *J. Immunol.* **168**, 4524–4530 (2002).
23. D. A. Piggott *et al.*, *J. Clin. Invest.* **115**, 459–467 (2005).
24. S.-E. Lamhamedi-Cherradi *et al.*, *J. Immunol.* **180**, 6000–6009 (2008).
25. K. C. Lim *et al.*, *Am. J. Trop. Med. Hyg.* **60**, 487–492 (1999).
26. M. Singh *et al.*, *J. Allergy Clin. Immunol.* **125**, 1369, e2 (2010).

Acknowledgments: The data presented in this paper are tabulated in the main paper and in the supplementary materials. Microarray data are available through the National Center for Biotechnology Information Gene Expression Omnibus, accession number GSE48609. We thank Y. Qian, T. Bird, and Y. Zhang for excellent technical assistance. Funding was provided by NIH grants HL75243, AI057696, and AI070973 (to D.B.C.); CA125123 (to C.J.C.); and T32GM088129 and R25GM56929 (to V.O.M.) and the C.N. and Mary V. Papadopoulos Charitable Fund from the Biology of Inflammation Center.

Supplementary Materials
www.sciencemag.org/cgi/content/full/341/6147/792/DC1
Materials and Methods
Figs. S1 to S9
References (*27*–*31*)

10 May 2013; accepted 18 July 2013
10.1126/science.1240342

Recurrent Insect Outbreaks Caused by Temperature-Driven Changes in System Stability

William A. Nelson,[1]* Ottar N. Bjørnstad,[2] Takehiko Yamanaka[3]

Insects often undergo regular outbreaks in population density but identifying the causal mechanism for such outbreaks in any particular species has proven difficult. Here, we show that outbreak cycles in the tea tortrix *Adoxophyes honmai* can be explained by temperature-driven changes in system stability. Wavelet analysis of a 51-year time series spanning more than 200 outbreaks reveals a threshold in outbreak amplitude each spring when temperature exceeds 15°C and a secession of outbreaks each fall as temperature decreases. This is in close agreement with our independently parameterized mathematical model that predicts the system crosses a Hopf bifurcation from stability to sustained cycles as temperature increases. These results suggest that temperature can alter system stability and provide an explanation for generation cycles in multivoltine insects.

One of the fundamental tenants in insect ecology is that temperature is a pacemaker of all vital rates (*1*, *2*). Temperature has a direct impact on ontogenetic development, survival, and reproduction and, through these, an indirect impact on generation time and population growth rate (*3*, *4*). The reliability by which temperature can predict development in insects is used to predict the number of generations per year (voltinism), and the timing at which different life stages appear (*5*, *6*). The latter is a critical component for scheduling pest control. While the influence of temperature on individual-level life-history traits is well understood, the impact on population-level dynamics, such as population cycles or outbreak frequency, is less clear. For multivoltine insects, temperature is thought to contribute to insect outbreaks early in the season when climate has helped synchronize the population stage structure through either induction of diapause (*7*, *8*) or differential winter mortality (*9*). Mathematical theory suggests that temperature could also destabilize dynamics of ectotherms (*10*–*13*); however, the role that temperature plays in sustained cycles or overall dynamics in real systems is poorly understood.

The smaller tea tortrix, *Adoxophyes honmai*, is a multivoltine lepidopteran that undergoes multiple outbreak cycles each year (*14*). The insect is a pest on tea plantations and of significant economic concern throughout Japan. Outbreak densities are higher at the peaks than the troughs by a rate between 100- and 4000-fold (Fig. 1). Our previous work (*15*) showed that summer outbreaks are most consistent with intraspecific mechanisms that involve the strongly stage-structured nature of the insect life cycle. The outbreak dynamics themselves, however, are highly variable throughout a season (Fig. 1), with outbreaks occurring during the warmer months of the season (typically May to September) but not during the cooler months. The classic explanation for such a pattern is that cool winter temperatures synchronize population stage-structure, which leads to transient generation cycles (*5*). This mechanism generally results in cohort synchrony and outbreak amplitudes that are greatest at the start of the season and decay through time. The decay in cohort synchrony through time is observed in other structured systems (*16*) and occurs because developmental plasticity and environmental variability cause development to become increasingly uncorrelated. However, in the smaller tea tortrix, developmental synchrony is enhanced rather than eroded through the season. We, therefore, studied an alternative explanation, motivated by mathematical models, whereby sustained cycles are the result of temperature-dependent changes in system stability—seasonal temperature increases cause the system to destabilize each spring, and cooling temperatures cause the system to restabilize each fall.

To test this idea, we studied the relation between temperature and stability in a stage-structured model of the tortrix life cycle (supplementary text). The model, which is a set of coupled integral delay-differential equations parameterized with individual-scale laboratory data, provides theoretical predictions that are fully independent of the time-series data and so can be used for a rigorous test of the hypotheses. Our model represents a dynamic description of life history that incorporates a more realistic nonlinear function for ontogenetic development than is found in the classic degree-day model from insect ecology (*17*). We studied local stability of the models using characteristic equations (supplementary text). The model predicts that the population dynamics should be strongly temperature-dependent with decay to extinction at low temperatures, transient fluctuations around a stable equilibrium at intermediate temperatures, and sustained generation cycles at higher temperatures (Fig. 2 and supplementary text). The predicted transition from stability to cycles is via a supercritical Hopf bifurcation at 12.6°C. This class of bifurcation generates a smooth increase in amplitude with increasing temperature once past the critical temperature threshold. The model provides two testable predictions that can be used to evaluate if the dynamics are driven by temperature-dependent destabilization: (i) cycle amplitude should show a threshold response to temperature, and (ii) above the thresh-

[1]Department of Biology, Queen's University, Kingston, Ontario K7L 3N6, Canada. [2]Departments of Entomology and Biology, Pennsylvania State University, University Park, PA 16802, USA. [3]Natural Resources Inventory Center, National Institute for Agro-Environmental Sciences, Tsukuba 305-8604, Japan.
*Corresponding author. E-mail: nelsonw@queensu.ca

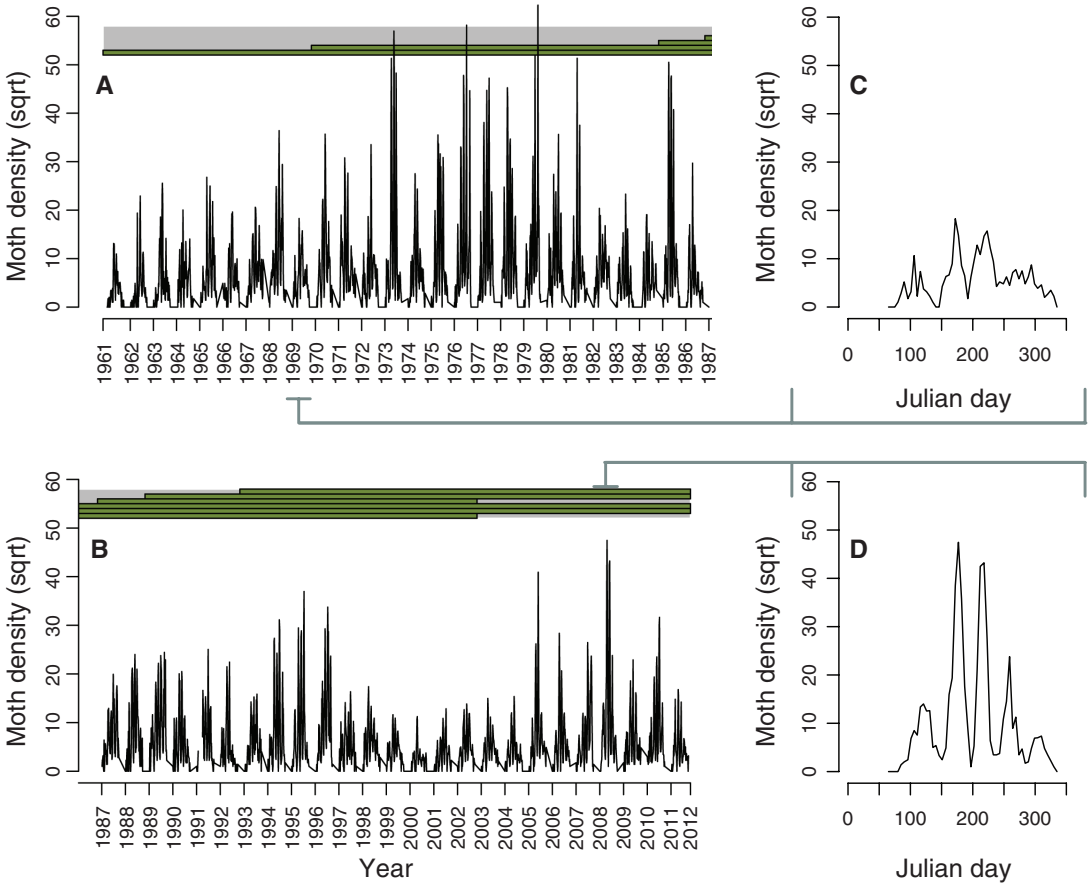

Fig. 1. Adult densities of the smaller tea tortrix, *Adoxophyes honmai*, over 51 years from light-trap census at the Kagoshima tea experiment station in Japan. (**A** and **B**) Adult densities. Sqrt, square root. (Right) Sample dynamics for years with relatively low-amplitude (**C**) and high-amplitude (**D**) outbreak cycles. Horizontal green bars show periods of time when different pest control strategies were used at the tea station (starting from the bottom: organophosphorus, carbamate, pyrethroid, insect growth regulator, *Bacillus thuringiensis*, and/or mating disruption compounds).

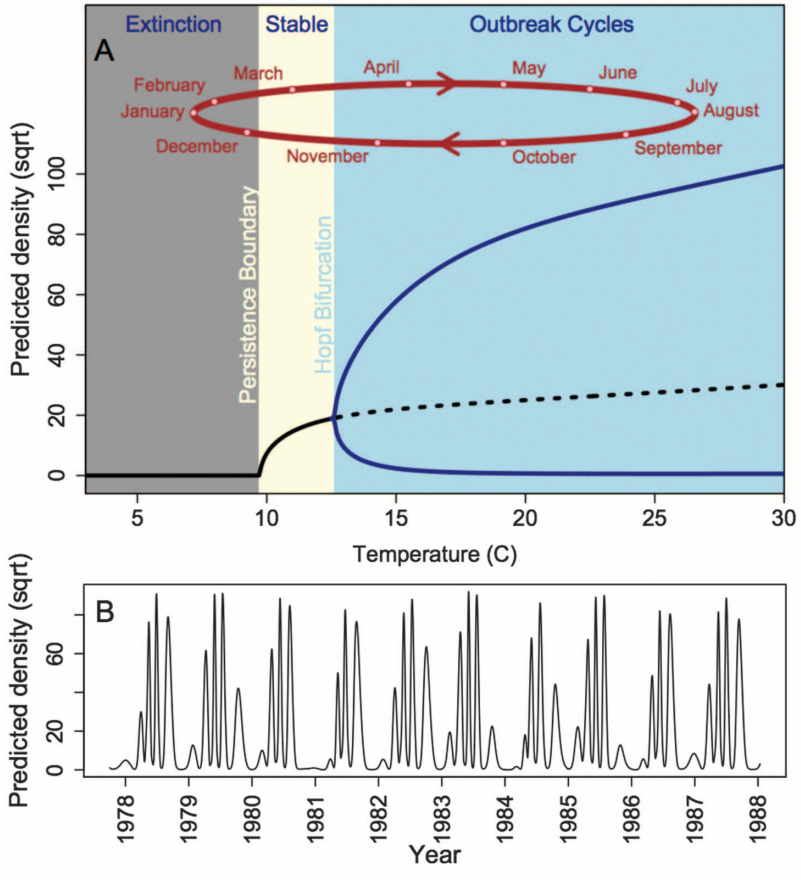

Fig. 2. Predicted temperature-driven changes in stability. (**A**) The system heads toward extinction at low temperature (gray), followed by stable population dynamics with densities that increase as temperature warms (yellowish white), followed by outbreak cycles at high temperatures with amplitudes that increase with temperature (blue). Solid black line denotes the stable equilibrium, dashed black line the unstable equilibrium. The solid blue line shows the minimum and maximum of outbreak cycles. Mean monthly temperature for the Kagoshima tea station is shown in red. (**B**) An example of predicted moth densities through time from the independently parameterized model driven with observed temperatures.

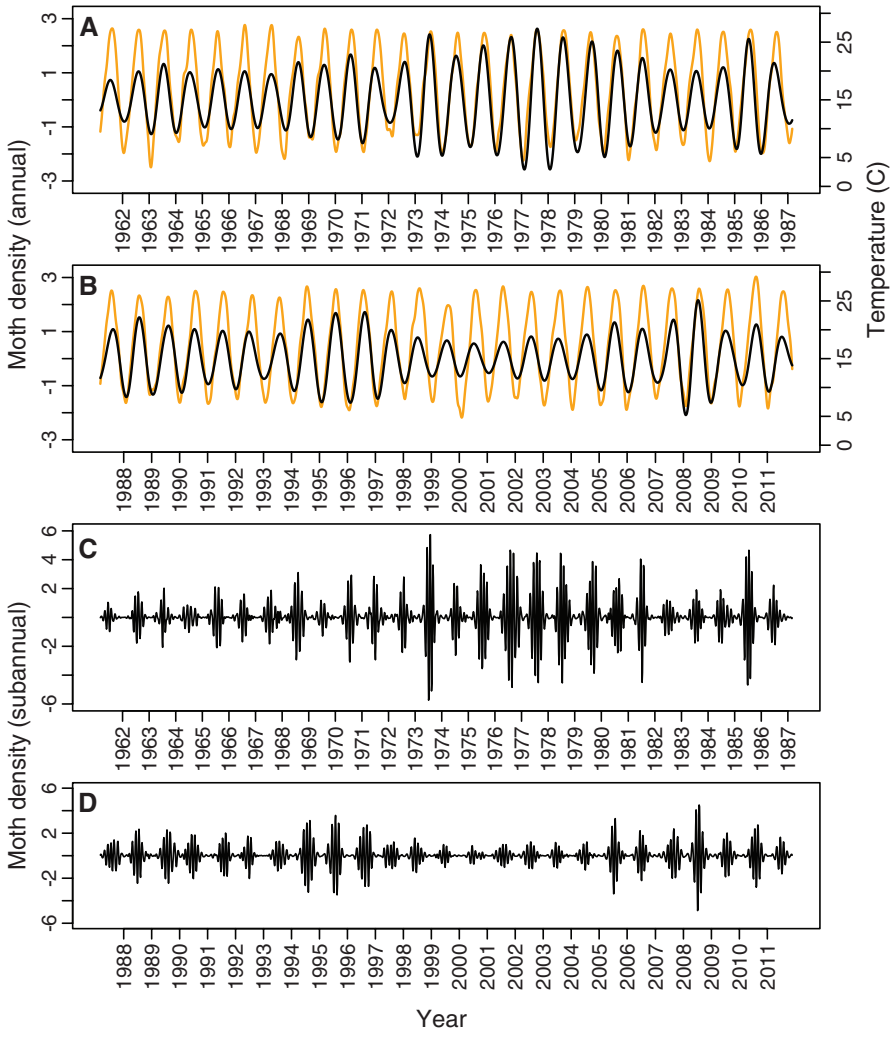

Fig. 3. Observed changes in moth density. Observed changes in moth density at the annual (**A** and **B**) and subannual (**C** and **D**) frequencies based on wavelet reconstruction. Scaled moth dynamics are shown with black lines, and smoothed mean daily temperature is shown in orange. Annual changes in moth dynamics are in phase with the observed temperature dynamics. The subannual cycles reveal striking nonstationary dynamics, with no cycles during the cold periods and large-amplitude outbreak cycles during the warm periods.

old, the cycle amplitude should increase roughly proportionally to temperature (Fig. 2). In contrast, if the cycles are simply due to the classic explanation of seasonally transient developmental synchrony, there should be no threshold relation between amplitude and temperature, and the amplitude should decrease with increasing temperature through the spring as cohorts smear into each other.

Wavelet analysis decomposes variability in a time-series into oscillations at different frequencies. In contrast to more traditional methods of spectral analysis, the wavelet also quantifies changes in cycle amplitude through time and accommodates nonstationarity in the data (*18*). Hence, it provides a useful framework to test our predictions. We applied the wavelet analysis to light-trap counts of adult moths recorded every 5 or 6 days from 1961 to 2012 at the Kagoshima tea station, Japan (*15*). The 51-year time series comprises more than 2500 observations and around 250 outbreaks. The analysis identifies two dominant patterns: a strong and relatively stationary signal that reflects an annual cycle and a pronounced, but punctuated, nonstationary signal that reflects the four to six distinct outbreak cycles that occur from late April through early October each year (Fig. 3 and supplementary text).

To test the predictions of the "classic" seasonal hypothesis versus the new temperature-induced destabilization hypothesis, we regressed outbreak amplitude against temperature using a mixed-effects linear and thresholded piecewise linear model. We modeled year as a random effect and used a first-order moving-average error structure to accommodate the serial dependence inherent in wavelet amplitudes (supplementary text). The thresholded regression model strongly outperforms the linear model for both spring and fall [likelihood ratio test: $\chi^2(24) = 689.6$, $P < 0.0001$, and $\chi^2(24) = 1338.8$, $P < 0.0001$, respectively]. Moreover, the best-fit model predicts a highly significant positive slope of amplitude against temperature above the threshold [spring slope (± SE): 34.3 ± 2.9; fall slope: 34.8 ± 3.8]. The profile likelihood for the threshold regression places the breakpoint at 15.0°C [confidence interval (CI): 14.5° to 15.5°C] for spring transitions and at 19.7°C (CI: 19.3° to 20.1°C) for fall transitions. These values are in good agreement but somewhat larger than the theoretical, temperature-induced Hopf bifurcation point expected under constant temperature. To investigate whether the discrepancy might be due to transient dynamics from the relatively rapid seasonal changes in temperature during the spring and fall transitions, we applied the same statistical protocol to numerical simulations of the model driven with observed monthly temperature data at the tea station for the last 50 years (supplementary text and fig. S23). The resultant regression patterns for the data and model are very close in terms of both the estimated threshold [simulated data, spring: 17.2°C (CI: 16.7° to 17.6°C), fall: 16.6°C (CI: 16.0° to 17.8°C)] and the estimated slope (Fig. 4). The analysis thus strongly supports the hypothesis that temperature destabilizes population dynamics and sustains recurrent outbreaks in this system.

Previous studies have shown that the population dynamics of some insect, fish, bird, and mammal species can be explained by single-species (*19*) or few-species (*20*) interactions even though they are embedded in complex food webs. Our results suggest that the outbreaks of the smaller tea tortrix share a similar level of dynamical sim-

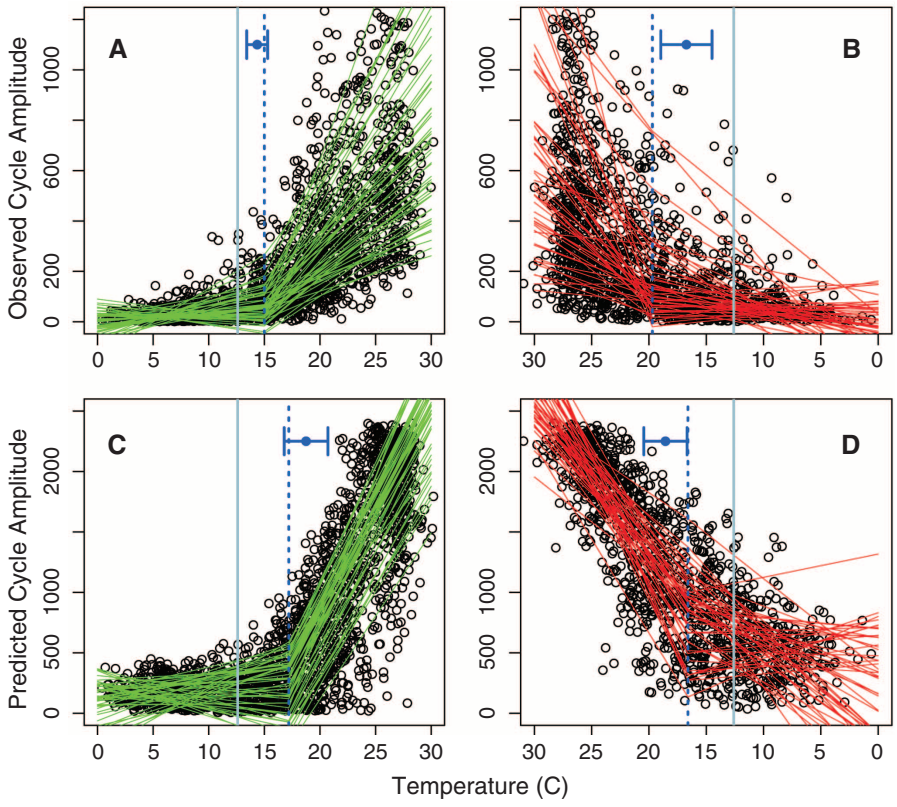

Fig. 4. Subannual cycle amplitude as a function of temperature. Observed cycle amplitude increases with increasing temperature (black circles) in the spring (**A**), with a fit threshold of 15°C (dashed blue line), and decreases with decreasing temperature in the fall (**B**), with a fit threshold of 20°C (dashed blue line). These compare very well with the theoretically predicted critical threshold temperatures of around 17°C for spring (**C**) and fall (**D**) from the independently parameterized model under seasonally driven temperatures (dashed blue line). Predicted constant temperature threshold is shown with the light blue solid line. Horizontal bars denote the mean and 95% confidence intervals from a variant of the model with year-specific transition points (supplementary text). Solid thin lines show fit of the piecewise regression model for each year (spring: green lines, fall: red lines).

plicity despite being part of a complex food web that includes parasitoids, predators, and competitors (*14*, *16*). We note, however, that the outbreak amplitudes are more variable between years than predicted by the model. This may be the signature of other interactions not included in our model that are of subdominant importance relative to the overall temperature pacemaker.

Theory predicts that environmentally induced changes in life-history traits can scale up to alter population and community dynamics, such that a system may be stable under certain conditions yet undergo cyclic or erratic dynamics in other environments (*21*–*24*). Various laboratory experiments manipulating productivity and mortality in consumer-resource systems provide essential proof-of-concept that dynamics can indeed undergo abrupt changes toward system instability in the face of gradual environmental gradients (*25*–*28*). Similar to other environmental drivers, mathematical models predict that temperature may cause abrupt changes in the stability of ectotherms through its ubiquitous influence on life-history rates (*10*–*13*). Despite these theoretical predictions and the enormous focus on contemporary and anticipated climate change, no previous studies have demonstrated that increased temperature may induce population cycles. Indeed, warming is linked to the loss of cyclicity in the larch budmoth in the Alps (*29*) and various other herbivores in northern latitudes (*30*). The smaller tea tortrix, however, demonstrates temperature-induced destabilization in a natural insect population.

References and Notes

1. J. F. Gillooly, J. H. Brown, G. B. West, V. M. Savage, E. L. Charnov, *Science* **293**, 2248–2251 (2001).
2. D. Atkinson, *Adv. Ecol. Res* **25**, 1–58 (1994).
3. J. Forster, A. G. Hirst, G. Woodward, *Am. Nat.* **178**, 668–678 (2011).
4. F. Taylor, *Am. Nat.* **117**, 1 (1981).
5. M. J. Tauber, C. A. Tauber, S. Masaki, *Seasonal Adaptations of Insects* (Oxford Univ. Press, Oxford, 1986).
6. D. A. Roff, in *Diapause and Life Cycle Strategies in Insects* (Junk, The Hague, 1983), pp. 253–270.
7. H. V. Danks, *Insect Dormancy: An Ecological Perspective* [Biological Survey of Canada (Terrestrial Arthropods), Ottawa, 1987].
8. W. S. C. Gurney, P. H. Crowley, R. M. Nisbet, *Theor. Popul. Biol.* **46**, 319–343 (1994).
9. J. A. Powell, J. L. Jenkins, J. A. Logan, B. J. Bentz, *Bull. Math. Biol.* **62**, 977–998 (2000).
10. D. A. Vasseur, K. S. McCann, *Am. Nat.* **166**, 184–198 (2005).
11. M. I. O'Connor, B. Gilbert, C. J. Brown, *Am. Nat.* **178**, 626–638 (2011).
12. S. Altizer *et al.*, *Ecol. Lett.* **9**, 467–484 (2006).
13. J. Ohlberger, E. Edeline, L. A. Vøllestad, N. C. Stenseth, D. Claessen, *Am. Nat.* **177**, 211–223 (2011).
14. Y. Tamaki, in *Tortricid Pests: Their Biology, Natural Enemies, and Control* (Elsevier, Amsterdam, 1991), pp. 541–551.
15. T. Yamanaka, W. A. Nelson, K. Uchimura, O. N. Bjørnstad, *Am. Nat.* **179**, 95–109 (2012).
16. T. M. Massie, B. Blasius, G. Weithoff, U. Gaedke, G. F. Fussmann, *Proc. Natl. Acad. Sci. U.S.A.* **107**, 4236–4241 (2010).
17. D. J. Lactin, N. J. Holliday, D. L. Johnson, R. Craigen, *Environ. Entomol.* **24**, 68–75 (1995).
18. R. Carmona, W. L. Hwang, B. Torresani, *Practical Time-Frequency Analysis*, vol. 9, *Gabor and Wavelet Transforms, with an Implementation in S* (Academic Press, San Diego, CA, 1998).
19. W. W. Murdoch *et al.*, *Nature* **417**, 541–543 (2002).
20. N. C. Stenseth, W. Falck, O. N. Bjørnstad, C. J. Krebs, *Proc. Natl. Acad. Sci. U.S.A.* **94**, 5147–5152 (1997).
21. R. A. Taylor, A. White, J. A. Sherratt, *Proc. Biol. Soc. B* **280**, 20122714 (2013).
22. S. Rinaldi, S. Muratori, Y. Kuznetsov, *Bull. Math. Biol.* **55**, 15–35 (1993).
23. M. L. Rosenzweig, *Science* **171**, 385–387 (1971).
24. A. Binzer, C. Guill, U. Brose, B. C. Rall, *Philos. Trans. R. Soc. London B Biol. Sci.* **367**, 2935–2944 (2012).
25. L. Becks, H. Arndt, *Ecology* **89**, 3222–3226 (2008).
26. G. F. Fussmann, S. P. Ellner, K. W. Shertzer, N. G. Hairston Jr., *Science* **290**, 1358–1360 (2000).
27. E. McCauley, R. M. Nisbet, W. W. Murdoch, A. M. de Roos, W. S. C. Gurney, *Nature* **402**, 653–656 (1999).
28. R. F. Costantino, J. M. Cushing, B. Dennis, R. A. Desharnais, *Nature* **375**, 227–230 (1995).
29. D. M. Johnson *et al.*, *Proc. Natl. Acad. Sci. U.S.A.* **107**, 20576–20581 (2010).
30. T. Cornulier *et al.*, *Science* **340**, 63–66 (2013).

Acknowledgments: We thank K. Uchimura for access to up-to-date light-catch data. W.A.N. was supported by Natural Sciences and Engineering Research Council Discovery grants. O.N.B. received support from the U.S. Department of Agricultures National Research Initiative. Raw time-series data are provided in Dryad (doi:10.5061/dryad.n11d4).

Supplementary Materials

www.sciencemag.org/cgi/content/full/science.1238477/DC1
Supplementary Text
Figs. S1 to S24
Tables S1 and S2
References (*31*–*42*)

29 March 2013; accepted 17 July 2013
Published online 1 August 2013;
10.1126/science.1238477

A Gut Lipid Messenger Links Excess Dietary Fat to Dopamine Deficiency

Luis A. Tellez,[1,2] Sara Medina,[1] Wenfei Han,[1,2,3] Jozelia G. Ferreira,[1,2] Paula Licona-Limón,[4] Xueying Ren,[1,2] TuKiet T. Lam,[5] Gary J. Schwartz,[6] Ivan E. de Araujo[1,2]*

Excessive intake of dietary fats leads to diminished brain dopaminergic function. It has been proposed that dopamine deficiency exacerbates obesity by provoking compensatory overfeeding as one way to restore reward sensitivity. However, the physiological mechanisms linking prolonged high-fat intake to dopamine deficiency remain elusive. We show that administering oleoylethanolamine, a gastrointestinal lipid messenger whose synthesis is suppressed after prolonged high-fat exposure, is sufficient to restore gut-stimulated dopamine release in high-fat–fed mice. Administering oleoylethanolamine to high-fat–fed mice also eliminated motivation deficits during flavorless intragastric feeding and increased oral intake of low-fat emulsions. Our findings suggest that high-fat–induced gastrointestinal dysfunctions play a key role in dopamine deficiency and that restoring gut-generated lipid signaling may increase the reward value of less palatable, yet healthier, foods.

Dopamine is the key neurotransmitter involved in the mediation of the reinforcing effects of foods and other rewards (*1*–*5*). Robust efflux of dopamine in dorsal striatum is observed during feeding in both rodents (*6*) and humans (*7*); conversely, preserved dopamine signaling in dorsal striatum is required for the expression of normal eating behaviors (*8*). This is consistent with a critical role for the nigrostriatal pathway in reward-seeking behaviors controlled by interconnecting dopaminergic circuits (*9*, *10*). Recently, the concept has emerged that overeating may represent a compensatory behavioral response to diminished responses within brain reward dopaminergic circuits (*1*, *11*–*14*). Dopamine receptor deficiency has been reported in the dorsal striatum of human obese participants (*11*, *15*), consistent with diminished striatal responses to food stimuli in overweight individuals (*13*). Critically, lentivirus-mediated knockdown of dorsal striatum dopamine receptors was found to be sufficient to induce compulsive-like caloric intake in rats (*16*).

Despite these advances, the physiological link between excess calorie intake and brain dopamine deficiency remains elusive. *N*-acylethanolamines form a family of appetite-regulating fatty acid amides (*17*–*21*) whose levels are reduced in response to excessive dietary fat (*22*, *23*). Because our own previous work revealed that gut stimulation with caloric nutrients induce robust striatal dopamine release (*6*, *24*, *25*), we set forth the hypothesis that high-fat–induced gastrointestinal *N*-acylethanolamine deficiency is physiologically linked to high-fat–induced dopamine deficiency.

We specifically hypothesized that reduced synthesis of the diet-derived satiety messenger oleoylethanolamine [OEA (*17*,*19*)] links excessive lipid intake to dopamine deficiency. By using liquid chromatography coupled to mass spectrometry, we confirmed that a high-fat diet produces in mice significant reductions in intestinal OEA synthesis, whereas no changes are detected in other tissues (fig. S1). Consistently, subchronic intraduodenal OEA treatment was sufficient to decrease weight gain and fat intake in high-fat–fed mice (fig. S2).

We first established that deficient dopamine release is recapitulated when food is delivered directly into the gastrointestinal tract, that is, bypassing the oral cavity. Low-fat– and high-fat–fed (henceforth LF and HF, respectively) mice were implanted with gastric catheters through which caloric fat emulsions were infused concomitantly to microdialysis sampling of extracellular dopamine levels in dorsal striatum. We found that HF mice failed to display the calorie-dependent dopamine effluxes observed in LF mice upon gut stimulation with lipids (fig. S3); that is, altered orosensation is not required for dopamine deficiency.

To evaluate the intestinal molecular basis of this dopamine deficiency, we administered OEA to LF and HF mice via intraperitoneal catheters during dopamine monitoring as above. Either con-

[1]The John B. Pierce Laboratory, New Haven, CT 06519, USA. [2]Department of Psychiatry, Yale University School of Medicine, New Haven, CT 06511, USA. [3]School of Stomatology, Tongji University, Shanghai 200072, China. [4]Department of Immunobiology, Yale University School of Medicine, New Haven, CT 06520, USA. [5]W. M. Keck Foundation Biotechnology Resource Laboratory, Yale University, New Haven, CT 06511, USA. [6]Albert Einstein College of Medicine, Yeshiva University, Bronx, NY 10461, USA.

*Corresponding author. E-mail: iaraujo@jbpierce.org

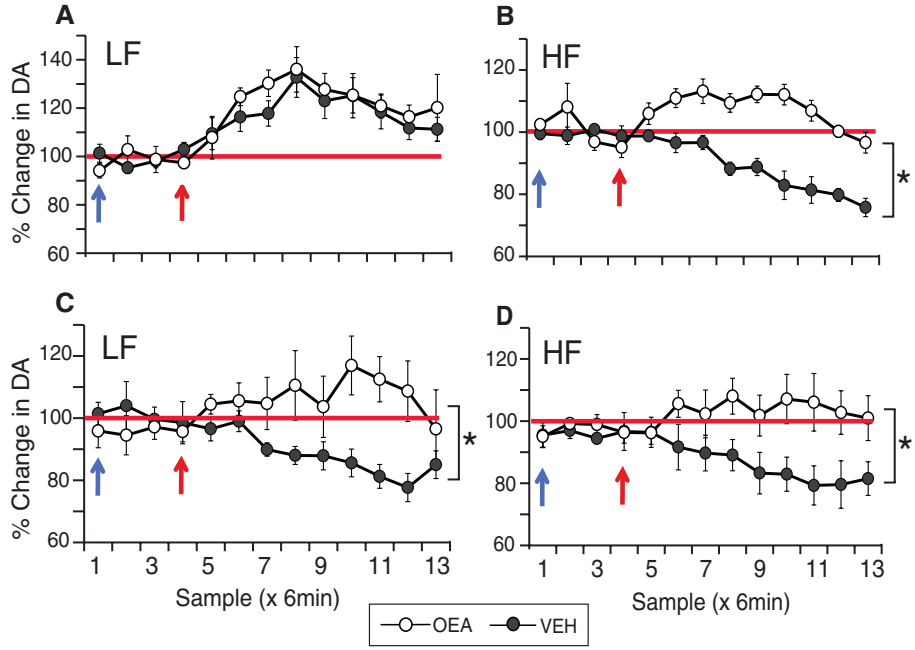

Fig. 1. Administration of OEA induces gut-stimulated dopamine release in high-fat–fed mice. LF ($N = 6$) and HF ($N = 6$) mice were implanted with gastric catheters, through which fat emulsions were infused. These mice were also implanted with intraperitoneal catheters, through which either OEA (10 mg/kg) or vehicle were injected 25 min before the gut fat infusions. Data correspond to time course of OEA effects on dopamine release of percent dopamine change with respect to baseline preinjection period (baseline = 100%, red horizontal trace). Blue vertical arrows represent time points when OEA or vehicle was injected, and red vertical arrows represent time points when the fat emulsion was infused. (**A**) In LF mice, OEA did not influence the increases in dopamine release stimulated by intragastric infusions of high-calorie emulsions [two-way repeated measures analysis of variance (RM-ANOVA), OEA treatment × sample time effect $F(12,60) = 0.68$, $P = 0.76$]. (**B**) However, in dopamine-deficient HF mice, OEA recovered dopamine release stimulated by intragastric infusions of high-calorie emulsions [two-way RM-ANOVA OEA treatment × sample time effect $F(12,60) = 7.1$, $^*P < 0.001$]. (**C**) In LF mice, unlike the case of high-calorie infusions, OEA produced significant effects on dopamine release after intragastric low-calorie emulsions [$F(12,60) = 3.5$, $^*P = 0.001$]. (**D**) In HF mice, likewise the case for high-calorie emulsions, OEA restored dopamine release stimulated by intragastric low-calorie emulsions [($F(12,60) = 4.7$, $^*P < 0.001$]. In (B) to (D), significant interaction effects (denoted by asterisks) are accounted for by the fact that OEA only affects dopamine efflux after the gut infusions. DA indicates dopamine; VEH, vehicle injections. Data shown as mean ± SE.

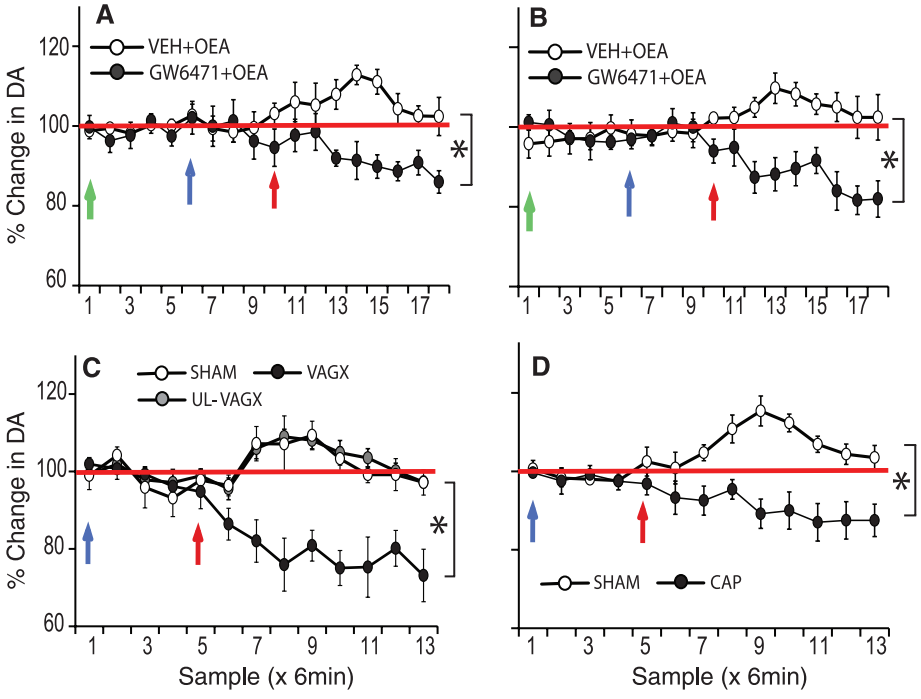

Fig. 2. The dopaminergic effects of OEA are mediated by PPARα and abolished by vagotomy or chemical deafferentation. (**A**) Intraperitoneal administration of the PPARα-specific antagonist GW6471 before OEA administration blocked the ability of OEA to potentiate dopamine efflux after intragastric infusions of low-calorie emulsions in LF mice [$N = 5$; two-way RM-ANOVA treatment effect $F(1,4) = 19.4$, $^*P = 0.012$]. Green vertical arrows indicate when GW6471 or vehicle was infused; blue and red vertical arrows are as above. (**B**) Similar results hold for HF mice [$N = 5$; two-way RM-ANOVA treatment effect $F(1,4) = 13.3$, $^*P = 0.02$]. (**C**) Subdiaphragmatic vagotomized (bilaterally vagotomized, VAGX, $N = 5$), unilaterally vagotomized (UL-VAGX, $N = 5$), and sham-operated (SHAM, $N = 5$) were treated exactly as described in Fig. 1. Blue vertical arrows represent time points when OEA or vehicle was injected intraperitoneally, and red vertical arrows represent time points when the fat emulsion was infused. Bilateral subdiaphragmatic vagotomies abolished the ability of OEA to potentiate dopamine efflux after intragastric infusions of low-calorie emulsions. The between-group difference (SHAM versus VAGX) is only apparent after the gut infusions [two-way RM-ANOVA group × sample time effect $F(12,96) = 5.2$, $^*P < 0.001$]. However, vagotomies restricted to the right vagal trunk, performed above the hepatic branch, produced no effect on OEA-stimulated dopamine release [SHAM versus UL-VAGX group effect $F(1,8) = 0.33$, $P > 0.5$]. (**D**) Intraperitoneal administration of the PPARα-specific agonist GW7647 recapitulates the ability of OEA to potentiate dopamine efflux after intragastric infusions of low-calorie emulsions in sham ($N = 6$), but not in capsaicin-treated (CAP), LF ($N = 6$) mice [two-way RM-ANOVA group × sample time effect $F(12,60) = 5.9$, $^*P < 0.001$]. Blue vertical arrows represent time points when GW7647 was injected, and red vertical arrows represent time points when the fat emulsion was infused. Data shown as mean ± SE.

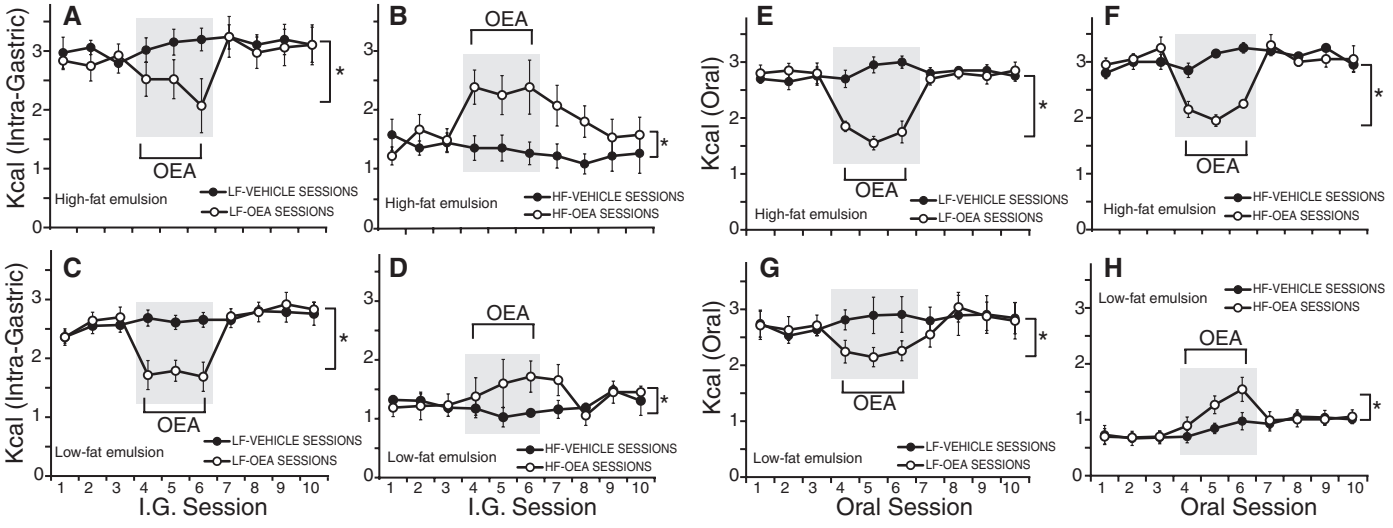

Fig. 3. Administration of OEA restores intragastric and oral feeding in high-fat–fed mice. As above, mice were conditioned to lick a dry spout to obtain intragastric (I.G.) infusions of fat emulsions. Mice were infused ~25 min before the onset of the intragastric feeding sessions with vehicle or 10 mg/kg OEA for 10 consecutive (daily) sessions. The initial three sessions (days 1 to 3) were performed after vehicle injections, followed by three sessions performed after OEA injections (days 4 to 6) and then four additional vehicle sessions (days 7 to 10). Additional 10 sessions using vehicle injections only were performed to control for potential time-derived confounds. OEA sessions performed on days 4 to 6 (and the corresponding vehicle-only sessions) are depicted within gray areas, and asterisks denote significant treatment × session interaction effects. (**A**) OEA treatment inhibited intragastric intake of high-calorie emulsions in LF mice ($N = 6$) on the third day of OEA testing [30% reduction; two-way RM-ANOVA for overall OEA treatment × session effect $F(9,90) = 1.7$, $^*P = 0.08$]. (**B**) OEA treatment stimulated intragastric intake of high-calorie emulsions in HF mice [$N = 6$; $F(9,90) = 2.5$, $^*P = 0.01$] to an extent that it matched caloric intake of LF mice. (**C**) OEA treatment inhibited intragastric intake of low-calorie emulsions in LF mice [$N = 6$; $F(9,90) = 12.4$, $^*P < 0.001$]. (**D**) OEA treatment stimulated intragastric intake of low-calorie emulsions in HF mice [$N = 6$; $F(9,90) = 2.0$, $^*P < 0.05$] to an extent that it matched intake in LF mice. (**E**) OEA treatment inhibited oral intake of high-calorie emulsions in both LF [$N = 6$; $F(9,90) = 12.3$, $^*P < 0.001$] and (**F**) HF mice [$N = 6$; $F(12,90) = 9.1$, $^*P < 0.001$]. (**G**) OEA treatment inhibited oral intake of low-calorie emulsions in LF mice [$N = 6$; $F(12,90) = 3.1$, $^*P < 0.004$]. (**H**) OEA treatment stimulated oral intake of low-calorie emulsions in HF mice [$N = 6$; $F(12,90) = 3.6$, $^*P = 0.001$]. Data shown as mean ± SE.

trol (vehicle) or 10 mg/kg OEA solutions were infused ~25 min before the onset of the intragastric fat infusions. Robust increases in striatal dopamine produced by intragastric high-calorie emulsions were observed in LF mice, an effect not altered by OEA injections (Fig. 1A). Remarkably, OEA administration to HF mice reversed HF-associated dopamine deficiency by inducing sustained dopamine effluxes after the gut fat infusions (peaking ~17% above baseline levels compared with ~20% decreases in vehicle sessions, Fig. 1B). Moreover, when the less-caloric emulsion was infused, we observed OEA-induced dopamine efflux in both LF (Fig. 1C) and HF (Fig. 1D) mice to an extent that OEA-induced dopamine efflux in LF versus HF mice became statistically indistinguishable.

We then investigated the neural and molecular pathways that may mediate OEA's dopaminergic effects. The anorectic effects of OEA are known to depend on the nuclear receptor peroxisome proliferator–activated receptor alpha (PPARα) (*26*). PPARα antagonism consistently abolished the OEA effect on gut-stimulated dopamine efflux in both LF (Fig. 2A) and HF (Fig. 2B) mice. These results were recapitulated in PPARα knockout mice (figs. S4 and S5). OEA anorectic effects are also known to be mediated by the vagus nerve (*17*). Indeed, intracerebral OEA infusions failed to influence dopamine release in either LF or HF mice (fig. S6). Moreover, OEA dopaminergic effects were completely abolished in both bilaterally vagotomized (Fig. 2C) and chemically deafferented (fig. S7) mice. Surgical vagotomies restricted to the right trunk (i.e., above the hepatic branch) failed to suppress gut-stimulated dopamine release (Fig. 2C), ruling out hepatic vagal influences on the above effects; indeed, intraduodenal OEA injections at doses ineffective systemically also restore dopamine efflux in HF mice (fig. S8). These effects were observed in the absence of any differences in striatal dopamine basal levels between the experimental groups (fig. S9). Last, because a PPARα-specific agonist recapitulated OEA dopaminergic actions in control but not in deafferented mice (Fig. 2D), we conclude that the OEA dopaminergic effect relies on a PPARα-gastrointestinal-brain axis.

We next investigated the behavioral consequences of the OEA-induced enhancement of dopamine efflux. Intragastric feeding in the absence of flavor input is a dopamine receptor–dependent operant behavior that induces striatal dopamine efflux in proportion to the amounts of calories self-infused to the gut (*6*, *25*). On the basis of the microdialysis studies, we reasoned that HF mice would display decreased motivation to feed themselves via the intragastric route. LF and HF mice were fitted with gastric catheters and trained to lick a dry spout in order to self-administer fat emulsions ad libitum via the gastric route (*6*). We observed markedly lower (~50 to 60%) intragastric feeding in HF compared with LF mice, irrespective of infusate volume (fig. S10A), concentration (fig. S10B), or hunger levels (fig. S10C). Altered responses in HF mice were neither due to early satiety (fig. S10D) nor to differences in gut lipase activity (fig. S11). Thus, diminished motivation to work for food in obese mice (*27*) is recapitulated when feeding is restricted to the gastrointestinal route. We additionally predicted that impaired flavorless intragastric feeding would coexist with low oral intake of less-hedonic stimuli, because high-fat–fed rodents show diminished oral acceptance of low-calorie fats (*14*, *28*, *29*). Accordingly, HF mice were less motivated to ingest the lesser-caloric emulsions during oral tests compared with LF mice (fig. S10, E and F). Both gut-related dopamine deficiency and deficient low-fat oral intake appear to result from chronic high-fat exposure, rather than from weight gain per se (fig. S12).

We then reasoned, again on the basis of the microdialysis studies, that OEA administration to HF mice would increase motivation for intragastric feeding. Mice were infused with vehicle or 10 mg/kg OEA ~25 min before the onset of the intragastric feeding sessions for 10 consecutive (daily) 1-hour sessions. As expected, OEA injections produced anorectic effects in LF mice self-administering the higher-calorie emulsion (Fig. 3A). Remarkably, the same OEA dose produced opposite, that is, orexigenic, effects in HF mice (Fig. 3B). Equally intriguing was the observation that LF and HF mice consumed comparable amounts of calories via the intragastric route when treated with the same dose of OEA (compare kcal in Fig. 3, A versus B). Analogous effects were observed during sessions in which mice self-administered the lesser-caloric emulsions (Fig. 3, C and D). The reinforcing effects produced by OEA on intragastric feeding are thus consistent with the dopaminergic effects produced by OEA during intragastric delivery of fats: In fact, HF mice showed significantly lower motivation to work for fat intragastric infusions during progressive ratio dry-lick tests, an effect that was attenuated by OEA administration (fig. S13).

Last, we predicted that OEA administration would increase the reward value of the lesser-caloric emulsion during oral tests in HF mice. As expected, OEA injections produced anorectic effects in both LF and HF mice during oral intake of high-calorie emulsion (Fig. 3, E and F). However, OEA produced anorectic effects during oral low-fat intake in LF mice (Fig. 3G) while stimulating low-fat intake in HF mice (Fig. 3H). Also in agreement with our overall hypothesis, OEA actions on low-fat intake were abolished by dopamine receptor antagonism in striatum, whereas deafferented mice remained insensitive to striatal dopaminergic blockade (fig. S14). Indeed, during oral tests LF and HF deafferented mice failed to converge their dissimilar caloric intake toward a congruent level after OEA treatment (fig. S15), consistent with HF deafferented mice showing abnormal long-term fat intake patterns (figs. S16 and S17).

Our results support the following conjectural model: Gut lipid messengers such as OEA may function as homeostatic signals that dictate the amounts of dietary fat to be ingested (i.e., by either stimulating or suppressing intake toward a set point). Such gut-derived signals would affect feeding by modulating a vagal-nigro-striatal pathway. High-fat–induced interference with this pathway would thus entail reward deficiency, that is, diminished attribution of reward value to less-palatable stimuli. Reestablishing gut-lipid signaling may thus enhance the reward value of low-calorie foods, presumably by restoring gut-stimulated dopaminergic function. Whether this concept can be developed into a useful weight-loss strategy will require further research.

References and Notes

1. N. D. Volkow, G. J. Wang, R. D. Baler, *Trends Cogn. Sci.* **15**, 37–46 (2011).
2. R. A. Wise, *Philos. Trans. R. Soc. London Ser. B* **361**, 1149–1158 (2006).
3. K. C. Berridge, *Neurosci. Biobehav. Rev.* **20**, 1–25 (1996).
4. A. Hajnal, G. P. Smith, R. Norgren, *Am. J. Physiol. Regul. Integr. Comp. Physiol.* **286**, R31–R37 (2004).
5. J. E. McCutcheon, J. A. Beeler, M. F. Roitman, *Synapse* **66**, 346–351 (2012).
6. J. G. Ferreira, L. A. Tellez, X. Ren, C. W. Yeckel, I. E. de Araujo, *J. Physiol.* **590**, 953–972 (2012).
7. D. M. Small, M. Jones-Gotman, A. Dagher, *Neuroimage* **19**, 1709–1715 (2003).
8. B. N. Sotak, T. S. Hnasko, S. Robinson, E. J. Kremer, R. D. Palmiter, *Brain Res.* **1061**, 88–96 (2005).
9. B. J. Everitt *et al.*, *Philos. Trans. R. Soc. London Ser. B* **363**, 3125–3135 (2008).
10. J. E. Murray, D. Belin, B. J. Everitt, *Neuropsychopharmacology* **37**, 2456–2466 (2012).
11. G. J. Wang *et al.*, *Lancet* **357**, 354–357 (2001).
12. P. J. Kenny, *Nat. Rev. Neurosci.* **12**, 638–651 (2011).
13. E. Stice, S. Spoor, C. Bohon, D. M. Small, *Science* **322**, 449–452 (2008).
14. H. R. Berthoud, *Proc. Nutr. Soc.* **71**, 478–487 (2012).
15. G. J. Wang, N. D. Volkow, P. K. Thanos, J. S. Fowler, *J. Addict. Dis.* **23**, 39–53 (2004).
16. P. M. Johnson, P. J. Kenny, *Nat. Neurosci.* **13**, 635–641 (2010).
17. F. Rodríguez de Fonseca *et al.*, *Nature* **414**, 209–212 (2001).
18. H. S. Hansen, T. A. Diep, *Biochem. Pharmacol.* **78**, 553–560 (2009).
19. G. J. Schwartz *et al.*, *Cell Metab.* **8**, 281–288 (2008).
20. V. Di Marzo, A. Ligresti, E. Morera, M. Nalli, G. Ortar, *Bioorg. Med. Chem.* **12**, 5161–5169 (2004).
21. K. Proulx *et al.*, *Am. J. Physiol. Regul. Integr. Comp. Physiol.* **289**, R729–R737 (2005).
22. A. Artmann *et al.*, *Biochim. Biophys. Acta* **1781**, 200–212 (2008).
23. T. A. Diep *et al.*, *FASEB J.* **25**, 765–774 (2011).
24. X. Ren *et al.*, *J. Neurosci.* **30**, 8012–8023 (2010).
25. I. E. de Araujo, J. G. Ferreira, L. A. Tellez, X. Ren, C. W. Yeckel, *Physiol. Behav.* **106**, 394–399 (2012).
26. J. Fu *et al.*, *Nature* **425**, 90–93 (2003).
27. J. F. Davis *et al.*, *Behav. Neurosci.* **122**, 1257–1263 (2008).
28. D. R. Reed, M. I. Friedman, *Appetite* **14**, 219–230 (1990).
29. H. Zheng, N. R. Lenard, A. C. Shin, H. R. Berthoud, *Int. J. Obes.* **33** (suppl. 2), S8–S13 (2009).

Acknowledgments: We thank M. Freire, M. LoPresti, and T. Abbott for surgical procedures, gut sample preparation, and MS data analysis respectively; Yale Clinical and Translational Science Award (UL1RR024139) for the 4000 QTRAP (AB Sciex) liquid chromatography (LC)–tandem mass spectrometry; and PerkinElmer for the Flexar ultra–high performance LC. I.E.d.A. is funded by NIH grants DC009997 and DK085579 and Ajinomoto USA. G.J.S. is funded by NIH grants DK020541 and DK026687. L.A.T. was supported by Instituto de Ciencia y Tecnología del Distrito Federal (México) BI10-164. W.H. was supported by China Scholarship Council (CSC) 201206260072.

Supplementary Materials

www.sciencemag.org/cgi/content/full/341/6147/800/DC1
Materials and Methods
Figs. S1 to S18
Table 1
References (*30*–*38*)

9 November 2012; accepted 12 July 2013
10.1126/science.1239275

MUFFLE FURNACES

A new range of 1,200°C muffle furnaces are now available which provide rapid and uniform heating in a compact, space-saving bench-top unit. The furnaces are available in chamber sizes ranging from 5.2 up to 20 L so there is a model that will suit the wide range of workloads typically required for most laboratory heating applications, such as quality control testing, ashing, heat treatment, preheating, melting, metallurgical research, and sample production. The inner chamber walls are constructed using insulated fire bricks which provide optimum insulation as well as protection against mechanical abrasion, thermal ageing, and deformation. A uniform temperature spread is achieved as the heating elements are located on both the sides and the top of the chamber and they are partially recessed and embedded in quartz sleeves. This, combined with a standard thickness of the inner chamber material, ensures additional protection and enhances uniform heating of the chamber.

Medline Scientific

For info: +44-(0)-1865-892987 | www.medlinescientific.com

CELL DIFFERENTIATION MEDIUM

OsteoMAX-XF is the first fully defined, xeno-free human mesenchymal stem cell differentiation medium for the differentiation of mesenchymal stem cells into osteocytes. Mineralization can be detected in less than one week, whereas competing products that contain serum require approximately 21 days to produce similar levels of bone formation. The formulation, licensed from Plasticell, produces more consistent and potent osteogenic differentiation than currently available formulations, enabling a more reproducible, efficient method for creating bone tissue and advancing research in bone disease and healing. EMD Millipore manufactures and distributes the medium globally for research purposes while Plasticell retains all rights over therapeutic applications. The OsteoMAX-XF differentiation media adds to EMD Millipore's comprehensive portfolio of mesenchymal stem cell products including primary human and rat mesenchymal stem cell lines, expansion media, antibodies, characterization kits, growth factors, and ECM proteins.

EMD Millipore

For info: 800-645-5476 | www.millipore.com/stemcell

PRECAST GELS

A new range of 10 x 10 cm Precast Gels which are ideally suited to all SDS-PAGE applications are now available. PAGE-PRO Precast gels provide fast run times from 45 to 75 minutes and a superior performance compared with traditional Laemmli gels. PAGE-PRO gels have a specially formulated proprietary gel matrix composition which ensures their enhanced performance and a guaranteed shelf-life of a minimum of 12 months. Available in single and gradient percentage acrylamide compositions, PAGE-PRO gels are manufactured using an automated filling technique that ensures total reproducibility between batches. They can also be used with standard Tris-MOPS, Tris-HEPES, and Tris Tricine SDS running buffers and are suitable for use with the omniPAGE mini vertical electrophoresis and blotting systems. They are available in 10- (30 µL per well) and 15-well (15 µL per well) formats and are compatible with most apparatus, including the XCell SureLock precast gel systems.

Cleaver Scientific

For info: +44-(0)-1788-565300 | www.cleaverscientific.com

UV VIEWING CABINETS

Spectroline CX-20 and CX-21 high-intensity ultraviolet (UV) viewing cabinets guarantee maximum ultraviolet irradiance and fluorescent contrast because they are designed for peak efficiency. The CX-20 and CX-21 cabinets combine separate long-wave and short-wave 8-watt UV light sources with uniquely designed specular aluminum reflectors to assure maximum intensity and exceptional fluorescent contrast. Both units have removable bottom panels so they can be easily placed over large objects or, to provide greater illumination, over a Spectroline UV transilluminator. The cabinets' housings are made of vinyl-clad aluminum for maximum durability. The flexible, contoured viewing eyepiece has a UV-absorbing window for comfort and safety. The window also eliminates "blue haze" interference and increases contrast between the fluorescent area and the background. Soft rubber curtains on both sides of the CX-20 allow easy entrance to its interior. A hinged metal door at the front of the CX-21 offers the convenience of using one hand to manipulate specimens.

Spectroline

For info: 800-274-8888 | www.spectroline.com

PROTEIN PURIFICATION SYSTEM

The new fraction collector and sample pump are specifically designed to enhance ÄKTA pure, the modular chromatography system for flexible, reliable and intuitive protein purification. Designed to handle both air and liquid, the sample pump together with the sample inlet valve, provides fast, automated, and complete loading of up to seven samples. The air-sensor integrated into the valve detects the final drop of sample, automatically preventing the introduction of air whilst ensuring the complete sample reaches the column. The sample pump also has a robust wash program that removes any air introduced between samples. In order to secure precious samples from dust and contaminants, the fraction collector is covered and it supports flexible combinations of collection vessels from deep-well plates to 250 mL bottles. In addition to spillage-free collection across the entire flow-rate range of ÄKTA pure, the fraction collector has inbuilt automatic detection of collection vessel type to ensure sample security.

GE Healthcare

For info: 800-526-3593 | www.gelifesciences.com/aktapure